

For Reference

NOT TO BE TAKEN FROM THIS ROOM

EX LIBRIS
UNIVERSITATIS
ALBERTAE NSIS



For Reference

NOT TO BE TAKEN FROM THIS ROOM

THE UNIVERSITY OF ALBERTA

THE EFFECT OF PRESSURE ON THE RADIATION INDUCED
CONDUCTANCE OF LIQUID HYDROCARBONS .

by



DAVID WALTER BRAZIER

A THESIS

SUBMITTED TO THE FACULTY OF GRADUATE STUDIES
IN PARTIAL FULFILMENT OF THE REQUIREMENTS FOR THE DEGREE
of

DOCTOR OF PHILOSOPHY

DEPARTMENT OF CHEMISTRY

EDMONTON, ALBERTA

July, 1968



Digitized by the Internet Archive
in 2020 with funding from
University of Alberta Libraries

<https://archive.org/details/Brazier1968>

THE UNIVERSITY OF ALBERTA
FACULTY OF GRADUATE STUDIES

The undersigned hereby certify that they have read,
and recommend to the Faculty of Graduate Studies for
acceptance, a thesis entitled

"THE EFFECT OF PRESSURE ON THE RADIATION INDUCED
CONDUCTANCE OF LIQUID HYDROCARBONS"

submitted by DAVID WALTER BRAZIER, M.Sc., in partial
fulfilment of the requirements for the degree of
Doctor of Philosophy.

A B S T R A C T

The effect of pressures up to 4000 bars upon the conductance induced in hydrocarbon liquids by γ -radiation was studied. The hydrocarbons investigated include n-pentane, n-hexane, n-octane, methylcyclohexane, cyclopentane and 2,2-dimethylbutane.

To relate the observed pressure dependence of the induced conductance to the yield of free ions generated in the hydrocarbons, it was necessary to determine the pressure dependence of the viscosity, dielectric constant and density of the hydrocarbons over the same pressure range. The pressure dependence of viscosity was determined by a rolling ball technique. For density determinations a bellows dilatometer was used.

At all pressures employed the induced conductance in the hydrocarbons was a linear function of the applied field at dose rates of 1 to 6×10^{14} eV/ml sec. The maximum applied field was 2500 V/cm. In 2,2-dimethylbutane the induced conductance is a function of the absorbed dose.

Because of uncertainties in the radiolytic ion mobilities, two limiting cases for the variation of G with pressure have been considered. (i) If Waldens rule is assumed to apply then G_{fi} decreases with increasing pressure, the relative G_{fi} at 4000 bars being 0.67

(n-pentane), 0.67 (n-hexane), 0.72 (n-octane), and 0.80 (methylcyclohexane and cyclopentane). (ii) Conversely, if G_{fi} is assumed to be independent of pressure then b at atmospheric pressure in

$$u \propto \eta^{-b}$$

is 1.20 for hexane, octane and methylcyclohexane, 1.40 for n-pentane and 0.96 for cyclopentane. The volumes of activation for the induced conductance are consistent with the ions being of molecular dimensions.

A C K N O W L E D G E M E N T S

The author would like to express his appreciation to his research director, Dr. G. R. Freeman, for his guidance throughout the course of this project.

Special thanks are also due to:

Mr. E. B. Cairns of the Radiation Research Centre, to the Staff of the Chemistry Department Workshop and especially Mr. R. G. Cox (supervisor), Mr. P. Bradbury and Mr. O. Halasz. To the National Research Council for a scholarship and to Mrs. M. Waters for typing this manuscript.

Finally, for her patience over the past years and for her assistance in the production of this thesis, the author expresses his gratitude to his wife, Judy.

T A B L E O F C O N T E N T S

	<u>Page</u>
Abstract	iii
Acknowledgements	v
List of Tables	x
List of Figures	xiii
Section 1	
INTRODUCTION	1 - 31
(A) Historical background	1
(B) The nature of radiation induced ion- ization processes	5
(1) Interaction of γ radiation with matter.	5
(2) Energy loss by energetic elect- rons	7
(3) Electron range.	9
(4) Spatial distribution of ionization events.	11
(C) Radiation induced conductance in dielectric liquids.	12
(1) Free ion yield and conductance.	12
(2) Ion mobilities in dielectric liquids	15
(3) Dependence of radiation induced conductance on dielectric con- stant	19
(4) G free ions	21
(5) Field dependence of radiation in- duced conductance	21

	<u>Page</u>
(D) Effect of pressure upon transport processes in liquids	23
(1) General considerations	23
(2) Effect of pressure upon ionic conductance	27
(E) Field of present investigation	31
Section II	
EXPERIMENTAL	32-120
(A) High pressure system	32
(1) Pressure production and measurement	32
(2) High pressure vessels	36
(3) Pressure vessel closures.	40
(4) Experimental procedure.	44
(B) High vacuum system.	46
(C) Materials	48
(D) Radiation sources and dosimetry	52
(1) Radiation sources	52
(2) Dosimetry	53
(E) Determination of the pressure dependence of the dielectric constant	60
(1) Apparatus	60
(2) Experimental procedure	65
(3) Capacitance calibration, dielectric constant determination and corrections	66

	<u>Page</u>
(F) Determination of the pressure dependence of density	72
(1) Apparatus	72
(2) Calibration and experimental procedure	78
(G) The pressure dependence of viscosity . . .	84
(1) Apparatus	84
(2) Electrical timing instrumentation . . .	92
(3) Experimental procedure.	95
(4) Calibration	99
(H) Radiation induced conductance measurements	100
(1) Conductance cell construction	100
(2) Electrical circuit and current measurement.	109
(3) Experimental procedure	115
Section III	
RESULTS	121-216
(A) Pressure dependence of dielectric constant	121
(B) Pressure dependence of density.	134
(C) Pressure dependence of viscosity	144
(1) Calibration	144
(2) Pressure dependence of viscosity . . .	157
(D) Pressure dependence of radiation induced conductance	173
(1) General	173
(2) n-hexane	174

	<u>Page</u>
(3) n-Octane.	191
(4) n-Pentane	201
(5) Cyclopentane	201
(6) Methylcyclohexane	206
(7) 2,2-Dimethylbutane	211
Section IV	
DISCUSSION	217-239
(A) G_{fi} at atmospheric pressure	217
(B) Effect of pressure on G_{fi}	224
(C) Radiation induced conductance	235
SUMMARY	240
REFERENCES	242

L I S T O F T A B L E S

<u>Table</u>		<u>Page</u>
I-C-I	G_{fi} and ion mobilities.	16
II-A-I	Conversion factors for various pressure units in common use.	37
II-C-I	Miscellaneous materials and their sources.	49
II-C-II	Hydrocarbon purity and most probable impurities.	51
II-D-I	Dose rates within the pressure vessels.	58
II-E-I	Dielectric cells.	62
II-E-II	Dielectric constants of standards and hydrocarbons.	69
II-G-I	Viscosity of standard and silicone oils.	101
II-G-II	Densities of standard and silicone oils.	102
II-G-III	Viscosity of hydrocarbons.	103
II-G-IV	Density of hydrocarbons.	104
II-H-I	Conductance cell spacer and electrode dimensions	110
II-H-II	Some typical correction factors for the micromicroammeters.	116
III-A-I	Relative dielectric constants n-pentane, n-hexane and n-octane at 30°C	125
III-A-II	Relative dielectric constants. Methylcyclohexane, cyclopentane, 2,2-dimethylbutane and carbon tetrachloride at 30°C.	128
III-B-I	Relative volume and density of n-pentane and n-hexane at 30°C.	135

<u>Table</u>		<u>Page</u>
III-B-II	Relative volume and density of n-octane, methylcyclohexane and cyclopentane at 30°C.	138
III-B-III	Relative volume of 2,2-dimethylbutane, heptane, diethyl ether and cyclopentanone at 30°C.	143
III-C-I	$(\rho_S - \rho_L)$ x roll time at various temperatures. Angle I.	149
III-C-II	$(\rho_S - \rho_L)$ x roll time at various temperatures. Angle II	150
III-C-III	Viscosity of n-hexane. Pressure dependence at 0, 30 and 60°C.	164
II-C-IV	Viscosity of n-octane. Pressure dependence at 0, 30 and 60°C.	166
III-C-V	Viscosity of cyclopentane and methylcyclohexane. Pressure dependence at 30°C.	169
III-C-VI	Viscosity of n-pentane and 2,2-dimethylbutane. Pressure dependence at 30°C.	171
III-D-I	Conductance and relative conductance. Hexane at 30°C.	183
III-D-II	Conductance and relative conductance. n-Hexane at 3°C.	187
III-D-III	Conductance and relative conductance. Hexane at 56°C.	190
III-D-IV	Conductance and relative conductance. Octane at 30°C.	194
III-D-V	Conductance and relative conductance. Octane at 3°C.	198
III-D-VI	Conductance and relative conductance. Octane at 56°C.	200
III-D-VII	Conductance and relative conductance. n-Pentane at 30°C.	202

<u>Table</u>		<u>Page</u>
III-D-VIII	Conductance and relative conductance. n-Pentane at 30°C.	203
III-D-IX	Conductance and relative conductance. Cyclopentane at 30°C	205
III-D-X	Conductance and relative conductance. Methylcyclohexane at 30°C.	209
III-D-XI	Conductance and relative conductance. 2,2-Dimethylbutane at 30°C.	215
IV-A-I	G_{fi} atmospheric pressure and ion mobilities	221
IV-B-I	G_{fi} hexane at one atmosphere and 4000 bars	234
IV-C-I	Volumes of activation for induced conductance	238

L I S T O F F I G U R E S

<u>Figure</u>		<u>Page</u>
II-A-1	High pressure production system	33
II-A-2	Section of high pressure vessel	38
II-A-3	Section of pressure vessel closure	41
II-B-1	High vacuum system	47
II-D-1	Absorbance versus radiation exposure time curves	57
II-E-1	Dielectric constant cell and assembly within the pressure vessel	61
II-E-2	Calibration dielectric cell P2 at 30°C	70
II-F-1	Bellows dilatometer (voltage divider removed)	74
II-F-2	(a) Slide wire contact and bellows head (b) Filling aperture closure	76
II-F-3	(a) Voltage divider (b) Electrical circuit employed with the voltage divider	77
II-F-4	Calibration of bellows volume	80
II-F-5	Voltage divider calibration	81
II-G-1	(a) Section of roll tube assembly on base plate (b) Detailed section of base plate	86
II-G-2	(a) Section of bellows roll tube holder (b) Detail of compression screw cap	87
II-G-3	Pressure vessel mounting for viscometric determinations	91
II-G-4	Block circuit diagram of viscometer timing apparatus	94

<u>Figure</u>		<u>Page</u>
II-G-5	Viscometer filling system	97
II-H-1	Bellows assembly of conductance cell	107
II-H-2	Electrode assembly of bellows conductance cell	108
II-H-3	Electrical circuit for conductance measurements in radiation cave	111
II-H-4	Electrical connections to the pressure vessel	113
II-H-5	Conductance cell filling system	118
III-A-1	Capacitance versus pressure cell P2	122
III-A-2	Relative dielectric constant versus pressure. n-Pentane, n-hexane and n-octane 30°C.	126
III-A-3	Relative dielectric constant versus pressure. 2,2-dimethylbutane, cyclopentane and methylcyclohexane 30°C	129
III-A-4	Clausius-Mossotti function versus density. n-pentane, n-hexane and n-octane 30°C	131
III-A-5	Clausius-Mossotti function versus density. Cyclopentane, methylcyclohexane and 2,2-dimethylbutane 30°C	132
III-B-1	Relative volume versus Pressure. n-Hexane, n-pentane	136
III-B-2	Relative volume versus pressure. n-Octane, methylcyclohexane and cyclopentane 30°C	139
III-B-3	Temperature dependence of hexane density at constant pressure	141
III-B-4	Temperature dependence of octane density at constant pressure	142

<u>Figure</u>		<u>Page</u>
III-C-1	Roll time versus temperature hydrocarbons	147
III-C-2	$(\rho_S - \rho_L) \times$ roll time versus $\text{Log} \eta$ 30°C	151
III-C-3	Temperature dependence of viscometer coefficient	154
III-C-4	Roll time versus pressure at constant temperature octane. Angle II	159
III-C-5	Roll time versus pressure at constant temperature methylcyclohexane. Angle I	160
III-C-6	Roll time versus temperature at constant pressure octane. Angle II	161
III-C-7	Roll time versus temperature at constant pressure methylcyclohexane. Angle I	162
III-C-8	Viscosity versus pressure, hexane, 0, 30 and 60°C.	165
III-C-9	Viscosity versus pressure, octane, 0, 30 and 60°C	167
III-C-10	Viscosity versus pressure, methylcyclohexane, 2,2-dimethylbutane, n-pentane, and cyclopentane 30°C.	170
III-D-1	Cell current versus voltage, hexane 30°C	175
III-D-2	Cell current versus Voltage, hexane 30°C	176
III-D-3	Conductance versus pressure, hexane 30°C	180
III-D-4	Conductance versus pressure, hexane 30°C	181
III-D-5	Relative Conductance versus pressure, hexane 30°C	185
III-D-6	Conductance versus pressure, hexane 3 and 56°C	186
III-D-7	Relative conductance versus pressure, hexane 3 and 56°C	189

<u>Figure</u>		<u>Page</u>
III-D-8	Cell current versus applied voltage at constant pressure, octane 30°C	192
III-D-9	Conductance versus pressure, octane 30°C	193
III-D-10	Relative conductance versus pressure, octane 30°C	195
III-D-11	Conductance versus pressure, octane 3°C	196
III-D-12	Relative conductance versus pressure n-octane 3 and 56°C	199
III-D-13	Relative conductance versus pressure pentane 30°C	204
III-D-14	Relative conductance versus pressure cyclopentane 30°C	207
III-D-15	Conductance versus pressure methyl- cyclohexane 30°C	208
III-D-16	Relative conductance versus pressure methylcyclohexane 30°C	210
III-D-17	Cell current versus absorbed dose, 2,2-dimethylbutane 30°C	212
III-D-18	Conductance versus pressure 2,2-di- methylbutane 30°C	213
III-D-19	Relative conductance versus pressure 2,2-dimethylbutane 30°C	216
IV-A-1	Ion mobility versus viscosity log log plot	220
IV-B-2	$(G_{fi}^P)/(G_{fi}^1)$ versus pressure	226
IV-B-2	$(G_{fi}^P)/(G_{fi}^1)$ versus pressure	227
IV-B-3	Power b in Relation IV-vii	230
IV-C-1	log κ versus pressure 30°C	236

Section I

I N T R O D U C T I O N

(A) Historical Background.

The ability of high energy radiations to ionize a medium through which they passed was one of the first properties of such radiations to be discovered. After the discovery of X-rays by Roentgen in 1895 (1,2), numerous authors (3-5) almost simultaneously reported that exposure of a gas to the new "Roentgen rays" resulted in the gas being rendered capable of supporting a flow of electricity. No such conductance was apparent in the absence of radiation.

A short time later, Curie (6) reported an induced conductance when such dielectric liquids as carbon disulphide, carbon tetrachloride, benzene and petroleum ether were exposed to X-rays and radium γ -rays. In 1902, Becquerel (7) found an induced current in a paraffin solid when the solid was exposed to radium γ -rays. The frequent use of the term "ionizing radiations" to describe high energy radiations is thus apparent.

Over the twenty year period after the discovery of X-rays and other high energy radiations, research into gas phase ionization proceeded at a tremendous rate. Interest in liquid and solid phase ionization on the other hand was small.

To cover the early work on gas phase ionization would require several volumes and the interested reader is referred to the numerous texts on gas ionization chambers and counters, (8,9).

Certain concepts, fundamental to the fate of ions produced during ionization and to radiation physics and chemistry in general, were developed over the early period of gas phase ionization investigations. The immediate concern of the investigators was to explain the observed dependence of the ion current upon the applied collecting electrical field. The characteristic ion current-applied field dependence is illustrated in Figure 1 for a typical gas. The actual shape of the curve is dose rate dependent and the curve illustrated is the type that is obtained at low dose rates.

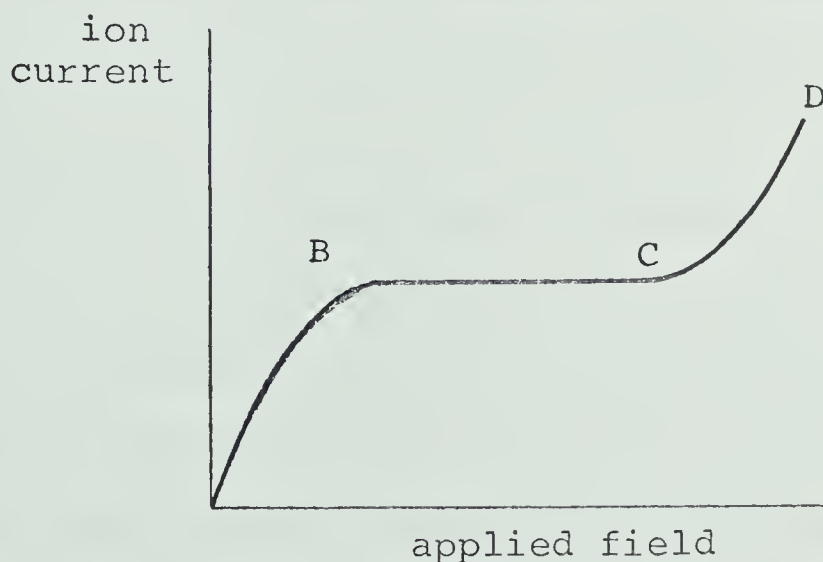


FIGURE -1

The shape of the curve was explained in terms of the effect of field strength on the competition between ion recombination processes and the collection of the ions at the electrodes (5,10,11). At low collecting fields (section AB of curve in Figure 1), the field is insufficient to collect all the ions produced and the observed ion current is field dependent. In this region ion recombination is appreciable. As the collecting field is increased the so called "saturation current", characterized by the plateau between B and C, is reached. All the ions are being collected over this region. Increasing the field beyond the point C results in acceleration of the electrons to an extent where they can cause further ionization and hence the ion current increases. In the case of liquids, dielectric breakdown occurs at applied fields much less than the field required to reach the saturation current and the saturation plateau is never reached (12).

In 1913, Jaffe (13) published his theory of "columnar ionization" for the ionization of fluids by heavy particles. The theory was successful in explaining the current-field characteristics observed in the α -particle ionization of gases (14,15). Qualitative agreement with the theory was also found for the X-ray (16,17) and γ -ray (18) ionization of liquids. A later modification of Jaffe's theory by

Kramers (19), also found only limited success (20,21).

The failure of Jaffe's theory when applied to radiations of low ionizing power is not surprising considering his assumption of a uniform ionization density. The spatial distribution of ionization events had been shown as early as 1911 (22) to be quite different for various radiations. A theory of initial recombination, developed by Onsager (23) for the recombination of isolated ion pairs generated in high pressure gases, has recently been applied successfully to the field dependence of conductance in dielectric liquids (24,25).

The scarce work available on the induced conductance in dielectric liquids prior to 1960, has been reviewed by several authors (26,27,28). A considerable number of the investigations were prompted by a need for the understanding of the intrinsic (or background) conductance of insulating oils. It is of historical interest to note that the intrinsic conductance of a dielectric liquid was once considered to arise from natural cosmic radiation (29,30). Today, the intrinsic conductivity is generally attributed to either, or both, ionic impurities and thermionic emission from the cathode (27).

Ionic processes do not alone account for the observed radiolysis products of various compounds. Measurements of W (31), the amount of energy required to produce an ion pair, showed that approximately equal amounts of excitation and

ionization result when a high energy radiation beam traverses a medium. Only the results of ionization events can contribute to an induced current.

Extensive radiolytic mechanisms involving excited neutral molecules and molecular fragments are to be found in the literature (32,33). A technique to distinguish the relative contributions of ionic and neutral processes to the overall radiolyses of gases was developed by Essex (34). The method consists of determining the ionic yield (number of molecules of a particular type produced or destroyed per ion pair formed) as a function of the applied electrical field.

(B) The Nature of Radiation Induced Ionization Processes.

The production of ion pairs in a medium exposed to electromagnetic radiation (x or gamma-rays), fast electrons or heavy charged particles, results from the physical interaction of the radiation with the orbital electrons of the molecules of the medium. A brief account of the nature of these interactions will now be given for gamma radiation and for fast electrons.

(1) Interaction of γ -Radiation with Matter.

Studies to be presented later, utilized the γ -emission of cobalt-60, a radioisotope produced from natural cobalt by neutron capture. ⁶⁰Cobalt decays with a half life

of 5.26 years (35) to nuclear excited states of ^{60}Ni ., the latter decaying to the ground state with the emission of two γ -rays with energies of 1.17 and 1.33 MeV.

The overall attenuation of electromagnetic radiation obeys the exponential law

$$I = I_0 e^{-\mu x} \quad (\text{I-i})$$

where I_0 is the incident beam intensity, I the intensity after travelling a distance x in the medium, and μ is the total linear absorption coefficient.

Energy is transferred to the medium by several processes, the most important of which are the photoelectric effect, pair production and Compton absorption (or scattering) (36).

The photoelectric effect results in the ejection of an orbital electron, with an energy equivalent to that of the incident photon less the binding energy of the electron. The greatest probability of interaction by the photoelectric effect occurs when the incident photon energy is comparable to, but just greater than, the binding energy of the electron (283 eV for a carbon K shell electron (37)). For gamma radiation from ^{60}Co . (energy > 1 MeV) the photoelectric effect does not contribute appreciably to ionization.

In pair production, the photon interacts with the nucleus of an atom and generates an electron-positron pair.

As the rest mass energy of an electron is 0.511 MeV, pair production can only occur with incident photons of energy greater than 1.02 MeV. The pair production cross section is negligible at energies less than 2 MeV (36) and the process does not contribute to ionization at ^{60}Co γ -ray energies.

Compton absorption, the only important mode of interaction for gamma energies around 1 MeV, occurs when the photon collides with an electron (either bound and free). The electron is ejected from the atom and the photon scattered, such that momentum between the ejected electron and the photon is conserved. The maximum energies of the ejected electrons (calculated using a relation given by Compton (39)) for incident gammas of 1.17 and 1.33 MeV are 0.96 and 1.12 MeV respectively. For 1 MeV gammas, the absorption and scattering coefficients are approximately equal (36) so the average energy of the ejected electrons for the two ^{60}Co gammas are 0.59 and 0.67 MeV. The primary interaction of a ^{60}Co gamma with matter thus produces an electron with an energy between zero and 1.12 MeV. The Compton electrons so produced are attenuated in a similar manner to fast electrons from other sources.

(2) Energy Loss by Energetic Electrons.

Energetic electrons lose energy to a medium by one or

more of the following three ways; inelastic scattering, elastic scattering, emission of radiation (Bremstrahlung).

For Compton electrons generated by ^{60}Co gammas essentially only inelastic collisions contribute to ionization. Bethe (39) developed the following relation for the rate of kinetic energy loss of electrons by collision as a function of path length traversed.

$$-\left(\frac{dT}{dX}\right)_{\text{coll}} = \frac{2\pi e^4 ZN}{M_0 V^2} \left[\ln \frac{M_0 V^2 T}{2I^2 (1-\beta^2)} - (2\sqrt{1-\beta^2} - 1 + \beta^2) \ln 2 + (1-\beta^2) + \frac{1}{8}(1-\sqrt{1-\beta^2})^2 \right] \quad (\text{I-ii})$$

where N is the number of atoms/cm³, Z is the number of electrons/atom, T is the relativistic kinetic energy of the electron with velocity V , I is the average excitation potential of the atom and β is the ratio v/c , when C is the velocity of light. The Bethe equation is only valid for incident electrons with kinetic energy in excess of the average excitation potential of the medium. The value of I may be calculated (40) but is generally obtained by fitting the Bethe equation to experimentally determined electron energy-range data (31).

The manner by which electrons with energies less than I lose their energy is uncertain. The Bethe equation has been used down to energies of about 20 eV by assuming only

the valence electrons contribute to attenuation, (25,41).

The excitation and ionization events along the track of a high energy particle are complete in approximately 10^{-15} secs. In this time, it has been estimated that a 1 MeV electron causes 3 to 4×10^4 ionization events and produces 5 to 8×10^4 excited molecules (42).

(3) Electron Range.

In recent studies of radiation induced conductance (25) and in some aspects of radiolysis in general (12) information as to the initial separation distances of the positive ion and its corresponding thermalised* electron (or negative species) has become increasingly important.

The range, R , of an electron may be calculated from the collisional energy loss relation (I-ii) by integration.

$$R = \int_I^T -dT / \left(\frac{dT}{dX} \right)_{\text{coll}} \quad (\text{I-iii})$$

The same limitations of $T \gg I$ placed on the Bethe equation applies to (I-iii). Comparison of experimentally determined electron ranges (43-45) indicates good agreement with those calculated by (I-iii) when the electron energy is greater than 20 keV (40,46) but below this energy

* A thermalised electron is an electron in thermal equilibrium with its environment.

there is serious discrepancy. In general, electron ranges calculated by relation (I-iii) are lower than the experimental values, the difference increasing as the electron energy decreases.

No satisfactory treatment of electron ranges for energies less than I exists. Samuel and Magee (47) estimated the range of a 15 eV electron in water to be 12.5 or 18 Å depending upon the fractional energy loss per collision that they assumed. These values were obtained by considering the electron to lose energy by collision and by interaction with the coulombic field of the parent positive ion. Platzman (48) on the other hand, has estimated the range of a 10 eV electron in water to be about 50 Å.

An alternative arbitrary procedure used by Freeman (24,25,49) consists of extrapolating the electron energy-range plot to lower energies. Employing the data of Lea (50) for the range of electrons in water with energies of 1 keV and greater, a range of 14 Å was obtained for a 15 eV electron by extrapolation using a parabolic function. Ranges in other liquids were calculated using the Bethe equation.

Hummel, Allen and Watson (46) found that in order to fit their radiation induced conductance data from n-hexane, the electron had to be given a range considerably greater

than that calculated by relation (I-iii). At the present time the range of low energy electrons is unknown with any certainty.

(4) Spatial Distribution of Ionization Events.

The rate of loss of kinetic energy of an energetic particle is often referred to as the LET value (Linear Energy Transfer) of the particle. The average LET of the Compton electrons generated in water by ^{60}Co gammas is 0.02 eV/\AA (51).

The minimum LET for an electron occurs at an electron energy of about 1 MeV and increases as the energy decreases. Taking the LET value of a 1 MeV electron as unity, the relative LET values of 100, 10 and 1 keV electrons are 2.1, 11.5 and 61.5 respectively (52). The density of ionization and excitation events therefore increases towards the end of an electron track.

The locations of excitation and ionization events along a particle track are called spurs. A spur may contain one or more ionization events. Occasionally a secondary electron may be ejected with sufficient energy to produce a true divergent track (δ -ray).

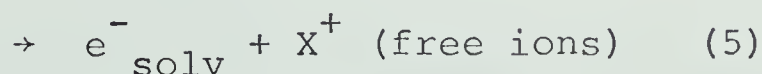
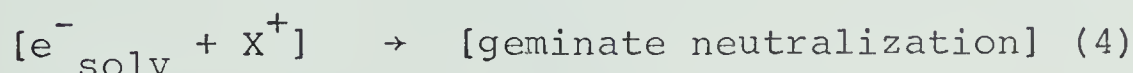
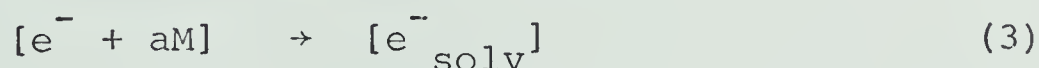
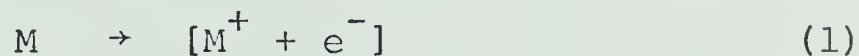
In a recent analysis of electron tracks (53) a track was divided into three entities, called spurs, blobs and short tracks, which were distinguishable in terms of the

amount of energy expended in their formation. A spur results from a glancing encounter of the incident electron and involves energy losses of up to 100 eV. Blobs and short tracks both arise from δ -rays, the former from low energy δ 's (~ 100 eV to ~ 500 eV) and the latter from relatively high energy δ 's (~ 500 eV to ~ 5 keV). As the energy of the electron increases the incidence of spurs increases whilst the formation of short tracks decreases. Blob formation on the other hand remains practically constant and independent of the incident electron energy.

(C) Radiation Induced Conductance in Dielectric Liquids.

(1) Free Ion Yield and Conductance.

The ionic reactions occurring during the initial stages of the radiolysis of a liquid may be represented by the following sequence (12,25,49).



Species inside a spur are shown in square brackets. If

reaction (2) does not occur then X^+ is M^+ in the above sequence.

The magnitude of the radiation induced conductance observed in such a liquid is determined by the competition between reactions (4) and (5). Ions removed by geminate neutralization cannot contribute to the ion current.

In general, geminate neutralization will occur if the coulombic attraction between the ions exceeds thermal energy. A critical distance, r_c , at which the coulombic interaction is equal to the thermal energy is given by

$$r_c = \frac{\xi^2}{\epsilon kT} \quad (\text{I-iv})$$

where ξ is the charge on the ions (e.s.u. units), ϵ is the dielectric constant and kT the thermal energy (4.07×10^{-14} ergs at 22°C).

At a steady state concentration of ions, i.e. when the applied field is low such that the majority of the free ions are disappearing by mutual neutralization, the yield of reaction 5 is given by (54-56)

$$G_{fi} = 100 \left[\frac{k\kappa^2}{Iu^2} \right] \quad (\text{I-v})$$

where G_{fi} is the number of free ions formed per 100 eV of energy absorbed, k is the geminate neutralization rate ($\text{cm}^3/\text{ion sec}$), I is the dose rate (eV/ml sec), u is the sum of the positive and negative ion mobilities ($\text{cm}^2/\text{V sec}$)

and κ is the conductivity.

In order to calculate G_{fi} directly from (I-v) the geminate neutralization rate constant k , and the mobilities would have to be known. As yet no method of measuring k directly is available but the ratio k/u is given by the Debye formulae (57)

$$\frac{k}{u} = \frac{4\pi e}{\epsilon} \quad (\text{I-vi})$$

where e is the charge on the ion (esu units) and ϵ is the dielectric constant. The value of u can be measured, so that of k can be obtained. Alternatively, when the value of u is unknown, both k and u may be estimated using theoretical and semiempirical relations (54). Assuming geminate neutralization to occur with unit encounter efficiency, k is given by the relation (58)

$$k = 4\pi r(D_+ + D_-) \quad (\text{I-vii})$$

where r is the interaction distance (or collision radius) and D is the diffusion coefficient of the respective ion. Relation (I-vii) was originally developed for the rate of coagulation of ions in colloidal suspensions and in the present application r may be equated to r_c (relation I-iv).

The diffusion coefficient in unassociated liquids may be obtained from the empirical equation (59)

$$D = 7.4 \times 10^{-10} \frac{T_M^{0.5}}{\eta V^{0.6}} \quad (\text{I-viii})$$

where η is the viscosity of the solution (poise), M is the molar weight of the solvent (grams) and V is the molar volume of the ions. The agreement between diffusion coefficients calculated by relation (I-viii) and those obtained experimentally is generally only fair especially at low temperatures (60).

The diffusion coefficient of an ion is related to the mobility of the ion by the equation (19)

$$D = \frac{ukT}{c} \quad (\text{I-ix})$$

where c is the charge on the ions in units of electronic charge. Suitable rearrangement of (I-vii, viii and ix) followed by substitution in (I-v) yields for G_{fi} , after proper conversion of units (54),

$$G_{fi} = 4.1 \times 10^{38} \frac{\eta V^{0.6}}{M^{0.5} I \epsilon} \kappa^2 \quad (\text{I-x})$$

Table I-C-I contains some representative literature data on G_{fi} and ion mobilities (positive and negative ions) in various liquids (25,55,56,61-68). Other values for mobilities are to be found in a recent review (69).

(2) Ion Mobilities in Dielectric Liquids.

The agreement between literature values, for the mobilities of ions in dielectric liquids is not good,

TABLE I-C-I

G_{fi} and Ion Mobilities. (\sim Room Temperature)

Compound	G_{fi}	$u_+ \times 10^3$ $\text{cm}^2/\text{V sec}$	$u_- \times 10^3$ $\text{cm}^2/\text{V sec}$	Reference
n-Pentane	0.12	0.82	1.50	61
	0.10	---	---	62
	0.145	---	---	68
n-Hexane	0.09	---	---	55
	0.10	---	---	25
	0.11	0.64	1.11	61
	0.09	0.85	0.91	62
	0.13	---	---	63
	0.10	0.66	1.27	56
	0.131	---	---	68
n-Heptane	0.09	0.65	0.72	62
n-Octane	0.124	---	---	68
	---	0.34 - 0.15	0.18	65
	---	0.24	0.44	66, 67
Cyclohexane	0.06	0.47	0.56	62
	0.11	0.21	0.38	61
	0.08	---	---	64
	0.148	---	---	68
2,2-dimethylbutane (neohexane)	0.40	0.48	0.97	61
	0.304	---	---	68
2,2-dimethylpropane (neopentane)	0.74	0.62	1.36	61
	0.857	---	---	68
2,2,4-trimethylpentane	0.332	---	---	68

cont'd....

TABLE I-C-I (continued)

cyclopentane	0.155	---	---	68
3-methylpentane	0.146	---	---	68
2,3-dimethylpentane	0.192	---	---	68
diethyl ether	0.350	---	---	68
	0.19	---	---	25
Carbon tetrachloride	0.068	0.43	0.43	56
	0.096	---	---	68
Carbon disulphide	0.314	---	---	68
Water	2.7	---	---	77
	----	---	1.8	77a

especially in the case of the negative ions. The question arises as to what negative species the determined mobility refers. The negative species are not quasi-free electrons* because the mobilities are too small. For example, in liquid argon, where the electron is considered to be quasi-free, its mobility is $500 \text{ cm}^2/\text{V sec}$, (71) compared to $0.22 \text{ cm}^2/\text{V sec}$ (72) in helium, in which the electron is localised. In most experiments with hydrocarbon liquids trace impurities capable of reacting with electrons to give molecular ions were probably present.

Addition of 2% carbon tetrachloride, which is known to capture electrons (73), did not alter the measured conductance or G_{fi} free ion of n-hexane (46) and only a small change in the negative ion mobility was observed. On the other hand the mobility was decreased by about a factor of two when 2% tetrahydrofuran was added. It is possible that the negative oxygen ion from oxygen electron capture is always present even in so-called degassed samples (46).

The dependence of the ion mobilities on the viscosity of the hydrocarbon has been generalized by the relation (69,74).

$$u \propto \eta^{-x} \quad (I-xi)$$

where x varies between 1 and 2 depending upon the liquid

* In a condensed medium the electron can never be completely free. An electron that is not localised is described as quasi-free (70).

and ion. For positive ions in hydrocarbons (65,66,75) x is about $3/2$ whereas for negative ions it is about 1 (67,76).

(3) Dependence of Radiation Induced Conductance on Dielectric Constant.

From equation (I-iv), the critical separation distance r_c may be calculated for different liquids. In cyclohexane, for example, ϵ is 2.02 and r_c is 280 \AA whereas, in water, r_c is 7 \AA for the static dielectric constant of 79. In water, therefore, assuming that the electron thermalization distance is approximately the same for both compounds, a larger fraction of ion pairs would be generated with separation distances greater than r_c . The free ion yield should therefore increase. The experimental value of G_{fi} for water is 2.7 (77) compared to 0.11 for cyclohexane (61).

Using Onsagers theory (23) for geminate neutralization, along with the distribution of ion-electron separation distances, Freeman and Fayadh (25) successfully interpreted the dielectric constant dependence of G_{fi} . The value of G_{fi} was calculated from the relation,

$$G_{fi} = \left[\frac{N(y) \phi(y) dy}{N(y) dy} \right] \times G_{(\text{total ionization})} \quad (\text{I-xii})$$

where $G_{(\text{total ionization})}$ is the yield of ions from reaction

1 (page 12), $N(y)$ is the relative number of thermalized secondary electrons that have an initial separation distance y from their parent positive ions and $\phi(y)$ is the probability that an ion pair of initial separation y will escape geminate neutralization. According to Onsager (23) the latter probability is given by $e^{-r_c/y}$.

Assuming $G_{(\text{total ionization})}$ was 3-4 (later estimates are closer to 4(12)), a satisfactory agreement between the observed and calculated G_{fi} was found for several compounds with dielectric constant between about 2 and 79 (12,25). Onsager's theory (23) has also been used in the interpretation of the observed temperature dependence of G_{fi} (46).

The dielectric constant dependence of the geminate neutralization rate constant is given in equation I-iii. Typical calculated values of k/u are 0.96×10^{-6} V/cm for n-hexane and 0.89×10^{-6} V/cm for cyclohexane. The value of k/u may be determined experimentally from the rate of decay of the induced current after a pulse of radiation (46,56,60). The value of k in n-hexane at room temperature is about 2×10^{-9} cm³/ion sec. The temperature dependence of the dielectric constant of low dielectric constant liquids is small and the major temperature dependence of k arises from variations in u with temperature.

(4) G free-ions.

The yield of free ions for straight chain hydrocarbons all are close to 0.1. However when methyl substituents are introduced into the chain the free ion yield increases (61,68). Gibaud (78) also noted a significant increase in the induced current when methyl substituents were present in the alkane chain, whereas little effect of methyl substituents in the aromatic ring was observed.

As yet none of the models for electron thermalization (25,79) can explain the higher free ion yields in liquids made up of more "spherical" molecules. It is considered (25) that the electron range prior to localization must increase so that the probability of geminate neutralization is reduced.

(5) Field Dependence of Radiation Induced Conductance.

Few studies have been made covering both a wide range of dose rates and field strengths (24,80). The variation in conductance with increasing field strength is dependent upon the dose rate. The variation may be summarized (a) at low dose rates ($\lesssim 10^{12}$ eV/ml sec) the number of ions undergoing neutralization at the electrodes is appreciable and increases as the applied field increases above about 1 kV/cm. The steady state concentration of ions in the liquid then decreases and the conductance falls.

(b) At high dose rates ($\sim 10^{15}$ eV/ml sec) the majority of the ions undergo random neutralization in the liquid. The conductance is then independent of applied field until the field is of sufficient magnitude (~ 2 kV/cm) to physically assist the ions in escaping each others coulombic attraction. The conductance then increases.

Onsagers theory (23) was shown to adequately describe the field dependence of the induced conductance at all dose rates employed (24).

Numerous other studies have been made on the field dependence of the induced ion current in the low dose rate region and the results have been discussed in several reviews (18,28,74). In general, the results were interpreted in terms of Jaffe's (13) or Kramer's (19) theories (see Section 1A) regardless of the LET of the radiation employed in the study.

Figure 2 shows the dependence of the induced current upon the applied field under low dose rate conditions (74).

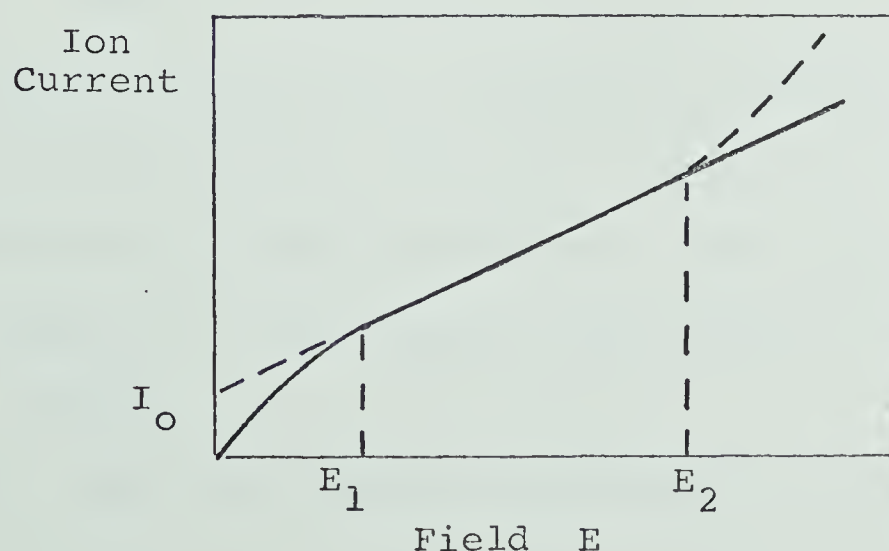


FIGURE 2.

The field dependence is described by the relation

$$I = I_0 + cE \quad (E > E_1) \quad (I\text{-xiv})$$

Values of G_{fi} calculated from I_0 in hexane at room temperature were 30% higher than those calculated from the low field conductance (81) and the physical significance of I_0 was questioned. The use of Jaffe's theory for radiation of low LET (X or γ) has also been objected to (12).

In some investigations (82,83) a rise in the induced current at high field strengths (dashed curve in Figure 2) was found and was attributed to ion multiplication processes as found in irradiated gases. Arguments for (84,85) and against (86) electron multiplication in very pure low dielectric constant liquids are to be found in the literature but as yet the problem remains unresolved.

(D) The Effect of Pressure upon Transport Processes in Liquids.

(1) General Considerations.

The ultimate interpretation of the mechanism of electrical conductance requires a knowledge of such transport properties as viscosity, diffusion and ion mobility. Unfortunately these processes in turn require an adequate description of the liquid state and no such description, as yet, exists.

The more rigorous treatments of the liquid state (87)

in terms of the intermolecular forces are hampered by difficult mathematics and a lack of availability of liquid correlation functions. Some simpler models (88-92) of the liquid state based upon the free volume and excess volume concepts, however, are more suited to a discussion of pressure effects because the major effect of pressure is to reduce the free volume. The latter fact is substantiated by compressibility measurements (93). The compressibility of organic liquids vary by approximately a factor of ten at atmospheric pressure whereas at about 12000 bars the variation is only by a factor of about 1.5. The compressibility also decreases as the pressure increases, the most rapid decrease being observed over the first 1000 bars.

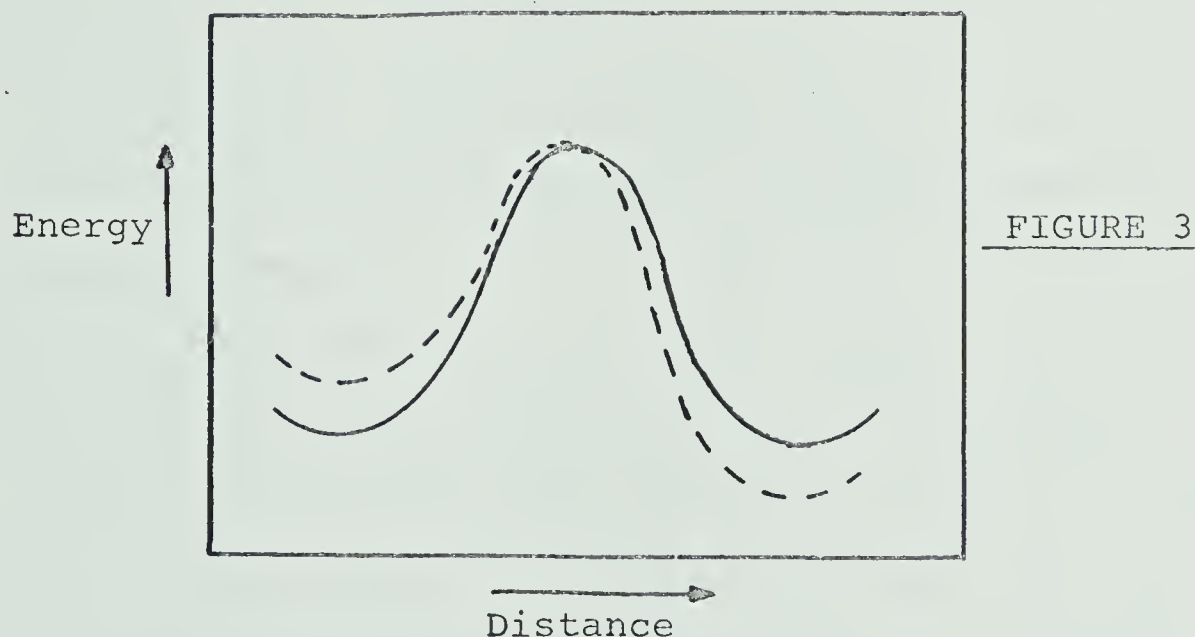
The free volume, V_f , of a liquid may be defined as the difference between the total volume of the liquid and the actual volume of the molecules themselves. For cubical packing (89,90)

$$V_f = 8(V^{1/3} - d)^3 \quad (\text{I-xv})$$

where V is the volume inhabited (molar volume/Avogadro's number) and d is the incompressible diameter of the molecule. The excess volume, as used in the significant structure theory (91,92) is the molar volume of the liquid state less the molar volume of the solid state. The excess volume per molecule is less than the free volume per molecule

because even in the closest possible packing a certain volume exists which is inaccessible to the molecules by virtue of their shape.

The application of the theory of rate processes (88, 90) to transport processes in liquids has met with some success. According to this theory in order for a molecule to be transported from one equilibrium position to another a potential barrier must be surmounted. The energy versus displacement distance diagram is depicted in Figure 3(90).



The solid line represents the situation with regards to diffusion for which the potential barrier is equal in all directions. The application of a force (e.g. a shearing force for viscosity or an electrical field for ion mobility) results in a reduction of the height of the barrier in the direction of the applied force (dashed line).

The pressure dependence of the rate constant for such a process may be expressed as follows (94,95)

$$-RT \frac{\partial \ln k}{\partial P} = \Delta V^\ddagger \quad (\text{I-xvi})$$

where ΔV^\ddagger represents the increase in volume on forming the transition state. Relation (I-xvi) is extensively used in high pressure reaction kinetic studies to interpret the observed pressure dependence of reaction rates (95,97).

If the sign of ΔV^\ddagger is known or may be estimated for a given reaction, the effect of pressure upon that reaction may be predicted on the basis of le Chatelier's principle.

Usually ΔV^\ddagger for transport processes is positive and the rate of such processes will therefore decrease with applied pressure. ΔV^\ddagger is considered (90) to be the increase in the volume of the system required for a molecule to move from one equilibrium portion to another.

Other simple models for transport processes in terms of the available volume in a liquid have been suggested (98,99) but, like the above, none is completely satisfactory (100). A more recent approach, the significant structure theory (92) leads to the conclusion that the rates of transport processes are dependent on the excess volume ($V_L - V_S$). The viscosity (or reciprocal fluidity) for example, is inversely proportional to the excess volume.

$$\eta \propto \frac{1}{V_L - V_S} \quad (\text{I-xvii})$$

This form is similar to that derived earlier by Batschinski (101).

It has been suggested (102-105) that pressure studies of conductance in conjunction with the transition state approach may lead to an understanding of the limiting molar conductance. However, as yet insufficient experimental data are available. None of the simple models allow for specific liquid or molecular structure effect on the transport processes when the pressure is applied. Liquid structure (93) and molecular structure (106), however are known to exercise an influence upon the pressure dependence of viscosity.

(2) The Effect of Pressure on Ionic Conductance.

The measurement of electrical conductance at elevated pressures is not only important for its own sake, but it also furnishes a technique for the study of ionic equilibrium at high pressures (95,97). The variation of conductance with pressure is generally interpreted in terms of the effect of pressure upon the density, viscosity and dielectric constant of the solvent.

The effect of pressure on the conductance of electrolytes in aqueous solutions may be summarized as follows (95).

(i) Strong Electrolytes.

At room temperature the limiting molar conductances

(LMC) of salts either increases or remains constant over the first 1000 bars, after which they decrease in a parallel manner with the viscosity.

At low temperature ($\lesssim 15^{\circ}\text{C}$), the viscosity of water initially decreases with increasing pressure (93,107), reaches a minimum at approximately 1000 bars, and then increases with a further increase in pressure. At 30°C the viscosity increases over the complete pressure range. The initial rise in conductance at room temperature ($\sim 25^{\circ}$) is attributed to extra structure being present in the water because of the presence of ions. The pressure dependence of the viscosity would then be similar to that at the lower temperatures.

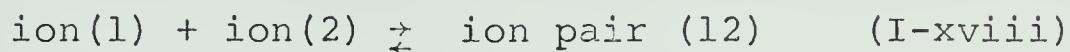
(ii) Weak Electrolytes.

The LMC of weak electrolytes increases with increasing pressure and reflects the effect of pressure upon the ionic equilibria between undissociated solute and ions. Since the LMC increases with applied pressure, the volume of activation (ΔV^{\ddagger}) for the process is negative. The negative ΔV^{\ddagger} is accounted for in terms of increased electrostriction i.e. the decrease in volume of the solvent in the vicinity of the ions (95).

Of more interest to the work to be presented later is the effect of pressure upon conductance in low dielectric constant media. When the dielectric constant of the solvent

is decreased, the coulombic interaction between the ions increases. The interaction energy is given by $\xi^2/\epsilon r$, where all symbols have the same meaning as in relation (I-iv) except r which is now the actual ion separation distance. A situation results in which the ions are associated in pairs, triplets and higher clusters depending upon the concentration of ions (108). The formation of an ion pair reduces the conductance because a neutral pair can no longer contribute to charge transport. An ion triplet, on the other hand, can transfer charge.

Increasing the pressure upon such a system alters the dynamic equilibrium for ion pairs



and also the equilibrium of higher ion aggregates. Superimposed upon this pressure effect is the decrease in conductance because of the increased viscosity of the solvent.

The critical concentration at 20°C, above which ion triplets are produced and below which ion pairs and free ion exist is given by (108)

$$C_o = 3.2 \times 10^{-7} \epsilon^3 \quad (\text{I-xix})$$

where C_o is the critical concentration and ϵ is the dielectric constant of the solvent. For hydrocarbons, ϵ is about 2 and C_o therefore is about $2.6 \times 10^{-6} M$.

The effect of pressure upon conductance in diethyl ether and benzene (109) toluene (110) and methanol (111) has been investigated and the results confirm the presence of ion pairs and higher aggregates. For the system tetra-isoamylammonium picrate in ether (109) at concentrations where ion triplets are present, the conductance increases with increasing pressure but a larger increase with pressure is observed at lower concentrations where ion pairs predominate. The variation of the pressure dependence of the conductance with concentration is explained in terms of the increased viscosity and dielectric constant of the ether. Increasing the dielectric constant decreases both ion pair and ion triplet association.

The steady state concentration of ions produced in a hydrocarbon during radiolysis is given by (25)

$$n = \frac{10^{-2} IG_{fi}}{k} \quad (I-xx)$$

where n is the concentration of ions (ions/cm³) and the other symbols have the same meaning as previously given in Section I-C. For n-hexane at room temperature, G_{fi} is 0.1 (25) and k is 2×10^{-9} cm³/ion sec, therefore at a dose rate of 1×10^{15} eV/ml sec, n is 2×10^{11} ions/cm³ or 3×10^{-10} M. Similar calculations for neopentane with G_{fi} 0.74 (61) still only gives a concentration of ions of 1×10^{-9} M. The average lifetime of the ions that escape

geminate neutralization is about 10^{-3} sec. The ions undergo random neutralization in this period of time and ion aggregate formation does not have to be considered.

E. Field of Present Investigations.

The present investigations are concerned with the effect of pressure (up to approximately 4000 bars) upon the induced conductance in hydrocarbon liquids. The hydrocarbons studied were n-pentane, n-hexane, n-octane, cyclopentane, methylcyclohexane and 2,2-dimethylbutane. Hexane and octane were investigated at three temperatures. All other studies were conducted at one temperature (30°C). Two dose rates were employed in each study.

In order to interpret the observed pressure dependence of the induced conductance the pressure dependence of the viscosity, density and dielectric constant of the hydrocarbon was required. The techniques used to obtain the pressure dependence of the latter variables are described together with the results obtained.

SECTION 11

E X P E R I M E N T A L

A. High Pressure Systems.

1. Pressure Production and Measurement.

Two high pressure systems of the same basic design were used. One was permanently installed in a radiation cave and used exclusively for the measurement of the effect of pressure upon radiation induced conductance. The second system was mounted on a mobile trolley and was used for the measurement of the effect of pressure upon the dielectric constant, viscosity and density of the various hydrocarbons investigated.

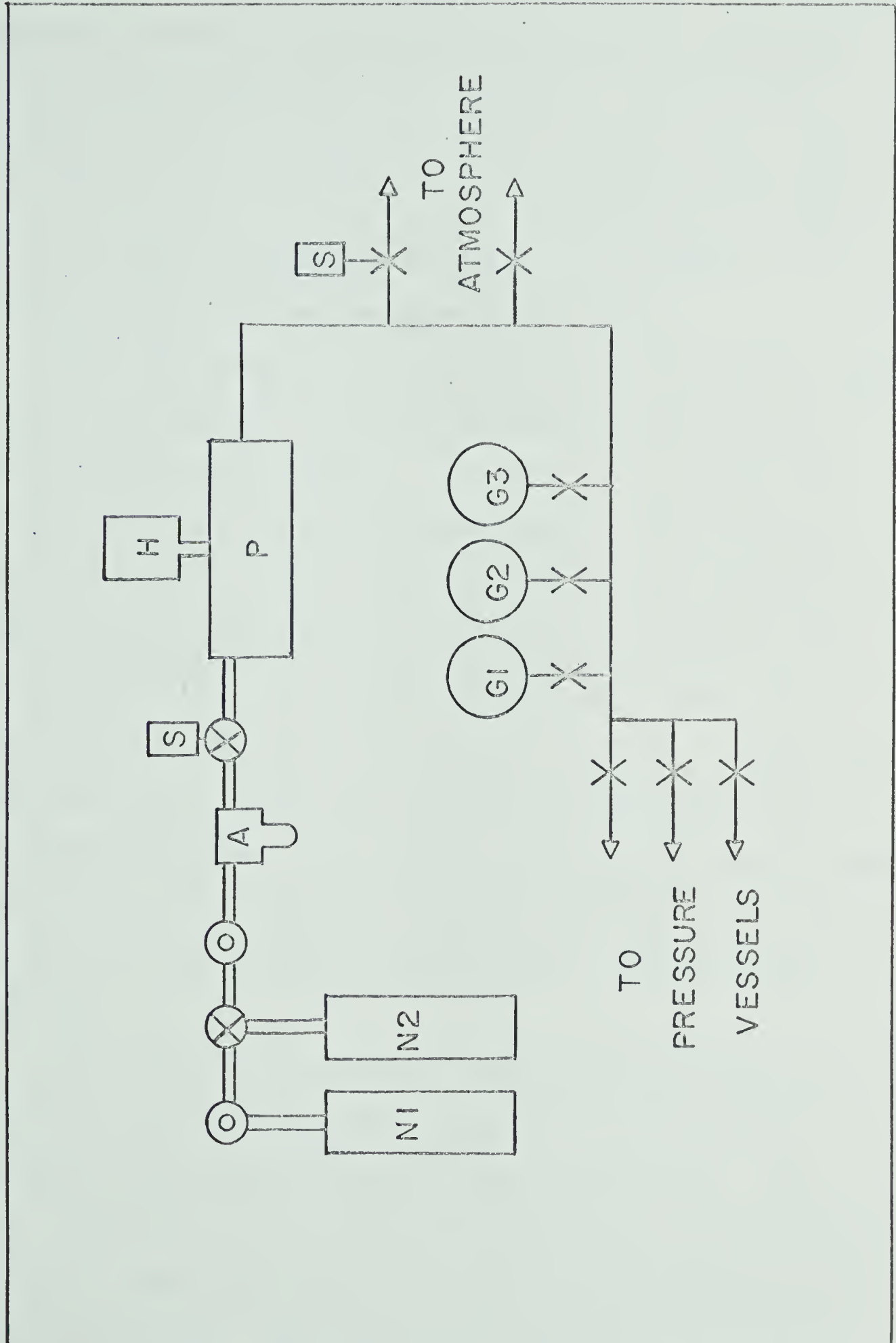
A schematic representation of the pressure producing apparatus is shown in Figure II-A-1. All components of the system, except for the actual pressure vessels and their auxiliary equipment, were obtained commercially.

Pressure was generated by a gas driven hydraulic pump supplied by Haskel Engineering and Supply Company, California (Type AO-602). These pumps are rated at a maximum output pressure of 75000 p.s.i. (5000 bars) for a maximum gas operating pressure of 150 p.s.i. Commercial grade nitrogen was supplied to the pump regulating valve at pressures between 20 and 150 p.s.i. from a ballast cylinder, which had previously been filled from a conventional compressed nitrogen cylinder. This procedure was

FIGURE II-A-1

HIGH PRESSURE PRODUCTION SYSTEM

N1	Nitrogen cylinder, 2000 p.s.i.
N2	Nitrogen cylinder, 150 p.s.i.
A	Filter and Moisture trap.
S	"Slo-Syn" synchronous motors. Type SS50/P3/RC.
H	Hydraulic fluid reservoir.
P	Haskel gas driven hydraulic pump. Type AO-602.
G1	4000 - 80000 p.s.i. Pressure gauge (Rough scale)
G2	0 - 15000 p.s.i. Pressure gauge (Fine scale)
G3	0-100000 p.s.i. Pressure gauge (Fine scale)
⊙	Conventional compressed gas cylinder valve and gauge.
⊗	Low pressure gas valves
x	High pressure valves.
—	High pressure tubing.
==	Iron tubing, one inch diameter.



adopted to prevent the accidental exposure of the pump to an excessive operating gas pressure. The pressure manifold, on the low pressure side of the pump, was constructed from one inch iron pipe. A combined filter and moisture trap of high flow capacity was included in the manifold just prior to the pump inlet valve.

The high pressure manifold was constructed from components supplied by the Superpressure Division of the American Instrument Company. The detailed construction of the components is given in the Superpressure Catalog Number 466 (1965). The pressure lines of the manifold were constructed from stainless steel tubing of internal diameter 0.063 ins, and external diameter 0.25 ins. All valves were of the non-rotating stem variety. Connections throughout the system were made with either straight or tee-shaped couplings and 0.25 ins high pressure union type connectors. All components are rated for use with a maximum hydraulic pressure of 100000 p.s.i. (approximately 7000 bars).

Two valves in the mobile system were controlled by "Slo-Syn" synchronous motors, supplied by the Superior Electrical and Supply Company, (Type SS50/P3/RC). The first motorised valve controlled the rate of flow of nitrogen to the pump and enabled the cycling speed of the pump to be controlled. The second motorised valve was used to

control the rate of release of hydraulic fluid during the release of the pressure.

Bayol 35 (formerly Bayol D), supplied by the Imperial Oil Company, was used as the hydraulic fluid. This product is a low viscosity deodourised kerosene oil.

The pressure in the manifold was measured with a variety of gauges, all of the Bourdon tube design. A Heise gauge (Heise Bourdon Tube Company, Conn.), calibrated in 100 p.s.i. divisions over the pressure range from zero (1 bar or 15 p.s.i. absolute) to 100000 p.s.i. (approximately 7000 bars) was primarily used to determine the pressure. An American Instrument Company gauge, calibrated from 4000 to 80000 p.s.i. in 2000 p.s.i. divisions, was used as a roughing gauge as the Heise gauge suffered violent oscillations if it was directly open to the system whilst the pressure was being increased. A third gauge, also supplied by the American Instrument Company, was used to cover the low pressure range from zero (1 bar or 15 p.s.i. absolute) to 15000 p.s.i. (1000 bars) and was calibrated in 100 p.s.i. divisions. The gauges were periodically returned to the manufacturers for recalibration.

Comparison of experimental results from various sources is tedious because of the use of different pressure units. Engineering data is almost exclusively reported using pounds per square inch as the pressure unit, other scientific

branches, however, use a variety of units.* The present results will be reported in terms of bars although the gauges were calibrated in pounds per square inch. The appropriate conversion factors for the more commonly used pressure units are listed in Table II-A-I.

(2) High Pressure Vessels.

The pressure vessels were manufactured by the Staff of the Chemistry Department Workshop. The design of such vessels is still somewhat arbitrary, because no reliable treatment of the rupture characteristics of thick wall cylinders under high internal pressure is available. Considerable experimental evidence indicates, however, that the maximum internal pressure that a vessel will withstand is far in excess of the normal tensile strength of its material (93).

The present vessels were constructed from Ultimo 4 steel (Atlas Steel Company, Ontario), a steel of high chromium and molybdenum content. The general features of the vessels are illustrated in Figure II-A-2. Three vessels were used, all of which had an internal diameter

*

In the System International d'Unites (SI Units), endorsed by the International Organization of Standardization, the unit of pressure is one newton per square metre (N/m^2). $1 \text{ bar} = 10^5 \text{ N/m}^2$ (97)

TABLE II-A-I

Conversion Factors for Various Pressure Units in

Common Use.

Unit	atmospheres	bars	kg/cm ²	p.s.i.
atmospheres	1	1.01325	1.0332	14.696
bars	0.98692	1	1.01971	14.504
kg/cm ²	0.96784	0.98067	1	14.223
p.s.i.	0.068046	0.68947	0.070307	1

FIGURE II-A-2

Section of High Pressure Vessel

not to scale

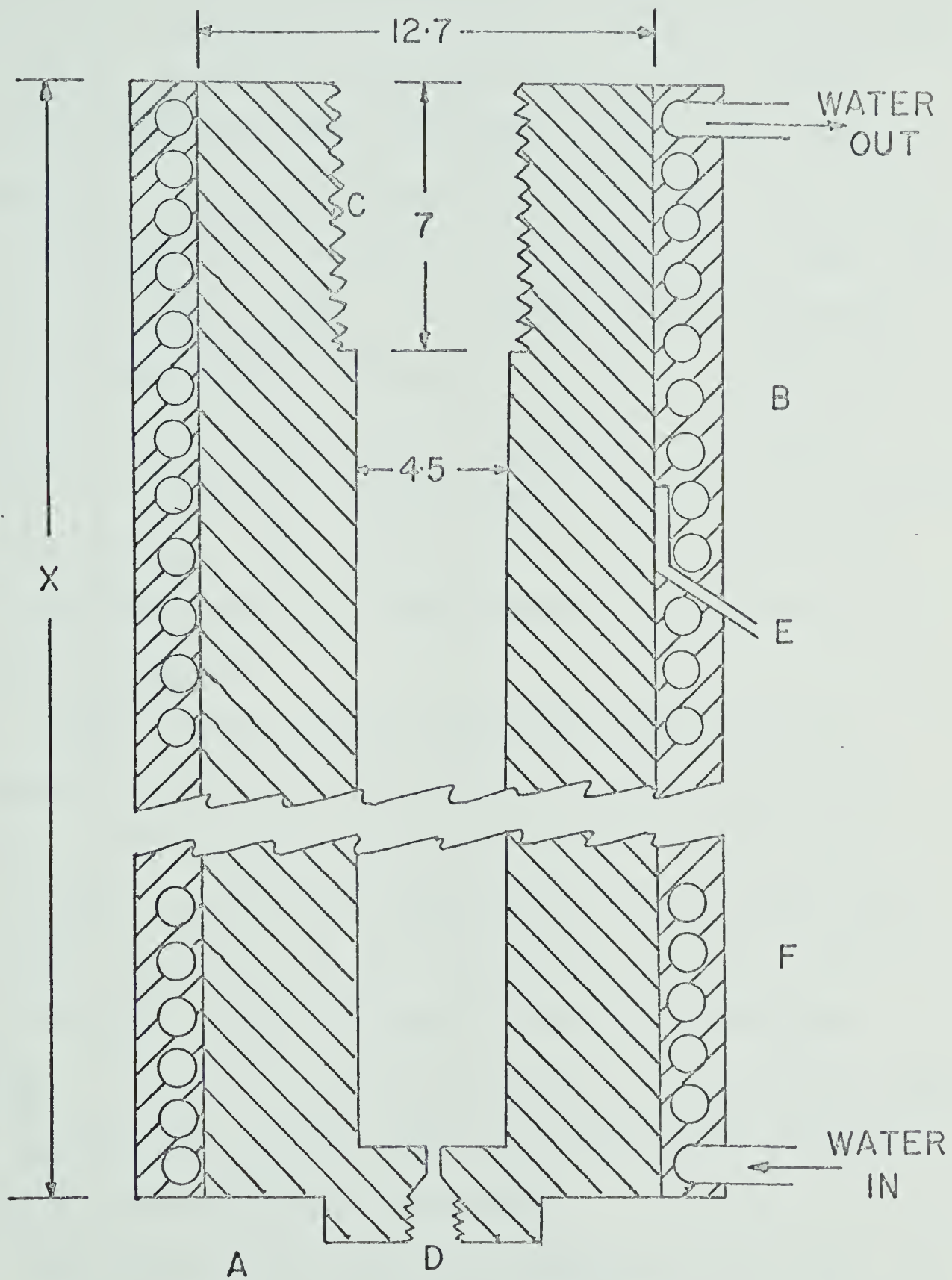
- A. Ultimo-4 steel pressure vessel
- B. Copper tubing (0.64 cm internal diameter)
- C. Closure thread (13 threads per inch)
- D. Hydraulic fluid entrance (0.25 ins. union-type connector. American Instrument Company)
- E. Thermocouple well
- F. Thermon T-85 heat transfer cement

All dimensions in cms

Three pressure vessels were used

Pressure vessel A and B $X = 32$ cm

Pressure vessel C $X = 50.8$ cm



of 4.5 cm and an external diameter of 12.7 cm. Two were identical in length, 32 cm, whilst the third was 50.8 cm in length. Pressure line connections to all vessels were made with American Instrument Company union type connectors. A square flange was milled onto the bottom of the vessels, and was used to reproducibly relocate the vessels in their holder. The pressure vessel mountings will be discussed in the relevant sections. After manufacture, the vessels were heat treated, the physical results of which will be mentioned in relation to pressure vessel closures. The interior bore of the vessels was finally honed such that the diameter was constant to within 0.002 ins.

Copper tubing (0.64 cm internal diameter) was wrapped around each of the pressure vessels such that about 0.3 cm separated each of the turns of the coil. The tubing was sealed to the surface of the vessel with a layer (approximately 1.3 cm thick) of Thermon T-85 heat transfer cement (Thermon Manufacturing Company, Texas). Prior to curing the cement, a thermocouple well, in the form of a narrow glass tube which went directly onto the vessel surface, was added.

The temperature within the pressure vessel was controlled by pumping water through the copper coil, using a Colora pumping bath (Colora Messtechnik GmbH, Lorch-Wurt). The temperature could be varied from approxi-

ately 2° to 80°C. To maintain temperatures below room temperature, the water in the bath was cooled by a Lanco portable bath cooler and by the addition of ice. The interior temperature of the pressure vessel equilibrated with the coil temperature in about 60 minutes, depending upon the extent of the temperature change. The temperature was measured with an iron-constantan thermocouple and at equilibrium varied by $\pm 0.5^{\circ}\text{C}$. To obtain less temperature variation within approximately 80 pounds of steel would require a far more sophisticated system.

(3) Pressure Vessel Closures.

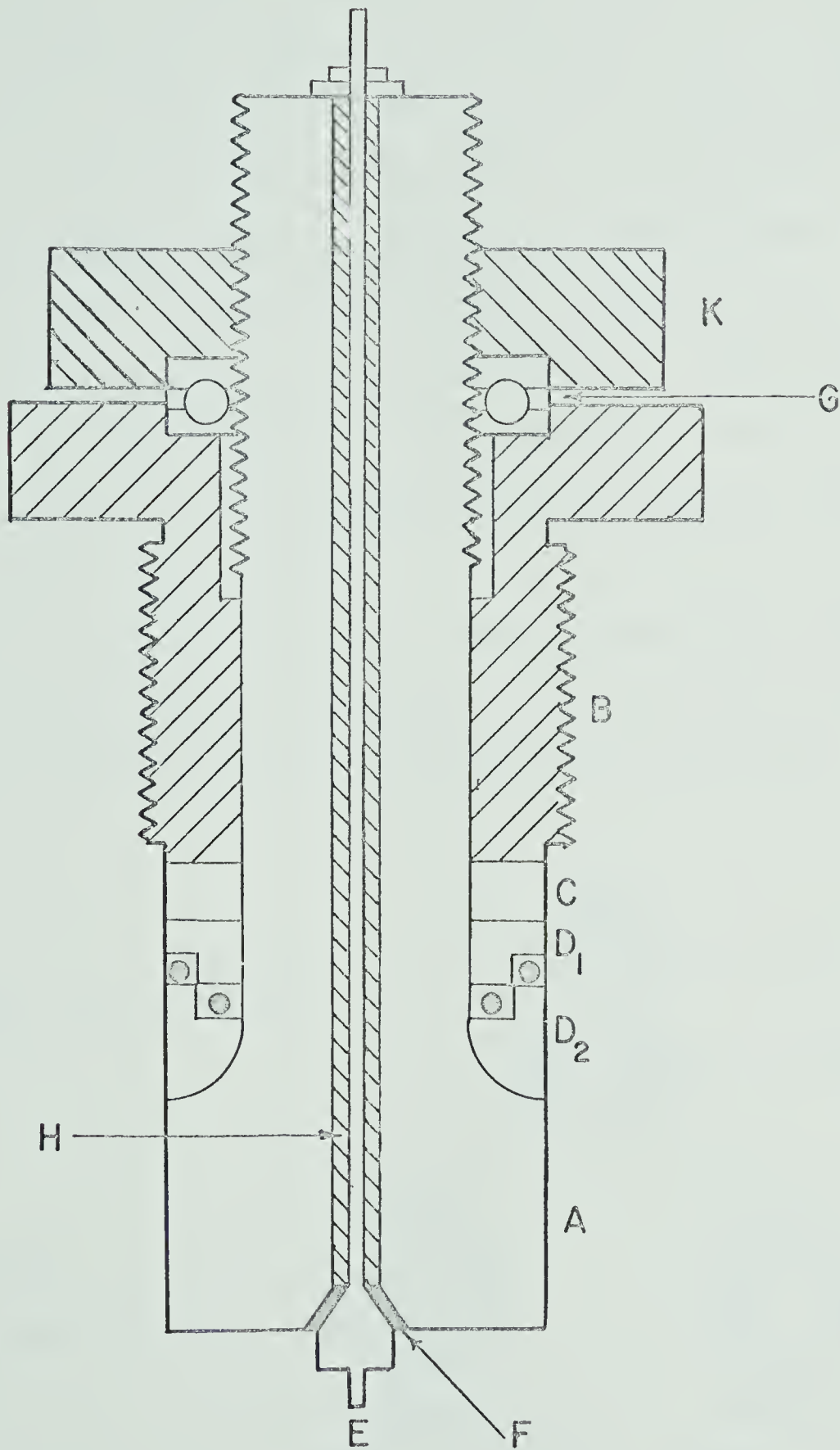
The closure of the high pressure vessels was accomplished using a modified Bridgman "unsupported area" design (93). The features of the closure are reproduced in Figure II-A-3 and, except for the use of Viton A "O" rings, are very similar to those of a closure used by Walling in his laboratory (112). Electrical connections are introduced into the vessel interior through the closure.

The piston and the nuts (A and B) were manufactured from the same material as the vessel. Two brass rings and one steel ring, the shapes of which are evident from the figure, were fitted onto the piston shaft. The brass rings fitted the inner bore of the pressure vessel with

FIGURE II-A-3

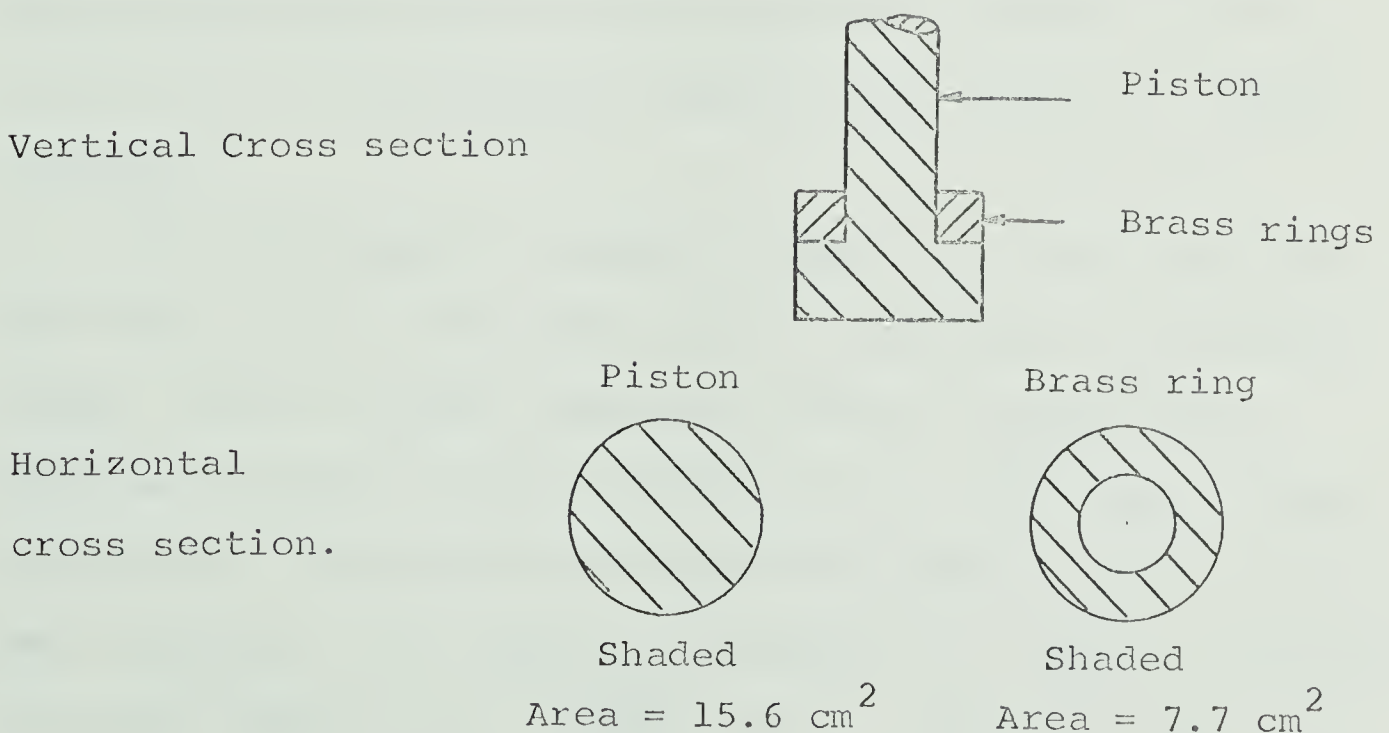
Section of Pressure Vessel Closure

- A. Pressure vessel piston. Ultimo 4 steel, 13 threads per inch on shaft.
 - B. Brass seal retaining nut, 12 threads per inch, Ultimo 4 steel.
 - C. Steel ring.
 - D₁D₂ Brass sealing rings
 - E. Self-sealing electrical connector (one of three shown in figure).
 - F. Teflon insulating cone and pressure seal.
 - G. Skefko thrust bearing.
 - H. Ceramic insulator.
 - K Piston extraction nut.
 - Viton A "O" rings.
-



a tolerance of about 0.005 ins. A similar clearance was allowed between the rings and the piston shaft. The steel ring prevents the brass rings from being extruded into the thread of the nut B prior to the spreading of the rings against the vessel bore and piston shaft. Two Viton "O" rings were placed in the recesses of the brass rings in the manner shown in the diagram. These "O" rings provide the initial seal, both against the bore of the vessel and against the piston shaft, and replace the more conventional rubber rings.

The closure operates by what Bridgman (93) called the "unsupported area principle". Consider the following oversimplified sketch of the piston and the brass rings.



The piston shaft is unsupported, apart from where it is in friction contact with the brass rings. The total force exerted by the fluid on the piston face is transferred to the brass ring. Since force is equal to the product of pressure and area, the pressure on the brass ring is greater than the pressure on the piston face. The pressure on the ring will exceed the pressure on the piston by a factor equivalent to the ratio of the area of the piston face to the area of the ring. In practice, this area ratio must be chosen with care, because if the pressure in the rings is too large the bursting pressure of the vessel may be exceeded. On the other hand, the only way the surface area of the ring can be increased is by decreasing the diameter of the hole in the ring. The piston shaft must be correspondingly reduced in diameter and if it becomes too thin it will pinch off under pressure.

In the present closures, a ratio of 2 to 1 was used for the area of the piston face to the area of the brass rings. Prior to heat treatment, Ultimo 4 steel has a tensile strength of about 140000 p.s.i. (9500 bars). After manufacture the piston and vessel was heat treated to Rockwell hardness C-39, which corresponds to a tensile strength of about 180000 p.s.i. (12000 bars). Using the above area ratio, a pressure of 135000 p.s.i. (9000 bars) would be

developed in the rings for the maximum internal pressure of 4500 bars used in the experiments. This is well within the limitations of the heat treated vessel. It is interesting to note, however, that a piston that was not heat treated after manufacture, showed a small amount of thinning of the shaft (pinch off) after each usage. The shaft contained three holes, spaced symmetrically around the shaft centre, through which electrical connections entered the pressure vessel (for clarity, only one is shown in Figure II-A-3). These holes further weaken the shaft.

The electrical connectors were obtained from the American Instrument Company are of a self-sealing cone design. The central conductor was insulated from the piston shaft with a ceramic tube. The breakdown voltage of the connector was increased to about 1000 volts by filling the air space with hydraulic fluid. A conical teflon washer provided both the electrical insulation and the pressure seal at the piston face. The conical washers required replacement after about three applications of pressure to 4500 bars. The method of connecting the outer terminal to the various electrical circuits used will be discussed in the appropriate section below.

(4) Experimental Procedure.

The closure was assembled and tested for electrical shorts prior to insertion within the pressure vessel. In

most experiments, air was bled from the vessel through one of the electrical connectors whilst the hydraulic fluid was gently pumped into the pressure vessel. The electrical connectors were then finally tightened at the piston head. The nut K was then tightened against the thrust bearing which resulted in the "O" rings being spread against the vessel bore and against the piston shaft. The pressure was then increased to the desired value. Occasionally, the brass rings would fail to seal and this was generally due to contamination of the brass surfaces with metal particles. The seal could always be attained by applying sufficient torque to the nut A, which results in the manual spreading of the brass rings.

After the release of pressure, difficulty was often experienced in removing the closure from the pressure vessel. The nuts A and B were first backed up the piston shaft. Tightening of the nut A against the thrust bearing then usually resulted in the extraction of the piston, but extreme torque was often required. In initial experiments the piston shaft had 16 threads per inch, which tended to strip under severe torque, and 13 threads per inch was found to be more satisfactory. The extraction process was facilitated by a liberal coating of Kopr-Kote on all threads. Kopr-Kote is an anti-seize compound that consists of finely divided

copper suspended in a penetrating oil. It was supplied by Jet Lube of Canada, Ltd. Occasionally the seal refused to break and hydraulic pressure was then applied to the vessel interior with both of the nuts A and B backed up the piston shaft. Pressures of 1000 bars were often reached before the seal finally broke, and the shock of sudden decompression was found to be extremely detrimental to any apparatus assembled within the pressure vessel.

The brass rings could only be removed from the piston shaft by a hand press and, in cases where the slightest pinch off had occurred, removal of the rings was extremely difficult. The inner and outer diameters of the rings had to be returned to size, by turning on a lathe, after each application of pressure, which resulted in the gradual thinning of the rings. Approximately twenty runs per set of rings was accomplished. The steel back-up ring underwent little distortion and rarely required returning to size. The Viton A "O" rings were replaced each run.

(B) High Vacuum System.

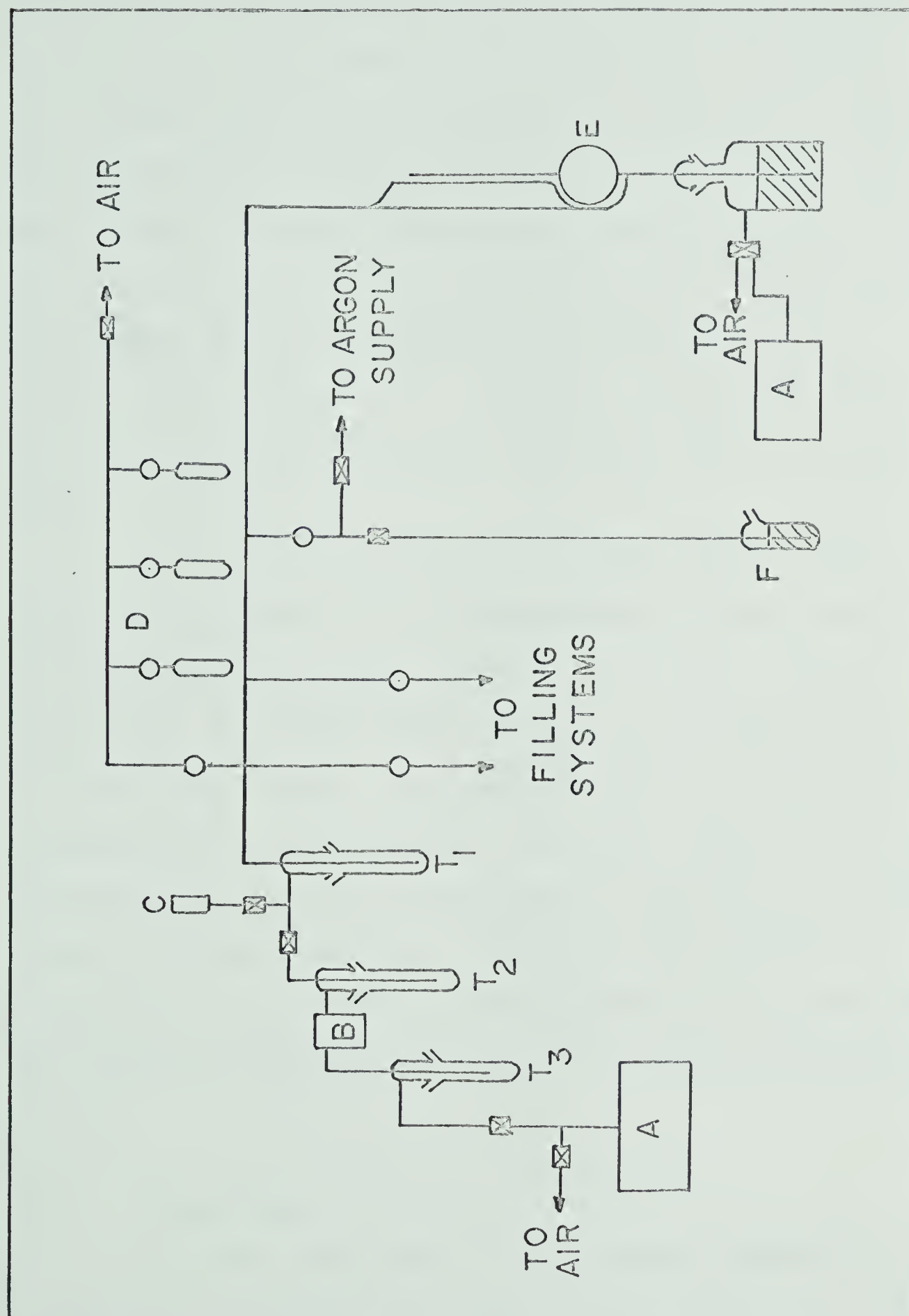
Several experimental procedures required the use of a high vacuum system. The techniques employed will be discussed in the relevant section and only a brief description of the high vacuum system will be necessary here.

The basic layout of the system is illustrated in Figure II-B-1. The apparatus is quite conventional in

FIGURE II-B-1

High Vacuum System

- A. Welch Duo-seal rotary Oil Pump.
- B. Glass mercury diffusion pump
- C. Pirani tube
- D. Storage manifold and bulbs (approx. 200 mls).
- E. McCleod gauge system
- F. Mercury exhaust valve
- T_{1,2,3} Liquid nitrogen traps
- O Greaseless stopcocks (Republic or Springham)
- ☒ Ground glass high vacuum stopcocks
- \\ 45/50 ground glass joints



construction and numerous detailed descriptions of such systems are to be found in the literature. Evacuation of the main manifold was accomplished with an all glass mercury diffusion pump in conjunction with a Welch Duo-Seal rotary oil pump. The pressure within the manifolds and associated lines was determined with a Pirani gauge. The Pirani gauge was periodically calibrated with a McCleod gauge. The latter gauge was constructed from a mercury calibrated capillary tube and a water calibrated bulb.

In all parts of the system where vapour from the sample came into contact with stopcocks, either Republic or Springham greaseless stopcocks were used. Unless specified, all other stopcocks were of the high vacuum ground glass variety. Dow Corning high vacuum silicone grease was used on all glass stopcocks. Facilities for the introduction of an atmosphere of argon into the apparatus were also available. Argon was supplied from a compressed gas cylinder and the system was protected from an excessive pressure of argon by a mercury filled exhaust valve.

(C) Materials.

The more important of the numerous materials used are listed, together with their source, in Table II-C-I.

TABLE II-C-I

<u>Compound</u>	<u>Source</u>
n-Hexane	Fisher Scientific. Spectro- grade
Benzene	Fisher Scientific. Spectro- grade
Dodecane	Eastman Organic Chemicals
Tetradecane	Eastman Organic Chemicals
Octadecane	Matheson, Coleman and Bell
Diethyl ether	Mallinckrodt. Analytical reagent. Eastman Organic Chemicals, Spectroscopic Grade.
Sulphuric acid	Baker and Adamson, Reagent grade.
Ferrous ammonium sulphate	British Drug Houses.
Sodium hydroxide.	British Drug Houses, Analar grade
Lithium aluminium hydride	Metal Hydrides Incorporated
Carbon tetrachloride	Eastman Organic Chemicals. Spectroscopic grade
Silicone Oils	Dow Corning
Viscometric Standard Oils	Cannon Instrument Company

The hydrocarbons used for the conductance experiments and as primary standards in various calibration procedures, are tabulated in Table II-C-II. The purities and the most probable impurities listed, are those indicated by the manufacturer. In addition to the listed impurities, however, all the saturated hydrocarbons were found to contain olefins, which presumably resulted from oxidation during the shelf life of the sample. The hydrocarbons were purified by removal of the olefin with sulphuric acid. The hydrocarbon (400 ml) was shaken with concentrated sulphuric acid (150 ml) for a period of at least 24 hours. The acid was changed at least three times until no yellow discolouration of fresh acid occurred. The hydrocarbon was then washed with three changes of 5% sodium hydroxide (150 ml) followed by many successive washings with doubly distilled water. Preliminary drying was accomplished with anhydrous magnesium sulphate. The hydrocarbon was finally distilled from lithium aluminium hydride through a 24 inch Vigreux column filled with glass helices. For high boiling hydrocarbons, external heating of the column was necessary. The first and last 10% of the distillate was discarded. The purified sample was then distilled directly into the high vacuum system, either for immediate use or for storage for a limited period of time. Samples that were stored were kept in the dark.

TABLE II-C-II

Hydrocarbon Purity and most probable impurities

<u>Compound</u>	<u>Purity Mole %</u>	<u>Most Probable Impurity</u>
n-Pentane	99.90	iso-pentane
n-Hexane	99.95	methylcyclopentane
n-Heptane	99.92	3-ethylpentane, cis-1,2-dimethylcyclopentene
n-Octane	99.88	n-paraffins and cyclo-paraffins
n-Decane	99.85	n-dodecane plus one unidentified
Cyclopentane	99.99	cyclopentene, 2,2-dimethylbutane
Cyclohexane	99.99	2,2-dimethylpentane
Methylcyclohexane	99.82	toluene
Benzene	99.91	toluene
2,2-Dimethylbutane	99.97	2,3-dimethylbutane 2-methylpentane.

All supplied by Phillips Petroleum Company Research Grade.

Benzene was purified by repeated partial recrystallisation, the supernatant liquid being discarded each time. Carbon tetrachloride and diethyl ether were used directly as supplied, a fresh can of ether being opened for each experiment.

All viscometric standard oils and silicone oils were used directly as supplied.

(D) Radiation Sources and Dosimetry.

(1) Radiation Sources

All radiation induced conductance measurements were performed in a radiation cave and utilised the γ -emission from the decay of ^{60}Co . Two sources of different strength were used. The first contained about 300 curies whilst the second, which was used for the results reported in this thesis, contained about 5500 curies.

The radiation cave adjoined the laboratory in such a manner that the source could be removed from its lead and steel container by the manual operation of a push-rod mechanism situated in the outer laboratory. The source travelled horizontally along a track and could be reproducibly placed at any desired position on the track. Only two positions were used in the present work and they will henceforth be referred to as track positions 1 and 2. Position 1 was the closest to the pressure vessel, the latter being mounted in a solid wall bracket adjacent to

the source track.

(2) Dosimetry.

The radiation beam intensity within the pressure vessel was determined using the Fricke chemical dosimeter, which is based upon the radiolytic oxidation of ferrous ion in acidic aqueous solution. The Fricke solution contained 1 mM ferrous ammonium sulphate, 1 mM sodium chloride and 0.8 N sulphuric acid. Triply distilled water was used in the preparation of the solution.

The concentration of ferric ion after radiation exposure was monitored using spectrophotometric techniques. A Beckman DU 2400 single beam spectrophotometer was used. Ferric ion exhibits an absorption maximum at 340 mμ, at which wave length the absorption of ferrous ion is negligible.

The dose rate in Fricke solution may be calculated from the relation

$$I = \frac{\text{Absorbance produced per second} \times N_0}{\epsilon \times [1 + 0.007 (t - 25)] \times 15.5 \times 10 \times D}$$

where I is the dose rate in eV/ml sec, N_0 is Avogadro's number, D is the light path length in the spectrophotometer cell (1 cm), ϵ is the extinction coefficient of the ferric ion (2201/molar cm at 25°C) and t is the temperature (°C) at which the absorbance was measured. Correction for the large temperature dependence of the ex-

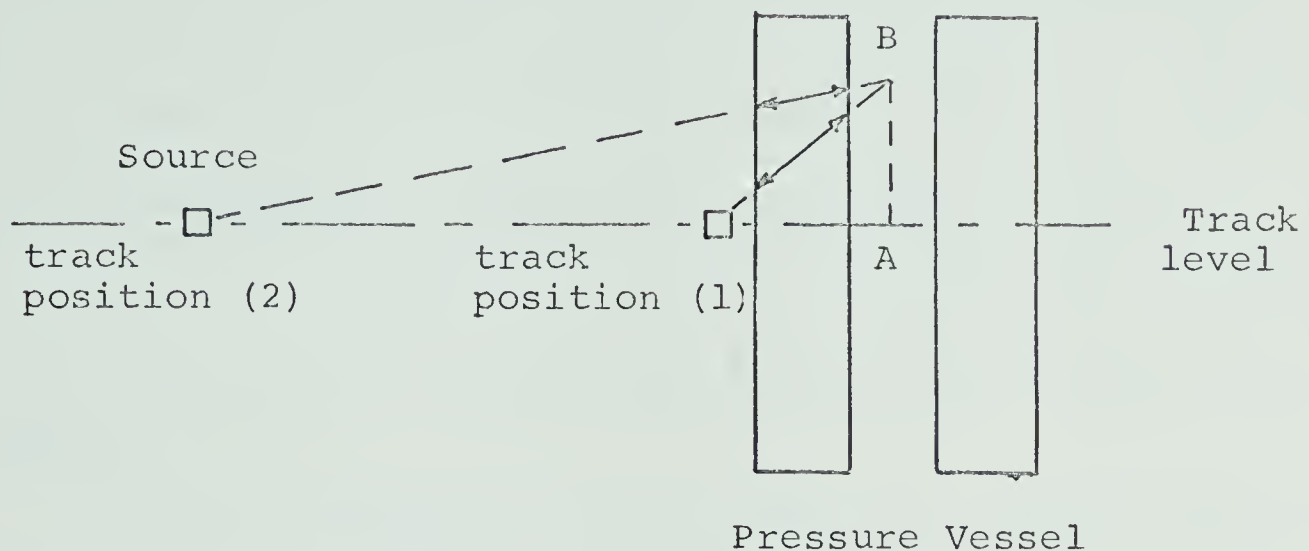
tinction coefficient (0.7% per centigrade degree between 20 and 30°C) was made by the factor $[1 + 0.007(t - 25)]$. The G value for ferric ion was taken as 15.5 for ^{60}Co γ -rays (113). However meticulously the solution was prepared, absorbance at 304 m μ was always present prior to exposure to radiation. The final absorbances were corrected for the blank absorbance.

The dose rate measured with Fricke solution was corrected for the variation in electron density when applied to other materials. The electron density of Fricke solution is 0.566 electron mole/ml.

The dose rate, expressed in eV/ml sec is not independent of pressure because the density of the hydrocarbons increases as the pressure is increased. Dose rate values obtained at atmospheric pressure were corrected for use at other pressures using the densities determined from the pressure-volume-temperature measurements.

The dose rate within the pressure vessel is dependent upon the path length in air and steel that the radiation beam has to traverse before reaching the interior of the vessel. The beam intensity of ^{60}Co γ -rays is attenuated by a factor of one hundred by 15 cm of iron (114). The following sketch shows the position of

the source with respect to the pressure vessel.



The maximum dose rate within the vessel, at any track position, is obtained at the point A, where A is on the same level as the source. The path length in steel is then at a minimum (4.2 cm in the present vessels). On rising above (or falling below) the level of the source (e.g. point B in the sketch), the path length in steel is increased and the dose rate reduced. For the same vertical rise within the pressure vessel, the change in the steel path length is less when the source is in track position 2 than when it is in track position 1. The variation in dose rate within the vessel is less when the source is at position 2. However, when the source is at track position 2 the total distance between the source and vessel has been increased and the beam intensity reaching the vessel has been reduced (inverse square law).

The volume of primary interest within the vessels is that contained between the electrodes of the conductance cells. In initial experiments the dosimeter solution was placed as close as possible to this position. To avoid the necessity of placing the conductance cell at exactly the same position for each experiment, the distribution of the dose rate within the pressure vessel was measured.

Typical absorbance versus radiation exposure time curves for four positions within pressure vessel A are illustrated in Figure II-D-1. The calculated dose rates for both track positions 1 and 2 are given in Table II-D-I. The values correspond to the average absorbance of 5 ml of Fricke solution. The height of 5 ml of solution in the cell is 1.9 cm. The dose rate distribution, relative to a point 14.4 cm from the top of the vessel, is illustrated in Figure II-D-2. Table II-D-II also contains the dose rate obtained for a single position in pressure vessel B with both the 300 and 5500 curie sources.

The dose rates were corrected for the natural decay of the ^{60}Co using the decay law

$$I_t = I_o \exp(-\gamma t)$$

where γ was taken as $1.09 \times 10^{-2} \text{ month}^{-1}$ and I_t corresponds

FIGURE II-D-1

Absorbance Versus Radiation Exposure Time Curves

Pressure vessel A. 5 ml samples of Fricke solution

Track position 1.

Curve	Distance from top of vessel
0	14.4 cm
Δ	17.2 cm
O	18.6 cm
A	19.8 cm

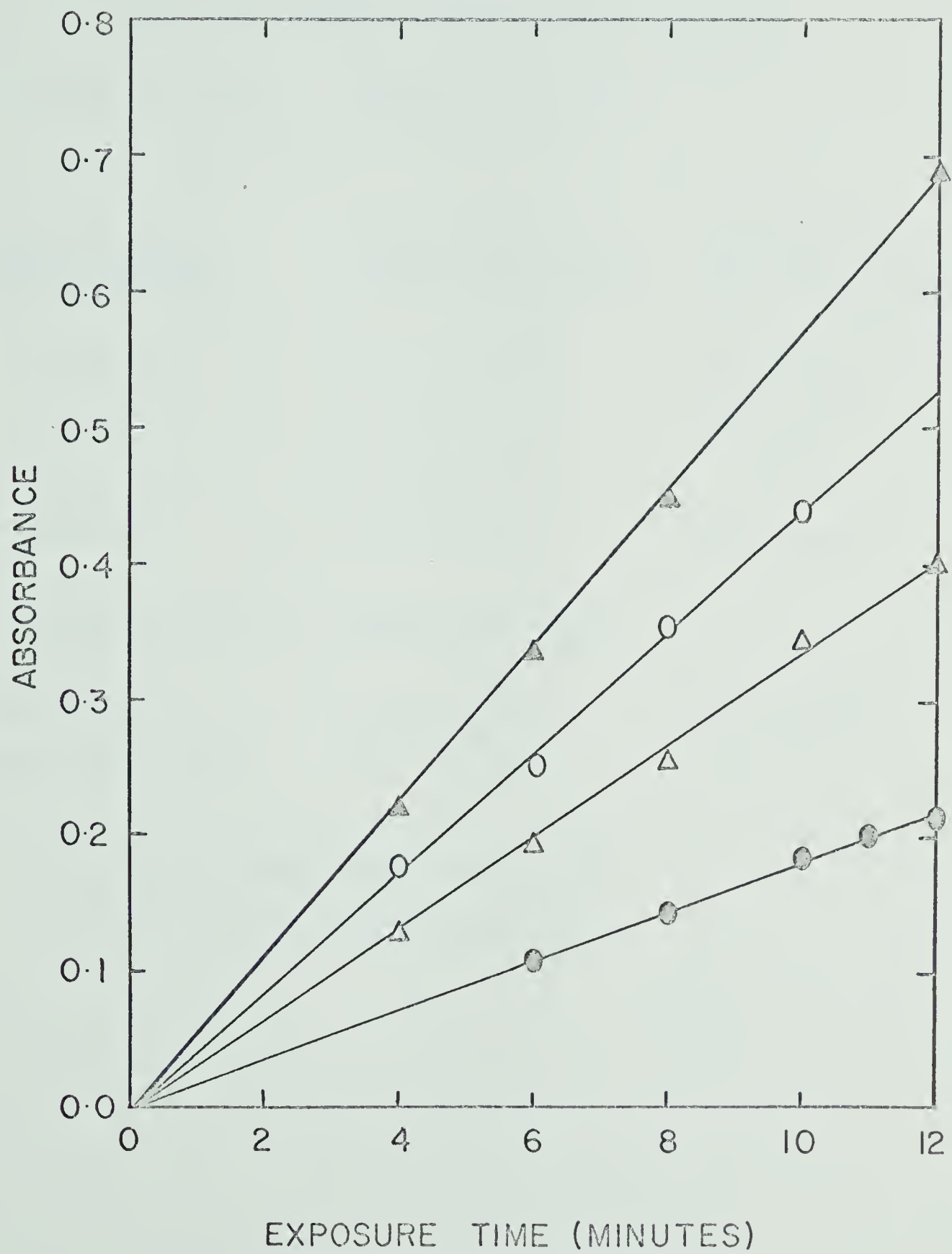


TABLE II-D-I

Dose Rates Within the Pressure Vessels

Pressure vessel A December 12, 1967

<u>Distance from top of vessel</u>	<u>Track Position 1 eV/ml sec Fricke</u>	<u>Track Position 2 eV/ml sec Fricke</u>
14.4 cm	0.54×10^{15}	2.0×10^{14}
17.2 cm	0.90×10^{15}	2.4×10^{14}
18.6 cm	1.29×10^{15}	-----
19.8 cm	1.73×10^{15}	2.7×10^{14}

Pressure Vessel B August 28, 1967

One position	0.94×10^{15}	2.3×10^{14}
Same Position ^a	4.2×10^{13}	-----

^a 300 Curie source September 7, 1965

All other values 5500 curie source.

FIGURE II-D-2

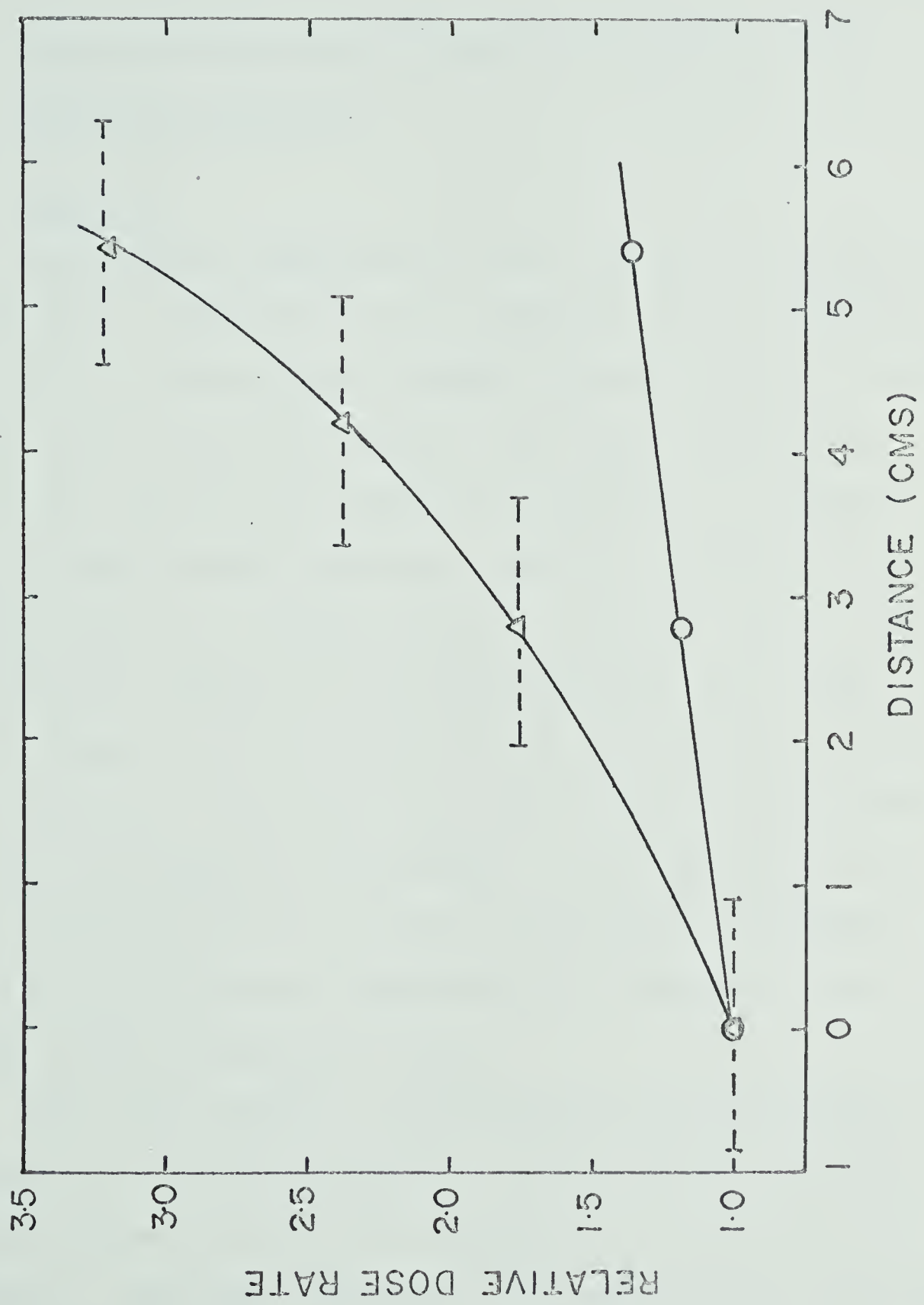
Dose Rate Distribution. Pressure Vessel A

Δ Track Position 1.

O Track Position 2.

Zero on the distance axis corresponds to a point 14.4 cm from the top of the pressure vessel. The distribution covers about 5.5 cm BELOW this point (see Figure II-A-2 and II-D-1)

----- Δ ----- Represents the distance over
which Δ is the average value.



to the dose rate at time t in months after the original determination I_0 .

(E) Determination of the Pressure Dependence of the Dielectric Constant.

(1) Apparatus

The pressure dependence of the dielectric constant of saturated hydrocarbons has received little attention compared to the numerous studies reported on polar liquids. Hexane (115, 116) and heptane (116) were studied in 1925 but only up to a pressure of 800 bars. Danforth (117) measured the dielectric constant of pentane up to 12000 bars in a general study of several liquids. The dielectric constants of the hydrocarbons of interest in the present study were obtained by determining the capacitance of a condenser (hereafter termed the dielectric cell) as a function of pressure. The dielectric cell was calibrated with a series of dielectric standards. The relation between capacitance and dielectric constant will be discussed later.

The basic design of the dielectric cell employed is reproduced in Figure II-E-I. Several cells were used, which differed only in the dimensions of the platinum plates. The plate dimensions for each cell are recorded in Table II-E-I.

FIGURE II-E-I

Dielectric Constant Cell and Assembly
within the Pressure Vessel

- A. Teflon cylindrical cell holder.
- B. Teflon piston
- C. Pressure vessel closure piston
- D. Stainless steel and teflon cell holder
- E. Supramica Plug
- F. Platinum electrodes (0.25 mm thick)
- G. Teflon cap over electrodes

For dielectric cell plate dimensions see
Table II-E-1.

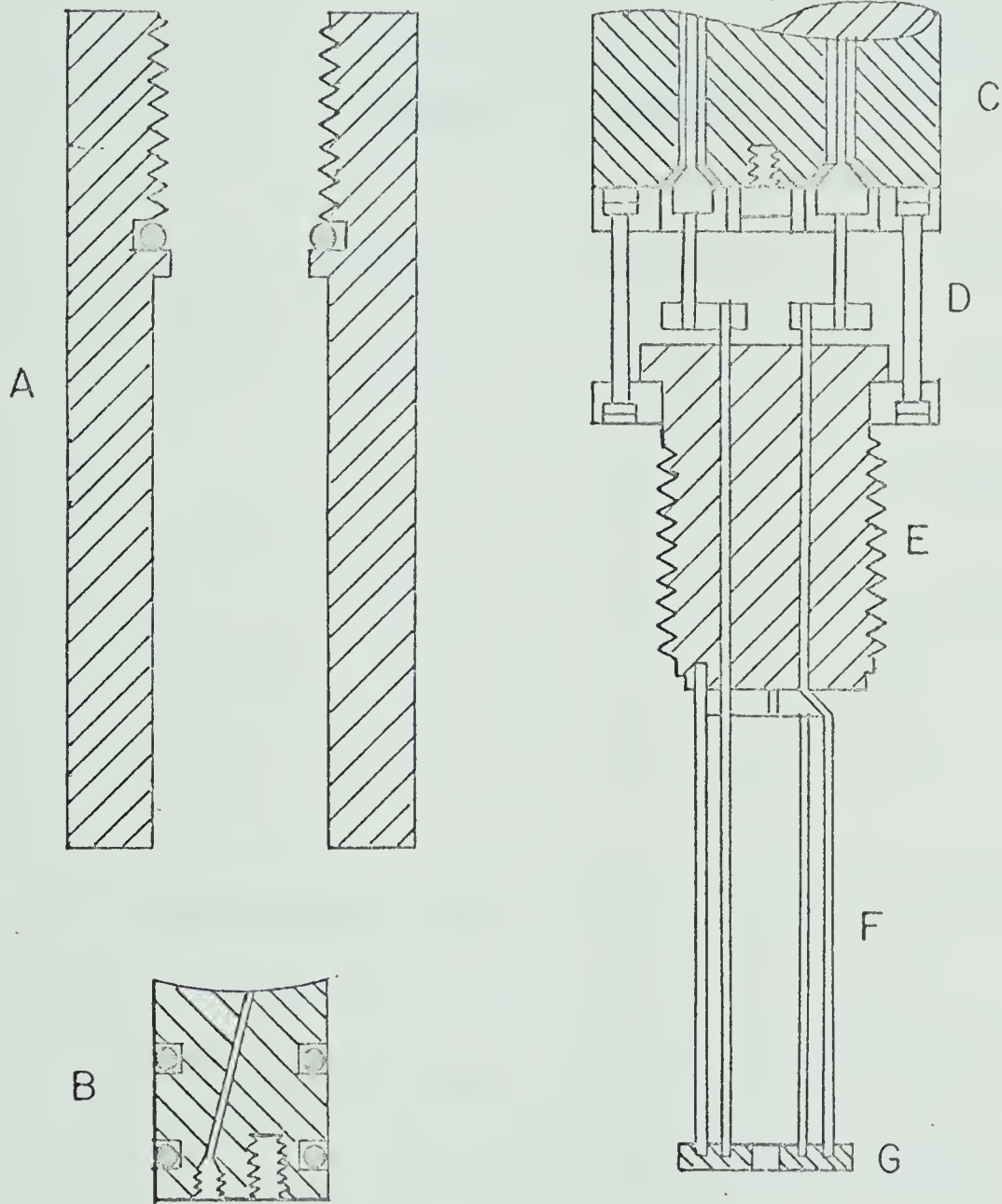


TABLE II-E-I

DIELECTRIC CELLS

<u>Cell</u>	Plate Diameter		<u>Plate Length</u>
	<u>Outer</u>	<u>Inner</u> ^a ^b	
P1	15.4	12.9	44.0
P2	16.1	13.1	40.3
P3	14.9	2.1	38.5
P4	15.5	5.0	40.0
	12.5	2.0	

All dimensions in mm. Plates 0.25 mm platinum

Cell P4 has four plates

^a

The internal diameter of the outer plate.

^b

The external diameter of the inner plate.

The sample was separated from the hydraulic fluid by a teflon cylinder (A) into which a movable teflon piston (B) fitted. The piston, by moving within the cylinder bore, allowed the pressure in the hydraulic fluid to be transmitted to the sample. The piston and cylinder are similar in design to those used by Jamieson (118) in a cell employed to determine the effect of pressure upon ionic conductance. Hydraulic fluid was prevented from leaking past the piston and into the sample by two Viton A "O" rings. The initial clearance between the piston and the cylinder bore was 0.002 ins. Care must be taken to ensure that the piston is not oversize because the cylinder is distorted immediately the pressure is increased, resulting in distortion of the platinum plates.

The piston contains an aperture by which air bubbles and excess sample were removed during the filling procedure. The aperture (0.06 ins diameter) entered the cell at the centre of the inner curved surface of the piston and was sealed at the outer surface by a small "O" ring and machine screw. The compressibility of teflon is greater than that of steel so the aperture closure is unlikely to leak as the pressure is increased. The piston also contained a threaded hole into which a bolt was inserted at the end of an experiment so that

the piston could be extracted from the cylinder.

The actual capacitance cell was assembled on a Supramica 500 ceramoplastic plug which screwed into the threaded end of the teflon cylinder. Supramica 500 cermoplastic, supplied by the Mycalex Corporation of America, is a machinable synthetic mica of high compressive strength. An "O" ring placed at the bottom of the thread prevented the hydraulic liquid from leaking past the plug. Platinum plates, 0.25 mm in thickness and cylindrical in shape, were mounted above the inner face of the plug on platinum supports. Electrical connections through the plug were made with 1 mm diameter platinum wire. The wire was sealed to the supramica with Armstrong epoxy resin cement. The seals were cured at 80°C for several days. Cured cement seals that were in contact with hexane and octane for about one year showed no visible deterioration and the dielectric constant of a sample of hexane in contact with the cement for four months was unaltered.

The complete cell assembly was connected to the face of the pressure vessel piston, using a steel and teflon support. The support was designed to allow the cell to be reproducibly placed on the piston face. Electrical connections, between the platinum contacts on the supramica plug and the central conductor of the leads through

the pressure vessel piston, were made with brass sleeves containing screw contacts (see Figure II-E-1).

A General Radio Impedance Bridge (Model 1608-A) was used to determine the total capacitance of the system. The bridge was placed directly above the pressure vessel in an inverted position so that the connecting cable could be as short as possible. Connection to the binding posts of the bridge were made with about 12 cm of coaxial cable, using silver plated BNC to banana plug adaptors. All capacitance values were determined at 1 kilocycle. The bridge was calibrated with an accuracy of ± 0.02 pf. The capacitance was always measured with the outer plate of the dielectric cell connected to the low potential terminal of the bridge.

(2) Experimental Procedure.

The cells were cleaned prior to use by washing in the hydrocarbon under investigation. The use of acid on supramica was found to be detrimental to the ceramic. Samples were not degassed for dielectric constant determinations. The purified sample (Section II-c) was poured into the cell and the piston inserted. Excess sample and air were removed through the piston aperture, the piston being forced into the cylinder bore until both "O" rings were in contact with the bore. The aperture was then closed and the cell assembled within the pressure vessel.

At least one hour was allowed for the system to attain thermal equilibrium. All measurements were taken at 30°C. Capacitance readings were taken both on the pressure increasing and pressure decreasing cycles. After each pressure change the system was allowed to sit at the new pressure for 20 minutes before measuring the capacitance. In cases where the atmospheric pressure values were identical, before and after the application of pressure, the cycle was repeated. If the atmospheric pressure values had altered the cell was recalibrated prior to the investigation of a second sample.

(3) Capacitance Calibration, Dielectric Constant Determination and Corrections.

The capacitance C_L of a dielectric cell when filled with a liquid, is related to the dielectric constant ϵ of the liquid by the equation

$$C_L = \epsilon \times C_V$$

where C_V is the capacitance of the same cell fitted with air. The above equation requires that the measured capacitances are those of an "ideal" dielectric cell, an "ideal" cell being one in which the measured capacitance arises entirely from the volume of dielectric between the cell plates. In most practical applications it is impossible to divorce the capacitance of the connections

and lines, joining the cell to the measuring circuit, from the actual cell capacitance. These extraneous contributions to the measured capacitance are large in the present investigations because of the necessity of using long leads and numerous connections to introduce the measuring circuit into the pressure vessel interior. The dielectric constant of a sample may still be obtained if the cell is calibrated with a standard of known dielectric constant. Provided the extraneous capacitances are constant, the unknown dielectric constant may be calculated from the relation

$$\frac{C_S - C_A}{C_L - C_A} = \frac{\epsilon_S - 1}{\epsilon_L - 1}$$

where C_S and C_L are the capacitances of the cell when filled with the standard and the unknown, respectively, C_A is the capacitance of the cell filled with air, and ϵ_S and ϵ_L are the dielectric constants of the standard and unknown. An alternative procedure is to determine the total capacitance of the complete assembly as a function of the dielectric constant of the liquid in the cell. The dielectric constant of the unknown is then determined by direct reference to the calibration. This procedure was adopted in these investigations.

The dielectric constants of the standards used for

calibration, together with the atmospheric pressure values for all the hydrocarbons investigated, are listed in Table II-E-II. A typical calibration plot for the cell P2 is shown in Figure II-E-2.

Corrections to the extraneous capacitance, arising when the pressure is increased, are small. It was established by experiment that the capacitance of the cable (exterior to the pressure vessel) and the pressure vessel closure piston was independent of the pressure within the vessel. A small pressure dependent contribution to the total capacitance arises where the connections pass through the hydraulic fluid. In a determination of the capacitance of the apparatus with the cell removed from the vessel but with the connections intact, the capacitance changed by less than 0.02 pf. on increasing the pressure to 4500 bars. The capacitance of the leads through the supramica plug could not be determined without removing the plates from the cell, however; it was assumed to be independent of pressure because the compressibility of supramica is small. The actual compressibility of supramica is not available but, on the assumption that it is similar to that of natural micas which have a compressibility about two orders of magnitude smaller than liquids (119), it may be neglected. A similar conclusion has been reached by other authors (109).

TABLE II-E-II

Dielectric Constants of Standards and Hydrocarbons

Compound	Dielectric Constant ϵ	Temperature °C	$\alpha \times 10^2$
n-Pentane	1.828	20.3	0.160
n-Hexane	1.880	25.0	0.155
n-Heptane ^b	1.924	20.0	0.160
n-Octane ^c	1.96 (0)	20.0	0.130
Cyclohexane	2.023	20.0	0.160
Methylcyclohexane ^e	2.020	20.0	---
Cyclopentane	1.977	25.0	---
Benzene ^d	2.274	25.0	0.200
2,2 Dimethylbutane ^f	1.866	25.0	---
Carbon tetrachloride ^{b,d}	2.239	20.0	0.190
Diethyl ether ^h	4.335	20.0	2.0

$$\alpha = d\epsilon/dt$$

b. W. M. Heston and C. P. Smythe, J. Am. Chem. Soc. 72, 99, (1950).

c. R. W. Dornte and C. P. Smythe, J. Am. Chem. Soc. 52, 3546, (1930).

d. Recommended dielectric constant standards.

e. F. H. Muller, Physik. Z., 38, 283, (1937).

f. Calculated from refractive index.

h. J. Clay, A. J. Dekker and J. Hennelrijk, Physica, 10, 768, (1943).

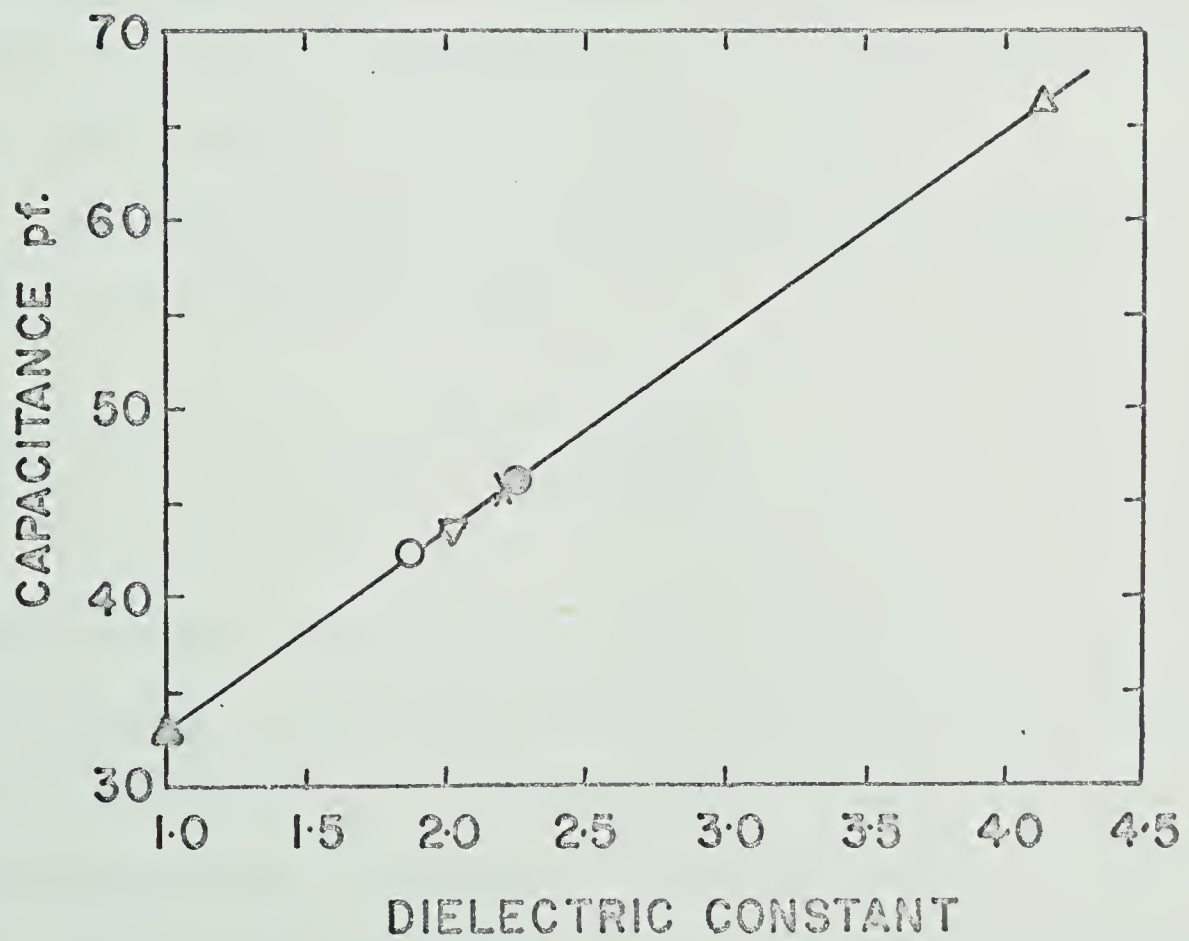
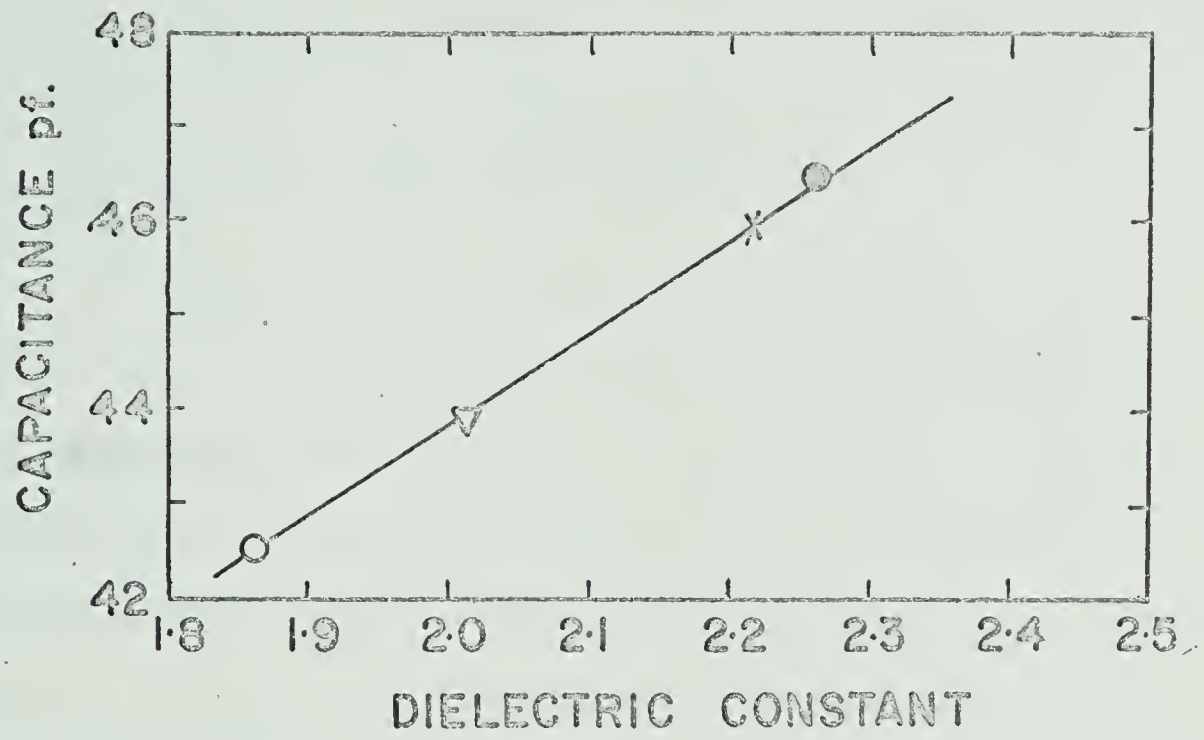
Other values taken from Timmermans "Physical-Chemical Constants of Pure Organic Compounds". Elsevier Publishing Co., New York, 1950.

FIGURE II-E-2

Calibration Dielectric Cell. P2 at 30°C

Total system capacitance against dielectric
constant of sample in cell

▲	Air
O	n-hexane
∇	cyclohexane
X	carbon tetrachloride
○	benzene
Δ	diethyl ether



The capacitance of the actual cell will change under pressure because of changes in the plate dimensions as they are compressed. The volume compressibility β of platinum may be calculated from the relation (93)

$$\beta = a \times 10^{-7} - 2 \times b \times 10^{-12} \times p$$

where a and b are constants with the values 3.60 and 1.8 respectively at 30°C, and p is the pressure in kg/cm^2 units. A value of 1.5×10^{-7} is obtained for the linear compressibility of platinum at 4000 kg/cm^2 (4088 bars) if it is assumed to be one third of the volume compressibility. For a typical cell used in the present determinations this would result in about 0.06% decrease in the plate length and the same percentage reduction in the thickness.

The capacitance of a cylindrical plate capacitor is given by the relation (120)

$$C = \frac{L}{2 \ln \frac{R_2}{R_1}}$$

where C is the capacitance in e.s.u. units (cm), R_1 is the outer radius of the inner plate, R_2 is the inner radius of the outer plate and L is the length of each plate. A decrease of plate thickness of 0.06% results, in the present cells, in an increase in R_2 of 0.002% and a similar percentage decrease in R_1 . The change in the radii of the

plates is therefore negligible. The plate length is reduced by 0.06% and C is reduced by approximately the same amount.

Whereas the cell capacitance decreases slightly because of decreasing plate length with increasing pressure, the extraneous contributions to the total measured capacitance increases with increasing pressure. The two corrections tend to cancel each other so the capacitance values were used as obtained.

(F) Determination of the Pressure Dependence of Density

(1) Apparatus

The results of pressure-volume-temperature measurements on liquids are generally reported in terms of the relative volume. The relative volume is the ratio of the volume of a certain mass of liquid at a given pressure and temperature, to the volume of the same mass of liquid at some chosen standard pressure and temperature (usually one atmosphere and 0°C). The relative volumes of several of the hydrocarbons investigated in the present work are to be found in the literature (93,121,122,123), but no experimental data has been reported for 30°C, the temperature used in most of the present studies.

The relative volume of the hydrocarbons was determined as a function of pressure at constant temperature

using a bellows dilatometer (or bellows piezometer). The bellows dilatometer was developed by Bridgman (93,121), who used the technique to determine the relative volume of liquids up to pressures of 50000 bars at temperatures from 0° to 95°C.

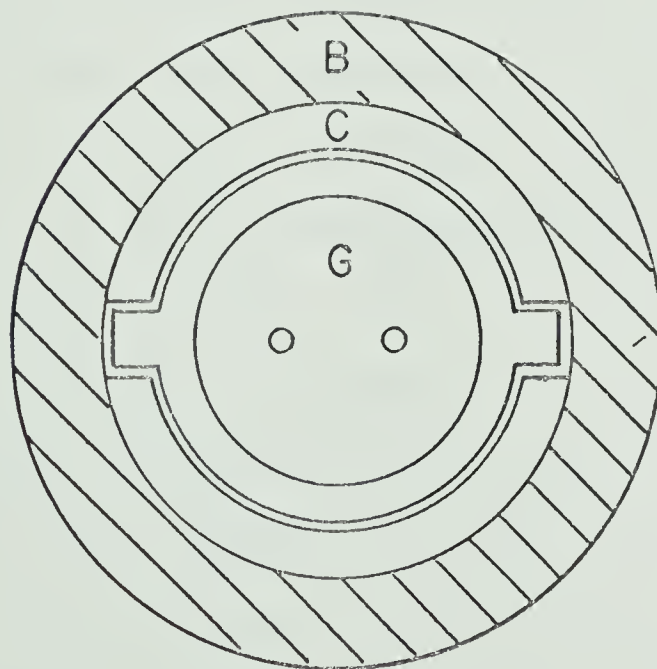
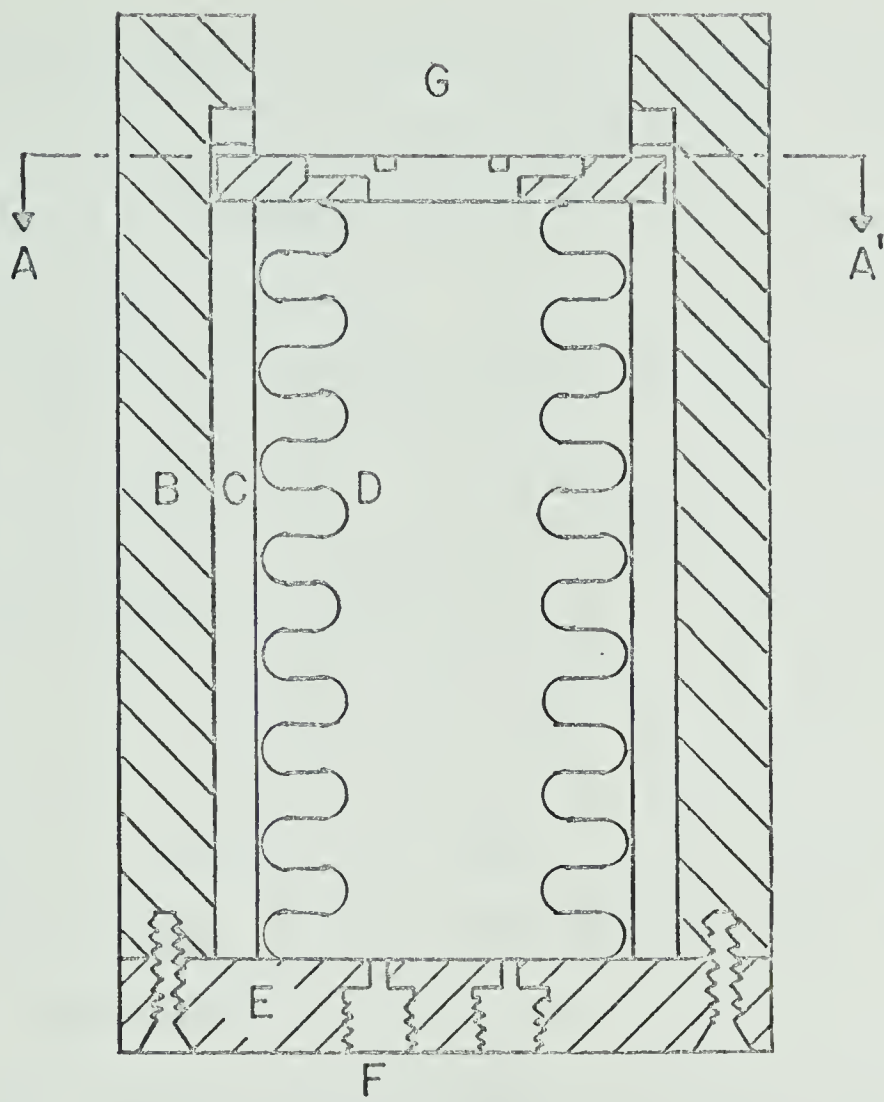
The basic dilatometer is illustrated in Figure II-F-1. It is quite similar in design to a dilatometer used by Brown (124) for the simultaneous determination of relative volume and dielectric constant of carbon tetrachloride up to a pressure of 600 bars. The complete apparatus, apart from the potentiometer wire and the electrical insulations, was constructed from stainless steel. The bellows, obtained from the Fulton Sylphon Division of Robertshaw Controls Ltd., Tennessee, contained 16 active corrugations in a length of 5.08 cm. The bellows had an external diameter of 2.64 cm, an internal diameter of 1.91 cm and an internal volume of approximately 20 ml. One end of the bellows was silver soldered to a base plate which served to hold the bellows within the holder and guide. The top end of the bellows was free to move under compression. Two lugs on the bellows head travelled in two milled slots in the inner guide and ensured that the bellows motion was only in the axial direction. The detailed construction of the bellows head is shown in Figure II-E-2a. The head contained a removable screw

FIGURE II-F-1

Bellows Dilatometer (Voltage Divider Removed)

- B. Outer holder for bellows and guide.
- C. Inner bellows guide.
- D. Bellows. Robertshaw Controls Limited
2.64 cm O.D. 1.91 cm I.D.
- E. Bellows base plate.
- F. Sample filling apertures
- G. Bellows head plate and screw cap.

All parts constructed from stainless steel.



SECTION ON A-A'

cap which facilitated cleaning of the bellows interior. The screw cap was sealed against leakage by a 0.005 in teflon washer, a technique that was found to be successful only for small closures. The use of "O" rings in screw seals was found to be quite unsatisfactory.

The base plate also contained two filling apertures which were sealed by a specially machined screw of the design illustrated in Figure II-F-2b. The screw seals are similar to those found in the closures of needle valves and proved quite satisfactory up to pressures of 4500 bars. The divider is essentially a small slide wire potentiometer. The sliding contact, fixed to the bellows head (Figure II-F-2a), consists of a silver wire, shaped in the form of a U, and rigidly held between two steel compression plates from which it was insulated with a thin layer of teflon. The divider wire assembly is illustrated in Figure II-F-3a. The wire, 30 gauge constantan, approximately 3.5 ohms per foot, was mounted under slight tension by means of a small spring. The wire holder was shaped in the form of a tee and was rigidly held in a similar shaped slot milled into the inner bellows guide. The wire was insulated from the assembly by a layer of teflon.

The electrical circuit associated with the divider is shown in Figure II-F-3b. Potential drops across the wire segments were determined with a differential voltmeter

FIGURE II-F-2a

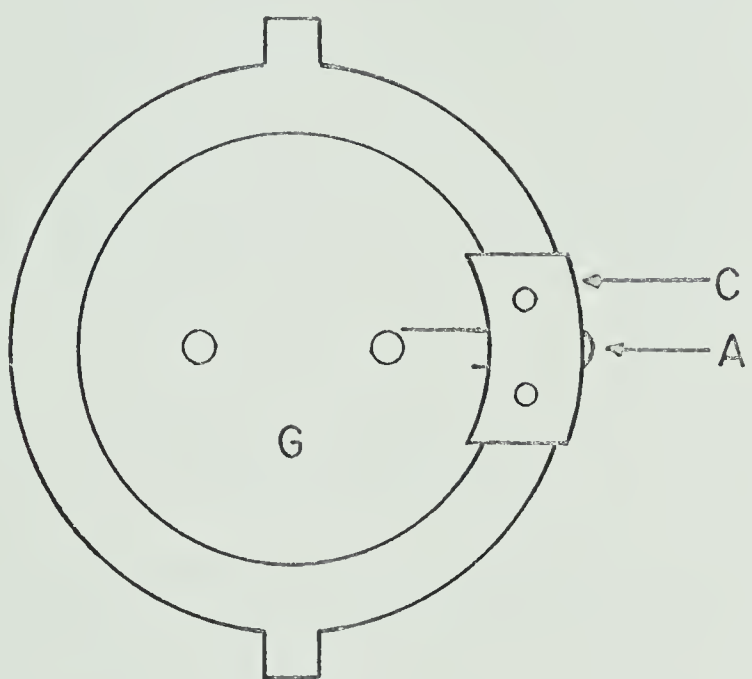
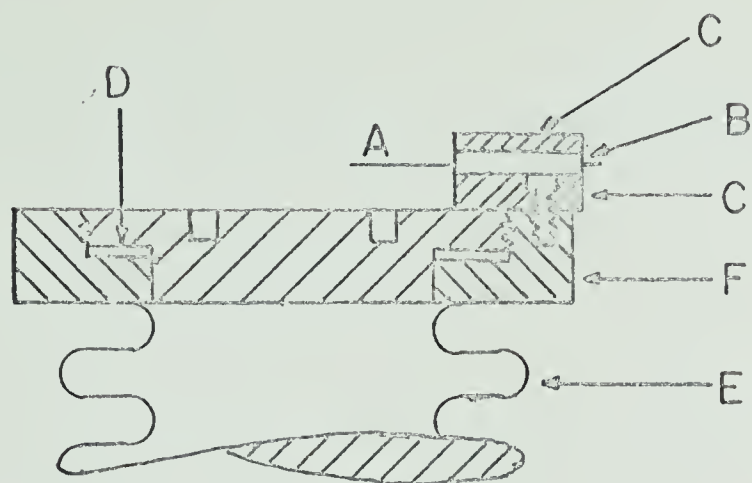
Slide Wire Contact and Bellows Head. (Section & Plan)

- A. Silver wire contact.
- B. Teflon insulation.
- C. Stainless steel compression plates.
- D. Teflon washer. 0.005 ins thick
- E. Dilatometer bellows
- F. Stainless steel ring.

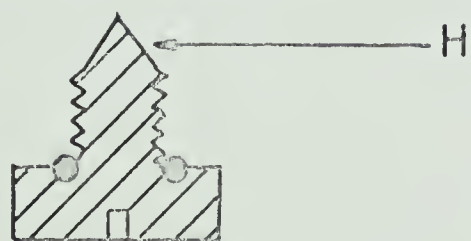
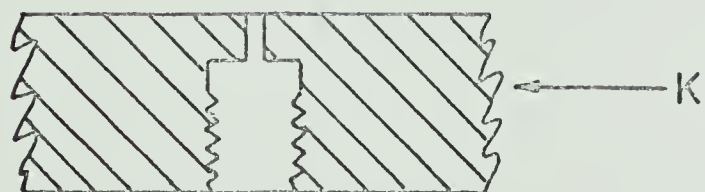
FIGURE II-F-2b

Filling Aperture Closure. (Section)

- H. Needle valve point.
- K. Bellows dilatometer base plate.
- . Rubber "O" ring.



(a)



(b)

FIGURE II-F-3a

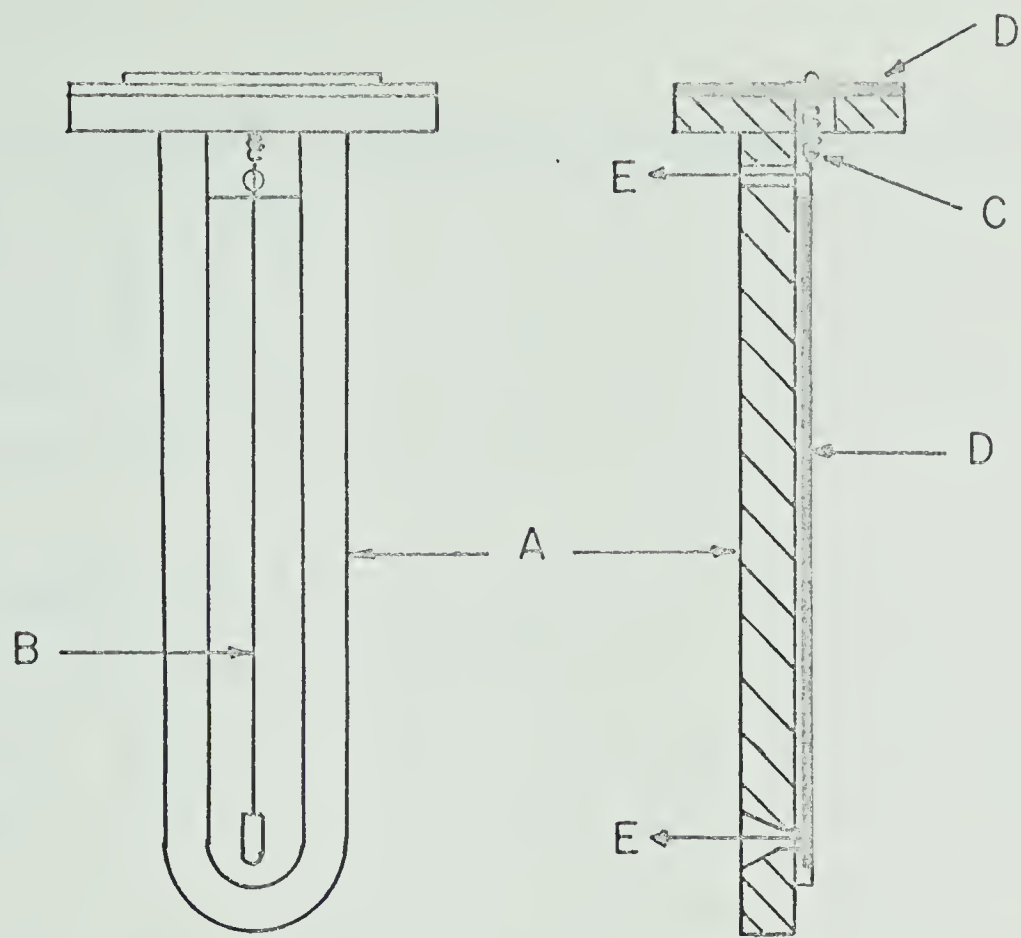
Voltage Divider

- A. Tee shaped stainless steel wire holder.
- B. Divider wire. 30 gauge constantan, 3.5 ohms per foot.
- C. Small helical spring.
- D. Teflon insulation.
- E. Connection to electrical circuit.

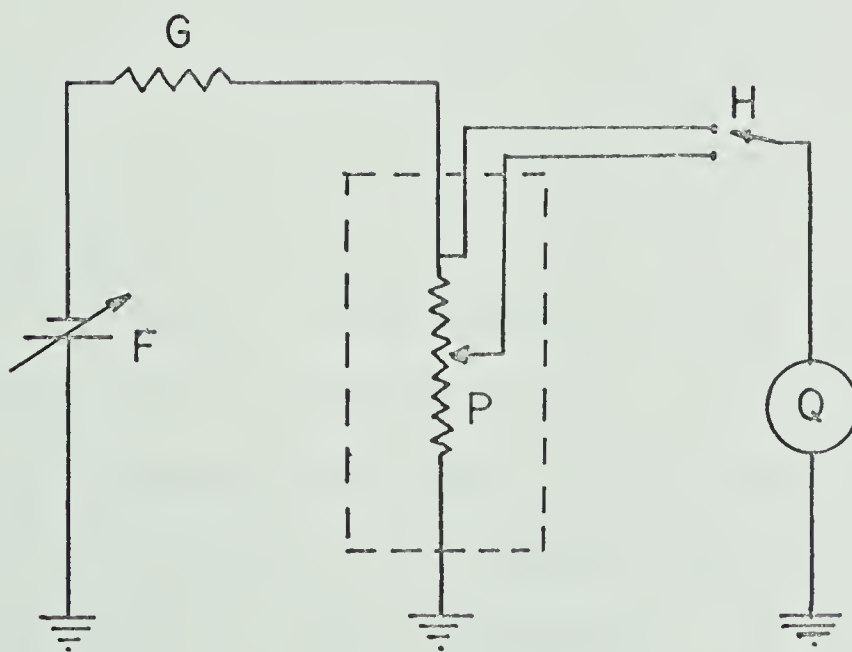
FIGURE II-F-3b

Electrical Circuit Employed with the Voltage Divider

- F. Variable power supply. Power Designs Inc. Model 105-TA.
 - G. 1000 ohm 10 watt resistor.
 - H. Switch.
 - P. Voltage divider
 - Q. Differential volt meter. Fluke Model 823A.
- Indicates part of circuit inside pressure vessel.



(a)



(b)

(Fluke, Model 823A), the potential being supplied by a variable power supply (Power Designs Inc., Model 105 TA). A 1000 ohm 10 watt resistor was included in the circuit and acted as a current limiting device which protected the divider wire from excessive currents.

(2) Calibration and Experimental Procedure.

Prior to any measurements, two calibrations are necessary. Firstly, it must be established that the resistance of the wire is a linear function of its length (i.e., the wire resistivity is uniform). Secondly, the relationship between the axial displacement of the bellows and the interior volume change of the bellows must be determined. An apparatus in which the bellows was held rigid at one end whilst undergoing compression from the opposite end, was constructed. The axial displacement of the bellows was measured to 0.01 mm with a micrometer. A mercury calibrated pipette (5 ml), attached by means of a hollow screw and a Kovar glass to metal seal, replaced one of the filling aperture screws. Octane or heptane was used as the calibrating fluid. The volume change in the bellows corresponding to an axial displacement from an arbitrary point was then determined. The bellows was always placed under slight compression before starting the calibration. The results of several calibrations are reproduced

in Figure II-F-4. The volume displaced from the bellows was directly proportional to the linear displacement up to the limit of the calibration (a 25% decrease in the total interior volume of the bellows).

At the same time as the volume was being calibrated, the potential drop across the divider wire was determined. The potential drop across the whole wire was always maintained constant at 0.10000 volts. Some typical results are illustrated in Figure II-F-5. The graphs show the potential ratio (potential drop across divider wire / potential drop across whole wire) as a function of the linear displacement along the wire from an arbitrary point. The resistivity of the wire was found to be uniform. A slight change in the slope of the plot of potential ratio against linear displacement was found after the wire had been subjected to pressure. The resistivity of the wire, however, remained uniform. The calibrations were checked periodically.

The sample was introduced into the bellows through one of the filling apertures by means of a syringe. Samples were not degassed for pressure-volume-temperature measurements. Air bubbles were removed from the bellows corrugations by rotation of the bellows, whilst flexing the corrugations. The presence of air bubbles in the bellows was readily detected by an irregular change in the bellows

FIGURE II-F-4

Calibration of Bellows Volume. Volume displaced versus displacement.

Δ O Two calibrations starting from a
different arbitrary point.
The calibrations were performed
about six weeks apart.

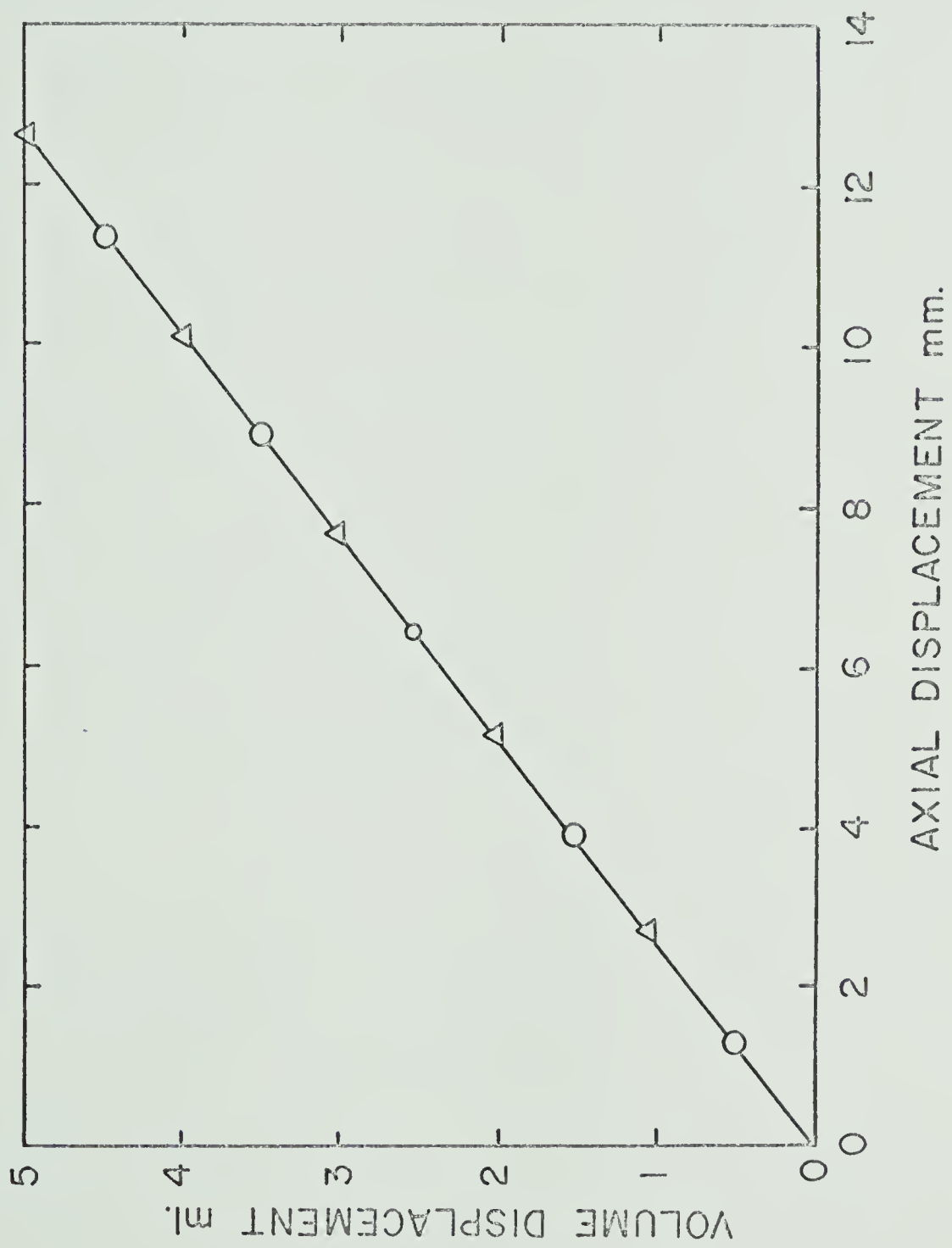


FIGURE II-F-5

Voltage Divider Calibration. Potential ratio versus linear displacement.

30 gauge Constantan wire. 30°C

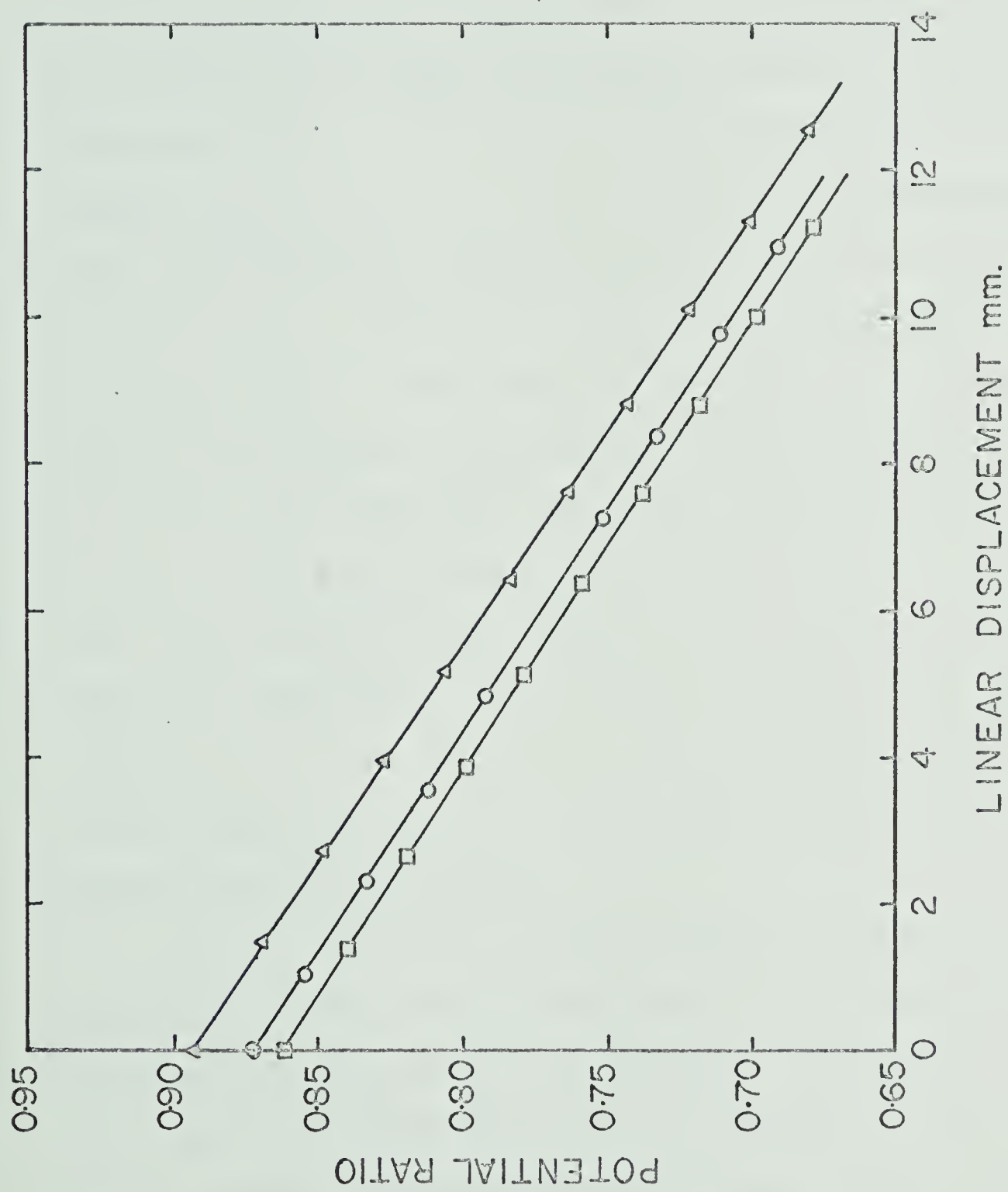
Potential ratio = P.D. across divider/P.D. across whole wire.

P.D. potential drop.

P.D. wire always maintained at 0.10000 volts.

- Δ Initial calibration new wire.
- O Same wire after four applications of 4500 bars.
- Same wire after removal and replacement in dilatometer.

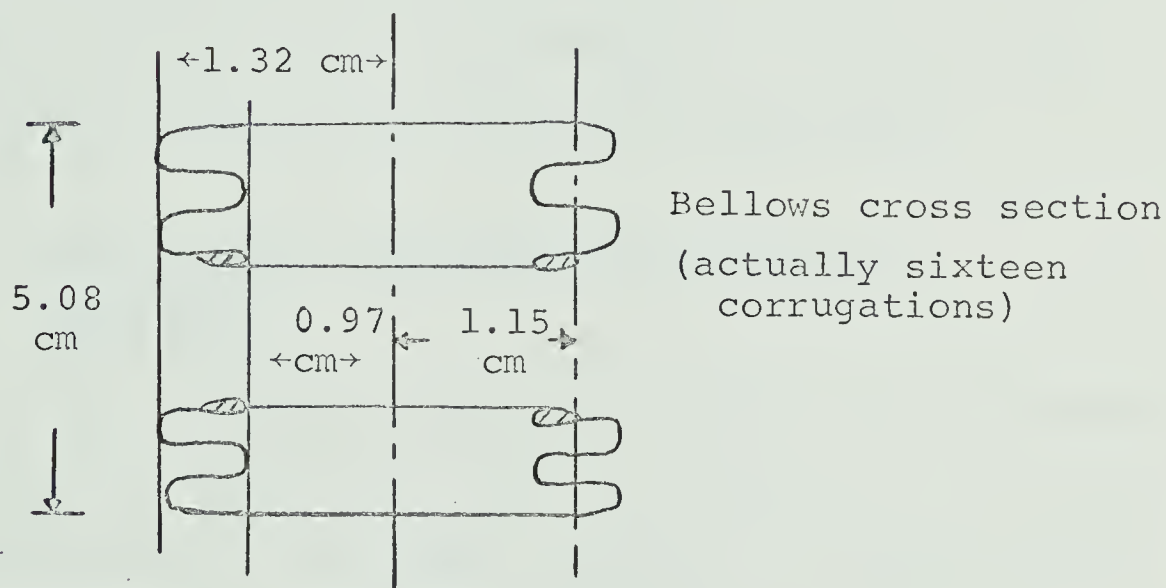
The difference in the initial value of the potential ratio arise from starting at different points on the divider wire corresponding to the relaxed position of the bellows.



volume at the beginning of the experiment. After filling, the cell was assembled within the guide and holder system and attached to the face of the pressure vessel closure piston by means of a 0.25 in bolt. The complete apparatus was then inserted into the pressure vessel, tested for electrical shorts and left for about one hour to attain thermal equilibrium. All experiments were conducted at 30°C. The potential drop across the divider wire was determined as a function of pressure, the potential drop across the whole wire being maintained at 0.10000 volts. Leaks in the bellows closures were readily detected, because if a leak occurred, after the pressure within the bellows had equilibrated with the pressure in the hydraulic oil, the bellows relaxed under its own tension arising from its compression. The relative volume of the sample in the bellows was calculated from the change in the potential ratio (see calibrations of the divider wire and the bellows volume given above).

A major correction arising from the change in resistivity of the wire as the pressure was increased, was eliminated by the use of the potential ratio rather than the simple potential drop across a segment of the wire. It was assumed that the change in resistivity of the wire with pressure was uniform along the length of the wire. The only remaining corrections to be considered are those

which arose from the change in volume of the materials of the apparatus as the pressure was increased. It was assumed that the compressibility of the silver contact was equal in all directions, in which case the point of contact with the divider wire should be unaffected by pressure. The change in volume of the bellows, because of compression of its stainless steel walls, may be shown to be negligible in the following manner.



The above sketch shows a cross-section of the bellows. Although the bellows was 5.08 cm in length, the actual length of steel that undergoes compression is 16.5 cm (the length of the bellows when fully extended). For calculation purposes, the bellows may be replaced by a cylinder of the same wall thickness (0.0127 cm) and with a radius equal to the average radius of the bellows (1.15 cm). Assuming stainless steel to have a similar linear compressibility to that of iron, a value of 1.89×10^{-7} is obtained at 4500 kg/cm^2

(4410 bars). The value was calculated by the same method described earlier (page 71), using Bridgman's values for the compressibility of iron (93). The change in volume resulting from the compression of the walls is negligible (less than 0.005%). The length of the walls is decreased by 0.08%. The decrease in length will have less effect when the steel is in the bellows configuration than in the cylinder configuration. The maximum volume change arising from the compression of the bellows material is less than 0.1% and was neglected.

(G) The Pressure Dependence of Viscosity.

(1) Apparatus.

The viscosity of the hydrocarbons was determined as a function of pressure using a rolling ball viscometer. Experimentally, the method consists of determining the time that a ball takes to roll between two points, a fixed distance apart, within a tube filled with the fluid whose viscosity is to be determined. The velocity with which the ball rolls is related to the viscosity of the fluid. The theory of the rolling ball viscometer has been extensively discussed by Hubbard and Brown (125). In practice, the instrument is not an absolute viscometer for low fluid viscosities and has to be calibrated with a series of standards of known viscosity.

The part of the viscometer apparatus that fitted within the pressure vessel was constructed in two major parts, a roll tube assembly, which is illustrated in Figure II-G-1a and b, and a bellows holder and pressure transmitting device shown in Figure II-G-2a and b. All parts, unless otherwise specified, were constructed from stainless steel.

The actual roll tube was cut from a length of precision bore fused quartz glass tubing supplied by the Thermal American Fused Quartz Company. The internal diameter of the tube was 7.99 ± 0.01 mm. The ball was selected from a number of steel bearings on the grounds of its uniformity in diameter. The selected ball had a diameter of 6.35 ± 0.01 mm and a density of 7.772 gms/ml at 25°C. The glass roll tube was held within three aluminium cylinders by a series of Viton A "O" rings which fitted tightly onto the glass surface. Two lucite sections were inserted between the aluminium cylinders. The lucite sections contained a slot, 0.025 cm wide, which terminated 0.013 cm from the surface of the glass roll tube. The distance between the slots was 13.3 cm when the sections were assembled on the tube. These slots held the coils of the timing device (described later). One end of the roll tube was closed by a perforated steel cap whilst the opposite end was fixed to a steel base plate. The base plate served three purposes, firstly it supported the

FIGURE II-G-Ia

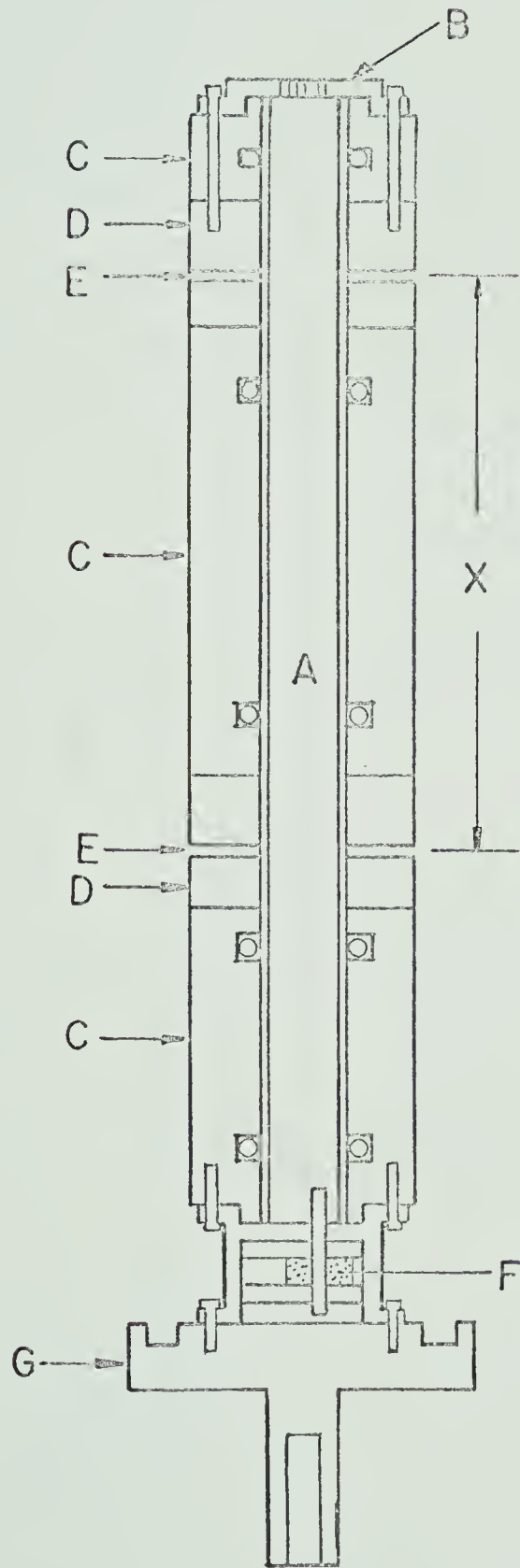
Section of Roll Tube Assembly on Base Plate

- A. Fused quartz roll tube. 7.99 ± 0.01 mm I.D.
- B. Perforated cap to retain ball in tube.
- C. Aluminium cylinder sections.
- D. Lucite cylinder sections.
- E. Slots containing the coils of the timing device.
- F. Iron core and coils of electromagnet.
- G. Stainless steel base plate.
- H. Threaded hole, to fix viscometer to pressure vessel piston.
- X. Roll distance between tuning coils (13.3 cms).
- O. Viton A "O" rings.

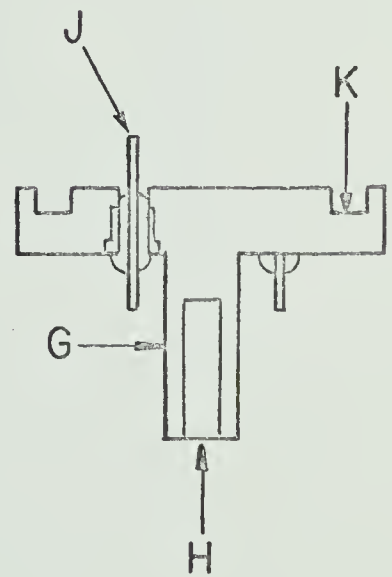
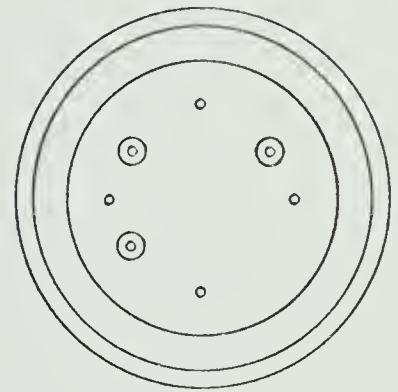
FIGURE II-G-Ib

Detailed Section of Base Plate

- K. "O" ring groove.
- J. Metal to ceramic terminal seal. Latronics Corporation.
- O. Shows the location of the three terminal seals in the base plate.



(a)



(b)

FIGURE II-G-2a

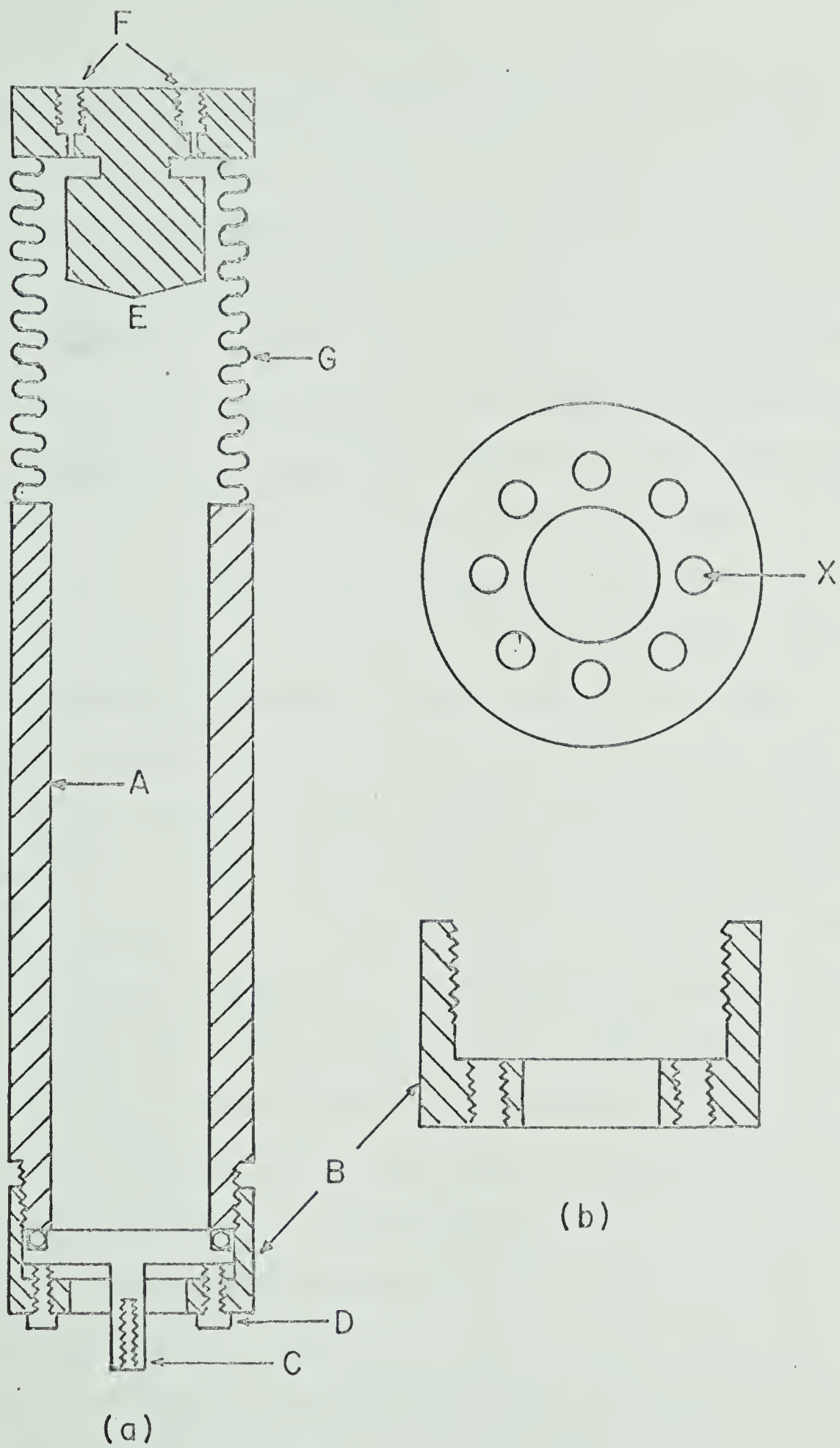
Section of Bellows Roll Tube Holder (Roll
tube removed).

- A. Stainless steel casing.
- B. Stainless steel compression screw cap.
- C. Roll tube base plate.
- D. Compression bolts.
- E. Solid steel plug.
- F. Filling apertures.
- G. Stainless steel bellows.
Robertshaw Controls Limited.
- O. Viton A "O" ring

FIGURE II-G-2b.

Detail of Compression Screw Cap

- X Shows location of the compression bolts.



electrical connections which passed through the baseplate into the tube interior. Secondly, it provided part of the seal between the tube interior and the surrounding hydraulic fluid, and lastly, it supported the magnet that was used to hold the ball at one end of the roll tube whilst the angle of tilt was being adjusted.

Electrical connections through the base plate were made with Latronics Corporation ceramic to metal terminal seals. The terminals were soldered to the stainless steel baseplate using a solder paste called Staintin, supplied by the Eutectics Welding Alloys Company of Canada. Seals between stainless steel and tin were found to be unreliable under vacuum when the surfaces were soldered with conventional solder (40:60 lead;tin). The high temperature necessary for silver soldering was found to part the tin to ceramic interface. The terminals required replacement after about five experiments to 4500 bars. The pressure was transmitted to the interior of the roll tube holder by bellows which were free to compress as the pressure was increased. The bellows (one-ply stainless steel, 4.17 cm outside diameter and 2.82 cm inside diameter) was constructed in two sections each of eight active corrugations. The bellows were supplied by Robertshaw Controls Limited. Two sections of bellows were necessary in order

to obtain sufficient compression without exceeding the elastic limit of the bellows. All stainless steel to stainless steel joins were silver soldered. The free end of the bellows was closed by a steel plate which contained two filling apertures. The plate had a solid plug attached to it on the bellows interior side. The plug significantly reduced the volume of sample required for the experiment and thereby, reduced the amount by which the bellows had to compress. The total volume of the system was approximately 80 ml. The filling apertures were similar in design to those described earlier in the bellows dilatometer (Figure II-F-2b).

The roll tube assembly fitted within the holder with a clearance of about 0.025 cm. A series of grooves along the sides of the aluminium cylinders allowed the sample to pass into all the dead spaces, and also allowed the electrical connections to pass up the tube. The seal of the sample from the hydraulic fluid was achieved by compression of the roll tube base plate against the lip of the tube holder, the two being separated by a Viton A "O" ring. Compression of the "O" ring was accomplished by eight bolts symmetrically placed around the holder screw cap (Figure II-G-2b).

The assembled viscometer was attached directly onto the face of the pressure vessel closure piston by means of

a bolt. A series of marks engraved on all parts of the viscometer ensured that the parts were always reassembled in the same position. Provided the instrument is calibrated the angle of tilt does not have to be known but it does have to be reproducible. The complete pressure vessel assembly (pressure vessel C weighed about 120 lbs) was mounted such that it could be rotated and fixed reproducibly at a series of angles. The mounting is illustrated in Figure II-G-3.

The pressure vessel was rigidly held in a solid steel structure mounted on a trailer axle and bearing. The angle of tilt of the pressure vessel was determined by a number of hardened steel stops which were located in a steel plate welded to the static stand. The stops were placed at 10° intervals from 10° one side of the horizontal to 60° the other side. Only one stop was used at a time, the others retracting into the steel plate. A spring loaded clamp was fixed to the pressure vessel assembly and rotated with the axle until it reached the stop in use. A hole in the clamp then mated with the stop. The angle of tilt, judging from reproducibility of the roll times, was found to be completely reproducible when adjusting away from and returning to the same stop. Pressure line connection to the vessel was made with a coil of high pressure tubing (see (A) this section). The coil contained

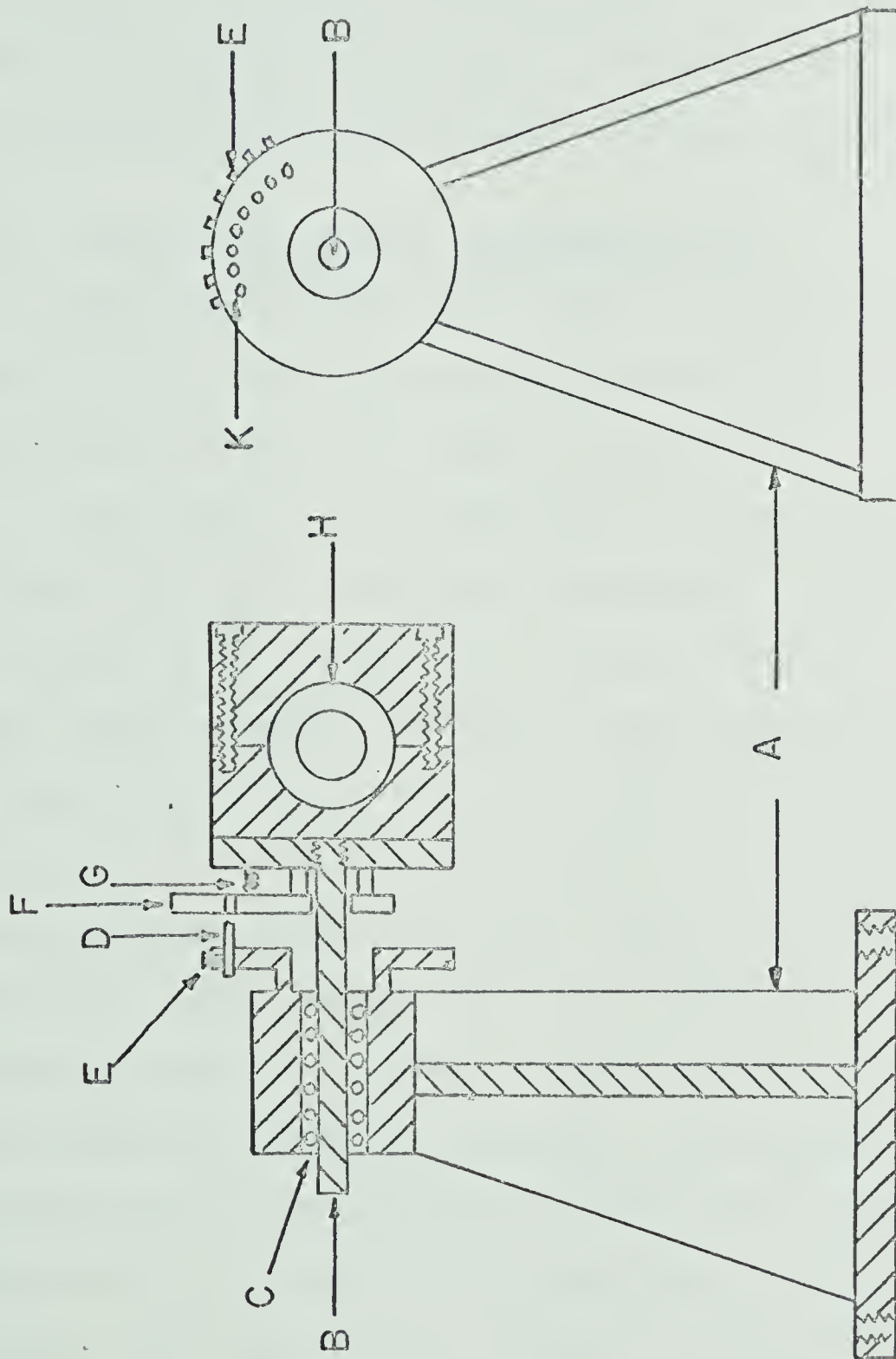
FIGURE II-G-3

Pressure Vessel Mounting for Viscometric Determinations

Side View Section

Front View (pressure vessel removed)

- A. Main Stand, bolts onto trolley.
- B. Axle (1 ins diameter)
- C. Axle bearings
- D. Hardened steel adjustable stops
- E. Adjustable stop tightening screws
- F. Clamp. Rotates with axle and holds on the stops.
- G. Spring
- H. Pressure vessel assembly
(pressure vessel C)
- K Adjustable stop location holes.



FRONT VIEW

SIDE VIEW SECTION

four turns and had an initial diameter of about 30 cm. The viscometer apparatus was mounted on the mobile pressure system, the trolley being raised on four solid steel stands for the measurements to ensure that the angle of the roll tube did not change. The level of the trolley was periodically checked using a series of spirit levels.

(2) Electrical Timing Instrumentation.

The time that the ball took to roll between the two coils of the roll tube was determined using the circuit shown in block notation in Figure II-G-4.

The coils, one in each slot of the lucite sections of the roll tube, contained approximately one hundred turns of magnet wire (Belden Wire Company 30 gauge). The coils were wound in series and had a combined resistance of about 10 ohms. A variable frequency constant amplitude AC generator was used to tune the coils to resonance, at which, the potential across the coils is at a maximum. The resonance frequency was generally between 0.75 and 0.85 megacycles but was dependent upon the applied pressure and the sample surrounding the coils. On passage of the ball through one of the coils the circuit was momentarily detuned resulting in a change in the potential in the circuit. The signal resulting from the change in potential in the circuit was filtered, differentiated and amplified prior to being fed to a Schmitt trigger.

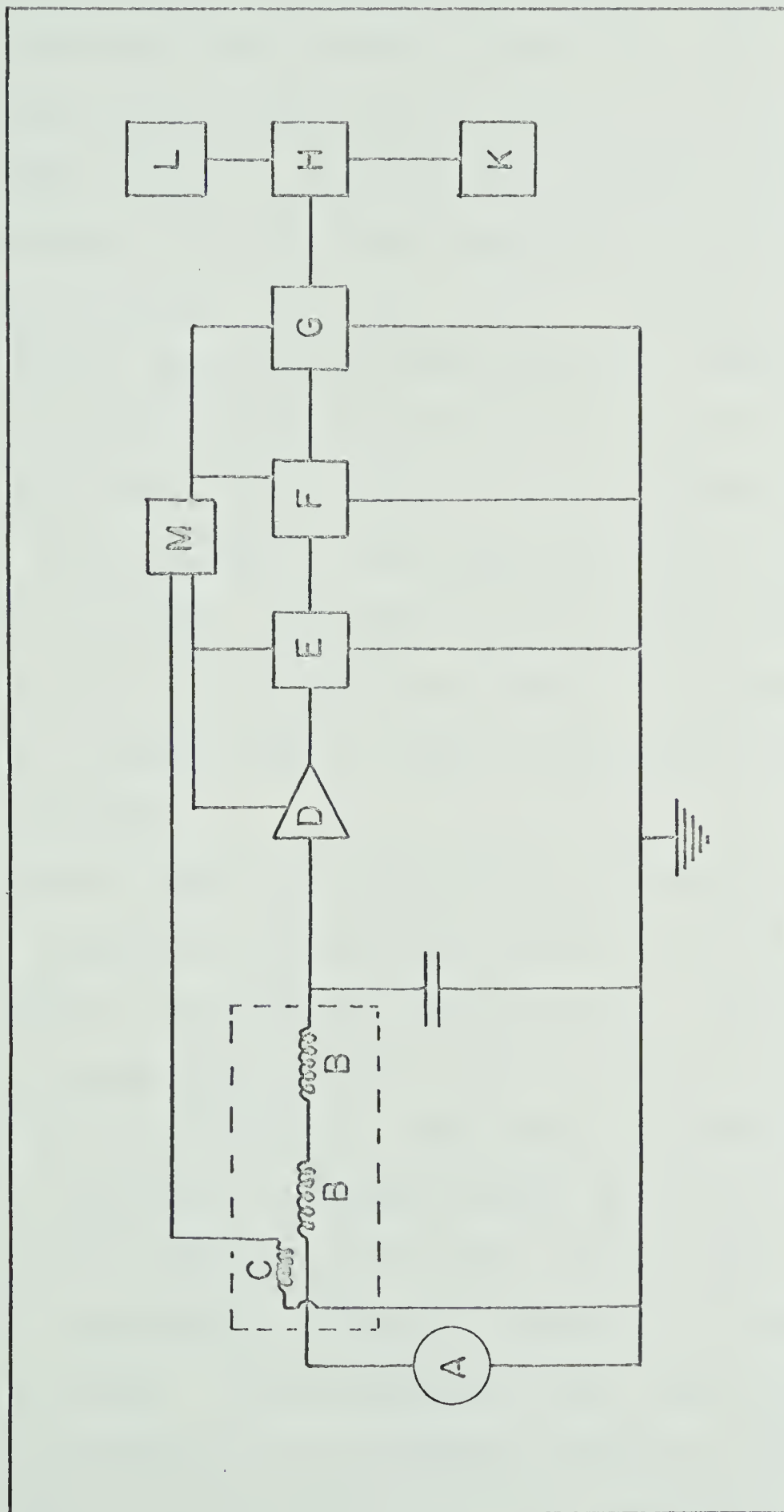
FIGURE II-G-4

Block Circuit Diagram of Viscometer Timing

Apparatus

- A. Constant amplitude sine wave generator.
Tektronix Type 190A.
- B. Viscometer coils.
- C. Magnet coil.
- D. Detector amplifier
- E. Schmitt trigger
- F. Bistable multivibrator (flip-flop)
- G. Emmitter follower (power amplifier)
- H. Gate
- K. Event counter (Transistor Specialties
Inc. Model 1535)
- L. Time mark generator (Tektronix, Type 184)
- M. Twin low voltage power supply. (Harrison
Laboratories Model 802B)
- Indicates part of circuit within pressure
vessel

D to G were mounted on a printed circuit board
and fixed directly onto the head of the pressure
vessel piston closure shaft.



The output pulse of the Schmitt trigger was used to activate a bistable multivibrator (flip-flop), the signal from which, after power amplification, was used to trigger a gate circuit. The gate, when opened, allowed the output pulses of a time mark generator to be fed into a pulse counter. The pulse counter recorded the number of pulses from the time mark generator between the on-off signals supplied to the gate as the ball passed through each coil in turn. The time marker was capable of giving pulses at time intervals from 10 nanoseconds up to seconds. For most of the present work pulses at 0.1 or 1 millisecond were used. The pulse counter had a digital read out and a resolution of one part per thousand.

The circuit, after the coils and up to the gate, was mounted on a printed circuit board and fixed directly onto the head of the pressure vessel piston. Little difficulty was encountered with the timing circuit provided the coils were in resonance. The amount of energy absorbed by the ball on passage through the coils is dependent upon the velocity of the ball and at very low velocities insufficient energy was absorbed to trigger the timing circuit. This problem was only encountered with methylcyclohexane at the highest pressure (4500 bars) and the lowest angle of tilt and lowest temperature. As

the roll velocity decreased with increasing pressure, the ball would proceed further into the coil before sufficient energy was absorbed to trigger the circuit, however, both coils were symmetrical so the overall error in timing would be nullified. The width of the coils accounted for about 0.3% of the total roll distance. The roll times were reproducible to better than 0.3% when the circuit was correctly tuned.

The magnet, which holds the ball at one end of the roll tube whilst the angle of tilt is being adjusted, was constructed from an iron core and the same magnet wire as was used for the coils. The circuit used for the magnet is also shown in Figure II-G-4. The magnet resistance was about 1.5 ohms and a current of about 0.1 amps was required to hold the ball. The ball was held for the minimum time possible to reduce local heating to a minimum.

(3) Experimental Procedure.

In all viscometric determinations, extreme care must be taken to ensure that the sample is free of foreign particles, for example, dust and metal fragments, because such contamination leads to unreproducibility in the measured times. All metal surfaces of the viscometer were cleaned with an air abrasive unit (S.S. White, Model F) which removed all solder chips and oxides that accumu-

lated on the surfaces during the soldering process. The components of the viscometer were then cleaned in a specially constructed Soxhlet extraction apparatus. The components were generally left in the Soxhlet apparatus overnight, which resulted in at least thirty washings in hot fresh solvent. If new terminal seals had been soldered into the roll tube base plate, the base plate was washed with water in the Soxhlet apparatus to ensure that traces of soldering flux were completely removed. Hexane, or the hydrocarbon under investigation, was used for the final washing.

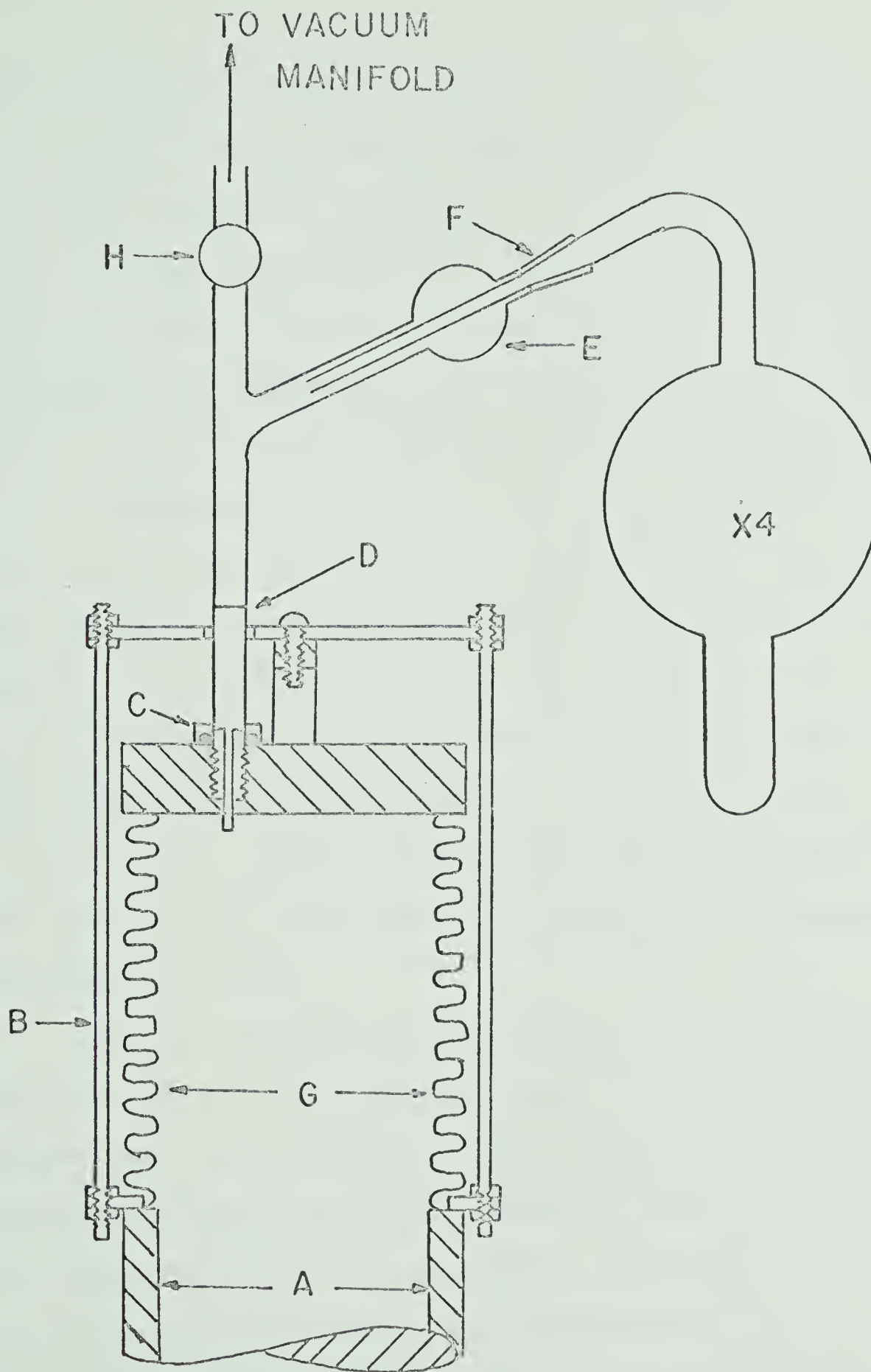
The cleaned components were assembled into the viscometer bellows holder and the apparatus attached to the vacuum manifold as shown in Figure II-G-5. A steel holder around the bellows prevented them from collapsing as their interior was evacuated. Connection to the vacuum manifold was made through one of the filling apertures using a glass to metal Kovar seal and a hollow screw. Failure to attain a satisfactory vacuum (less than one micron) was generally traced to leaks at the soldered joints of the terminal seals. A helium leak detector (Consolidated Electrodynamics Model 24-120B) was used to trace leaks in the metal to metal joints.

When a satisfactory vacuum was obtained, the sample was introduced into the bulb X4, from the storage mani-

FIGURE II-G-5

Viscometer Filling System

- A. Viscometer main casing.
- B. Steel holder. Prevents bellows from collapsing during evacuation.
- C. Hollow screw adaptor in filling aperture.
- D. Kovar seal (0.25 ins)
- E. Small bulb (approximately 10 ml)
- F. 10/30 extended ground glass joint
- G. Viscometer bellows
- H. Republic greaseless valve
- X4 Sample bulb. 200 ml



fold (see Figure II-B-1), by trap to trap distillation. For the high boiling hydrocarbons and the calibrating oils this procedure was found to be tedious because of their low vapour pressures and they were introduced directly into X4 by means of a long needled syringe. Samples introduced in this manner were degassed in X4 by the freeze-thaw technique. The sample was then transferred to the viscometer by rotation of the bulb about the extended 10/30 ground glass joint. The latter joint was greased (Dow Corning Silicone Grease) over the outer 50% of its ground glass surface. Extreme care was taken to ensure that the sample did not come into contact with the joint (any contact was readily apparent from the wetting of the ground glass). A small bulb, blown just below the joint, was found to be advantageous in preventing the sample from reaching the joint.

After filling the viscometer, an atmosphere of argon was allowed into the manifold and the viscometer removed from the manifold. The sealing screw was then inserted and the viscometer assembled onto the face of the pressure vessel closure piston. All electrical connections were soft soldered and checked for shorts, prior to inserting the viscometer into the pressure vessel. About one hour was allowed for the system to attain thermal equilibrium. The roll time of the ball was then

determined as a function of pressure at constant temperature. The roll time at each pressure was determined at two angles of tilt of the pressure vessel. Readings were taken both with the pressure increasing and decreasing, at least twenty minutes being allowed before the reading was taken after increasing or decreasing the pressure. The temperature was then adjusted and the procedure repeated.

(4) Calibration.

As previously mentioned the rolling ball viscometer has to be calibrated. All hydrocarbons investigated were used as calibrating standards at atmospheric pressure. For higher viscosities, higher molecular weight hydrocarbons and a series of oils were used.

In cases where the viscosity of the calibrating fluid was not available in the literature, the viscosity was determined using a Ubbelohde viscometer. These instruments were calibrated by the manufacturer (Cannon Instrument Company). The calibration was periodically checked with a standard oil. The viscosity was determined by multiplying the measured efflux time of the sample by the viscometer constant. The viscosity obtained is in units of centistokes and the density of the sample is required to convert this to units of centipoise. Densities, when not available from the literature, were determined using a single necked pycnometer. The pycnometer was constructed

from a 1 ml pipette and a 10 ml pyrex bulb. The volume of the bulb and pipette was determined as a function of temperature by calibration with mercury. Samples were introduced into the pycnometer using a long fine-needled syringe.

The viscosities (centipoise) as a function of temperature for the standard and silicone oils are given in Table II-G-I. The densities of the same oils are shown in Table II-G-II. All values for the standard oils are those determined by the Cannon Instrument Company. Table II-G-III contains the viscosities of the hydrocarbons from 0 to 60°C at atmospheric pressure. These values were either determined in the present work or taken from various sources in the literature. Table II-G-IV list the densities of the same hydrocarbons at atmospheric pressure.

The rolling ball viscometer was calibrated in exactly the same manner as described for the pressure experiments except that the pressure remained at one atmosphere. The results of these calibrations will be given in the next section.

(H) Radiation Induced Conductance Measurements.

(1) Conductance cell construction.

The magnitude of the radiation induced currents observed in the hydrocarbons during the present investi-

TABLE II-G-I

Viscosity of Standard and Silicone Oils. Centipoise

		Atmospheric Pressure					
		Temperature °C					
Oil	O	10	20	30	40	50	60
A(20)	-	24.10 ^a	21.60	17.85	15.00	12.75	11.00
B(10)	14.45	11.70	9.55	8.00	6.70	5.65	4.87
C(5)	7.98	6.45	5.40	4.55	3.86	3.27	2.82
D(2)	-	-	-	1.84	-	-	-
N1	-	-	-	0.8531 ^b	-	-	-
N4	-	-	-	0.2947 ^b	-	-	-
S3	-	-	3.528	3.102 ^b	-	-	-
S6	-	-	9.490	7.913 ^b	-	-	-

a Values at 15°C

b Values at 25°C

A to D Silicone oils

N and S Cannon Instrument Company. Standard Oils.

TABLE II-G-II

Densities of Standard and Silicone Oils (gm/ml). Atmospheric Pressure

Oil	Temperature °C						
	0	10	20	30	40	50	60
A(20)	0.9715	0.9626	0.9537	0.9448	0.9358	0.9269	0.9179
B(10)	0.9535	0.9445	0.9356	0.9268	0.9177	0.9068	0.8995
C(5)	0.9397	0.9305	0.9215	0.9125	0.9033	0.8942	0.8850
D(2)	0.8828	0.8733	0.8636	0.8540	0.8442	0.8346	0.8250
N1	---	---	---	0.7260 ^b	---	---	---
N4	---	---	---	0.6554 ^b	---	---	---
S6	---	---	0.8627	0.8593 ^b	---	---	---
S3	---	---	0.8391	0.8356 ^b	---	---	---

b Value at 25°C

A-D present values determined by pycnometer

N and S manufacturers values

TABLE II-G-III

Viscosity of Hydrocarbons Centipoise. Atmospheric Pressure

Compound	Temperature °C						
	0	10	20	30	40	50	60
n-pentane	0.279	0.255	0.235	0.216	---	---	----
n-hexane	0.3810	0.3846	0.3126	0.2854	0.2619	0.2512	0.2223
n-octane	0.7125	0.6203	0.5466	0.4865	0.4368	0.3947	0.3587
n-decane	1.304	1.091	0.9284	0.8018	0.7010	0.6192	0.5517
n-dodecane	2.278	1.833	1.508	1.265	1.079	0.9321	0.8147
n-tetradecane	---	2.940	2.342	1.910	1.590	1.345	1.154
n-octadecane	---	---	---	3.891	3.093	2.516	1.912
methylcyclohexane	0.993	0.850	0.734	0.641	0.564	0.500	0.446
cyclopentane	0.555	0.492	0.439	0.394	0.356	0.323	---
2-2dimethylbutane	---	0.422	0.374	0.330	-----	-----	---

Values taken from F. D. Rossini "Selected Values of Physical and Thermodynamic Properties of Hydrocarbons and Related Compounds", American Petroleum Institute Research Project #44 Carnegie Press Pittsburgh 1953.

TABLE II-G-IV

Densities of Hydrocarbons (gm/ml). Atmospheric Pressure

Compound	Temperature °C					
	0	10	20	30	40	50
n-pentane	0.6454	0.6360	0.6263	0.6165	-----	-----
n-hexane	0.6769	0.6683	0.6595	0.6505	0.6412	0.6318
n-octane	0.7185	0.7102	0.7022	0.6942	0.6860	0.6778
n-decane	0.7447	0.7398	0.7297	0.7221	0.7146	0.7072
n-dodecane	-----	0.7563	0.7488	0.7416	0.7343	0.7270
n-tetradecane	-----	0.7663 ^a	0.7626	0.7563	0.7495	0.7428
n-octadecane	-----	-----	-----	0.7751	0.7684	0.7616
methylcyclohexane	0.7868	0.7734 ^a	0.7693	0.7606	0.7514	0.7425
cyclopentane	0.7648	0.7504 ^a	0.7454	0.7359	-----	-----
2,2dimethylbutane	0.6677	0.6541 ^a	0.6491	0.6443 ^b	-----	-----
a. values at 15°C			b. values at 25°C			

Values taken from F. D. Rossini "Selected Values of Physical and Thermodynamic Properties of Hydrocarbons and Related Compounds" American Petroleum Institute Research Project #44 Carnegie Press, Pittsburgh 1953.

gations varied from 10^{-10} to 10^{-7} amperes, depending upon the experimental conditions. In order to measure such small induced currents accurately, the conductance of the sample in the absence of radiation must be at least two orders of magnitude smaller (they were actually 10^{-14} mho or less). The conductance cell was designed such that it was amenable to rigorous cleaning and such that it could be filled with the minimum possibility of introducing ionic impurities. Cells used for the measurement of radiation induced currents at atmospheric pressure are generally constructed from glass (54,56). However, of numerous glass cells constructed, for the present work, none were found that would withstand a pressure of 4500 bars without fracturing. Failure always occurred at the glass to metal seals which were required to introduce electrical connections into the cell. Glass to metal seals that were constructed from all combinations of tungsten, platinum and Kovar with Pyrex, soda and uranium glass, were found either to fracture when subjected to a pressure of 4500 bars, or to shatter at various lengths of time after the release of pressure. A seal constructed from a very fine platinum wire (0.005 ins diameter) sealed into soda glass withstood 4500 bars without fracturing, but when the diameter of the wire was increased to a point where it could support an electrode, the

seal once more fractured under pressure.

Initial investigations were conducted using the same cells that were employed for the measurement of the effect of pressure upon dielectric constant (Figure II-E-1). These cells were unsatisfactory because of the large volume occupied by the cylindrical electrodes, which introduced a large variation in the dose rate over the volume of the cell. The cell design ultimately adopted, permitted the cell to be filled under degassed conditions, the final seal of the cell being made under an atmosphere of argon. The bellows cell is illustrated in Figure II-H-1 and details of the electrode assembly are reproduced in Figure II-H-2.

The bellows section of the cell was constructed from two sections of one-ply stainless steel bellows, each of 10 active corrugations, joined by the same method as described in (G) of this section. A stainless steel ring was silver soldered to each end of the bellows and formed part of the "O" ring seal. The outer surface of the steel ring contained an annular slot into which a Viton A "O" ring was fitted. The ends of the bellows were closed by stainless steel caps which compressed against the "O" rings. Compression was applied by eight bolts placed symmetrically around the stainless steel caps. Electrical connections into the bellows interior were

FIGURE II-H-1

Bellows Assembly of Conductance Cell

- A. Stainless steel bellows. Robertshaw Controls Limited
- B. Stainless steel closure caps.
- C. Stainless steel rings
- D. "O" ring groove
- E. Compression bolts.
- F. Bracket by which bellows is attached to the pressure vessel piston.
- G. Metal to ceramic terminal seals. Latronics Corporation.
- H. Filling aperture (see Figure II-F-2b)
- I. Viton "O" ring.

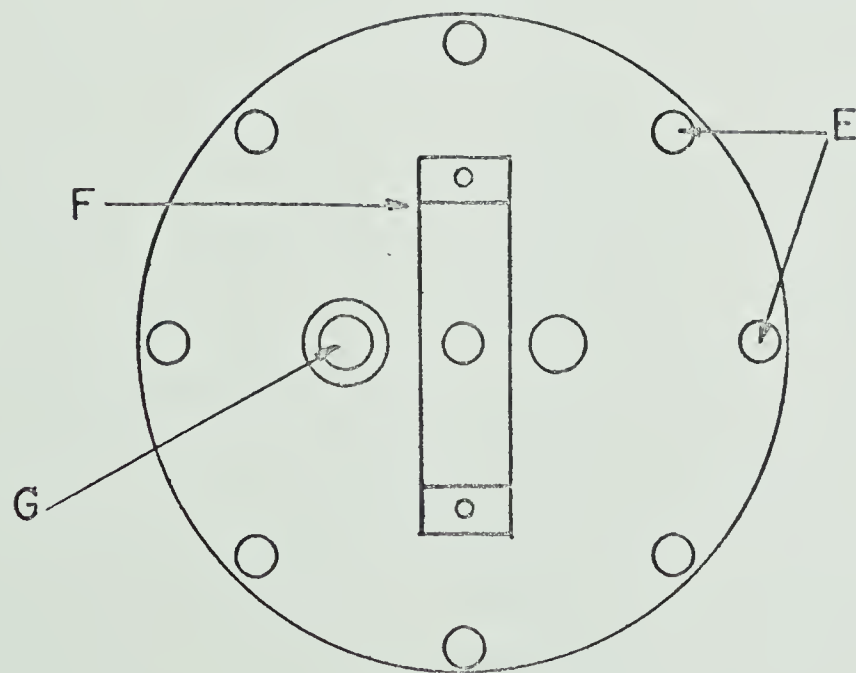
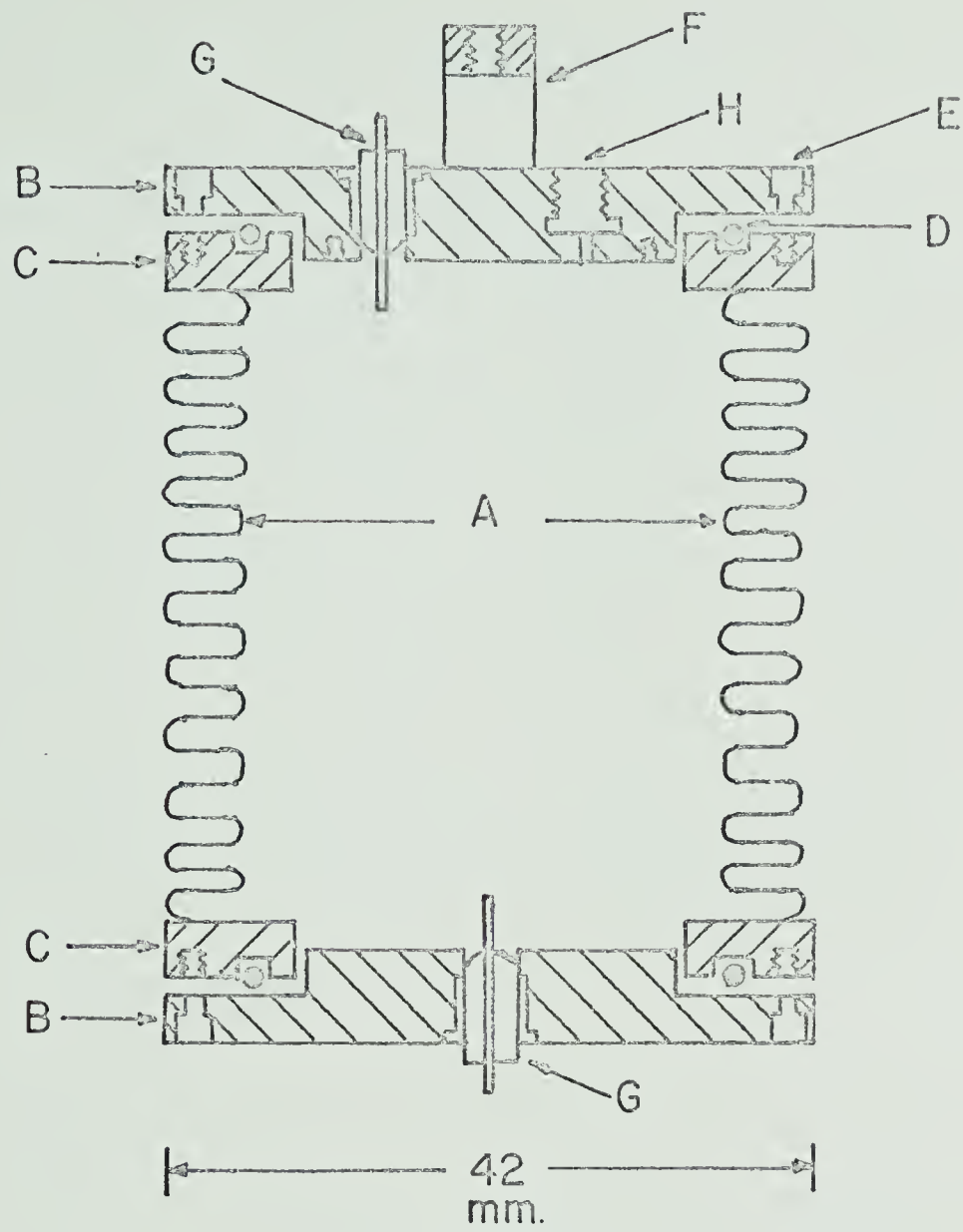


FIGURE II-H-2

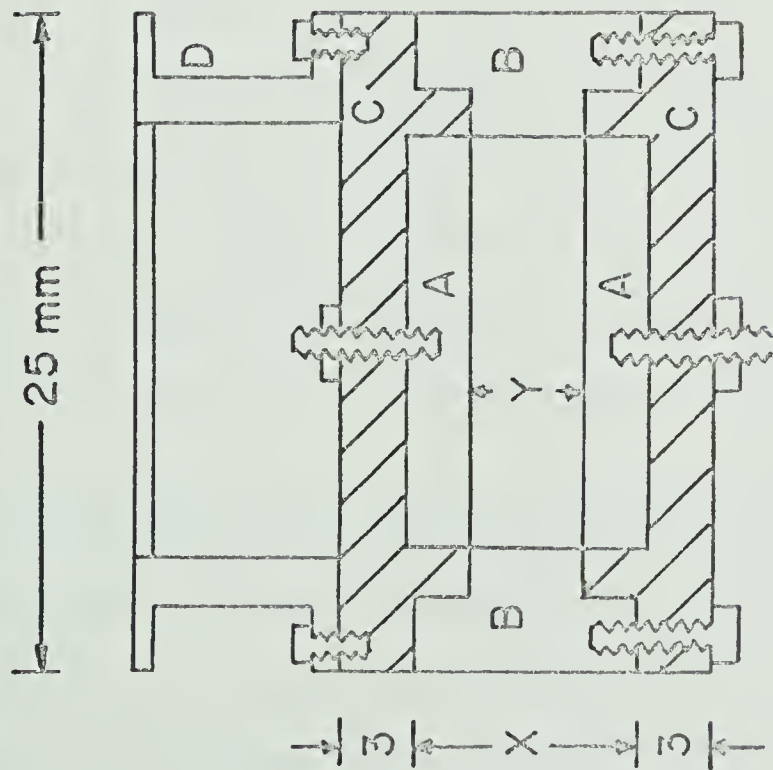
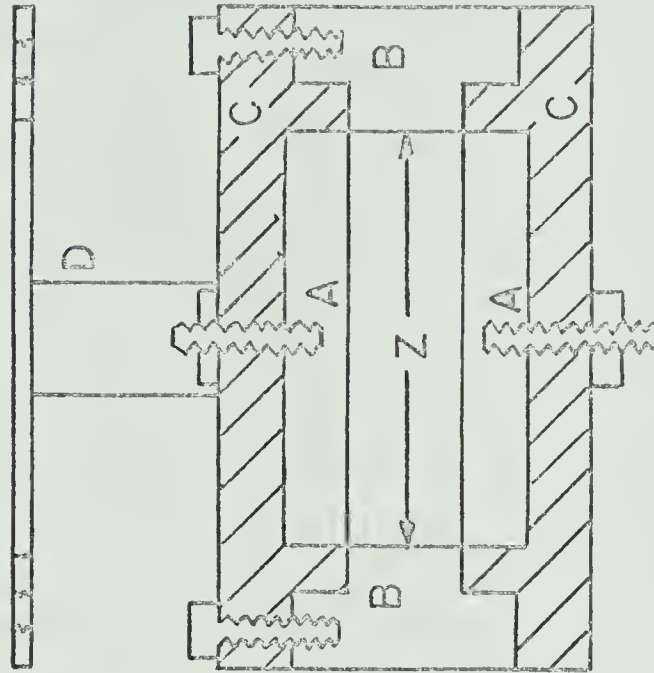
Electrode Assembly of Bellows Conductance
Cell

- A. Stainless steel electrodes 2mm thick
- B. Supramica cermoplastic interchangeable spacer.
- C. Supramica electrode holders
- D. Stainless steel bracket by which electrode assembly was reproducibly placed on the inner surface of the top bellows closure cap.

The distance X varied with the spacer in use

The distance Y corresponds to the electrode spacing as determined by the spacer dimensions given in Table II-H-I.

Z is equivalent to the electrode diameter



made with Latronics Corporation metal to ceramic terminal seals (see (G), this section). One sealing cap contained two filling apertures of similar design to those used in the bellows dilatometer (Figure II-F-2a).

The electrode assembly (Figure II-H-2) consisted of two stainless steel electrodes held a fixed distance apart by a Supramica cermoplastic spacer. The electrode separation was varied from 2 mm to 10 mm using a series of interchangeable spacers. Table II-H-I lists the various combinations of spacers and electrodes used for the conductance determinations. Except in one cell, which contained a guard ring, the electrodes were all about 16 mm in diameter. Electrical connections within the bellows were made with copper wire and soft soldered connections. The electrode, closest to the top of the bellows, when assembled in the pressure vessel, was always used as the collector electrode. The lower electrode was connected to the lower sealing cap by a coil of copper wire. The coil was of sufficient length to allow for the compression of the bellows as the pressure was increased.

(2) Electrical Circuit and Current Measurement.

The electrical circuit employed for the measurement of the current is illustrated in Figure II-H-3. Considerable care has to be taken in the construction of the circuit to avoid the incidence of radiation induced currents

TABLE II-H-I

Conductance Cell Spacer and Electrode Dimensions

Cell	Spacer mm	Electrode Diameter mm	$\frac{L}{A}^b \text{ mm}^{-1}$
A	1.9	16.1	0.0093
B	2.0	15.9	0.0101
C	2.7	15.9	0.0136
D	3.2	16.1	0.0157
E	3.6	16.1	0.0176
F	3.9	16.6	0.0180
G	4.0	16.1	0.0196
H	5.5	16.1	0.0270
J	7.0	11.1 ^a	0.0874
K	9.5	16.1	0.0466

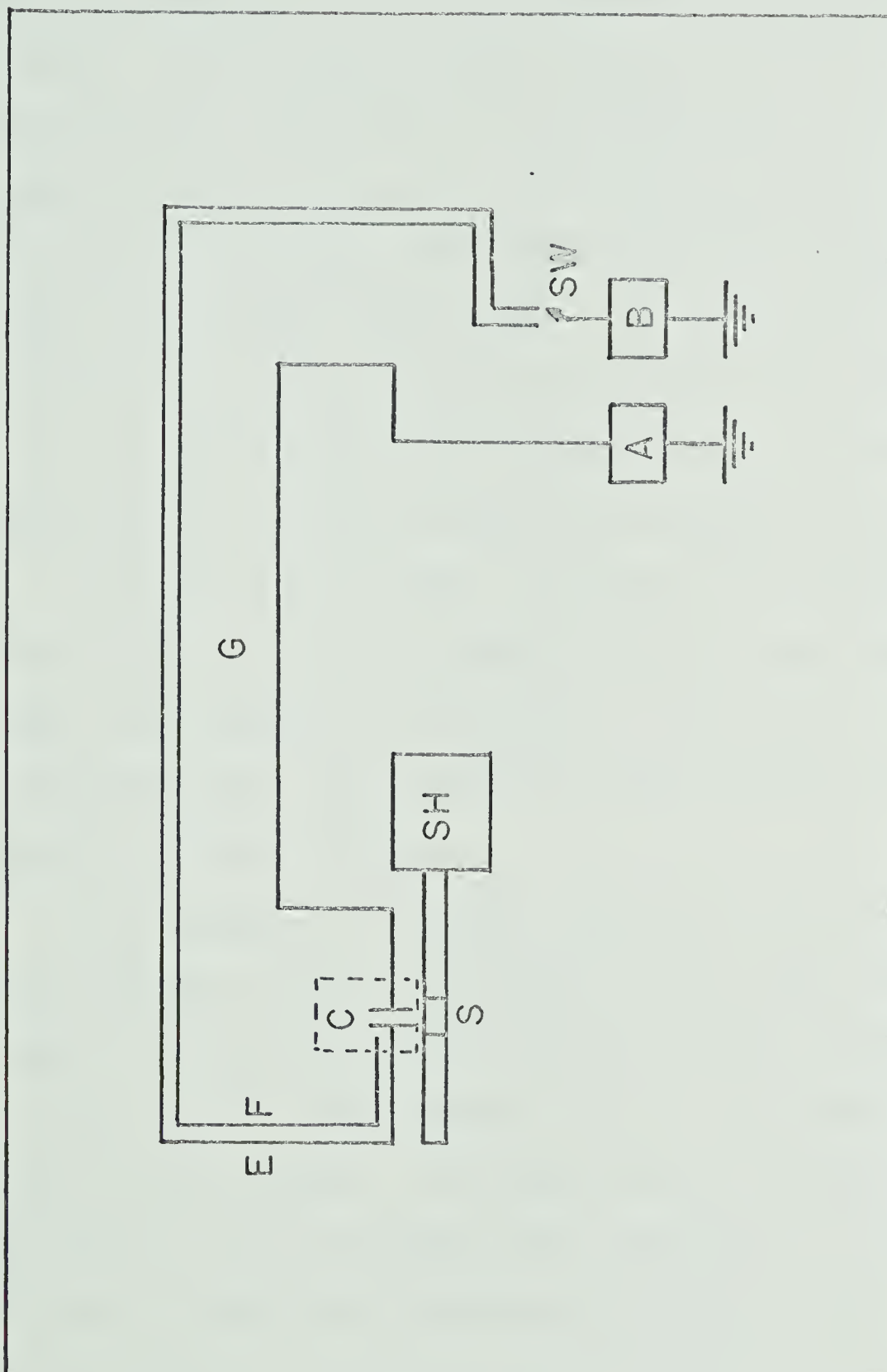
^aElectrode used in conjunction with a guard ring.

^b L/A is the ratio of the electrode separation to the area of the collector electrode.

FIGURE II-H-3

Electrical Circuit for Conductance Measurements in
Radiation Cave

- A. 0 - 1000 volt power supply. Keithly Model 240
- B. Micromicroammeter. Beckman Model 5 or E. H. Laboratories Model 240
- C. Conductance cell (Inside pressure vessel not shown)
- S Radiation source and track
- SH Source housing
- SW Switch
- E Current measuring cable
- F Dummy cable
- G Power cable



between the cable of the circuit. Such currents can be reduced to a negligible level but cannot be completely eliminated. Three coaxial cables (Type RG 8/U) were introduced around the maze of the radiation cave and were about 30 feet in length. Two cables symmetrically spaced about 2 ins apart over their complete length, were used to determine the current. One of these cables terminated just prior to the bellows conductance cell and was used to determine the current arising between the cables of the circuit under the influence of radiation. A third coaxial cable, separated by at least two feet from the current measuring cables, was used to supply the potential to the cell. All three cables were suspended from the ceiling of the radiation cave on lengths of rubber tubing.

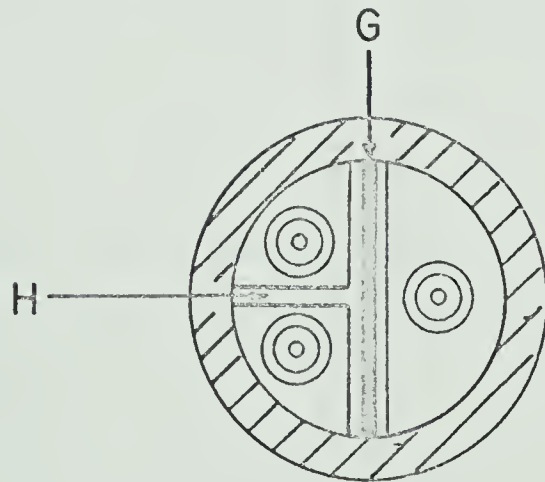
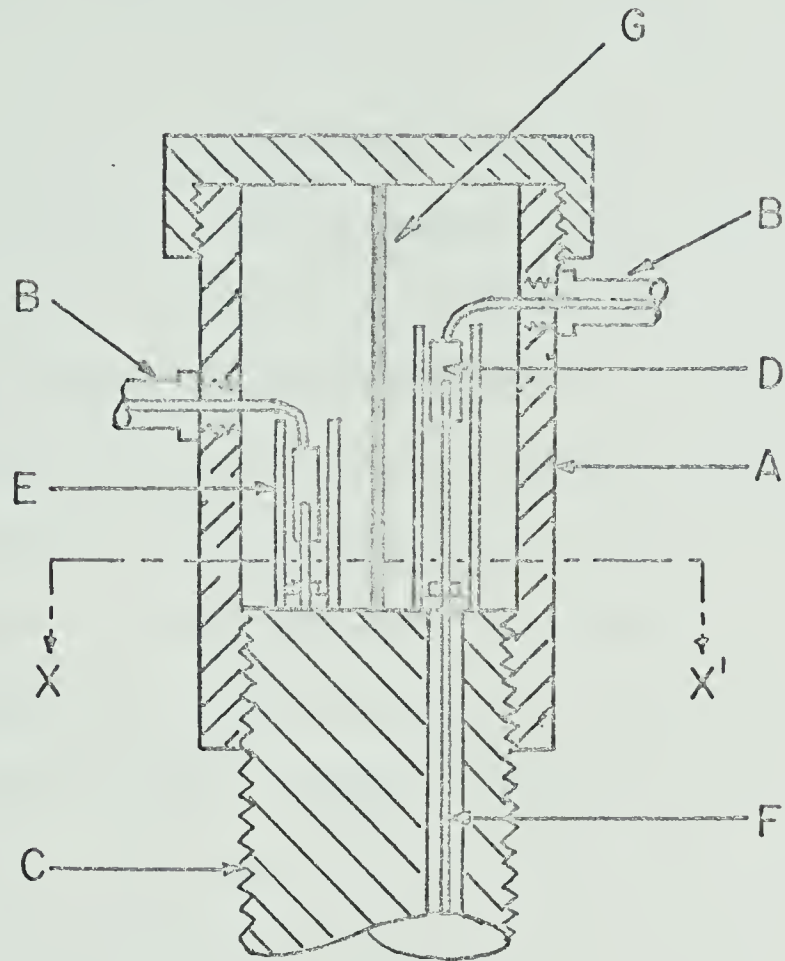
In the absence of special shielding, radiation induced currents between the cables at the point where the cables passed through the pressure vessel closure were large ($\sim 10^{-9}$ amps) because of the unavoidable proximity of the cables. To reduce these currents to a negligible level the cables were connected to the piston head in the manner depicted in Figure II-H-4. A brass cap screwed directly onto the piston shaft and the cables were introduced into the interior of the cap by three BNC silver plated connectors, symmetrically

FIGURE II-H-4

Electrical Connection to the Pressure Vessel Closure

Piston

- A. Brass cap
- B. Silver plated BNC coaxial cable connectors.
- C. Pressure vessel closure piston
- D. Brass sleeves
- E. Polyethylene tubing
- F. Ceramic insulated electrical connections
to the pressure vessel interior
- G. Grounded copper plate.
- H. Rubber sheeting



SECTION ON X-X'

placed at 120° with respect to each other. Interior connections were made with copper wire and soft solder, care being taken to ensure that no cold soldered connections were present. Cold soldered connections (high resistance joints in which the solder has crystallized) introduced contact potentials into the circuit. In order to obtain contact with the central conductor of the electrical leads through the pressure vessel closure piston, it was found to be necessary to silver plate the outer threaded terminals. Connections were made to a brass sleeve screwed directly onto the silver plated thread. All connections within the cap were insulated with polyethylene tubing and a grounded copper plate was placed between the potential and current cables. The interior of the cap was finally filled with the hydraulic fluid. The cables exterior to the pressure vessel were separated by a rubber sheet.

The current was measured with two micromicroammeters, a Beckman Model 5 and an E. H. Laboratories Model 240. The potential was supplied from a Keithley Model 240 variable power supply. The potential, calibrated with a Hewlett Packard digital voltmeter Model 3440A, was consistent with the dial read-out of the power supply to within 1% over the range from 10 to 1000 volts. The ammeters were calibrated with known currents produced by

applying known voltages to calibrated resistors. A series of Victoreen resistors, covering the range from 10^9 to 10^{13} ohms were calibrated using a General Radio megohm bridge (Model 1644-A), which, after calibration by the manufacturer was claimed to be accurate to within 1%. The resistance of megohm resistors is very dependent upon the applied voltage. To cover the complete range of currents required for calibration of the ammeters, the resistors were calibrated with applied potentials from 10 to 100 volts. Table II-H-II contains some typical correction factors determined for the ammeters. The correction factors do not reflect upon the general manufacture of the ammeters but indicate the care which must be taken in the operation of such instruments. Seriously overloading a given current range changed the calibration factor for that range.

(3) Experimental Procedure

The cell components were cleaned using the Soxhlet apparatus described previously ((G) this section). Cells not in immediate use were left in the Soxhlet apparatus and cleaned for several days. If the terminal seals had been replaced in the bellows cap, cells were initially cleaned in boiling water to ensure that all traces of soldering flux were removed. All metal surfaces, apart

TABLE II-H-II .

Some Typical Correction Factors for the Micromicro-
ammeters.

<u>Scale</u>	<u>Instrument</u>	<u>Correction Factor</u>	
1 x 10 ⁻⁸	E-H Laboratories	0.87 ^X	0.89 ^Y
3 x 10 ⁻⁸	"	0.89	0.90
1 x 10 ⁻⁹	"	0.96	1.01
3 x 10 ⁻⁹	"	1.01	1.02
1 x 10 ⁻¹⁰	"	1.02	1.01
3 x 10 ⁻¹⁰	"	1.01	1.02
3 x 10 ⁻⁷	Beckman	1.03	
3 x 10 ⁻⁸	"	1.02	
10 x 10 ⁻⁸	"	1.02	
3 x 10 ⁻⁹	"	1.02	
10 x 10 ⁻⁹	"	1.00	
3 x 10 ⁻¹⁰	"	1.03	
10 x 10 ⁻¹⁰	"	1.03	
3 x 10 ⁻¹¹	"	0.99	

Correction factor - Amps_{meter}/Amps_{true}

X January 1968

Y August 1965

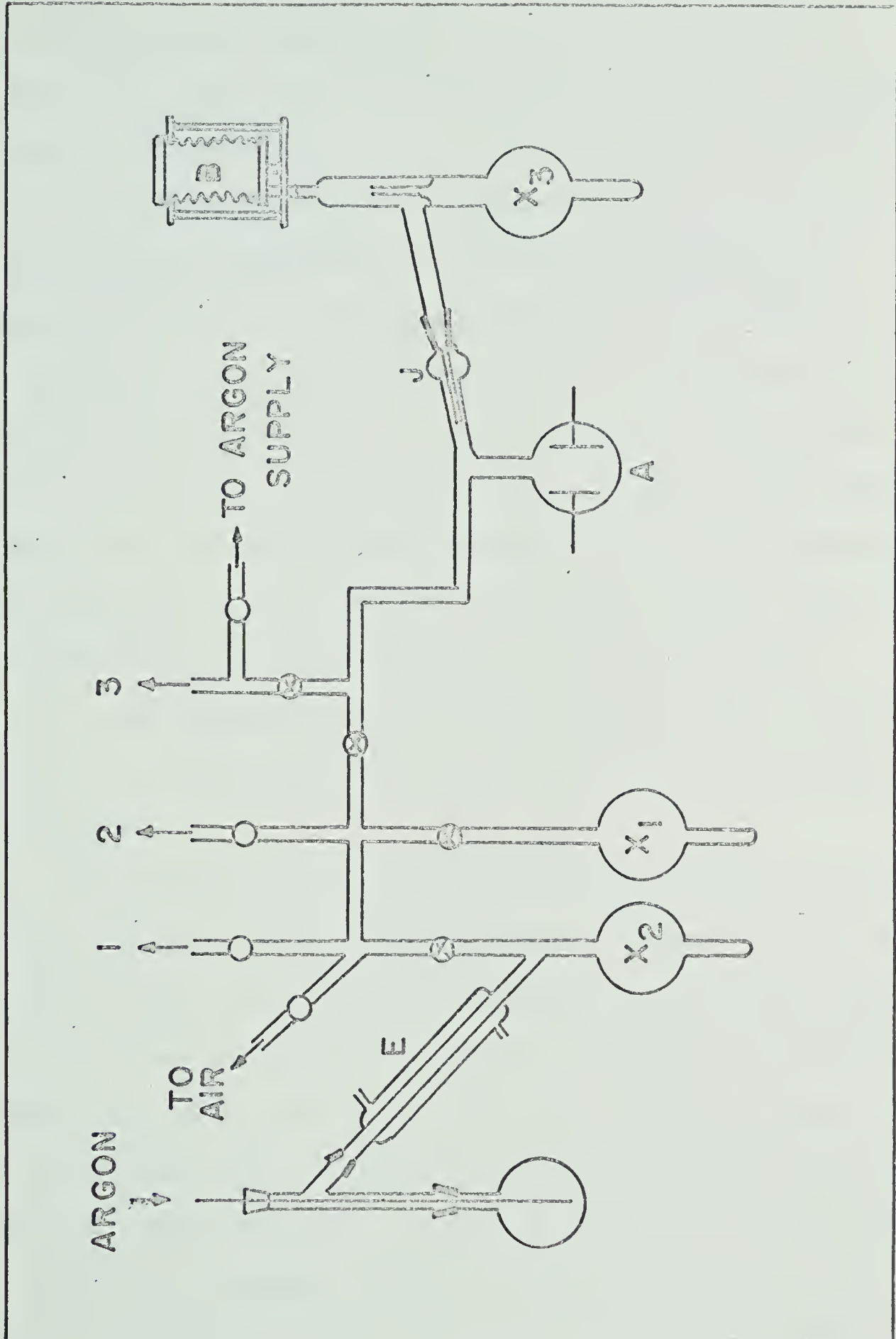
from the bellows interior, that were in contact with the sample were cleaned with an air abrasive unit, prior to the Soxhlet cleaning. Hexane was used as the cleaning solvent. After cleaning, the bellows and cell was assembled and tested for leaks with the helium leak detector. If no leak was apparent the bellows cell was attached to the filling system illustrated in Figure II-H-5. The chemically purified sample (see (B) this section), was either distilled directly into the bulb X1 by trap to trap distillation from the manifold, or distilled into bulb X2 under an atmosphere of argon. Samples introduced by the latter technique were degassed in X2 by the freeze-thaw technique prior to distillation under vacuum into X1. The sample was finally distilled into the bulb X3 and the filling system isolated from the manifold.

Upon thawing, the sample was transferred to the cell for a preliminary washing of the cell. The transfer was accomplished by rotation of bulb X3 and the cell about the extended ground glass 10/30 joint. This procedure was described in (G) of this section. The transfer was facilitated by cooling the metal surface of the bellows. A further rotation of the cell through 180° transferred the sample into the electrolytic cleaning bulb A. The sample was prevented from returning into

FIGURE II-H-5

Conductance Cell Filling System

- $X_1 X_2 X_3$ Bulbs (approximately 200 mls)
- A. Electrolytic cleaning bulb
- B. Bellows cell and holder
- J. 10/30 extended ground-glass joint
- E. Condensor
- ∇∇ Ground glass joints
- O. High vacuum ground glass joints
- ⊗ Greaseless stopcocks (Springham
or Republic)
1. To storage manifold
2. To vacuum manifold
3. To mercury exhaust valve.



the bulb X3 by a pouring spout situated in the neck of the bulb X3. The bulb A contained two platinum electrodes (3.8 cm in diameter and 6.4 cm apart) to which a potential of up to 30 kilovolts could be applied. The potential was supplied by a Spellman High Voltage Company power supply (Model PN-30). The electrolysis of the sample was continued for several hours prior to distilling the sample back into the bulb X3, by cooling the latter bulb in liquid nitrogen. The sample was transferred back into the cell and the conductance determined with the equipment discussed above. The complete cycle was repeated until the conductance of the sample was 10^{-14} mho or less. The cell was removed from the filling system after introduction of an atmosphere of argon, and the sealing screw was inserted.

The filled cell was connected to the face of the pressure vessel closure piston by means of the bracket and a 0.25 in bolt. Electrical connections between the terminals of the bellows cell and the central conductor of the leads through the piston were made with soft soldered copper wire. All connections were insulated with polyethylene tubing and by layers of rubber sheeting. Prior to insertion of the assembly within the pressure vessel, it was connected to the current measuring circuit to ensure that no large contact potentials were present. At least one hour was allowed for the system to attain thermal equilibrium.

The radiation induced current was determined as a function of applied voltage at constant temperature and pressure. The pressure was increased in stages up to about 4500 bars and thirty minutes was allowed before the current determinations after each increase in pressure. The procedure was repeated on the pressure release cycle. The complete cycle was then repeated.

Section III

R E S U L T S

In this section the results obtained for the pressure dependence of the dielectric constant, the density, the viscosity and radiation induced conductance are reported. It is not proposed to discuss the results obtained for the dielectric constant, density and viscosity, at a later time, so a very brief discussion is given under each in the section. All results are reported in relative terms, the standard state (unless otherwise specified) being chosen as one atmosphere pressure (1.0133 bars) and 30°C. A detailed discussion of the radiation induced conductance will be given in a later section.

(A) Pressure Dependence of Dielectric Constant.

The dielectric constants of the hydrocarbons were determined as functions of pressure at 30°C, using the apparatus and experimental technique previously described in Section II-E.

The observed variation in the total capacitance of the system with pressure is shown in Figure III-A-I for several hydrocarbon samples. In some experiments, the total measured capacitance at atmospheric pressure, prior to the application of pressure, was different from the value at atmospheric pressure after the release of

FIGURE III-A-I

Capacitance versus Pressure

Cell P₂, 30°C

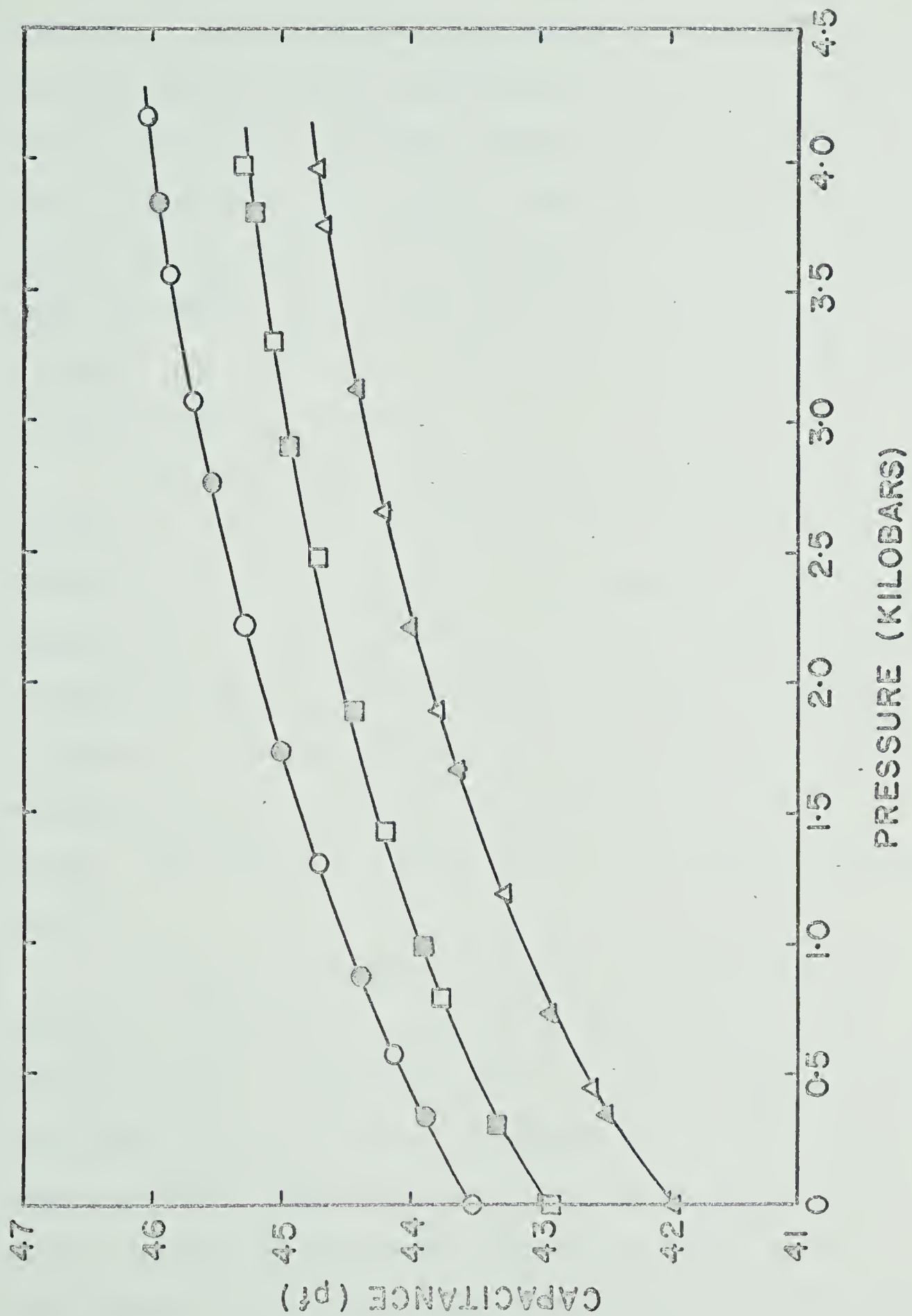
O Methylcyclohexane

□ n-octane

Δ n-hexane

open points pressure increasing cycle

closed points pressure decreasing cycle



pressure. The difference never amounted to more than 0.5%, except in the case where carbon tetrachloride was investigated. The latter compound underwent solidification at about 1500 bars at 30°C, which resulted in permanent distortion of the cell. If the capacitance values at atmospheric pressure, before and after the application of pressure, were different, the cell was recalibrated and the investigation repeated.

The capacitance determined immediately after an increase of pressure was usually higher than the value determined after an elapse of about twenty minutes of the new pressure. This effect results from a slight decrease in pressure which was always observed after an increase in pressure. The equilibrium pressure was reached after a shorter period of time if the pressure was raised slowly. The effect was reversed on the pressure decreasing cycle.

Attempts to detect a change of temperature accompanying an increase or decrease of the pressure within the pressure vessel were unsuccessful. In the present system, the temperature would have to change by at least 5°C before an effect would be observed on the measured capacitance, because of the small temperature dependence of the dielectric constant of the hydrocarbons (Table II-E-II).

The total capacitance of the system, measured at

500 bar increments of pressure up to a maximum of 4000 bars, was obtained from the smooth curve drawn through the points of the plot of observed capacitance versus experimental pressure (Figure III-A-1). The capacitance values were converted to dielectric constants by direct reference to a calibration graph, an example, of which was given in Figure II-E-2. The values reported are the average of at least two determinations. The reproducibility in the dielectric constant from experiment to experiment was within 0.5%.

The relative dielectric constant at 500 bar intervals of pressure are recorded in Table III-A-1 for n-pentane, n-hexane and n-octane. The pressure dependence of the relative dielectric constant for these hydrocarbons is illustrated in Figure III-A-2. The relative dielectric constant of pentane, calculated from the results of Danforth (117) after adjustment from pressures reported in atmospheres, is also shown as a function of pressure in Figure III-A-2. The present results are in good agreement with those of Danforth (117). A similar comparison for hexane using the data of Mopsik (126) is also illustrated. The present results were obtained at 30°C, whilst those of Mopsik refer to 25°C. The absolute agreement between the two sets of results is quite satisfactory, but is not as close as Figure III-A-2

TABLE III-A-I

Relative Dielectric Constants at 30°C

<u>Pressure (Bars)</u>	<u>Compound</u>		
	<u>n-Pentane</u>	<u>n-Hexane</u>	<u>n-Octane</u>
1	1.000	1.000	1.000
500	1.045	1.036	1.026
1000	1.074	1.060	1.047
1500	1.096	1.078	1.064
2000	1.114	1.094	1.077
2500	1.129	1.107	1.087
3000	1.142	1.118	1.096
3500	1.153	1.129	1.106
4000	1.163	1.138	1.113
<hr/>			
	$\epsilon^{30^\circ\text{C}^a}_{1 \text{ atm}} = 1.812$	$\epsilon^{30^a}_{1 \text{ atm}} = 1.872$	$\epsilon^{30^a}_{1 \text{ atm}} = 1.940$

1 atmosphere - 1.0133 Bars

^a Values calculated from temperature dependence of ϵ and values of ϵ given in Table II-E-II.

FIGURE III-A-2

Relative Dielectric Constant versus Pressure

n-pentane, n-hexane and n-octane 30°C

I n-pentane

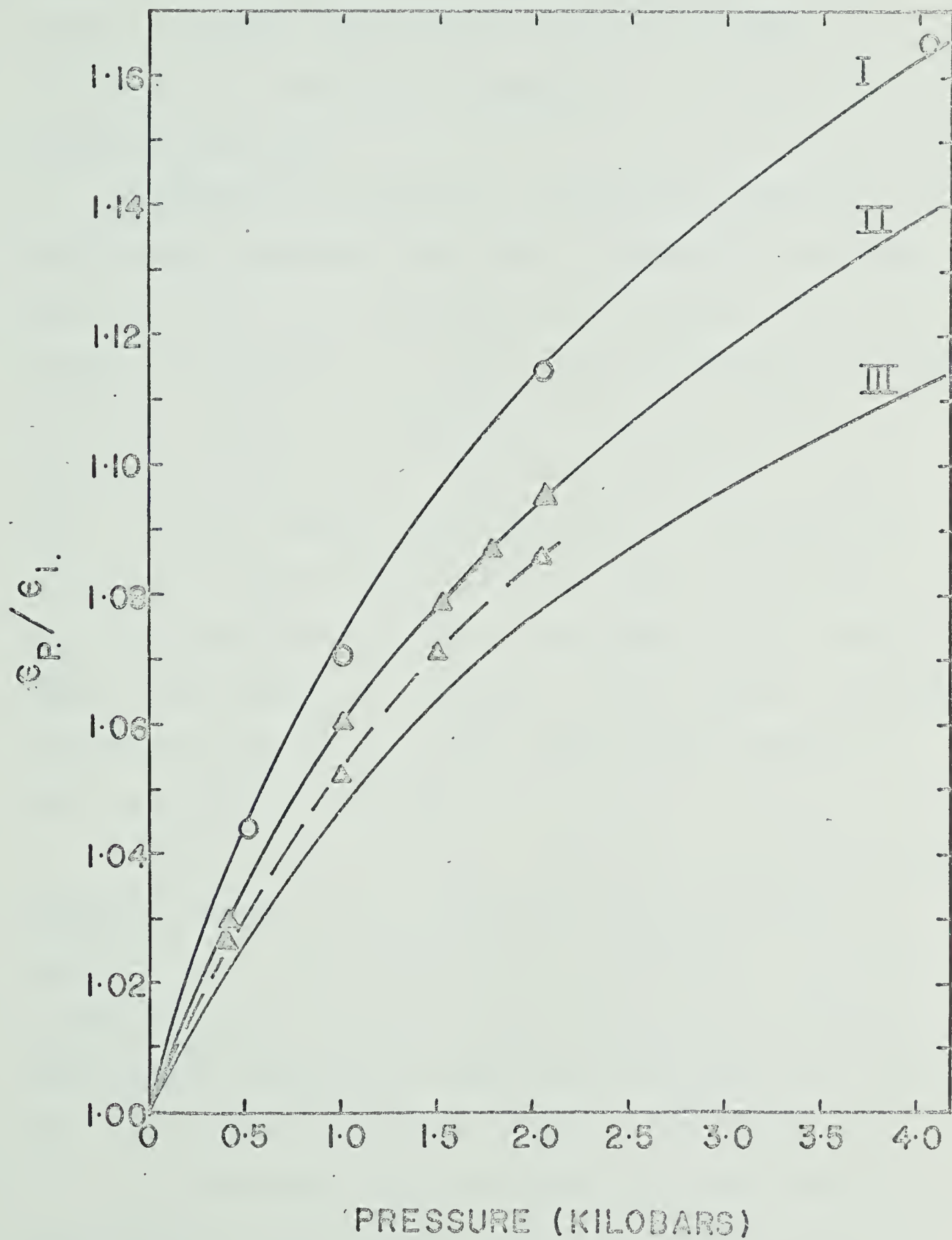
II n-hexane solid lines, present
work

III n-octane

O n-pentane 30°C W.E. Danforth (117)

A n-hexane 25°C F.I. Mopsik (126)

Δ n-hexane 0°C F.I. Mopsik (126)



suggests because of the temperature difference. The results of Mopsik (126) at 0°C are also included to illustrate the temperature dependence of the relative dielectric constant.

The present results for n-hexane are also in satisfactory agreement with those of Chang for the same compound (127). As was pointed out by Mopsik (126) although the limited data on the pressure dependence of the dielectric constant generally parallel one another, systematic differences in the absolute values are present. In the present work knowledge of the amount of variation of the dielectric constant with pressure is more important than an accurate knowledge of the absolute value of the dielectric constant. To the author's knowledge, comparative data for the other hydrocarbons studied in this work are not available.

The relative dielectric constants for cyclopentane, methylcyclohexane and 2,2-dimethylbutane are given in Table III-A-II and their pressure dependence is illustrated in Figure III-A-3. Table III-A-II also contains some values obtained for carbon tetrachloride up to 1500 bars (the freezing pressure at 30°C is 1470 bars (128)).

For non-polar liquids, such as the hydrocarbons investigated in the present work, the molecular polarization of the liquid is generally related to the dielectric

TABLE III-A-II

Relative Dielectric Constant at 30°C

Pressure (Bars)	<u>Compound</u>			
	Methylcyclo- hexane	Cyclopentane	2,2-Dimethyl- butane	Carbon tet- rachloride
1	1.000	1.000	1.000	1.000
500	1.028	1.037	1.039	1.034
1000	1.047	1.060	1.068	1.055
1500	1.063	1.079	1.087	1.069 ^c
2000	1.074	1.094	1.102	-----
2500	1.089	1.108	1.116	-----
3000	1.099	1.121	1.128	-----
3500	1.108	1.133	1.139	-----
4000	1.116	1.144	1.149	-----
<hr/>				
	$\epsilon^{30^\circ\text{C}^a}=2.004$ 1 atm	$\epsilon^{30^\circ\text{C}^a}=1.968$ 1 atm	$\epsilon^{30^\circ\text{C}^b}=1.857$ 1 atm	$\epsilon^{30^\circ\text{C}^a}=2.220$ 1 atm

^a Values calculated for temperature dependence of ϵ and values of ϵ given in Table II-E-II

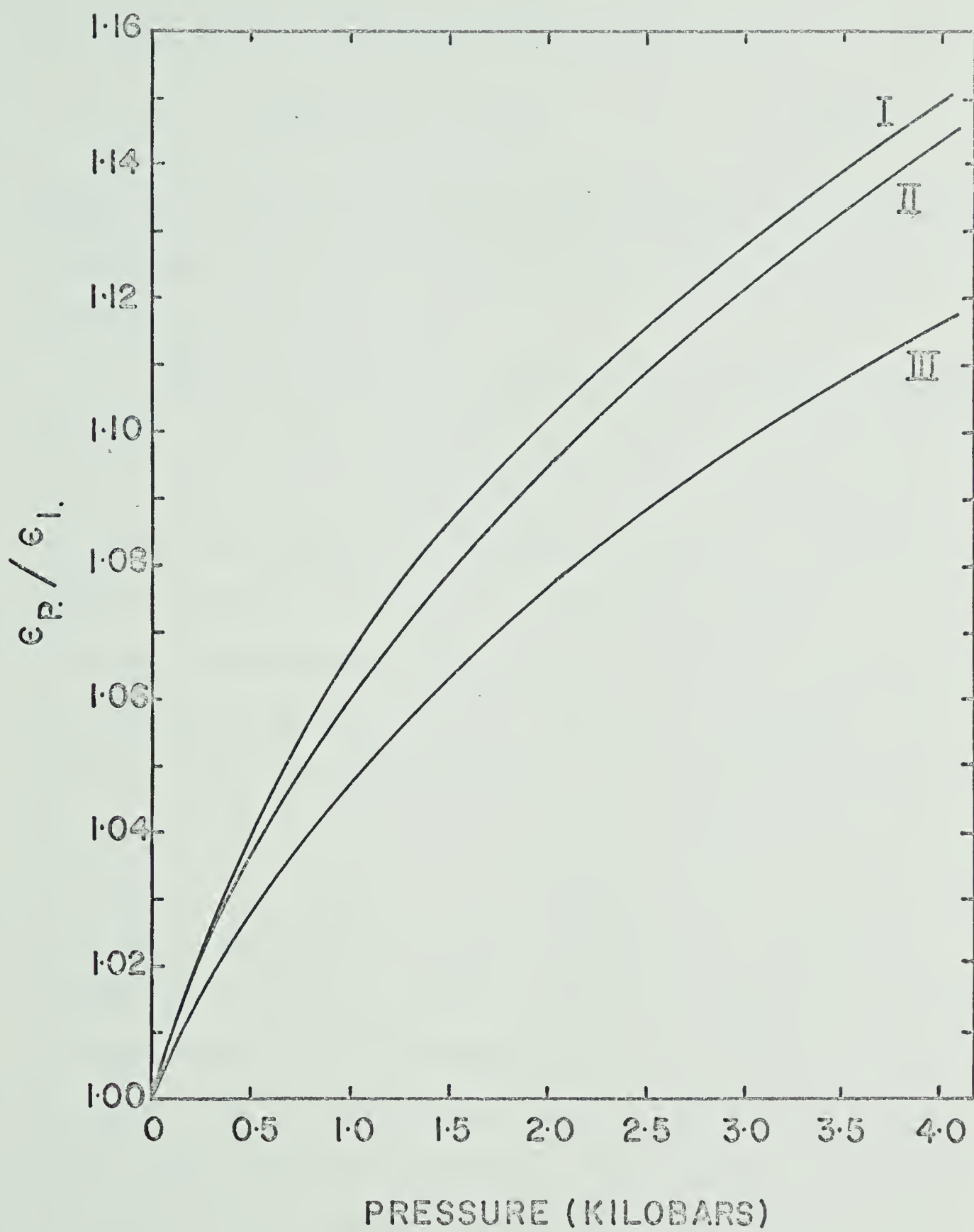
^b Calculated from refractive index square

^c Freezes at 1473 bars at 30°C (128)

FIGURE III-A-3

Relative Dielectric Constant versus Pressure

- I 2,2-dimethylbutane 30°C
- II Cyclopentane 30°C
- III Methylcyclohexane 30°C



constant of the liquid by the equation (129)

$$\frac{\epsilon - 1}{\epsilon + 2} V = \frac{4}{3} \pi N \alpha \quad (\text{III-i})$$

where V is the molar volume of the liquid, ϵ is the static dielectric constant, N is Avogadro's number and α is the molecular polarizability.

Equation (III-i) is identical to the general Debye equation (130) for all liquids the term for the orientation contribution to the polarization having been removed because of the absence of a permanent dipole. The left hand side of equation (III-i) is generally referred to as the Clausius Mossotti function. Equation (III-i) predicts that if the polarizability of the liquid is independent of density (and therefore pressure), the Clausius Mossotti function (CM) should be constant and independent of the density of the liquid. The variation of the CM with density is illustrated in Figure III-A-4 for n-pentane, n-hexane and n-octane. Similar plots for methylcyclohexane, cyclopentane and 2,2-dimethylbutane are shown in Figure III-A-5. The CM function is found to decrease, in all cases, with increasing density. The scatter in the data is greater for n-pentane and cyclopentane than for the higher boiling hydrocarbons. The observed reduction in the CM function with increasing density (and pressure) is consistent with other observations reported in the liter-

FIGURE III-A-4

Clausius Mossotti Function versus Density 30°C

▲ n-pentane

○ n-hexane

□ n-octane

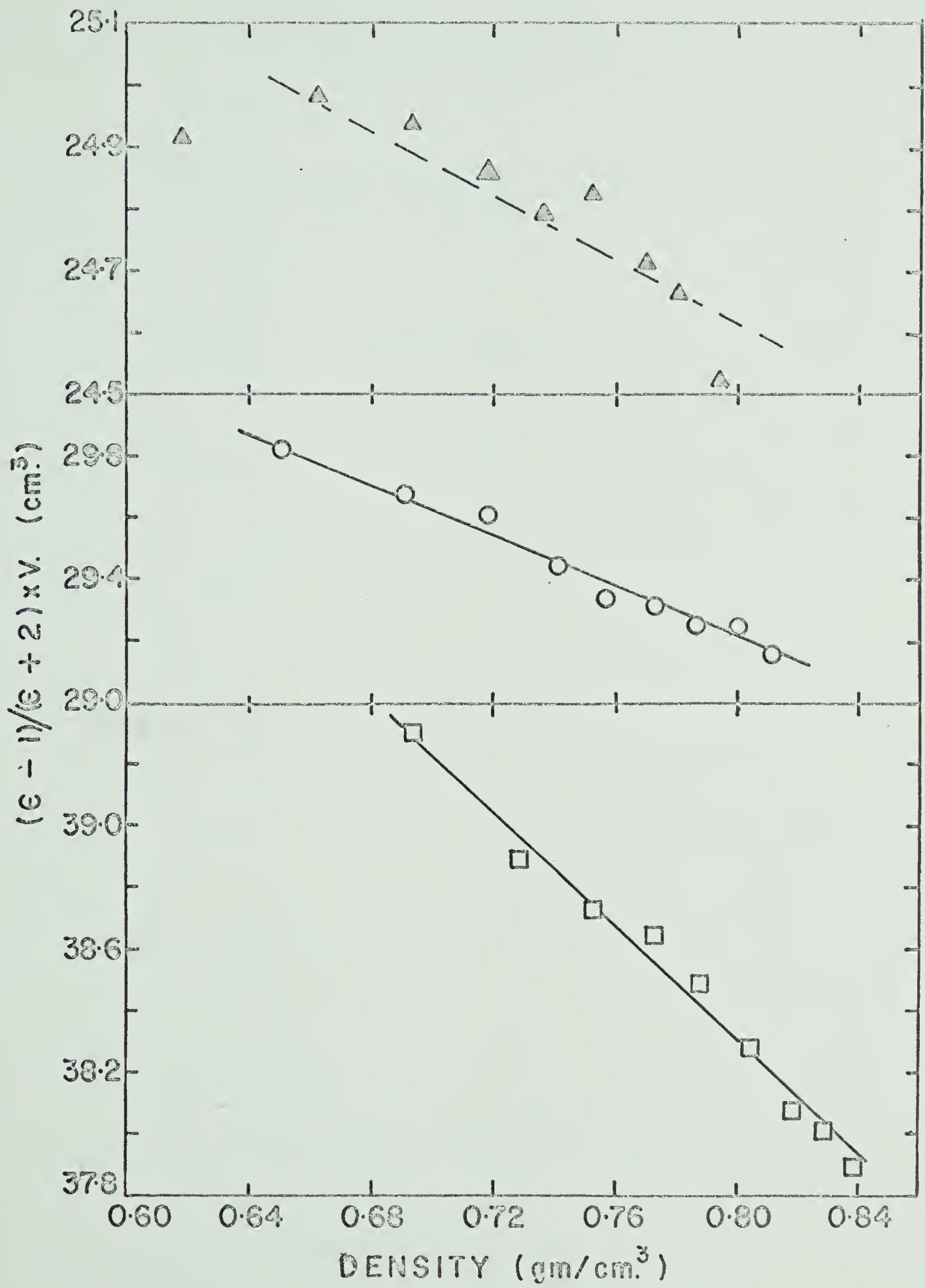


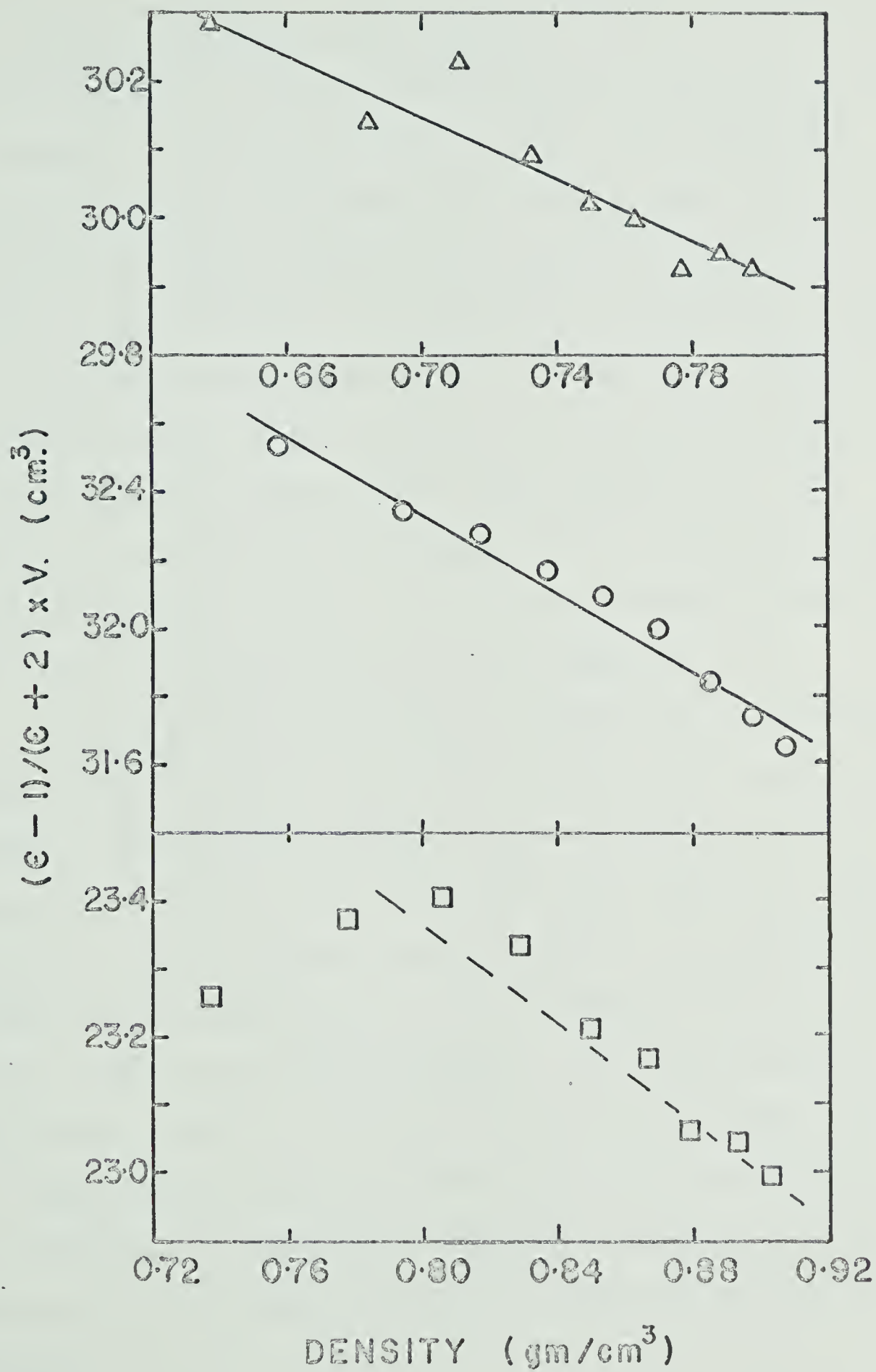
FIGURE III-A-5

Clausius Mossotti Function versus Density 30°C

Δ Cyclopentane

O Methylcyclohexane

\square 2,2-dimethylbutane



ature (116,117,126,131). The non-consistency of the CM function has led to the general validity of equation (III-i) at increased densities being questioned. Two possibilities have been generally suggested, namely, that the form of the CM function is incorrect at high densities, or that the polarizability of the molecules is pressure dependent. Some recent investigations by Mopsik (126) indicated the possibility of hexane having a small permanent dipole, which, if correct, would require the addition of a term to the right hand side of equation (III-i), yielding the general Debye equation (130). No alternative and satisfactory form of the CM function has yet been suggested.

The possibility that the polarizability is pressure dependent has received some attention, but only in the case of gases. As long ago as 1936, Kirkwood (132) concluded that equation (III-i) was strictly valid only for a perfect gas. The CM function has been found to be independent of pressure for hydrogen (133) and nitrogen (134) at least up to a pressure of 1000 atmospheres. The function for argon (134), however, and for several organic gases (136, 137) exhibits an initial increase with pressure followed by a decrease. Theoretical calculations (138) for argon indicate that the polarizability of argon may be pressure dependent.

(B) Pressure Dependence of Density

The pressure-volume relationship was determined at 30°C for all the hydrocarbons (except 2,2-dimethylbutane, for which Bridgman's (121) data were used) used in the radiation induced conductance investigations. The potential ratio was determined as a function of pressure up to a maximum pressure of 4500 bars. The values of the potential ratio at one atmosphere before the application of pressure and after the release of pressure generally agreed to within 0.1%. No hysteresis was ever apparent. The change in the potential ratio with pressure was converted to the change in volume using calibration curves, typical examples of which were given in Figures II-F-4 and II-F-5. The reported relative values are the average of at least two determinations. The reproducibility in relative volume from experiment to experiment was about 0.002 (approximately 0.25% of the actual relative volume depending upon the sample) at 4000 bars and was better than 0.002 at lower pressures.

The relative volumes of n-pentane and n-hexane, and the corresponding calculated densities are given in Table III-B-I and are illustrated in Figure III-B-I. The values at 500 bar increments of pressure were obtained by plotting the measured relative volume against the

TABLE III-B-I

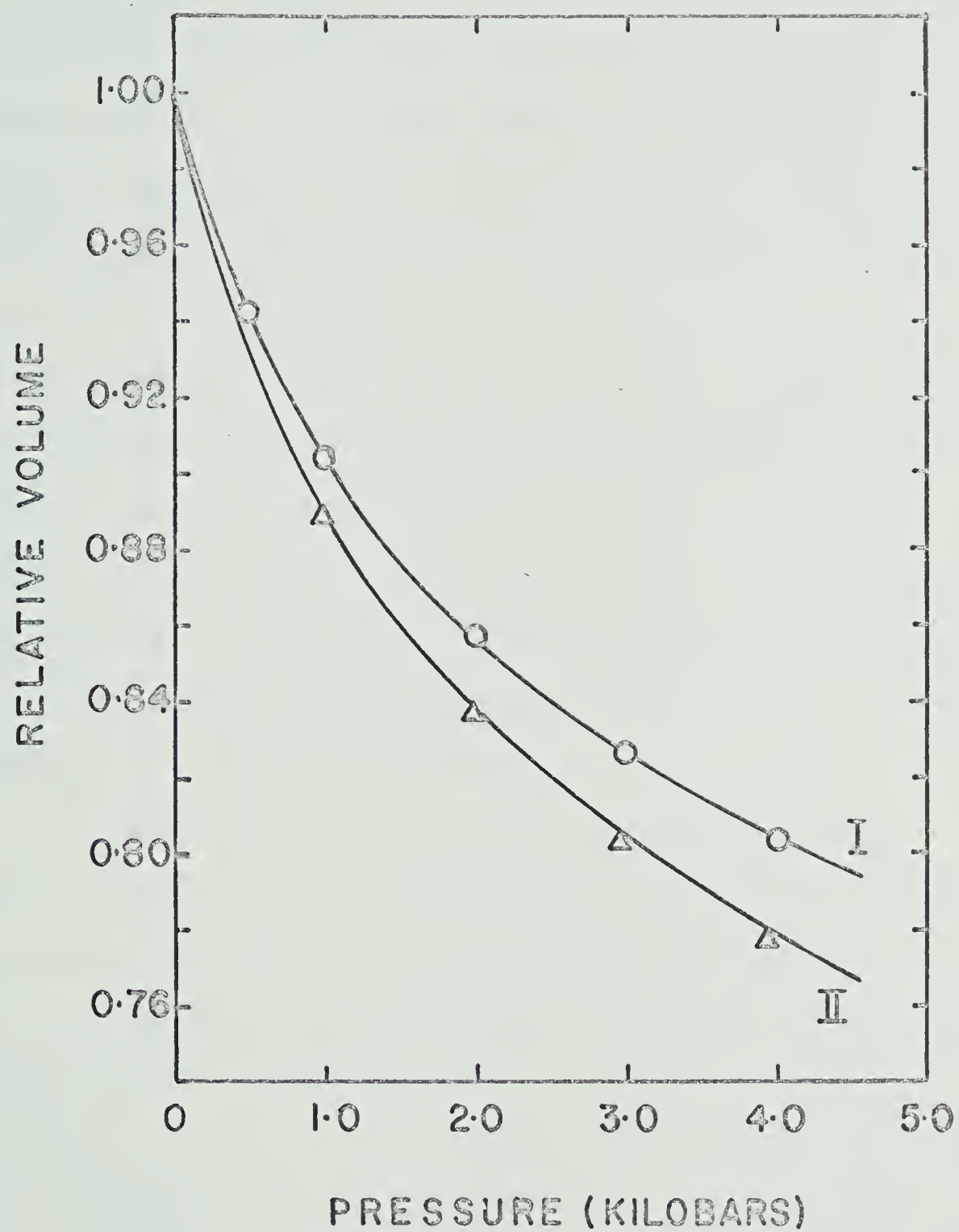
Relative Volume and Density of Pentane and Hexane at 30°C

Pressure Bars	n-Pentane		n-Hexane	
	Relative Volume	Density gm/cm ³	Relative Volume	Density gm/cm ³
1	1.000	0.6165	1.000	0.6505
500	0.930	0.6629	0.941	0.6912
1000	0.889	0.6934	0.905	0.7188
1500	0.859	0.7176	0.877	0.7409
2000	0.836	0.7374	0.858	0.7581
2500	0.821	0.7509	0.841	0.7734
3000	0.804	0.7667	0.826	0.7865
3500	0.791	0.7793	0.814	0.7991
4000	0.778	0.7924	0.803	0.8101
4500	0.767	0.8037	0.796	0.8172
Molar Volume (30°C 1 atm)		Molar Volume (30°C 1 atm)		
= 117.03 cm ³		= 132.46 cm ³		
Molecular Weight - 72.15		Molecular weight - 86.17		

FIGURE III-B-I

Relative Volume versus Pressure

- I n-Hexane full line, present results 30°C
- II n-Pentane full line, present results 30°C
- O n-Hexane values interpolated from data
 at 0, 25, 45 and 60°C (121)
- Δ n-Pentane values interpolated from data
 at 0, 50 and 95°C (121).



experimental pressure, drawing a smooth curve through the points, and reading the values at the desired pressure directly from the curve. The relative volume of n-pentane at 30°C, estimated graphically from the results of Bridgman (121) at 0, 50 and 95 C after correction from pressure units of kg cm^{-2} are also shown in Figure III-B-I.

The present values for n-pentane are somewhat higher than the values estimated from Bridgman's data the discrepancy amounting to about 1% at 4000 bars and less at lower pressures. A similar comparison for n-hexane, using the data of Bridgman (121) and Eduljee, Newitt and Weale (123) is also illustrated in Figure III-B-I. The agreement is quite satisfactory.

The relative volumes and densities of n-octane, methylcyclohexane and cyclopentane at 500 bar increments of pressure up to 4500 bars are listed in Table III-B-II and illustrated in Figure III-B-2. Comparative data for octane at 30°C, estimated from the results of Eduljee et al. (123) at 0, 25, 40 and 60°C after adjustment from pressures reported in atmospheres, are also shown. The agreement is excellent. No comparative data are available for methylcyclohexane or cyclopentane. Bridgman (139) has studied methylcyclohexane but did not report the temperature of his relative volume measurements other

TABLE III-B-II

Relative Volume and Density of n-Octane, Methylcyclohexane and Cyclopentane at 30°

n-Octane			Methylcyclohexane		Cyclopentane	
Pressure	Relative	Density	Relative	Density	Relative	Density
Bars	Volume	gm/cm ³	Volume	gm/cm ³	Volume	gm/cm ³
1	1.000	0.6942	1.000	0.7606	1.000	0.7357
500	0.953	0.7284	0.956	0.7956	0.947	0.7768
1000	0.921	0.7537	0.928	0.8196	0.914	0.8049
1500	0.898	0.7730	0.906	0.8395	0.888	0.8284
2000	0.879	0.7897	0.888	0.8565	0.867	0.8485
2500	0.863	0.8044	0.872	0.8722	0.850	0.8655
3000	0.848	0.8186	0.858	0.8865	0.837	0.8789
3500	0.837	0.8293	0.846	0.8991	0.825	0.8917
4000	0.827	0.8394	0.836	0.9098	0.815	0.9026
4500	-----	-----	0.828	0.9186	0.807	0.9116

Molar Volume
(30°C 1 atm) 164.53 cm³
Molecular weight 114.22

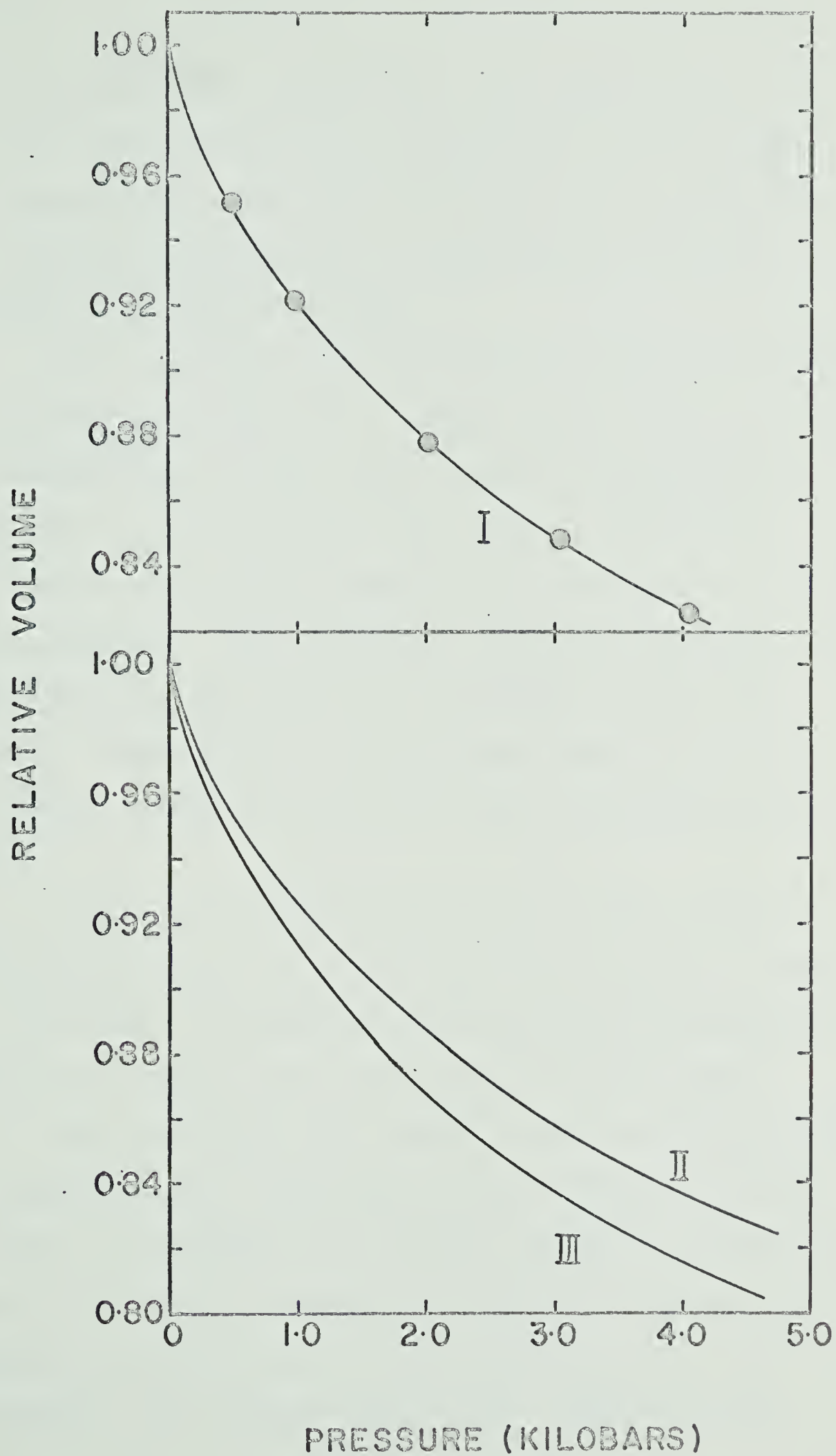
Molar Volume
(30°C 1 atm) 129.08 cm³
Molecular weight 98.182

Molar Volume
(30°C 1 atm) 95.32 cm³
Molecular weight 70.130

FIGURE III-B-2

Relative Volume versus Pressure

- I Octane 30°C full line Present results
- Values interpolated from data at 0, 25,
 40 and 60 (123)
- II Methylcyclohexane 30°C - Present results
- III Cyclopentane 30°C - Present results



than that they were obtained at room temperature. If this was approximately 25°C, the results of his study and the present study are in good agreement, assuming the temperature dependence of the relative volume to be similar to that of octane .

The pressure dependence of the density of hexane and octane were required at temperatures other than 30°C. The present data at 30°C and the data of Eduljee et al. (123) at 0, 25, 40 and 60C were used to construct a plot of the variation of density with temperature at constant pressure. The calculated variations are shown in Figure III-B-3 for hexane and in Figure III-B-4 for octane. The density at the required temperature and at 500 bar intervals of pressure were obtained from the plots.

Table III-B-III contains the relative volume of 2,2-dimethylbutane calculated from the results of Bridgman, at several pressures, and some results obtained on some other liquids during the course of this study.

Cyclopentanone was studied because of its relevance to another project undertaken in this laboratory (140). Attempts to determine the freezing pressure of cyclopentanone at 25°C (the experimental temperature of the results reported in Table III-B-III for cyclopentanone) were unsuccessful. The sample froze if the temperature was

FIGURE III-B-3

Temperature Dependence of Hexane Density
at Constant Pressure

- O Present results 30°C
- Δ Eduljee, Newitt and Weale (123) 0,
40 and 60°C
- P. W. Bridgman (121) 50°C

Pressure in kilobars.

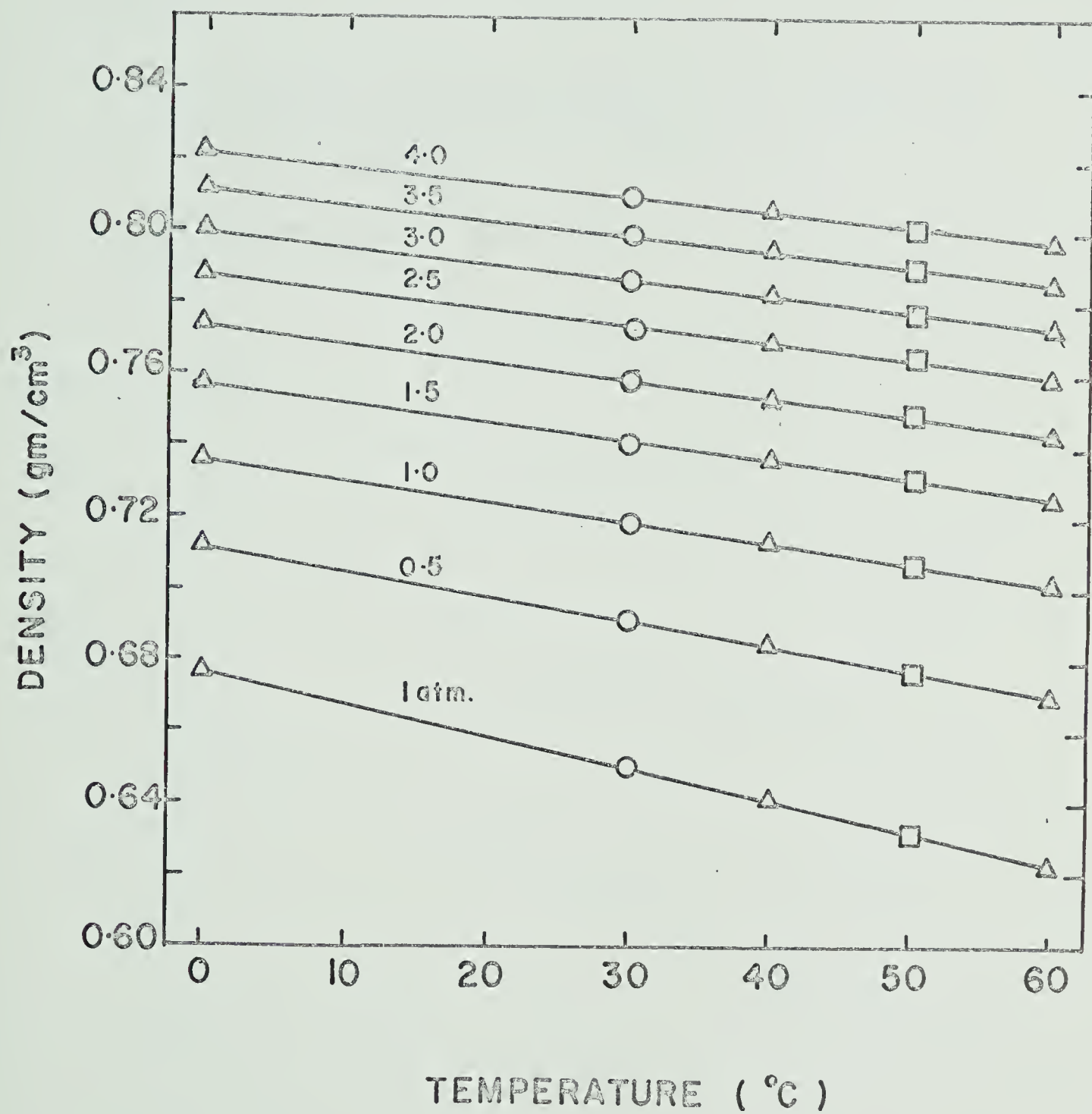


FIGURE III-B-4

Temperature Dependence of n-Octane Density
at Constant Pressure

O Present results 30°C

Δ Eduljee, Newitt and Weale (123)
0, 25, 40 and 60°C.

Pressure in kilobars.

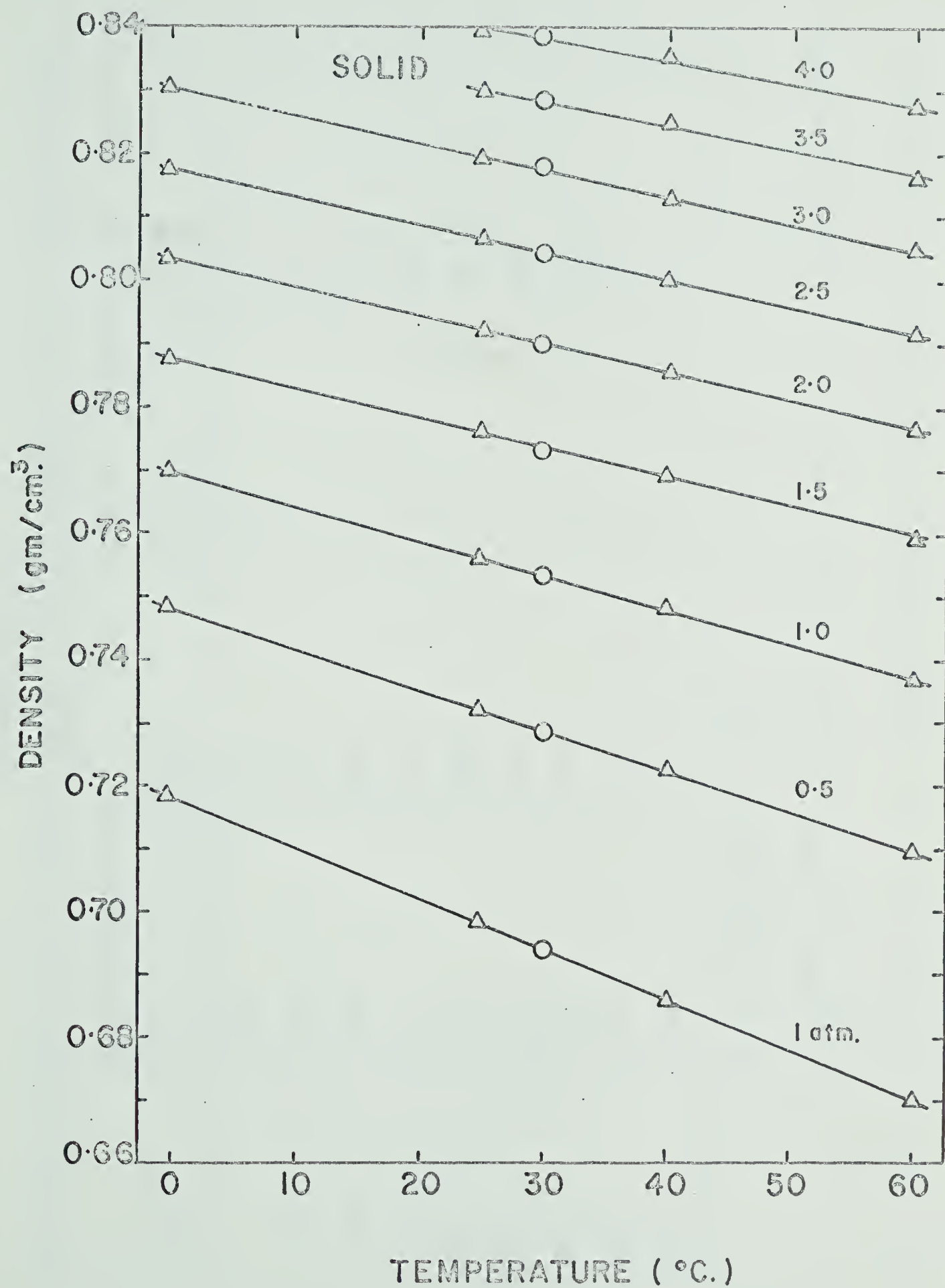


TABLE III-B-III

Relative Volume of 2,2-Dimethylbutane, Heptane, Diethyl ether, Cyclopentanone at 30°C

Pressure Bars	2,2-Dimethylbutane ^b		Heptane		Diethyl ether		Cyclopentanone ^a	
	Relative Volume	Density gm/cm ³	Relative Volume	Relative Volume	Relative Volume	Relative Volume	Relative Volume	Relative Volume
1	1.000	0.6397	1.000	1.000	1.000	1.000	1.000	1.000
500	0.935	0.6841	0.945	0.939	0.939	0.964	0.964	0.964
1000	0.900	0.7108	0.909	0.893	0.893	0.938	0.938	0.938
1500	0.872	0.7336	0.882	0.866	0.866	0.899	0.899	0.899
2000	0.853	0.7499	0.863	0.842	0.842	0.884	0.884	0.884
2500	0.837	0.7642	0.848	0.824	0.824	0.872	0.872	0.872
3000	0.823	0.7772	0.834	0.811	0.811	0.860	0.860	0.860
3500	0.812	0.7878	0.823	0.799	0.799	0.850	0.850	0.850
4000	0.802	0.7976	0.813	0.786	0.786	0.841	0.841	0.841

Molar Volume 30°C 1 atm
= 134.70 cm³

Molecular weight = 86.14

(a) Values at 25°C

(b) Bridgman's Data (121) 30°C values calculated from data at 0, 50 and 95°C.

lowered to about 20°C after increasing the pressure to about 3500 bars, however the rapid change in volume associated with the change of state resulted in distortion of the dilatometer slide wire. It is possible that the values reported for cyclopentanone at the higher pressures refer to the liquid state in excess of its freezing pressure.

The results obtained for the various hydrocarbons studied require little comment. They all fit into the general pattern observed by Bridgman (93) that most organic compounds decrease in volume by between 15% and 25% on increasing the pressure to 4000 bars. The compressibility (defined as $-\frac{1}{V} \frac{\partial V}{\partial P}$) where V is the volume and P is the pressure decreases as the pressure increases.

(C) Pressure Dependence of Viscosity.

(1) Calibration

The system of a ball rolling within an enclosed tube was first suggested for use as a viscometer by Flowers (141) in 1914 and first applied to higher pressure viscometric determinations in 1928 (142). The variables of the system are generally correlated by the equation

$$\eta = \frac{C(\rho_S - \rho_L)}{V} \quad \text{(III-ii)}$$

where η is the viscosity in poise (gm/cm sec) of the medium

in which the ball is rolling, ρ_S and ρ_L are the densities (gm/ml) of the ball material and the medium, respectively, V is the velocity (cm/sec) of the ball and C is a coefficient which is usually determined by experiment with liquids of known viscosity and density.

The general form of the above calibrating equation has been obtained both from dimensional analysis (125,143) of the system and by the application of a modified form of Stokes Law to include the rotational motion of the ball (144). In the present investigations, the distance that the ball rolls was maintained constant from investigation to investigation and the calibration equation was used in the form

$$\eta = K(\rho_S - \rho_L)T \quad (\text{III-iii})$$

where T is the time, in seconds, required for the ball to roll the fixed distance. The new viscometer coefficient K is simply the old coefficient C divided by the fixed distance.

The viscometer was calibrated at atmospheric pressure, using a series of standards of known viscosity and density (see Tables II-G-III and II-G-IV). All hydrocarbons investigated were also used as standards at one atmosphere pressure the viscosity at atmospheric pressure being either determined with an Ubbelohde viscometer or taken from

the literature (section II-G). Two angles of inclination of the roll tube were used which corresponded to a tilt of approximately 20.5 and 30.5 degrees from the horizontal. The angles of inclination, hereafter referred to as angle I ($\sim 20.5^\circ$) and angle II ($\sim 30.5^\circ$), were not known with great accuracy, but they were accurately reproducible.

The roll time was determined at each angle over the temperature range, 0 to 60°C , except in cases where the freezing temperature or the boiling point of the sample was reached. Figure III-C-I illustrates the variation of roll time with temperature and angle of inclination for several hydrocarbons. The scatter in the measured roll times never exceeded 0.3% provided the timing circuit was correctly tuned (see Section II-G). The roll time was reproducible from sample to sample to within 0.2% under the same experimental conditions.

No attempt was made to adjust the temperature to exactly the required value because this process was found to be tedious owing to the long period of time required for the system to equilibrate after a temperature change. The roll time at the required temperature was obtained from the plots of roll time against experimental temperature. Fewer values of the roll times were determined for temperatures below 10°C because of either the sample freezing or the viscosity increasing rapidly outside the

FIGURE III-C-1

Roll Time versus Temperature. Hydrocarbons

Δ n-Tetradecane Angle I

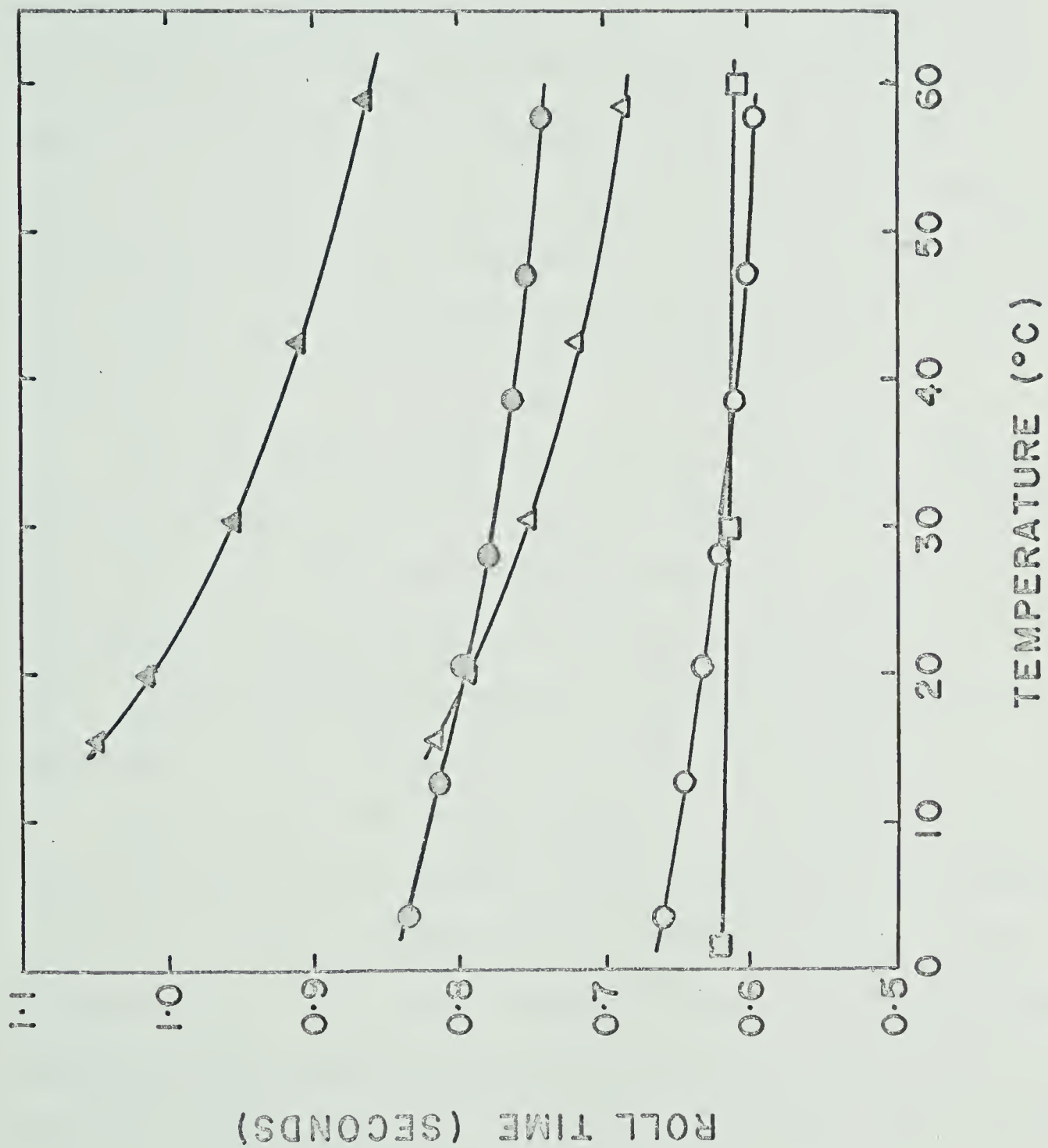
Δ n-Tetradecane Angle II

● Methylcyclohexane Angle I

○ Methylcyclohexane Angle II

□ n-Hexane Angle I

Atmospheric pressure.



range of interest as the temperature was lowered.

The value of the $(\rho_S - \rho_L) T$ term of the calibrating equation was calculated at 0, 30 and 60°C, using the graphically interpolated roll times and the density of the sample at the temperature of the interpolated roll time. The density of the steel ball (7.7733 gm/cm³ at 25°C) was corrected for use at other temperatures taking the thermal expansion coefficient of steel to be 11×10^{-6} per C (145). The total correction between 0 and 60°C amounts to about 0.07%

The calculated values of $(\rho_S - \rho_L) T$ for both angles of inclination at 0, 30 and 60°C are listed in Tables III-C-I and III-C-II. The viscosity dependence of $(\rho_S - \rho_L) T$ is illustrated in Figure III-C-2 for both angles I and II at 30°C. The viscosity is actually plotted in terms of the logarithm of the viscosity expressed in millipoise.

The straight chain hydrocarbons, the standard oils (a mixture of high molecular weight straight chain hydrocarbons) and the silicone oils with a viscosity of 5 cP or greater all fall upon a smooth curve. The cyclic hydrocarbons, methylcyclohexane and cyclopentane and the silicone oil with a viscosity of 1.82 cP at 30°C, fall below the straight chain hydrocarbon curve.

The cause of the difference observed in the calibration points obtained with different types of compounds is un-

TABLE III-C-I

$(\rho_S - \rho_L) \times T$ at Various Temperatures. Atmospheric Pressure				
Compound	$(\rho_S - \rho_L) \times RT$	gm sec/cm ³		
		0°C	30°C	angle 1 ($\sim 20^\circ$) 60°C
n-Pentane	-		4.575	-
n-Hexane	4.866		4.672	4.486
n-Octane	5.431		5.097	4.846
n-Decane	6.051		5.535	5.172
n-Dodecane	7.224		6.130	5.572
n-Tetradecane	7.347*		6.715	6.038
n-Octadecane	-		8.401	6.875
2,2-Dimethylbutane	-		4.879	-
Methylcyclohexane	5.875		5.470	5.204
Cyclopentane	-		5.116	-
S-3-65-1c	-		7.655	6.506
S-6-57-2E	14.93		10.93	7.761
2 cts	-		6.790	-
5 cts	12.32		9.180	7.706
10 cts	15.10†		11.85	9.200

* 15° † 10°

TABLE III-C-II

 $(\rho_S - \rho_L) \times T$ at Various Temperatures

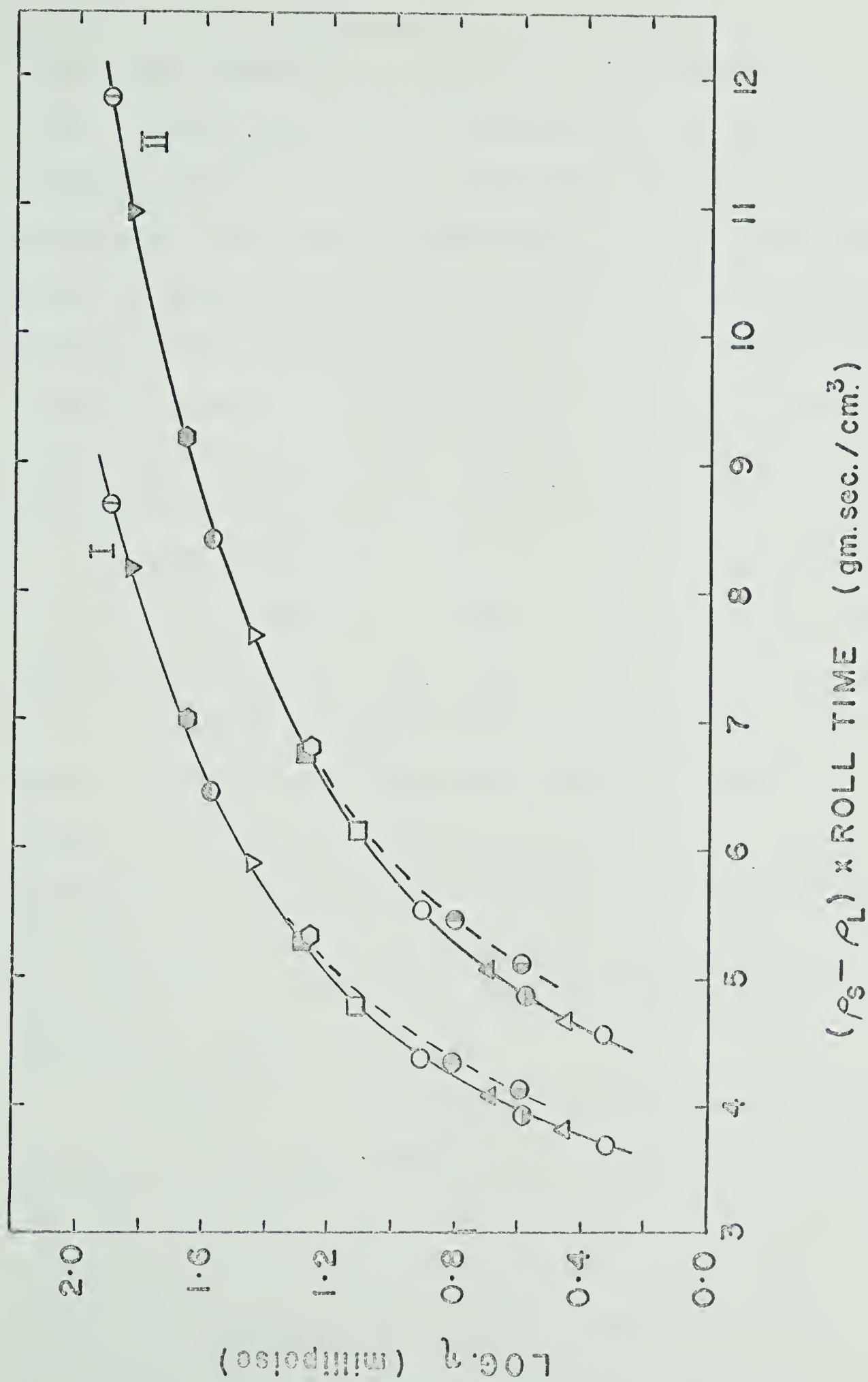
Compound	Atmospheric Pressure		
	$(\rho_S - \rho_L) \times \text{Roll Time}$	gm sec/cm ³	angle 2 ($\sim 30^\circ$)
	0°	30°	60°
n-Pentane	-	3.709	-
n-Hexane	-	3.841	3.575
n-Octane	4.315	4.071	3.889
n-Decane	4.714	4.386	4.134
n-Dodecane	-	4.851	4.451
n-Tetradecane	5.749 [*]	5.284	4.808
n-Octadecane	-	6.471	5.425
2,2-Dimethylbutane	-	3.938	-
Methylcyclohexane	4.658	4.348	4.170
Cyclopentane	-	4.145	-
S-3-65-1c	-	5.893	5.181
S-6-57-1E	10.919	8.162	6.0286
2 cts	-	5.321	-
5 cts	9.031	6.971	5.952
10 cts	11.92 [†]	8.681	6.996

* 15°
[†] 10°

FIGURE III-C-2

$(\rho_S - \rho_L) \times \text{Roll Time versus } \log \eta \text{ } 30^\circ\text{C}$

O	n-pentane	
Δ	n-hexane	
Δ	n-octane	
o	n-decane	
\square	n-dodecane	
\blacksquare	n-tetradecane	
e	n-octadecane	
o	cyclopentane	
o	methylcyclohexane	
e	2,2-dimethylbutane	
∇	S-3	Standard oils
∇	S-6	
o	B(10)	Silicone oils
\bigcirc	C(5)	
I	Angle I	
II	Angle II	



known. The calibration points were reproducible within 0.02%. It may tentatively be suggested that the molecular structure of the liquid may play some role in the observed effect, but to reconcile molecular structure with such a bulk property as viscosity is difficult. In the present viscometer the velocity of the ball is high at low liquid viscosities and, as will be further discussed later, the effect may arise from the occurrence of turbulent rather than from streamline flow of the liquid past the ball.

The dashed lines in Figure III-C-2 indicate the calibration curves used for the cyclic compounds. The only justification in using these curves, at the present time, is that if turbulent flow is dependent upon molecular structure, such dependency should disappear as the region of streamline flow is approached. The latter assumption may be partially justified by the observation that the silicone oils of about 5 and 8 cp fit, within experimental error, onto the high viscosity end of the hydrocarbon calibration curve.

The non linearity of the calibration plot (Figure III-C-2) has been observed by numerous authors (125, 142-144, 146, 147). The calibration plot is generally found to be linear when the viscosity of the fluid is greater than about 10 cP. However the actual point of departure from linearity is dependent upon the experi-

mental conditions.

The viscometer coefficient, K , is viscosity dependent. The form of the viscosity dependence of K may be illustrated from the observed temperature dependence of K . Figure III-C-3 illustrates the observed variation of the viscometer coefficient with temperature for *n*-decane and methylcyclohexane. These compounds were chosen as typical examples of straight chain and cyclic hydrocarbons because they were amenable to study over the complete temperature range from 0 to 60°C. A similar variation was found for all hydrocarbon and silicone oils.

According to the theory of Hubbard and Brown (125), the viscometer coefficient is given by the relation

$$K = \frac{5\pi}{42} C g \sin \theta d(D+d) \quad \text{(III-iv)}$$

where g is the acceleration due to gravity, θ the angle of inclination, d the ball diameter, D the tube diameter and C is a correlation factor. The correlation factor is given by (125)

$$C = \frac{\eta h u}{R} \quad \text{(III-v)}$$

where η is the viscosity in poise, h is the equivalent diameter, u is the average velocity of the liquid through the space between the ball and tube, and R is the resistive force on the motion of the ball. For non-circular channels, such as the crescent shaped channel between the

FIGURE III-C-3

Temperature Dependence of Viscometer Coefficient

$$\frac{K_O}{K_T} = \frac{\text{Viscometer coefficient } 0^\circ\text{C}}{\text{Viscometer coefficient } T^\circ\text{C}}$$

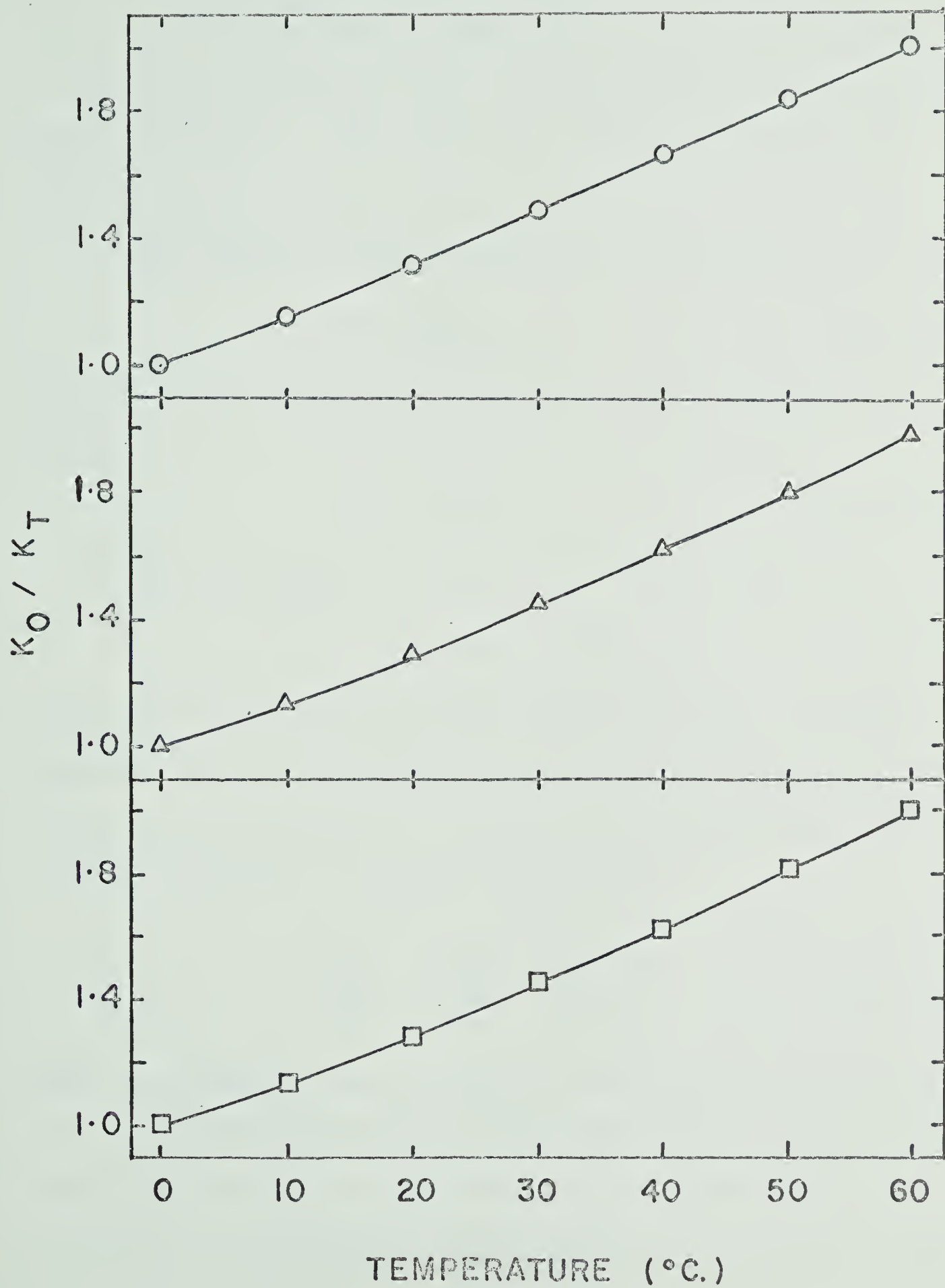
Full lines Values calculated relation III-iii

Points Values calculated relation III-ix

O n-Decane Angle I

Δ methylcyclohexane Angle I

methylcyclohexane Angle II



ball and the tube, the equivalent diameter is given by four times the hydraulic radius, the latter being defined as the cross-sectional area of the channel divided by the wetted perimeter. The value of h is therefore given by the term $(D-d)$.

The average fluid velocity u is given by

$$u = \left(\frac{d^2}{D^2 - d^2} \right) V \quad (\text{III-vi})$$

where V is the velocity of the ball. In the present system

$$u = 1.708 V \quad (\text{III-vii})$$

The resistance factor R may be calculated from

$$R = \frac{5}{7} g \sin \theta \frac{\pi d^3}{6} (\rho_S - \rho_L) \quad (\text{III-viii})$$

where all symbols have the meaning given above. Assuming that the change in d and D with temperature may be neglected, suitable rearrangement of the above equations yields for the relative variation of K with temperature

$$\frac{K_1}{K_2} = \frac{\eta_1 u_1}{\eta_1 u_2} \frac{\rho_{S_2} - \rho_{L_2}}{\rho_{S_1} - \rho_{L_1}} \quad (\text{III-ix})$$

where the suffix 1 and 2 refer to two different temperatures.

The relative values of the ratio K_1/K_2 , calculated from equation III-ix are illustrated in Figure III-C-3 as a function of temperature. The values are plotted as K_O/K_T

where K_0 refers to 0°C and K refers to $T^\circ\text{C}$. The relative variation in K_0/K_T calculated from the calibrating equation III-iii is in excellent agreement with the variation calculated from equation III-ix. The rolling ball viscometer appears to be functioning in accordance with the theory of Hubbard and Brown (125) for both the straight chain and cyclic hydrocarbons.

Whereas the non-linear dependence of equation (III-ii) on viscosity at low liquid viscosities (< 10 cP) is well established, the cause of the departure from linearity is still uncertain. It is generally attributed to a transition from laminar to turbulent flow. Block (144) believes the transition to result from increasing inertia of the liquid as the ball velocity increases in low viscosity liquids. Another possible explanation (148) is that the boundary layer at the solid-liquid interface separates when the ball velocity is high.

In order to use the calibration plot (Figure III-C-2) obtained at atmospheric pressure at high pressures it must be assumed that the only change in the viscometer constant with pressure arises from the increased viscosity of the liquid. The effect of pressure on the dimensions d , D and the roll distance may be neglected (d and D alter by less than 0.1% on increasing the pressure to 4500 bars). Block (144) suggested that the value of K may change with pressure

if the motion of the ball is altered from a pure rolling motion to a rolling and slip motion. However, it was concluded by Block that the occurrence of slip depended only upon the angle of inclination and not upon the viscosity of the liquid separating the two solid interfaces. This observation is in accordance with the theory of lubrication (149) which states that the coefficient of friction is independent of the viscosity of the lubricant.

It would appear that up to this time, no objections have been voiced to the use of the viscometer coefficient obtained at an atmosphere pressure being employed at higher pressures.

(2) Pressure Dependence of Viscosity

The roll time of the ball was determined as a function of pressure at constant temperature for each hydrocarbon. Experimentally the procedure was analogous to that described for the calibration of the viscometer at atmospheric pressure (Section II-G), except that the pressure was altered between readings. For most hydrocarbons, the variation of the roll time with pressure was determined at four or five temperatures. The boiling point or freezing point of the sample was never exceeded and care was taken to ensure that the freezing pressure at the temperature of the experiment was not exceeded.

The roll time was recorded at both angles of inclination for each pressure. Some typical results obtained for the variation of the roll time with pressure are illustrated for n-octane in Figure III-C-4 and for methylcyclohexane in Figure III-C-5.

The recorded roll times are the average value of at least ten determinations. The scatter in the observed roll time at a fixed pressure was 0.2 to 0.3% for angle I and 0.1 to 0.2% for angle II. The small deviation of the points from a smooth curve (Figures III-C-4) probably arises from the inaccuracy in the pressure reading rather than the timing device.

The roll time at 500 bar increments of pressure and at the experimental temperature was determined by interpolation from graphs such as shown in Figures III-C-4 and 5. The interpolated roll times were then plotted against temperature at constant pressure and the roll time obtained at any desired temperature, between the limits of the experimental temperatures, by a further interpolation. Extrapolation beyond the temperature range of the determinations is difficult at low temperatures because of the rapid rate of change of roll time with temperature.

The variation in roll time with temperature at constant pressure is shown in Figure III-C-6 for n-octane and Figure III-C-7 for methylcyclohexane. In order to convert

FIGURE III-C-4

Roll Time versus Pressure at Constant

Temperature

n-Octane

Angle II

O Pressure increasing cycle

Δ Pressure decreasing cycle

I 3.5°C

II 16.7°C

III 29.2°C

IV 43.5°C

V 58.5°C

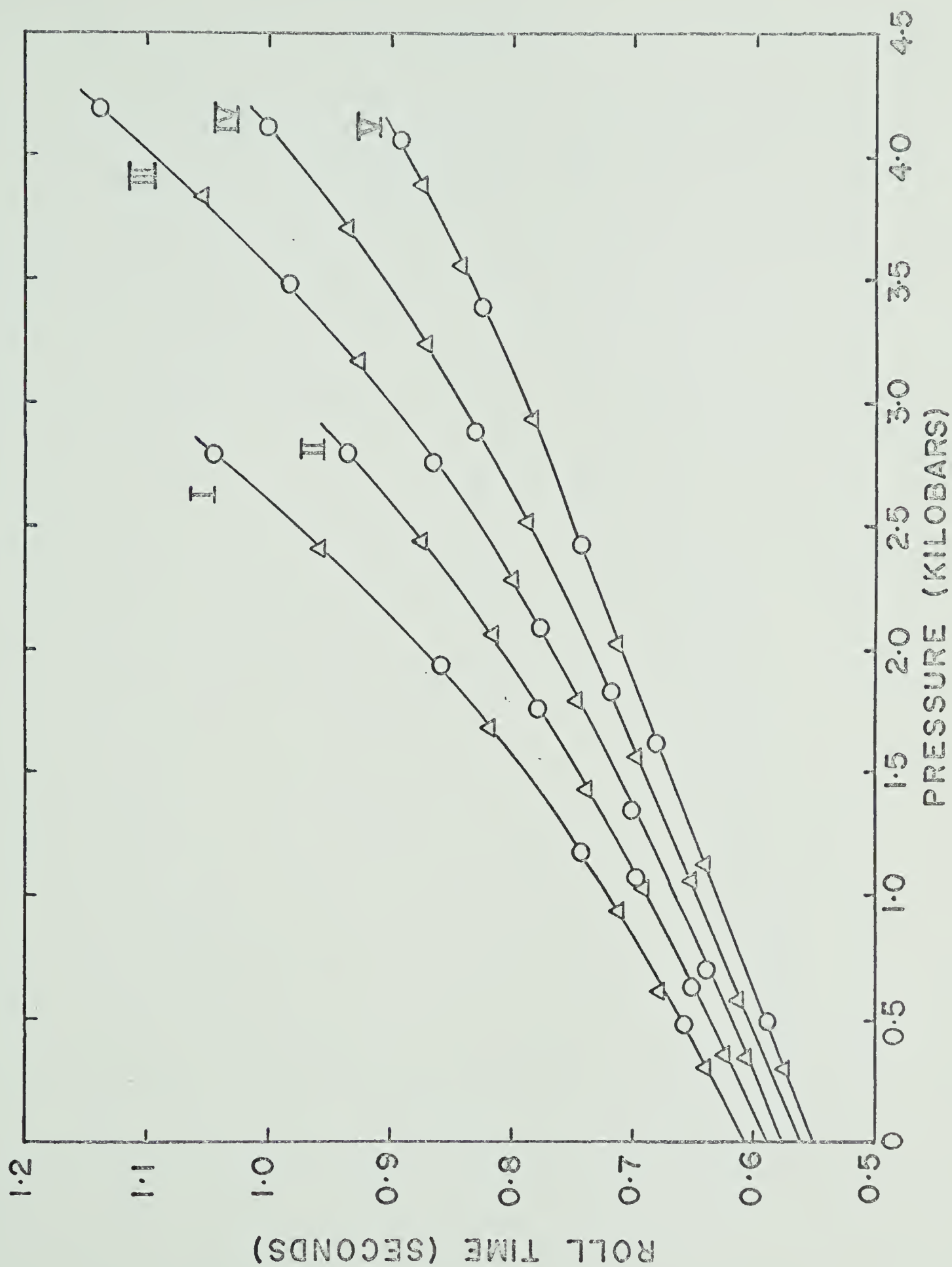


FIGURE III-C-5

Roll Time versus Pressure at Constant Temperature. Methylcyclohexane Angle I

I 11°C

II 29°C

III 43°C

IV 59.5°C

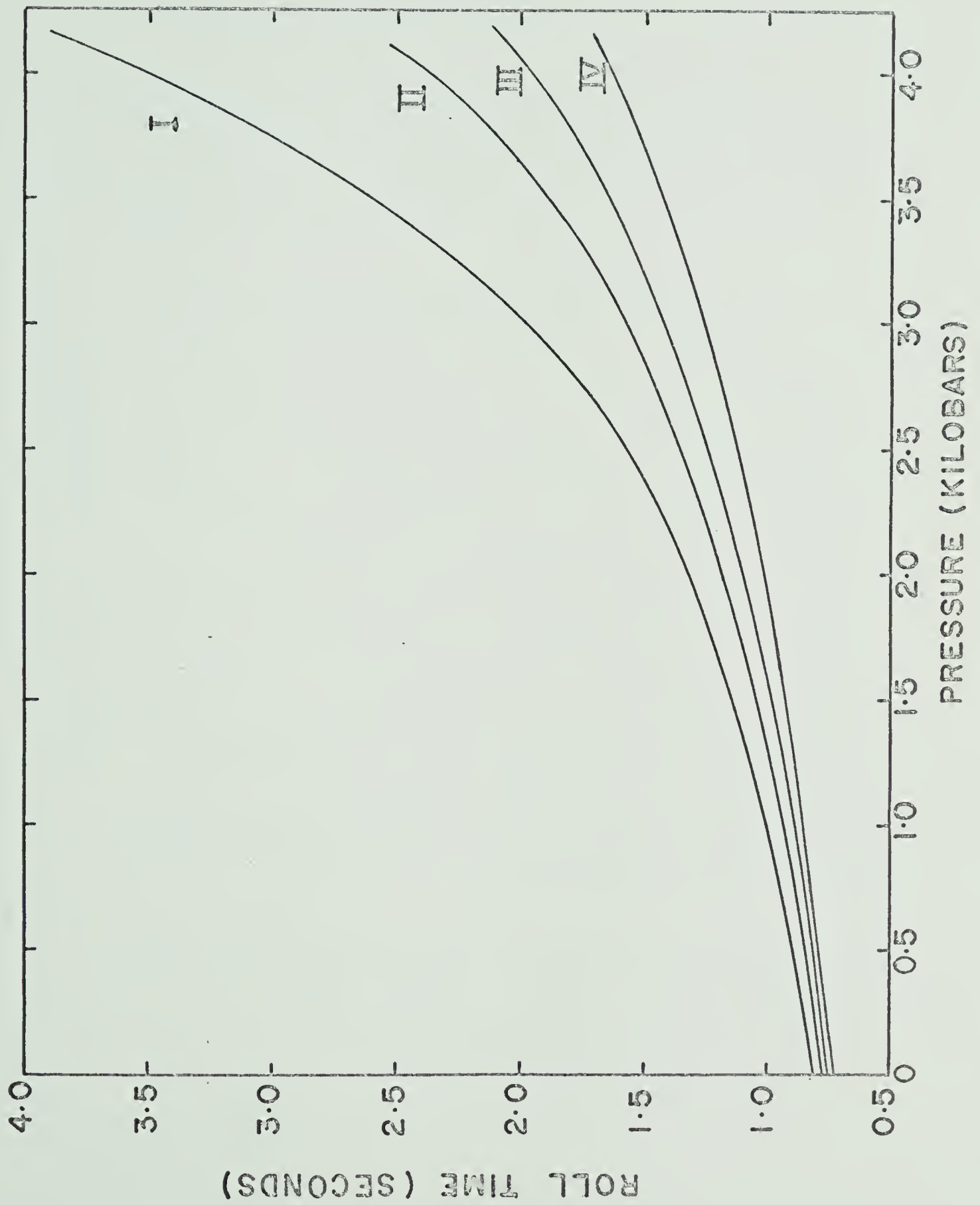


FIGURE III-C-6

Roll Time versus Temperature at Constant
Pressure. n-Octane. Angle II

Pressure in Kilobars (except 1 atm)

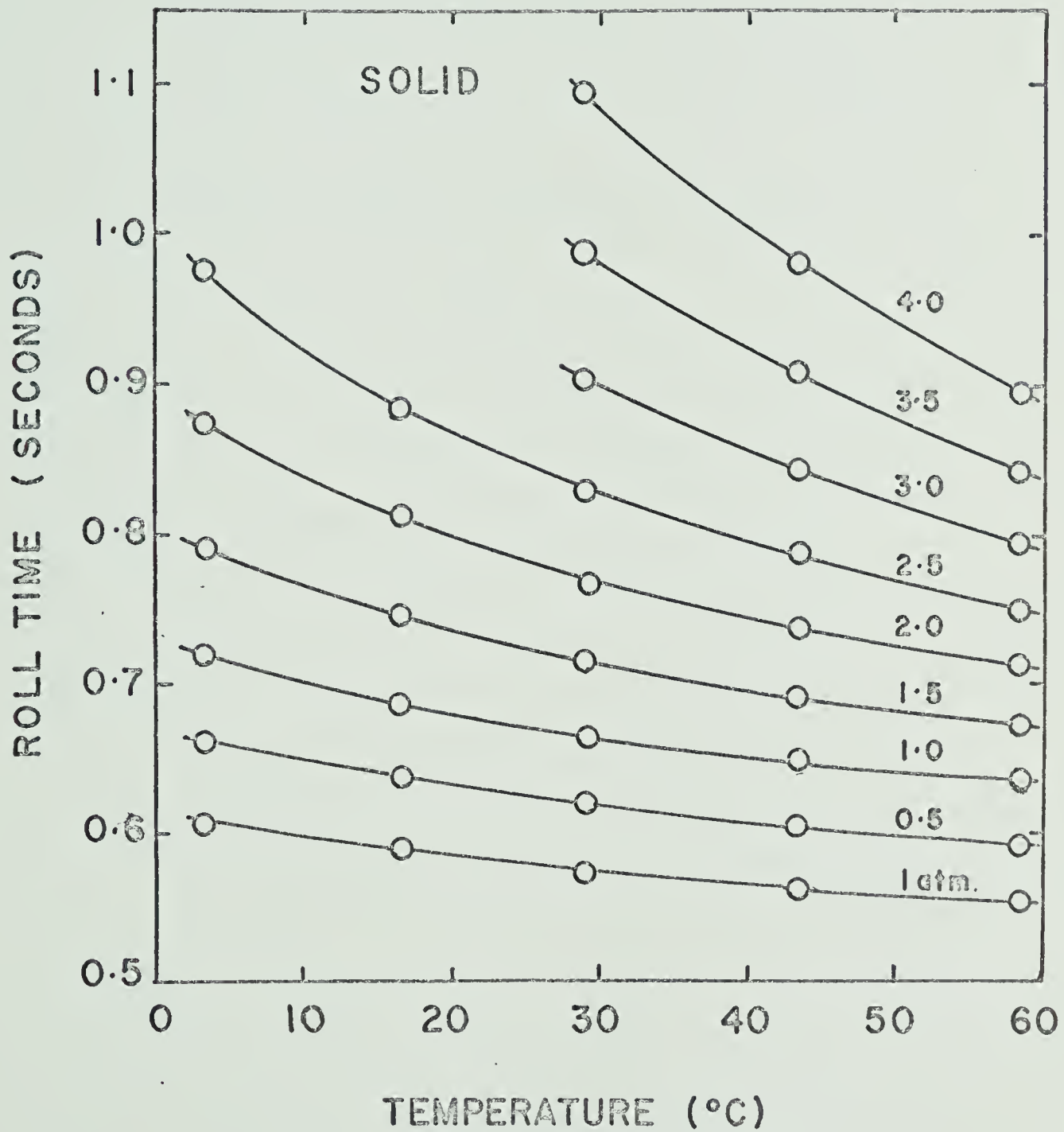
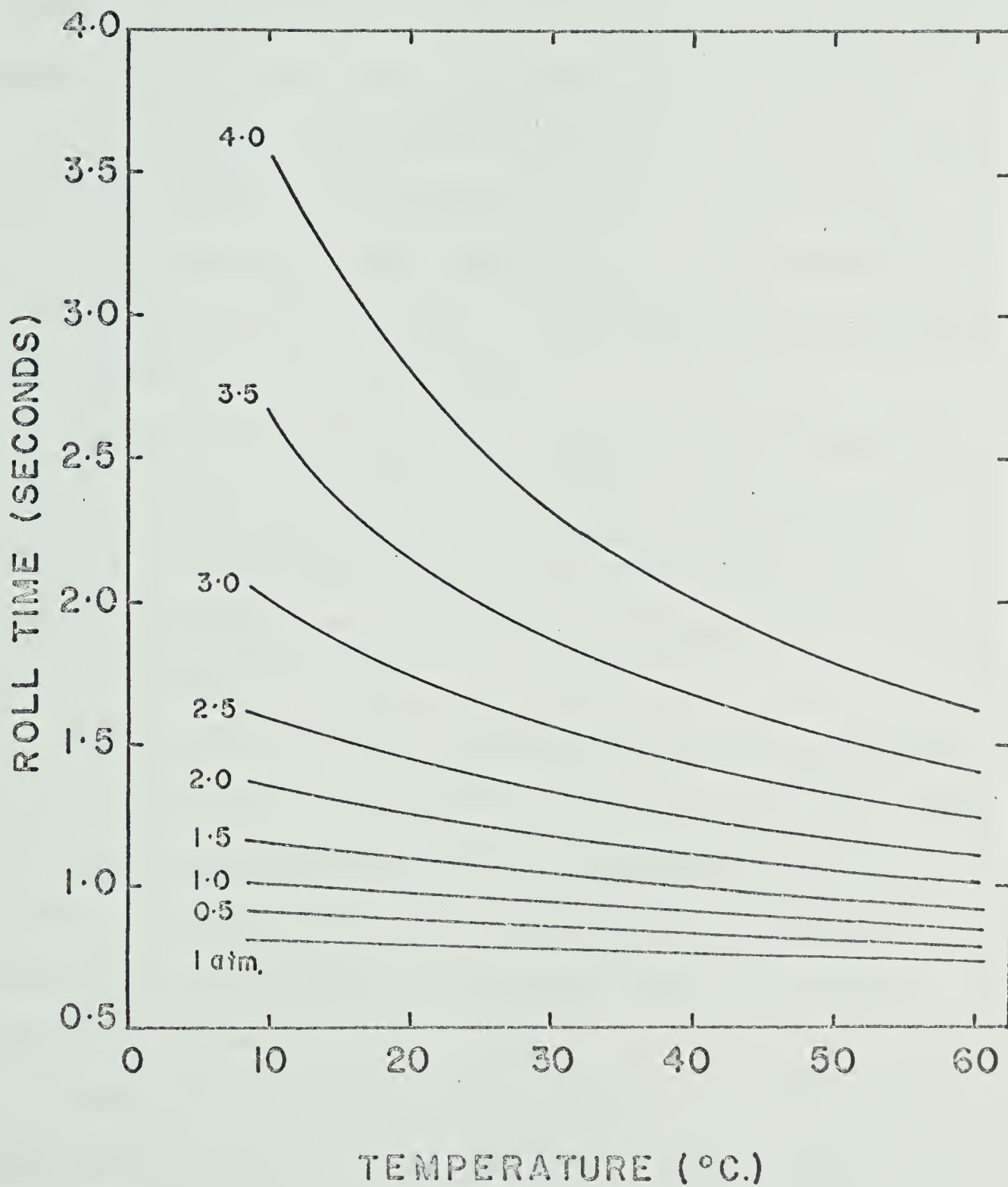


FIGURE III-C-7

Roll Time versus Temperature at Constant
Pressure. Methylcyclohexane Angle I

Pressure in Kilobars (except 1 atm).



the interpolated roll time to viscosity, the term $(\rho_S - \rho_L) T$ of the calibrating equation III-iii was calculated. The pressure dependence of the density of the hydrocarbon (ρ_L) was taken from the results presented in Section III-A. The density of the ball, ρ_S , was corrected for changes in temperature but not for changes in applied pressure. The viscosity was then determined by comparison of the $(\rho_S - \rho_L) T$ term with the calibration plot (Figure III-C-2 for example).

Table III-C-III lists the viscosity of n-hexane as function of pressure at 0, 30 and 60°C. The relative viscosity at each temperature is also recorded. The viscosity of hexane as a function of pressure is illustrated in Figure III-C-8.

Figure III-C-8 also includes the results of Bridgman (93, 150) for the viscosity of n-hexane at 30°C. The agreement between the results is satisfactory up to a pressure of about 1000 bars, after which the present results fall below those of Bridgman, the discrepancy amounting to about 8% at 4000 bars.

Table III-C-IV lists the values of the viscosity found for n-octane at 0, 30 and 60°C. These results are illustrated as a function of pressure in Figure III-C-9. The results at 30°C are again below those of Bridgman (93,150) at 30°C at pressures greater than 2000 bars, the

TABLE III-C-III

Viscosity n-Hexane. Pressure Dependence

Pressure Bars	Viscosity Centipoise					
	0°C		30°C		60°C	
	Absolute	Relative	Absolute	Relative	Absolute	Relative
1	0.381	1.000	0.285	1.000	0.223	1.000
500	0.62	1.63	0.45	1.58	0.36	1.61
1000	0.84	2.20	0.62	2.18	0.50	2.24
1500	1.11	2.91	0.80	2.81	0.63	2.82
2000	1.40	3.67	0.98	3.44	0.77	3.45
2500	1.73	4.54	1.24	4.35	0.93	4.17
3000	2.17	5.70	1.51	5.30	1.11	4.98
3500	2.67	7.01	1.84	6.47	1.27	5.69
4000	3.29	8.63	2.21	7.75	1.52	6.82

1 = 1.0133 Bars (1 Atm)

FIGURE III-C-8

Viscosity versus Pressure n-Hexane

□ 0 °C

Δ 30 °C

○ 60 °C

▲ 30 °C P. W. Bridgman's data (150)

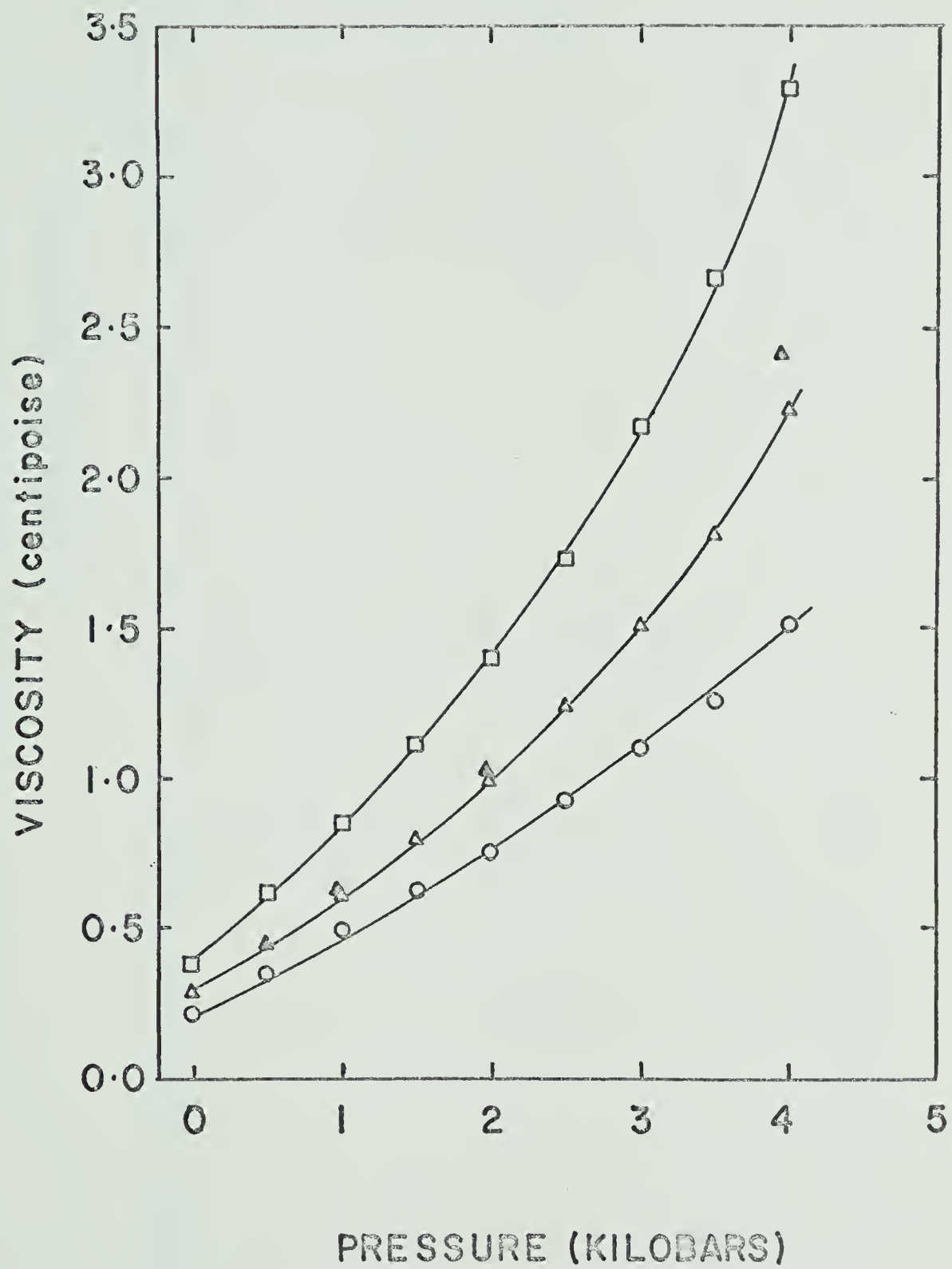


TABLE III-C-IV

Viscosity of n-Octane. Pressure Dependence

Pressure Bars	Viscosity Centipoise					
	0°C		30°C		60°C	
	Absolute	Relative	Absolute	Relative	Absolute	Relative
1	0.712	1.00	0.487	1.00	0.359	1.000
500	1.21	1.70	0.79	1.62	0.56	1.56
1000	1.73	2.43	1.10	2.26	0.80	2.23
1500	2.35	3.30	1.52	3.12	1.06	2.95
2000	3.12	4.38	1.99	4.09	1.34	3.73
2500	4.45	6.25	2.57	5.28	1.66	4.62
3000	-----	-----	3.33	6.83	2.08	5.79
3500	-----	-----	4.31	8.85	2.72	4.58
4000	-----	-----	5.67	11.64	3.57	9.95

1 = 1.0133 Bars (1 atm)

FIGURE III-C-9

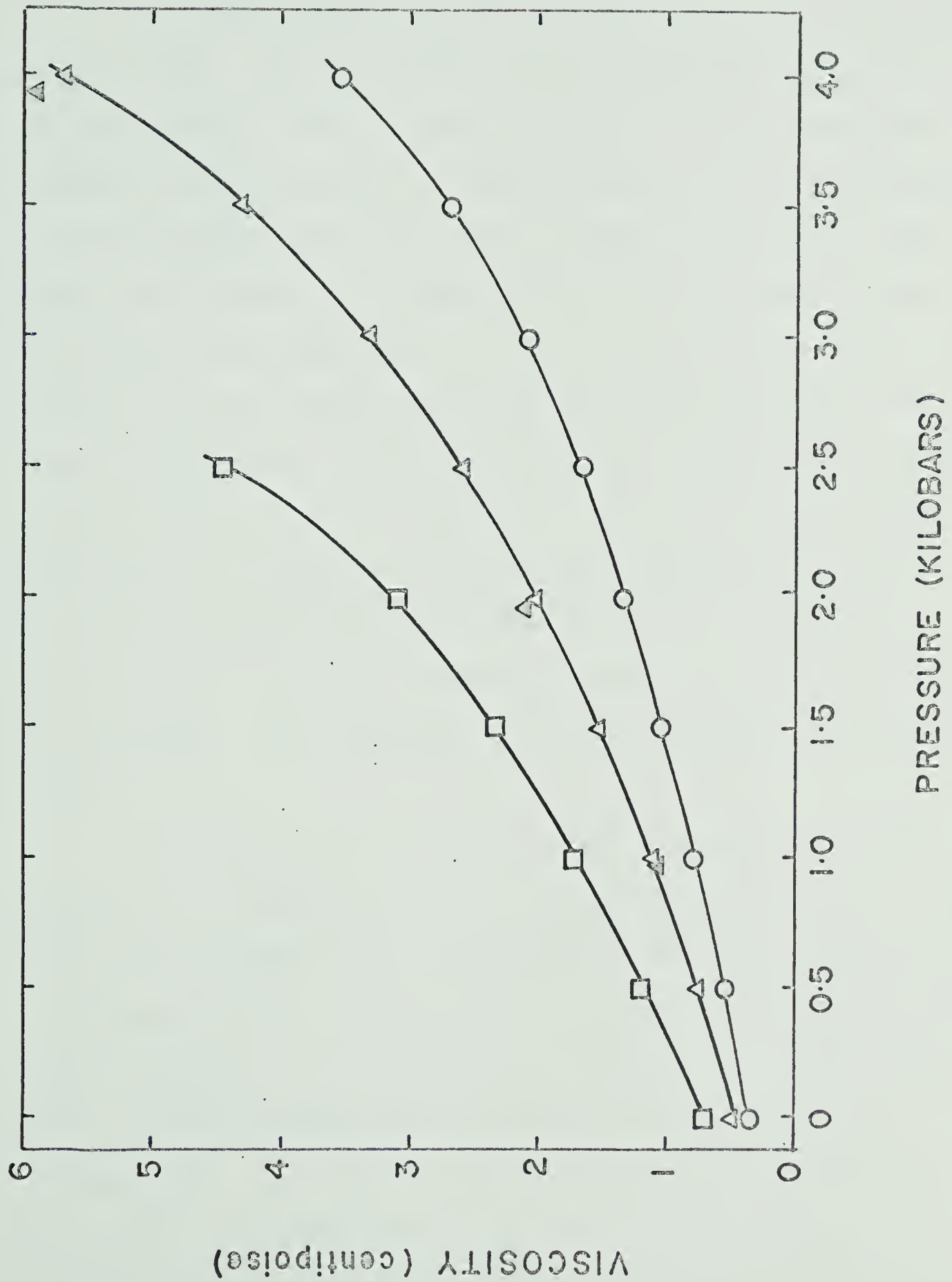
Viscosity versus Pressure n-Octane

□ 0°C

Δ 30°C

○ 60°C

▲ P. W. Bridgman's Data (150) 30°C



difference at 4000 bars amounting to 8%.

The viscosity of all other hydrocarbons was obtained only at 30°C. The viscosities of cyclopentane and methylcyclohexane are given in Table III-C-V. The pressure dependence of the density of these compounds is not available at temperatures other than 30°C. Table III-C-V also contains the observed roll times at some other temperatures. If the pressure dependence of the density of these compounds at other temperatures should become available, the viscosities may be calculated using the calibration results given in Table III-C-I (angle I). The variations of the viscosity with pressure for methylcyclohexane and cyclopentane are illustrated in Figure III-C-10. Bridgman's (93,150,151) values for methylcyclohexane are also included in the Figure. No comparative data is available for cyclopentane.

Table III-C-VI lists the results obtained for the viscosity of n-pentane and 2,2-dimethylbutane at 30°C. The roll times at some other temperatures are also included for 2,2-dimethylbutane. The viscosity pressure dependence for these compounds is also shown in Figure III-C-10. Bridgman's (93,150) results for n-pentane at 30°C are also illustrated. The present results are in good agreement with those of Bridgman up to a pressure of between 1000 and 2000 bars. At higher pressures the present results con-

TABLE III-C-V

Viscosity of Cyclopentane and Methylcyclohexane. Pressure Dependence at 30°C

Pressure Bars	Cyclopentane			Methylcyclohexane		
	Viscosity cP	Relative Viscosity	Roll Time (sec) 10°C	Viscosity cP	Relative Viscosity	Roll Time (sec) 10°C
1	0.390	1.00	0.755	0.641	1.00	0.819
500	0.64	1.64	0.808	1.07	1.67	0.900
1000	0.92	2.36	0.861	1.65	2.50	1.010
1500	1.17	3.00	0.912	2.20	3.59	1.143
2000	1.51	3.87	0.967	3.32	5.18	1.341
2500	1.81	4.64	1.028	4.55	7.10	1.579
3000	2.19	5.62	1.094	6.58	10.30	2.009
3500	2.69	6.90	1.167	9.12	14.23	2.641
4000	3.16	8.10	1.255	11.80	18.41	3.852

FIGURE III-C-10

Viscosity versus Pressure 30°C

- I Methylcyclohexane
- II 2,2-dimethylbutane
- III Cyclopentane
- IV n-Pentane
- Δ Methylcyclohexane P.W. Bridgman (151)
data 30°C
- O n-pentane P.W. Bridgman (150) data 30°C

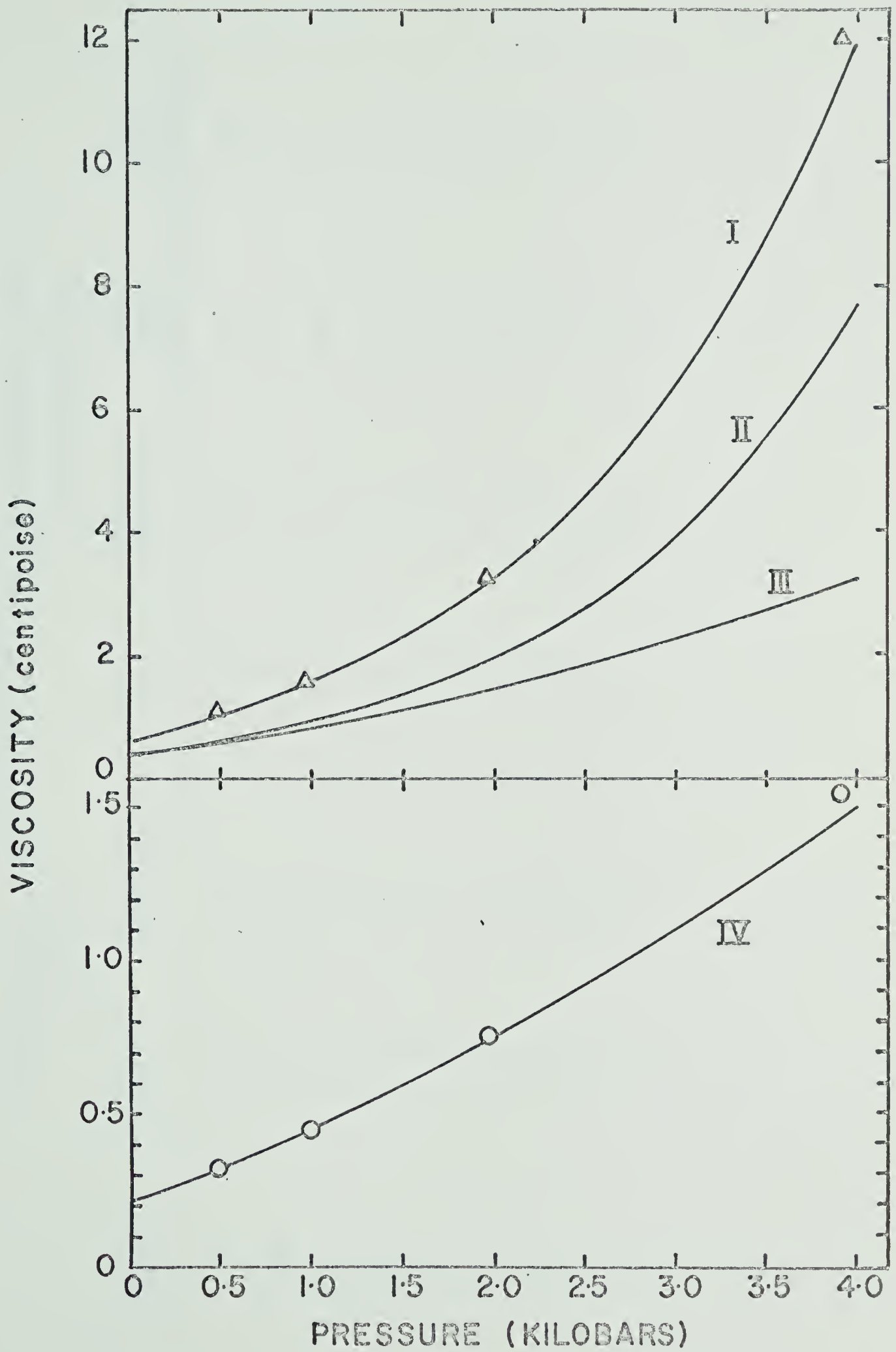


TABLE III-C-VI

Viscosity of n-Pentane and 2,2-Dimethylbutane at 30°C

Pressure Bars	<u>n-Pentane</u>		<u>2,2-Dimethylbutane</u>			
	Viscosity cP	Relative Viscosity	Viscosity cP	Relative Viscosity	Roll Time (secs) 15°C	Roll Time (secs) 40°C
1.	0.216	1.00	0.330	1.00	0.704	0.661
500	0.33	1.53	0.66	2.00	0.781	0.725
1000	0.45	2.08	1.00	3.03	0.842	0.791
1500	0.59	2.73	1.47	4.44	0.943	0.859
2000	0.75	3.47	2.00	6.05	1.079	0.943
2500	0.90	4.17	2.75	8.33	1.218	1.040
3000	1.08	5.00	3.98	12.06	1.425	1.168
3500	1.28	5.93	5.47	16.57	1.730	1.321
4000	1.50	6.95	7.76	23.52	2.214	1.526

sistently fall below those of Bridgman, the discrepancy amounting to about 7% at 4000 bars.

As the present results are constantly below those of Bridgman at pressures greater than 2000 bars, it is possible that a systematic correction should have been applied. However, the origin of any such correction is not immediately apparent. Greater discrepancies are to be found in the literature (93) so they may be due to differences in the experimental equipment used.

Although the present viscometer was operated in the region of turbulent flow, the discrepancies arise at the higher pressures, where, the flow is more laminar and not, as might be expected, at the low pressures. Additional independent determinations of the pressure dependence of the viscosities of the hydrocarbons would be of interest.

The viscosities of all of the hydrocarbons studied increased with increasing pressure in roughly an exponential manner. The relative increase in viscosity with pressure varied widely from hydrocarbon to hydrocarbon, the greatest variation being observed for the branched hydrocarbons. Whereas the relative volumes of all the hydrocarbons changed by between 15 and 22% at 4000 bars, the viscosity variation was much larger (700 to 2400%) over the same pressure range. The latter is consistent with Bridgman's observation (93) that any satisfactory theory for the pressure dependence of

viscosity cannot depend solely upon the pressure dependence of the volume. No attempt was made to fit the present results to the numerous empirical and theoretical equations cited for the pressure dependence of the viscosity (152, 153).

(D) Pressure Dependence of Radiation Induced Conductance

(1) General

The effect of pressure upon the current induced in an hydrocarbon on exposure to radiation was determined as described in Section II-H. The cell current was monitored as a function of the applied electrode voltage, up to 500 volts, at constant temperature and at a series of constant pressures.

Several conductance cells were used that differed in their physical dimensions (Table II-H-I) and in order to correlate the results obtained with different cells, the relative conductance is used. The necessity of using several cells arose because of the limited lifetime of the supramica spacers. Cells of the type used for the dielectric constant measurement (Figure II-E-1) were unsatisfactory for radiation induced conductance measurements because of the large dose rate variation over the ion collecting volume and because of large background currents ($\gtrsim 10^{-10}$ amps).

The relative conductance is defined by the relation

$$\left(\frac{i}{v}\right)_{P.T.} / \left(\frac{i}{v}\right)_{1 \text{ atm.} T.}$$

where i is the cell current (amperes), v is the applied voltage (volts), P is the pressure (bars) and T is the experimental temperature. The conductivity, κ , of a sample in a given cell with parallel plate electrodes is given by

$$\kappa = \frac{i}{v} \frac{L}{A} \text{ mho/cm}$$

where L is the electrode separation (cm) and A is the electrode surface area (cm^2). It is assumed in the present results that the ratio L/A is independent of temperature and pressure. The relative conductivity is then simply the ratio of the conductance at the given pressure to that at one atmosphere, both being determined at the same temperature.

The experimental observations made during the course of these investigations with numerous hydrocarbons will be discussed in some detail for n -hexane and n -octane only. The comments made for the latter hydrocarbons apply in general to the other hydrocarbons investigated, except where special note has been made.

(2) n -Hexane

Typical results obtained for the variation of the cell current with applied voltage at 30°C and at several pressures are illustrated in Figures III-D-1 and III-D-2. The

FIGURE III-D-1

Cell Current versus Voltage. n-Hexane 30°C

Cell D. Pressure Vessel A

Dose Rate 4.3×10^{14} eV/ml sec.

I 1 atmosphere

II 747 bars

III 1140 bars

IV 1600 bars

V 2690 bars

VI 3450 bars

VII 4068 bars

O Pressure increasing cycle

● Pressure decreasing cycle

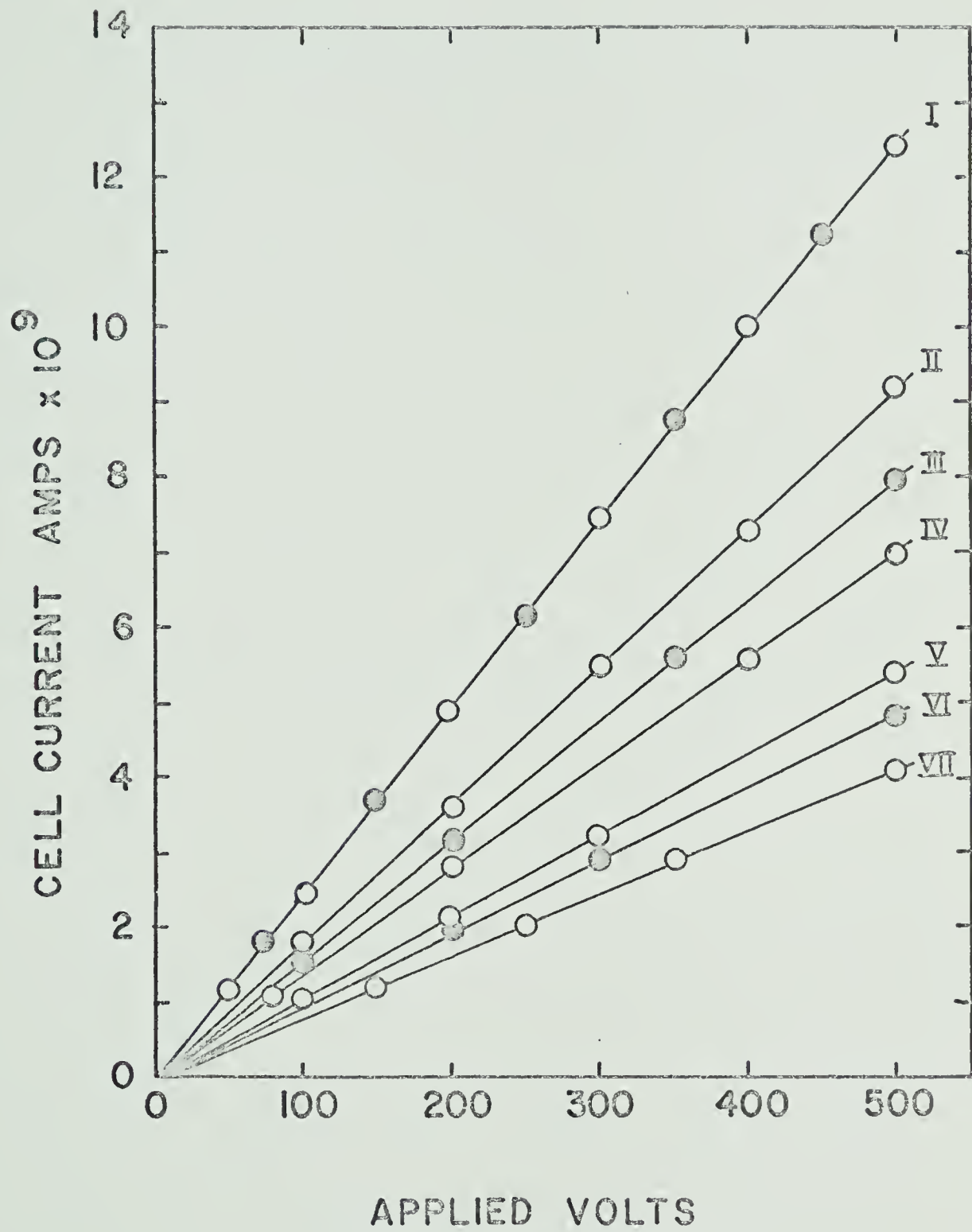


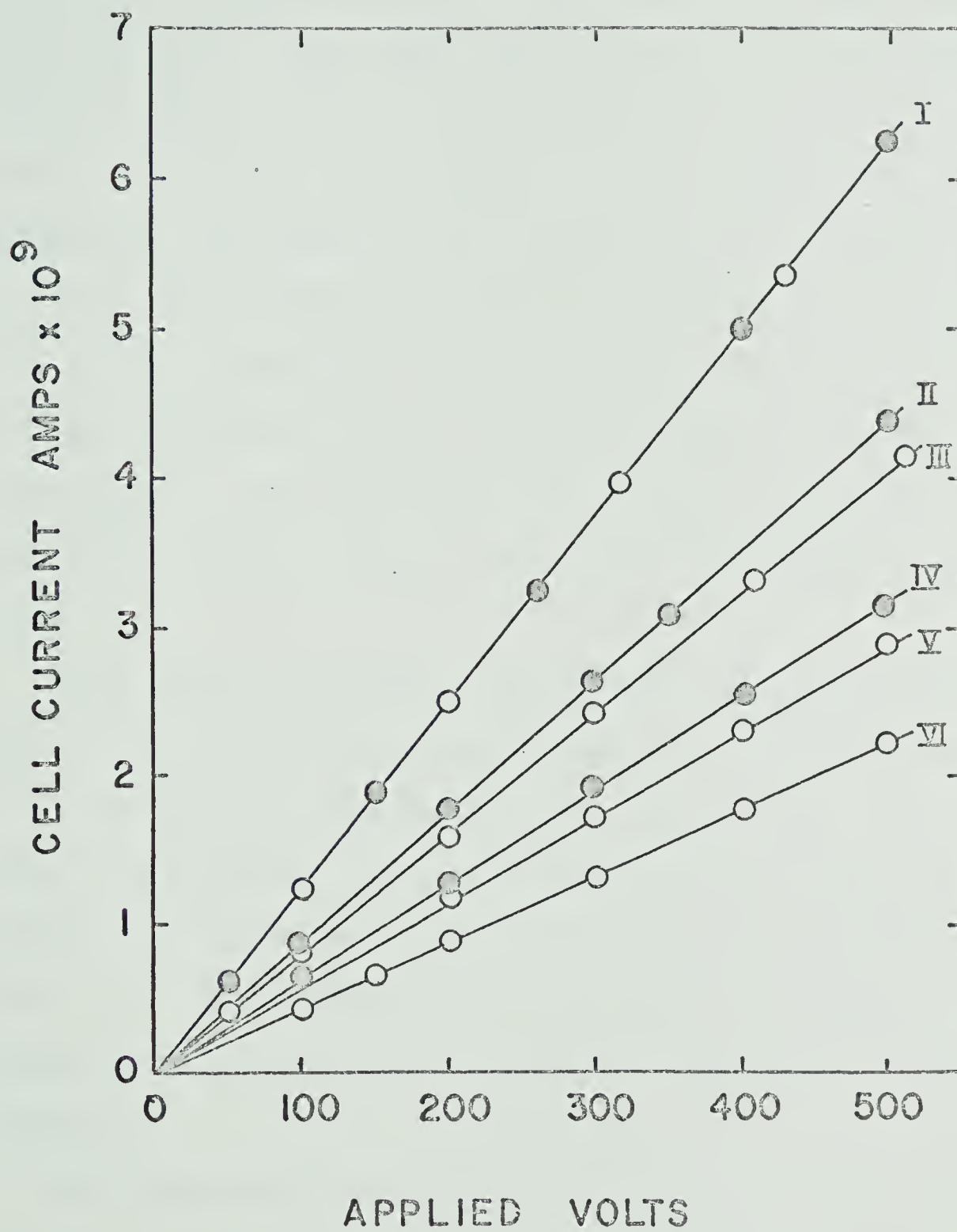
FIGURE III-D-2

Cell current versus Voltage. n-hexane 30°C

Cell D. Pressure Vessel A.

Dose Rate 1.40×10^{14} eV/ml sec.

- I. 1 atmosphere
- II. 993 bars
- III. 1255 bars
- IV. 2206 bars
- V. 2620 bars
- VI. 4033 bars
- O Pressure increasing cycle
- Pressure decreasing cycle



variations shown were obtained using Cell D at a dose rate of 4.3×10^{14} eV/ml.sec (Figure III-D-I) and 1.4×10^{14} eV/ml sec (Figure III-D-2). The dose rates were calculated from the dose rate distribution within the pressure vessel (Figure II-D-2), the position of the cell being known. All dose rates quoted in this section refer to one atmosphere pressure and the temperature of the experiment.

The cell currents recorded in Figure III-D-I and III-D-2 are experimentally observed values after subtraction of the background current in the absence of radiation, when applicable. The background current never exceeded 1% of the radiation induced current for any of the results reported here.

The initial background current was generally less than 0.5% of the radiation induced current, but rose slowly with the time that the sample was left in the cell. The latter rise in background current probably results from the slow removal of ionic impurities from the metallic surfaces of the cell. The background current also rose after prolonged exposure of the sample to radiation (see later in this section).

The radiation induced cell current was found to be a linear function of the applied cell voltage at all pressures and temperatures studied. The current-voltage plot was linear for both dose rates used, although the absolute

magnitude of the current was less at the lower dose rate for the same applied voltage.

The cell current versus applied voltage graphs always exhibited a positive voltage intercept which was not reproducible from investigation to investigation. The intercept varied from about 0.5 volts to 10 volts and was generally greater at the lower dose rate. It was also pressure dependent in a non-reproducible manner, either increasing, decreasing or remaining constant as the pressure in the system was altered.

The voltage intercept has been noted by several authors (56, 156) and is believed to be the result of radiation induced currents in the cables of the measuring circuit and of contact potentials in the circuit. The current induced in the cables by radiation, as determined by the dummy current line (Figure II-H-3) was not reproducible but rarely exceeded 1×10^{-11} amperes, provided the shielding illustrated previously in Figure II-H-4 was employed. The pressure dependency of the voltage intercept probably arises from changing contact potentials in the circuit within the pressure vessel because, within experimental error, the radiation induced current in the cables was independent of pressure.

The conductance of the sample was determined from the slope of the cell current versus applied voltage plot. Some

typical results for the pressure dependence of the conductance of n-hexane at 30°C are shown in Figures III-D-3 and III-D-4. The results illustrated in Figure III-D-3 were obtained using cells C, D and E at dose rates of 4.3×10^{14} eV/ml sec and 6.0×10^{14} eV/ml sec. Cell E was used in conjunction with pressure vessel B whilst all other cells were used with pressure vessel A (see Table II-D-II for the difference in dose rates within these vessels). The results illustrated in Figure III-D-4 were obtained with cells A, C and D at the lower dose rates of 1.40×10^{14} and 1.47×10^{14} eV/ml sec.

In some experiments the conductance at atmospheric pressure was lower after the release of pressure than before the application of pressure. A micrometer dial gauge placed on the pressure vessel piston closure indicated that the piston moved upward in a non-reproducible manner as the pressure was initially increased. The movement varied from zero to about 3 mm and was dependent upon the amount of movement that the packing rings (Figure II-A-3) of the piston closure underwent before sealing against the bore of the pressure vessel. Such movement was never observed on a second pressure cycle. The observed discrepancy results, therefore, from a change in dose rate (about 2% per mm).

It was possible that the discrepancy might have

FIGURE III-D-3

Conductance versus Pressure n-Hexane 30°C

Δ Cell D. Dose rate 4.3×10^{14} eV/ml sec.

O Cell C. Dose rate 4.3×10^{14} eV/ml sec

\square Cell E. Dose rate 6×10^{14} eV/ml sec

Cells D and C Pressure vessel A

Cell E Pressure vessel B.

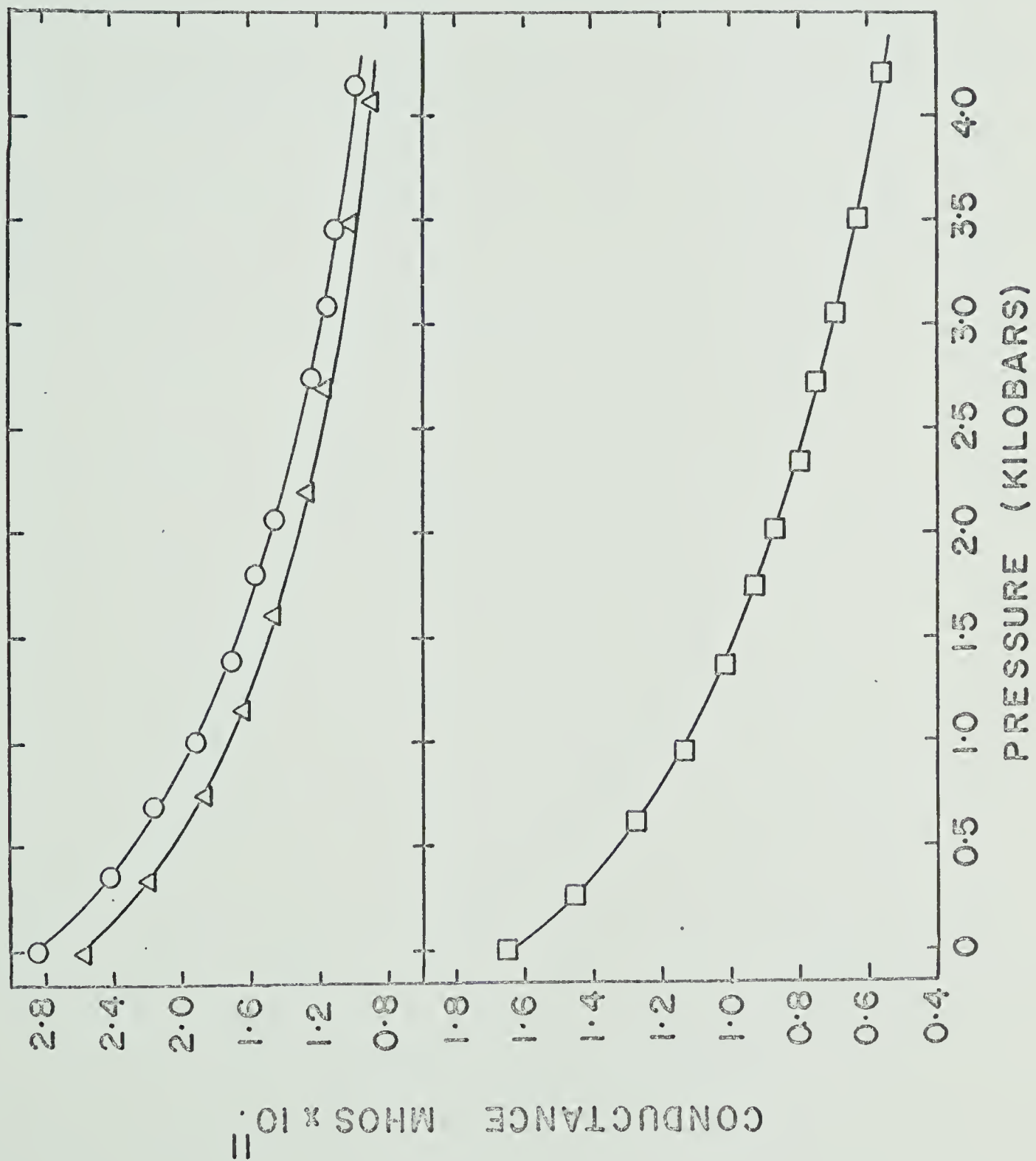


FIGURE III-D-4

Conductance versus Pressure. n-Hexane 30°C

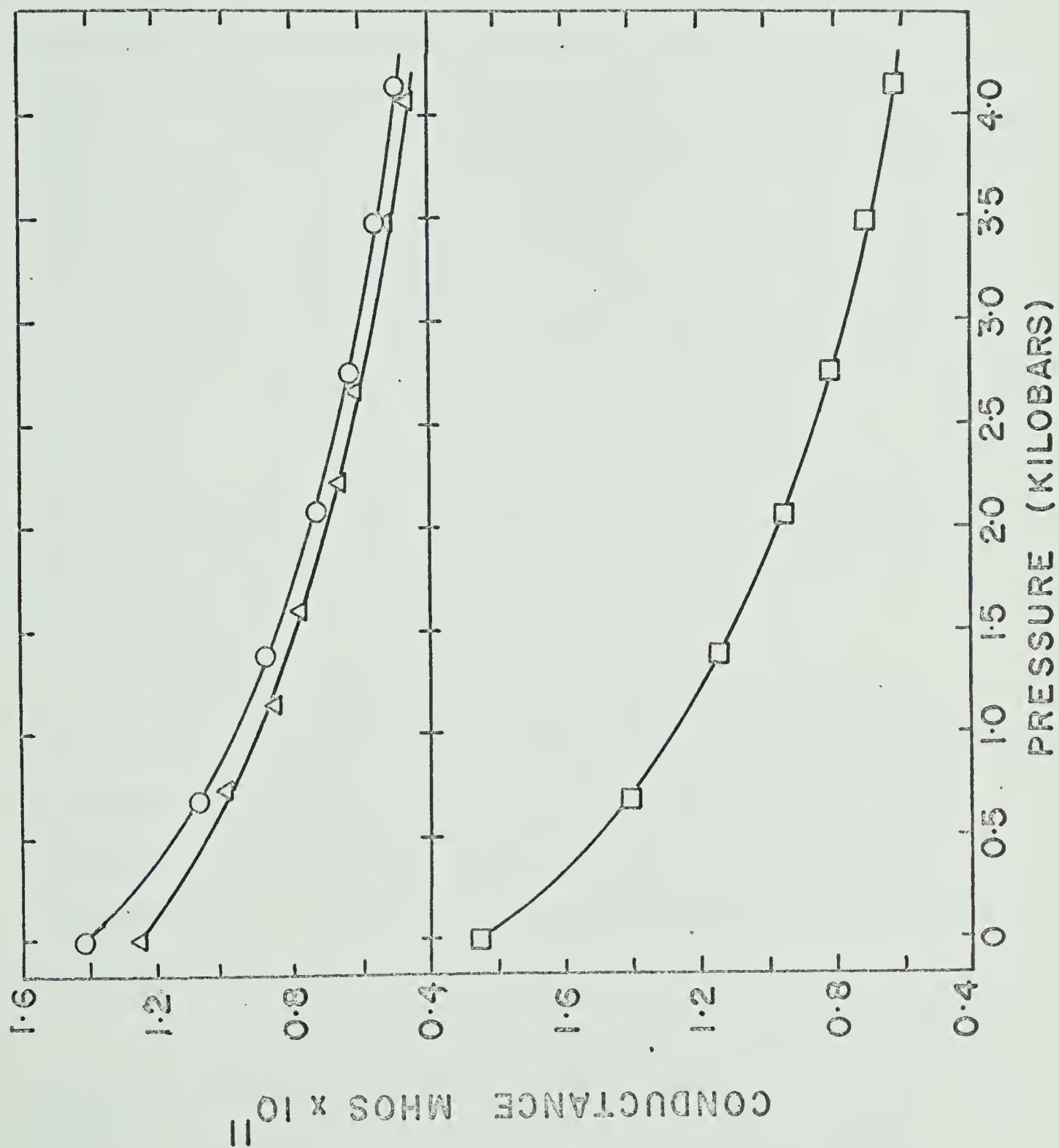
Δ . Cell D. Dose rate 1.4×10^{14} eV/ml sec.

O Cell C. Dose rate 1.4×10^{14} eV/ml sec

\square Cell A. Dose rate 1.47×10^{14} eV/ml sec

All pressure vessel A.

Experimental values



arisen because of the build up of hexane radiolysis products as the total dose increased. The conductance of a sample of hexane that was exposed to the radiation for a period of 280 minutes at a dose rate of 4.0×10^{14} eV/ml sec showed, within experimental error, no increase, apart from a small increase attributable to an increased background current. The radiation induced current at 100 volts increased from $2.46 \pm 0.02 \times 10^{-9}$ amperes to $2.48 \pm 0.02 \times 10^{-9}$ amperes, whilst over the same period of time the background current increased from 0.8×10^{-11} to 1.9×10^{-11} amperes. No effect of radiolysis products was observed for any of the hydrocarbons investigated, except in the case of 2,2-dimethylbutane which will be discussed later.

The conductance values reported in this section are those obtained when no discrepancy in the atmospheric pressure values was apparent or those obtained on a second pressure cycle. The measured conductance was reproducible to within 10% from filling to filling of the same cell.

The conductance of hexane as a function of pressure is recorded in Table III-D-I for several different cells and dose rates employed. The values, given at 500 bar intervals of pressure, were interpolated from the smooth curve drawn through the experimental plot of conductance versus pressure (e.g. Figure III-D-3). The

TABLE III-D-I

Conductance and Relative Conductance Hexane 30°C

I = conductance mhos $\times 10^{11}$

II = relative conductance

Pressure bars	Cell D		Cell C		Cell E		Cell D		Cell C		Cell A	
	I	II	I	II	I	II	I	II	I	II	I	II
	4.3 $\times 10^{14}$ eV/ml sec	4.3 $\times 10^{14}$ eV/ml sec	4.3 $\times 10^{14}$ eV/ml sec	4.3 $\times 10^{14}$ eV/ml sec	6.0 $\times 10^{14}$ eV/ml sec	6.0 $\times 10^{14}$ eV/ml sec	1.4 $\times 10^{14}$ eV/ml sec	1.4 $\times 10^{14}$ eV/ml sec	1.40 $\times 10^{14}$ eV/ml sec	1.40 $\times 10^{14}$ eV/ml sec	1.54 $\times 10^{14}$ eV/ml sec	1.54 $\times 10^{14}$ eV/ml sec
1	2.56	1.00	2.84	1.00	1.65	1.00	1.25	1.00	1.41	1.00	1.85	1.00
500	2.04	0.80	2.28	0.80	1.33	0.81	1.05	0.84	1.15	0.82	1.51	0.82
1000	1.73	0.68	1.92	0.68	1.13	0.68	0.90	0.72	0.98	0.70	1.28	0.69
1500	1.50	0.61	1.67	0.59	0.99	0.60	0.79	0.63	0.85	0.60	1.11	0.60
2000	1.32	0.52	1.47	0.52	0.88	0.53	0.70	0.56	0.75	0.53	0.97	0.52
2500	1.16	0.45	1.32	0.46	0.78	0.47	0.62	0.50	0.67	0.48	0.86	0.46
3000	1.05	0.41	1.18	0.42	0.70	0.42	0.56	0.45	0.60	0.43	0.77	0.42
3500	0.95	0.37	1.07	0.38	0.63	0.38	0.50	0.40	0.55	0.39	0.69	0.37
4000	0.87	0.34	0.98	0.35	0.57	0.35	6.46	0.37	0.50	0.35	0.63	0.34

183

relative conductance at each pressure is also listed in Table III-D-I. Figure III-D-5 illustrates the pressure dependency of the relative conductance. The points shown are the average values of the relative conductance at each pressure obtained with cells C and D at the higher dose rates of 4.3×10^{14} eV/ml sec and with the same cells at the lower dose rate of 1.4×10^{14} eV/ml sec. It is apparent from Figure III-D-5 that, within experimental error, the pressure dependence of the relative conductance is independent of the dose rate over the present range of dose rates used.

The conductance of n-hexane at 3 and 56°C is illustrated as a function of pressure in Figure III-D-6. The results shown for 3°C were obtained with cell C at a dose rate of 4.5×10^{14} eV/ml sec and with cell A at a dose rate of 6.5×10^{14} eV/ml sec. The observed decrease in conductance as the temperature was lowered from 30° to 3°C at atmospheric pressure amounted to 34%. The background current decreased, over the same temperature range, by approximately a factor of ten.

The interpolated conductances at 500 bar intervals of pressure are given in Table III-D-II. As well as the results obtained with cells A and C, which were illustrated in Figure III-D-6, the results obtained with cell D at a dose rate of 1.50×10^{14} eV/ml sec are given. The calcu-

FIGURE III-D-5

Relative Conductance versus Pressure

n-Hexane 30°C

○ Average results two cells C & D

Dose rate 4.3×10^{14} eV/ml sec

● Average results cells C & D

Dose rate 1.4×10^{14} eV/ ml sec

⊙ Coincident points

All interpolated values.

Pressure Vessel A

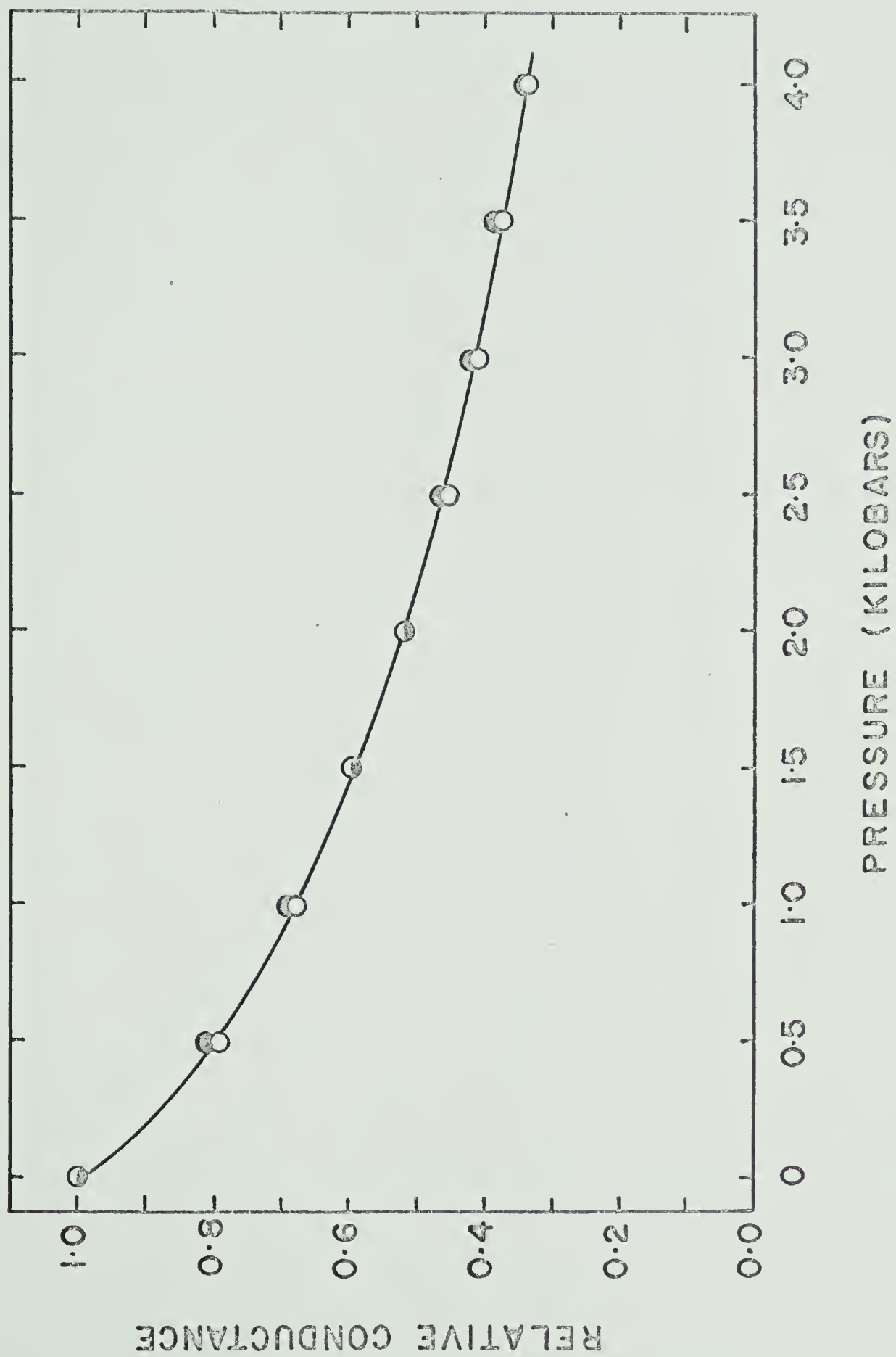


FIGURE III-D-6

Conductance versus Pressure n-hexane

3 and 56°C

□ Cell A 56°C 6.1×10^{14} eV/ml sec

○ Cell C 56°C 4.1×10^{14} eV/ml sec

○ Cell A 3°C 6.5×10^{14} eV/ml sec

Δ Cell C 3°C 4.5×10^{14} eV/ml sec

All Pressure vessel A.

Experimental values

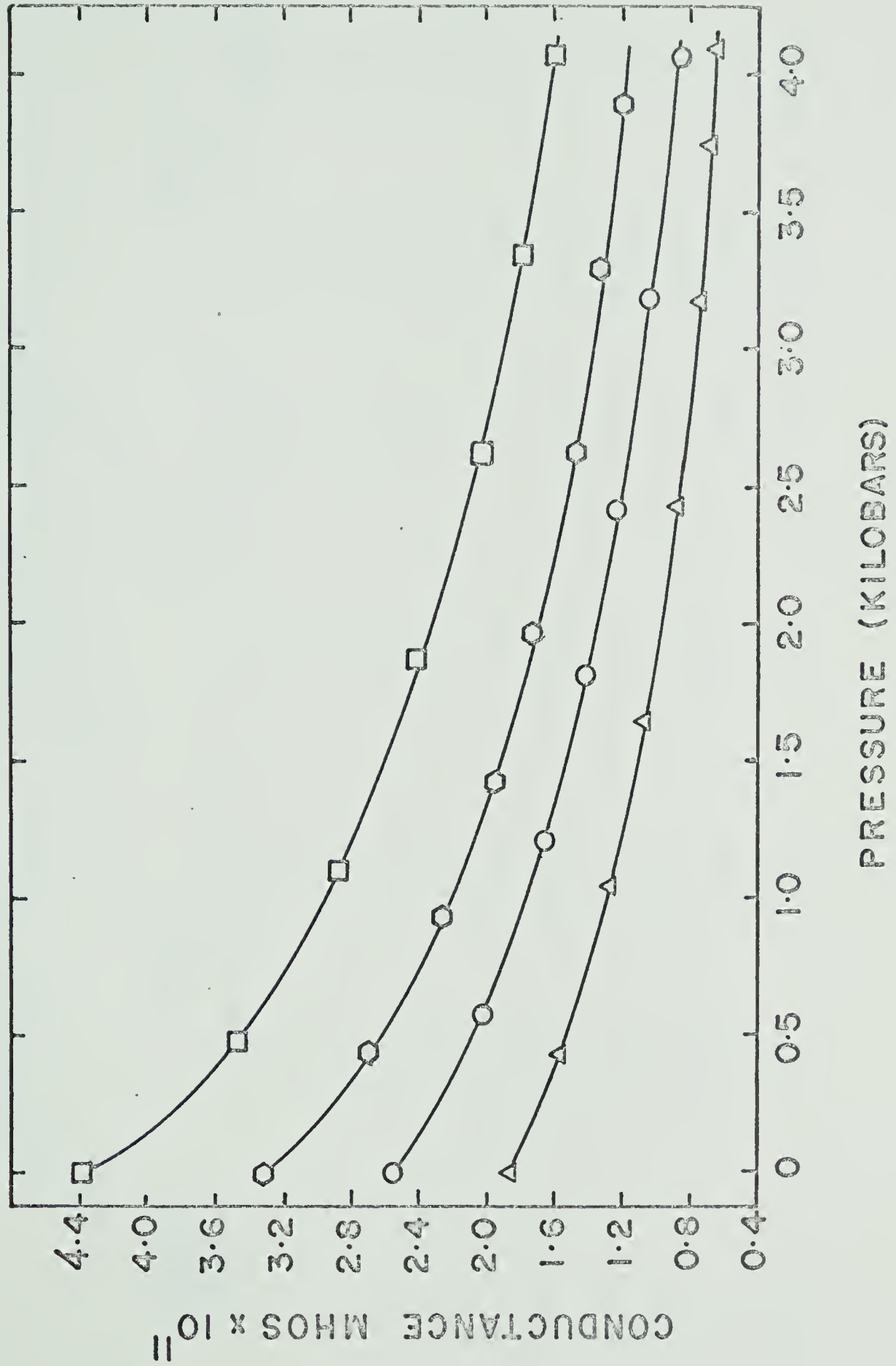


TABLE III-D-II

Conductance and Relative Conductance n-Hexane 3°CI = Conductance mhos $\times 10^{11}$

II = Relative conductance

Pressure Bars	Cell A		Cell C		Cell D	
	6.5×10^{14} eV/ml sec		4.5×10^{14} eV/ml sec		1.50×10^{14} eV/ml sec	
	I	II	I	II	I	II
1	2.56	1.00	1.87	1.00	1.55	1.00
500	2.07	0.81	1.51	0.81	1.29	0.83
1000	1.78	0.70	1.29	0.69	1.12	0.72
1500	1.59	0.60	1.12	0.60	0.98	0.63
2000	1.36	0.63	0.98	0.52	0.86	0.55
2500	1.21	0.47	0.87	0.47	0.76	0.49
3000	1.08	0.42	0.79	0.42	0.66	0.43
3500	0.97	0.38	0.72	0.38	0.58	0.37
4000	0.88	0.34	0.66	0.35	0.53	0.34

lated relative conductances are also listed in Table III-D-II and their pressure dependency illustrated in Figure III-D-7.

The agreement in the pressure dependence of the relative conductance of hexane at 3°C for the two dose rates, 6.5×10 and 1.5×10 eV/ml sec, is within 3% over the complete pressure range. This variation is within experimental error.

The results shown in Figure II-D-6 at an experimental temperature of 56°C were obtained using cells A and C with dose rates of 4.1 and 6.1×10^{14} eV/ml sec respectively. The conductance at atmospheric pressure increased by approximately 12% over that observed in the same cell at 30°C. The background current increased by about a factor of five over the same temperature range. The interpolated conductances for hexane at 56°C are given in Table III-D-III. The pressure dependence of the relative conductance of n-hexane at 56°C is illustrated in Figure III-D-7. Within experimental error, the pressure dependence of the relative conductance is independent of the dose rate over the range 6.1 to 1.35×10^{14} eV/ml sec.

The relative conductance of n-hexane at 4000 bars and at 3, 30 and 56°C is 0.34, 0.35 and 0.37 respectively. These values are the average results obtained from the experiments reported in Tables III-D-I, II and III. Al-

FIGURE III-D-7

Relative Conductance versus Pressure n-Hexane.

3°C

- O Average Cells A and C
 - Cell A 6.5×10^{14} eV/ml sec
 - Cell C 4.5×10^{14} eV/ml sec
- Cell D Dose rate 1.5×10^{14} eV/ml sec.

56°C

- O Average Cells A and C
 - Cell A 6.1×10^{14} eV/ml sec.
 - Cell C 4.1×10^{14} eV/ml sec
- Average cells A and C
 - Cell A 1.48×10^{14} eV/ml sec
 - Cell C 1.35×10^{14} eV/ml sec
- Coincident points (3 and 56°C)
 - All Pressure Vessel A
 - All interpolated values.

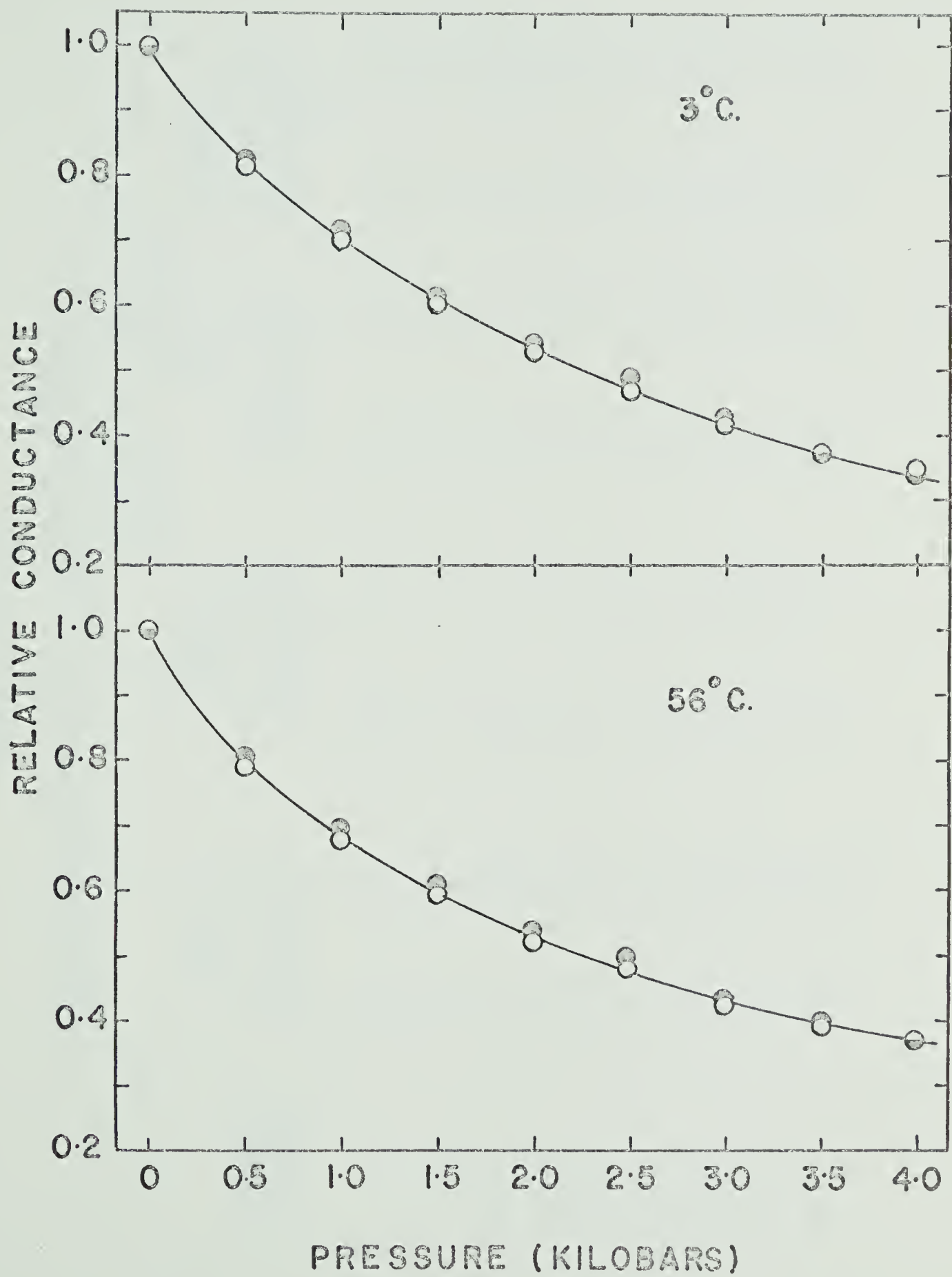


TABLE III-D-III

Conductance and Relative Conductance Hexane 56°C

Pressure Bars	I = conductance mhos $\times 10^{11}$					
	II = relative conductance					
	Cell C		Cell A		Cell C	
	I	II	I	II	I	II
	4.1 $\times 10^{14}$ eV/ml sec	1.00	6.1 $\times 10^{14}$ eV/ml sec	1.00	1.35 $\times 10^{14}$ eV/ml sec	1.48 $\times 10^{14}$ eV/ml sec
1	3.32	1.00	4.38	1.00	1.64	2.11
500	2.62	0.79	3.45	0.79	1.34	1.71
1000	2.23	0.67	2.95	0.67	1.15	1.47
1500	1.95	0.59	2.60	0.59	1.01	1.29
2000	1.72	0.52	2.33	0.53	0.89	1.16
2500	1.55	0.47	2.10	0.48	0.80	1.05
3000	1.40	0.42	1.85	0.42	0.72	0.93
3500	1.30	0.39	1.75	0.40	0.67	0.87
4000	1.20	0.36	1.62	0.37	0.61	0.79

though a definite trend to decrease the pressure dependence of the relative conductance is observed as the temperature is increased, the experimental technique is of insufficient sensitivity to observe the exact variation.

(3) n-Octane

n-Octane was studied at three temperatures, 3, 30 and 56°C, using two cells and two dose rates. Some typical results obtained for the variation of the cell current (after correction for the background current) with applied voltage are illustrated in Figure III-D-8. These results were obtained with cell D at 30°C and at two dose rates of 4.6×10^{14} and 1.5×10^{14} eV/ ml sec. The cell current versus voltage plot was linear over the complete pressure range studied (1-4000 bars) at both dose rates.

The values of the conductance, calculated from the slope of results such as those shown in Figure II-D-8, are illustrated in Figure III-D-9. The conductances shown were obtained with cells D and F at dose rates of 4.6 and 1.5×10^{14} eV/ ml sec and at 30°C. Table III-D-IV records the interpolated conductances, for each cell and dose rate, at 500 bar intervals of pressure. The relative conductances, given in Table III-D-IV are shown as a function of pressure in Figure III-D-10.

Results obtained for the pressure dependence of octane at 3°C in cells D and F are shown in Figure III-D-11.

FIGURE III-D-8

Cell Current versus Applied Voltage at
Constant Pressure n-octane 30°C

Cell F. A. Dose Rate 1.5×10^{14} eV/ml sec

 B Dose Rate 4.6×10^{14} eV/ml sec

 I. 1 atmosphere

 II. 792 bars

 III 1648 bars

 IV 2690 bars

 V 4150 bars

Pressure Vessel A

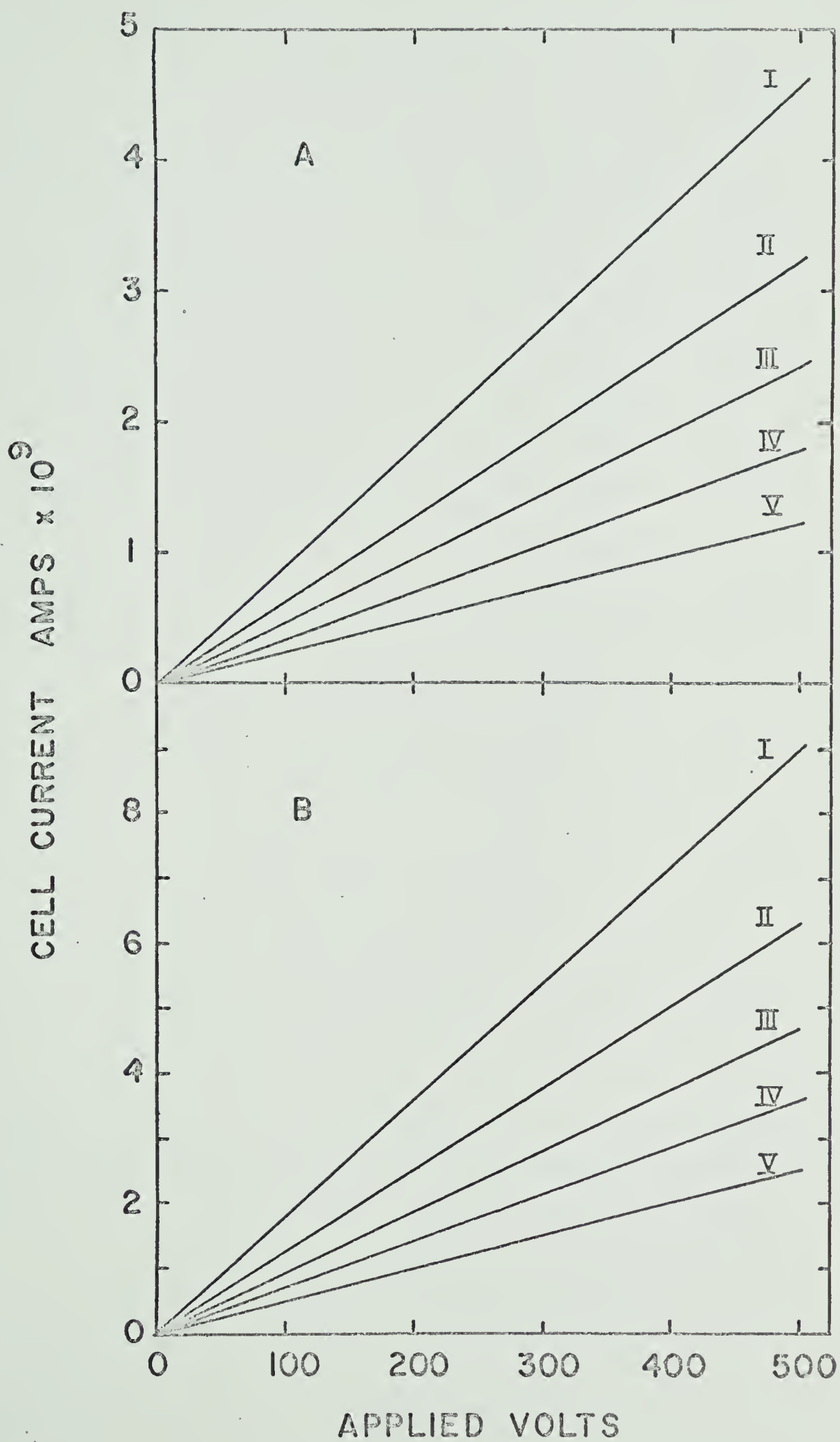


FIGURE III-D-9

Conductance versus Pressure n-Octane 30°C

O Cell D Dose rate 4.6×10^{14} eV/ml sec

o Cell D Dose rate 1.5×10^{14} eV/ml sec

□ Cell F Dose rate 4.6×10^{14} eV/ml sec

■ Cell F Dose rate 1.5×10^{14} eV/ml sec

Pressure Vessel A

Experimental Values

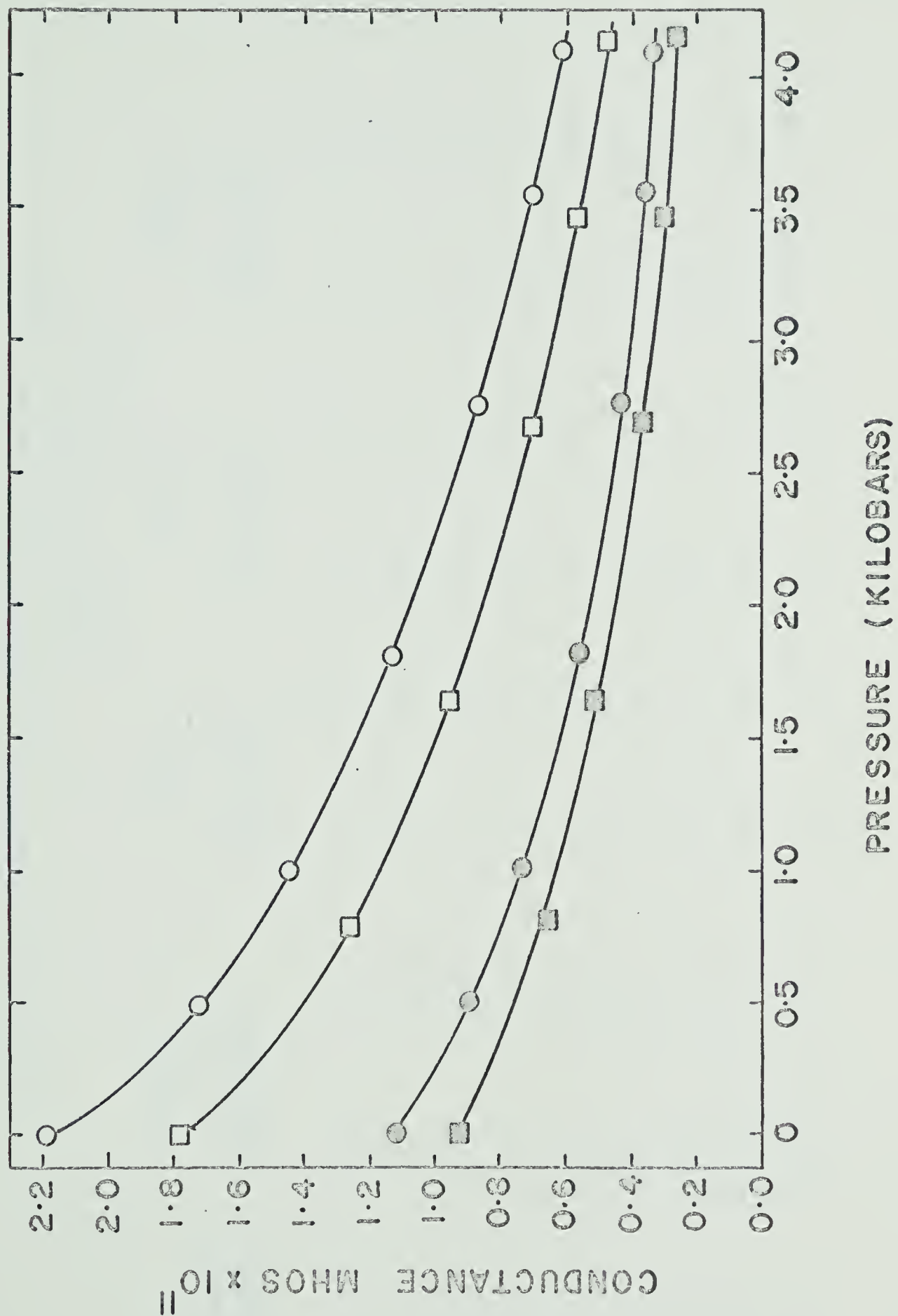


TABLE III-D-IV

Conductance and Relative Conductance n-Octane 30°C

Pressure Bars	I = Conductance mhos $\times 10^{11}$		II = Relative conductance		Cell F		Cell D		Cell F		Cell D		Cell F		Cell D		Cell F		Cell D	
	I		II		I		II		I		II		I		II		I		II	
	4.6 $\times 10^{14}$ eV/ml sec	1.5 $\times 10^{14}$ eV/ml sec	4.6 $\times 10^{14}$ eV/ml sec	1.5 $\times 10^{14}$ eV/ml sec	4.6 $\times 10^{14}$ eV/ml sec	1.5 $\times 10^{14}$ eV/ml sec	4.6 $\times 10^{14}$ eV/ml sec	1.5 $\times 10^{14}$ eV/ml sec	4.6 $\times 10^{14}$ eV/ml sec	1.5 $\times 10^{14}$ eV/ml sec	4.6 $\times 10^{14}$ eV/ml sec	1.5 $\times 10^{14}$ eV/ml sec	4.6 $\times 10^{14}$ eV/ml sec	1.5 $\times 10^{14}$ eV/ml sec	4.6 $\times 10^{14}$ eV/ml sec	1.5 $\times 10^{14}$ eV/ml sec	4.6 $\times 10^{14}$ eV/ml sec	1.5 $\times 10^{14}$ eV/ml sec	4.6 $\times 10^{14}$ eV/ml sec	1.5 $\times 10^{14}$ eV/ml sec
1	2.19	1.00	1.78	1.00	1.78	1.12	1.00	1.00	1.78	1.12	1.00	1.00	1.78	1.12	1.00	1.00	1.78	1.12	1.00	1.00
500	1.72	0.78	1.40	0.79	1.40	0.87	0.78	0.78	1.40	0.87	0.78	0.78	1.40	0.87	0.78	0.78	1.40	0.87	0.78	0.80
1000	1.45	0.66	1.17	0.66	1.17	0.73	0.65	0.65	1.17	0.73	0.65	0.65	1.17	0.73	0.65	0.65	1.17	0.73	0.62	0.67
1500	1.24	0.57	1.00	0.56	1.00	0.63	0.56	0.56	1.00	0.63	0.56	0.56	1.00	0.63	0.56	0.56	1.00	0.63	0.54	0.58
2000	1.07	0.49	0.86	0.48	0.86	0.54	0.48	0.48	0.86	0.54	0.48	0.48	0.86	0.54	0.48	0.48	0.86	0.54	0.46	0.50
2500	0.97	0.44	0.75	0.42	0.75	0.48	0.43	0.43	0.75	0.48	0.43	0.43	0.75	0.48	0.43	0.43	0.75	0.48	0.40	0.43
3000	0.81	0.37	0.65	0.37	0.65	0.42	0.37	0.37	0.65	0.42	0.37	0.37	0.65	0.42	0.37	0.37	0.65	0.42	0.34	0.37
3500	0.71	0.32	0.55	0.31	0.55	0.37	0.33	0.33	0.55	0.37	0.33	0.33	0.55	0.37	0.33	0.33	0.55	0.37	0.30	0.32
4000	0.63	0.29	0.51	0.29	0.51	0.34	0.30	0.30	0.51	0.34	0.30	0.30	0.51	0.34	0.30	0.30	0.51	0.34	0.27	0.29

FIGURE III-D-10

Relative Conductance versus Pressure

n-Octane 30°C

O Cell D Dose rate 4.6×10^{14} eV/ml sec

● Cell F Dose rate 1.5×10^{14} eV/ml sec

Pressure Vessel A

Interpolated Values

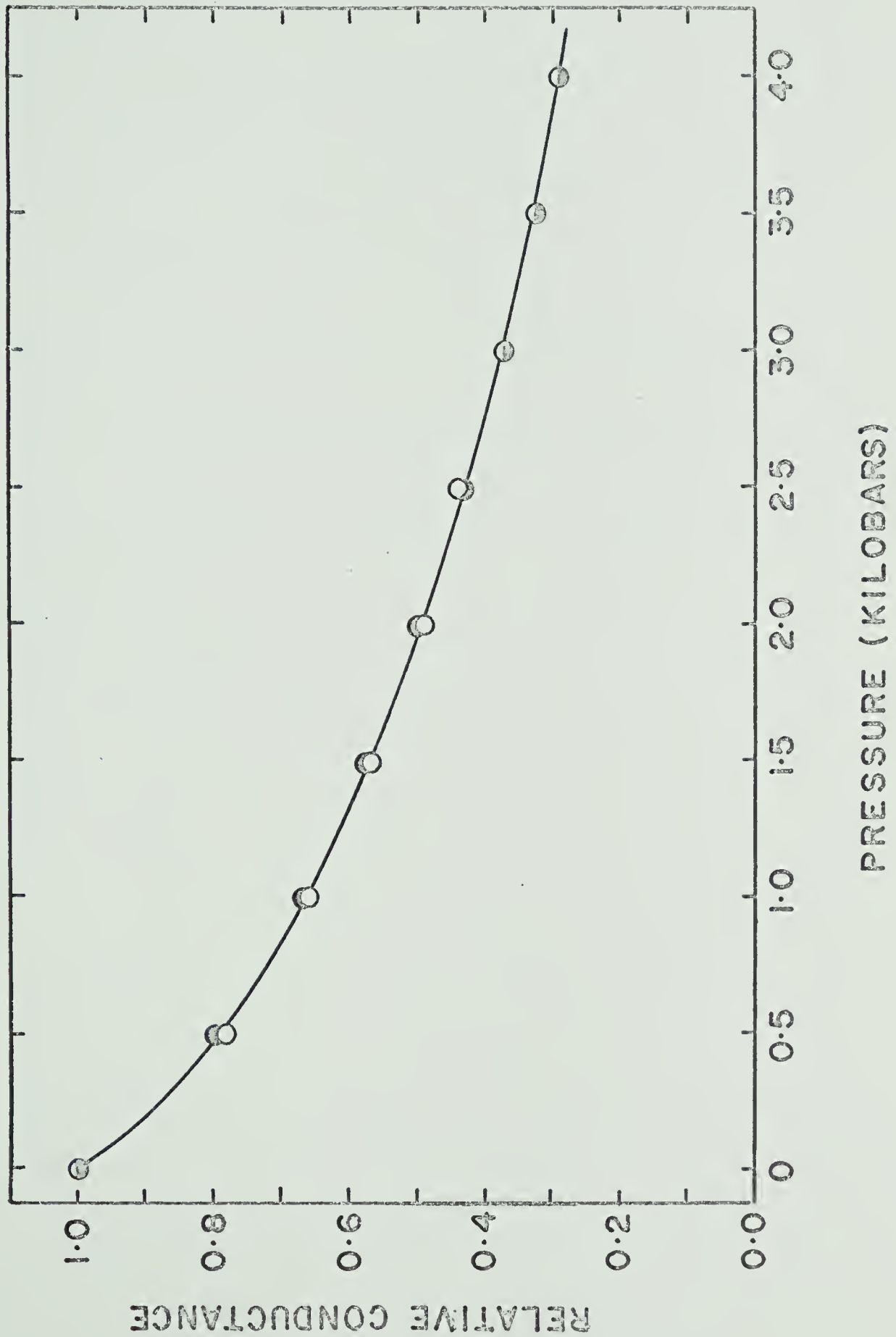


FIGURE III-D-11

Conductance versus Pressure

n-Octane 3°C

O Cell D Dose rate 4.7×10^{14} eV/ml sec

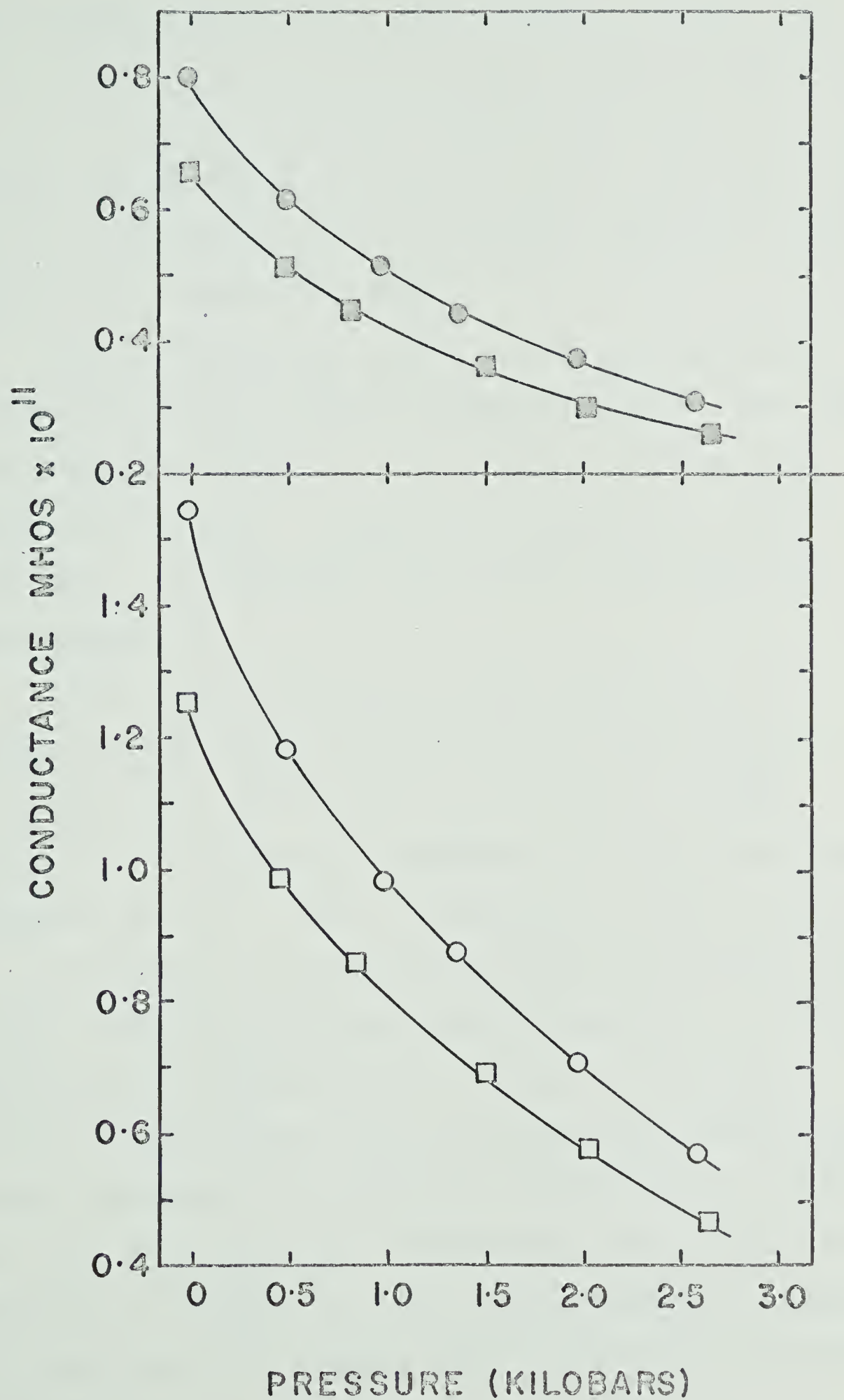
O Cell D Dose rate 1.6×10^{14} eV/ml sec

□ Cell F Dose rate 4.7×10^{14} eV/ml sec

■ Cell F Dose rate 1.6×10^{14} eV/ml sec

All Pressure Vessel A.

Experimental Values



The maximum pressure used with octane at 3°C was 2600 bars because octane freezes at approximately 3000 bars at 0°C. The dose rates for the results illustrated in Figure III-D-11 were 4.7 and 1.6×10^{14} eV/ml sec. These values were calculated from the known temperature dependence of the density of octane.

The interpolated values of the conductance of octane at 3°C are listed in Table III-D-V for each cell and dose rate employed. The relative conductance of octane is shown as a function of pressure in Figure III-D-12. The agreement for each cell and dose rate is satisfactory.

The results obtained for the conductance of n-octane at 56°C, using cells D and F at dose rates of 4.46 and 1.45×10^{14} eV/ml sec, are given in Table III-D-VI. The pressure dependence of the relative conductance at 56°C is also illustrated in Figure III-D-12.

The effect of temperature variation upon the relative conductance is greater than in the case of n-hexane. The relative conductances at 2500 bars of n-octane at 3, 30 and 56°C are 0.39, 0.43 and 0.45 respectively, which correspond to a change in conductance by a factor of 2.56, 2.33 and 2.22. At 4000 bars the relative conductance of n-octane at 30°C and 56°C indicate changes in conductance by factors of 3.45 and 3.22 respectively.

TABLE III-D-V

Conductance and Relative Conductance n-Octane 3°C

I = Conductance mhos $\times 10^{11}$

II = Relative conductance

Pressure Bars	Cell D		Cell F		Cell D		Cell F	
	I	II	I	II	I	II	I	II
	4.74 $\times 10^{14}$ eV/ml sec		4.74 $\times 10^{14}$ eV/ml sec		1.55 $\times 10^{14}$ eV/ml sec		1.55 $\times 10^{14}$ eV/ml sec	
1	1.55	1.00	1.25	1.00	0.80	1.00	0.66	1.00
500	1.18	0.76	0.97	0.78	0.61	0.76	0.51	0.77
1000	0.98	0.63	0.81	0.65	0.51	0.64	0.42	0.64
1500	0.83	0.54	0.69	0.55	0.42	0.53	0.36	0.55
2000	0.70	0.45	0.58	0.46	0.36	0.45	0.30	0.45
2500	0.59	0.38	0.49	0.39	0.32	0.40	0.27	0.41
2600	0.57	0.37	0.47	0.38	0.31	0.39	0.26	0.39

FIGURE III-D-12

Relative Conductance versus Pressure
n-octane at 3 and 56°C

56°C O Cell D 4.46×10^{14} eV/ml sec

■ Cell F 4.46×10^{14} eV/ml sec

Interpolated Values

3°C Δ Cell D 4.74×10^{14} eV/ml sec

▲ Cell D 1.55×10^{14} eV/ml sec

Experimental Values

● Coincident points

Pressure Vessel A

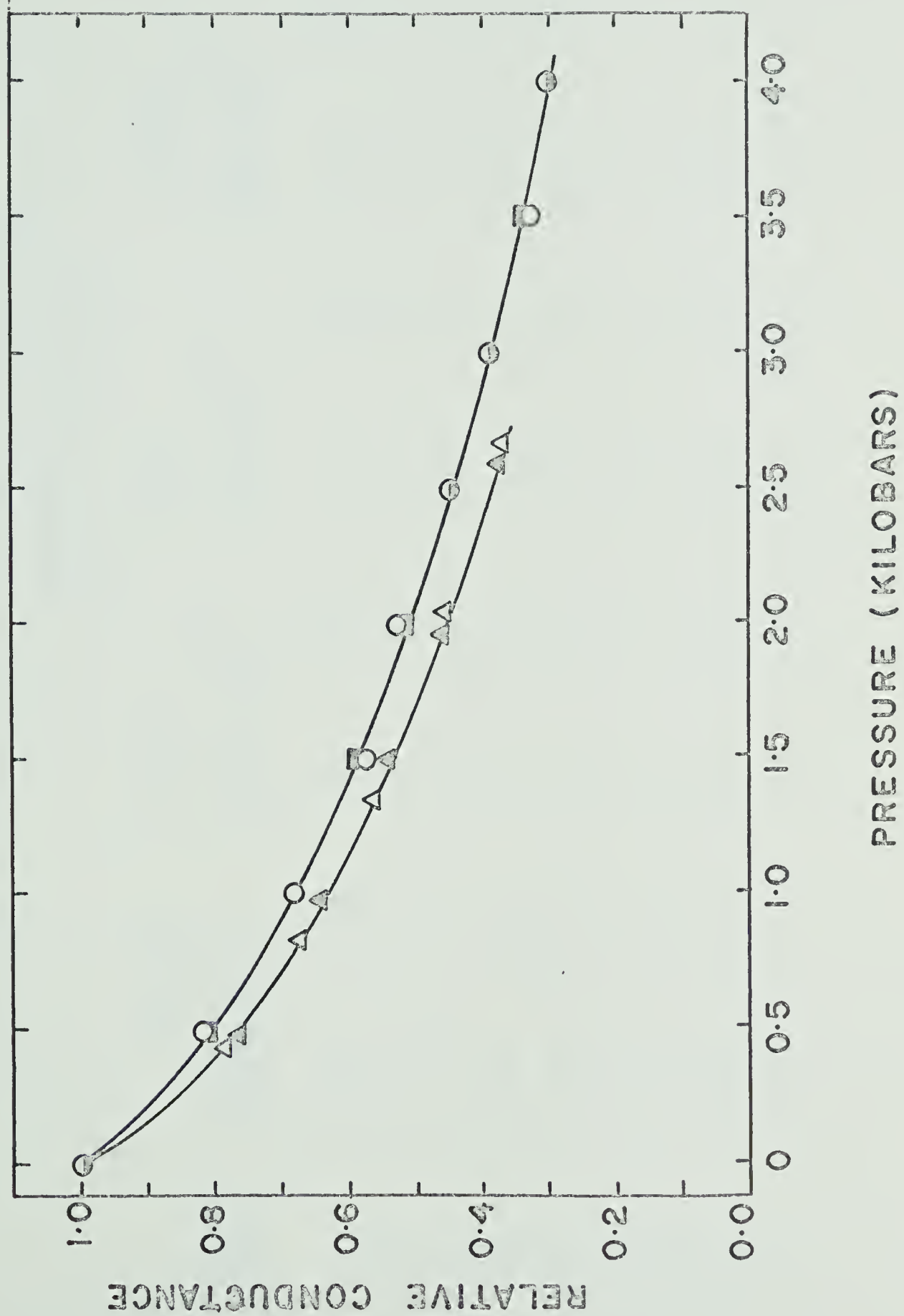


TABLE III-D-VI

Conductance and Relative Conductance n-Octane 56°C

I = Conductance mhos $\times 10^{11}$

II = Relative conductance

Pressure Bars	Cell D		Cell F		Cell D		Cell F		Cell F	
	4.46 $\times 10^{14}$ eV/ml sec	I	II	4.46 $\times 10^{14}$ eV/ml sec	I	II	1.45 $\times 10^{14}$ eV/ml sec	I	II	1.45 $\times 10^{14}$ eV/ml sec
1	2.59	2.18	1.00	2.18	1.33	1.00	1.08	1.00	1.00	1.00
500	2.07	1.77	0.80	1.77	1.06	0.81	0.89	0.80	0.82	0.82
1000	1.74	1.48	0.67	1.48	0.90	0.68	0.72	0.68	0.67	0.67
1500	1.50	1.24	0.58	1.24	0.76	0.58	0.62	0.57	0.57	0.57
2000	1.29	1.13	0.50	1.13	0.68	0.52	0.57	0.51	0.53	0.53
2500	1.17	0.98	0.45	0.98	0.61	0.45	0.49	0.44	0.45	0.45
3000	1.01	0.87	0.39	0.87	0.52	0.40	0.42	0.39	0.39	0.39
3500	0.88	0.72	0.34	0.72	0.44	0.33	0.36	0.33	0.33	0.33
4000	0.80	0.68	0.31	0.68	0.41	0.32	0.33	0.31	0.31	0.31

(4) n-Pentane

n-Pentane was only studied at 30°C. The interpolated conductances at 500 bar intervals of pressure, obtained in several experiments, are given in Tables III-D-VII and VIII. The results shown were obtained using cells B and C at dose rates of 4.0 and 1.32×10^{14} eV/ml sec. The agreement in the measured conductance between two consecutive experiments in cell C with fresh samples of n-pentane is about 6% and varies somewhat over the pressure range studied. This variation was typical of all the hydrocarbons studied where consecutive experiments with the same cell were possible. The pressure dependence of the relative conductance of n-pentane at 30°C is illustrated in Figure III-D-13. The results obtained with both cells B and C are in good agreement. The relative conductance is independent of the dose rate over the dose rate range studied.

(5) Cyclopentane

Cyclopentane was studied at 30°C. The interpolated conductances at 500 bar intervals of pressure are recorded in Table III-D-IX. The results shown were obtained at dose rates of 4.7 and 1.6×10^{14} eV/ml sec with cells B and C.

The calculated relative conductances of cyclopentane are also given in Table III-D-IX and are illustrated as a

TABLE III-D-VII

Conductance and Relative Conductance n-Pentane 30°C

I = Conductance mhos $\times 10^{11}$

II = Relative Conductance

Pressure Bars	Cell C		Cell C		Cell B	
	4.0×10^{14} eV/ml sec	II	4.0×10^{14} eV/ml sec	I	4.0×10^{14} eV/ml sec	II
1	3.30	1.00	3.39	1.00	4.30	1.00
500	2.61	0.79	2.66	0.78	3.51	0.82
1000	2.25	0.68	2.28	0.67	2.95	0.69
1500	1.96	0.59	2.01	0.59	2.54	0.59
2000	1.74	0.53	1.80	0.53	2.22	0.52
2500	1.58	0.48	1.64	0.48	2.02	0.47
3000	1.45	0.44	1.50	0.44	1.85	0.43
3500	1.34	0.41	1.39	0.41	1.70	0.40
4000	1.26	0.38	1.29	0.38	1.61	0.37

TABLE III-D-VIII

Conductance and Relative Conductance n-Pentane 30°C

I = Conductance mhos $\times 10^{11}$

II = Relative Conductance

Pressure Bars	Cell C		Cell C		Cell B	
	1.32×10^{14} eV/ml sec	II	1.32×10^{14} eV/ml sec	I	1.32×10^{14} eV/ml sec	II
1	1.59	1.00	1.70	2.14	1.00	1.00
500	1.27	0.80	1.31	1.66	0.77	0.78
1000	1.08	0.68	1.11	1.42	0.65	0.66
1500	0.96	0.60	0.98	1.26	0.58	0.59
2000	0.86	0.54	0.88	1.12	0.52	0.53
2500	0.80	0.49	0.81	1.03	0.48	0.48
3000	0.73	0.46	0.75	0.94	0.44	0.44
3500	0.68	0.43	0.70	0.86	0.41	0.40
4000	0.63	0.39	0.64	0.81	0.38	0.38

FIGURE III-D-13

Relative Conductance versus Pressure n-Pentane 30°C

- Average two experiments Cell C
Dose Rate 4.0×10^{14} eV/ml sec
- Average two experiments Cell C
Dose Rate 1.32×10^{14} eV/ml sec
- ⊙ Coincident points

Pressure Vessel A

Interpolated Values

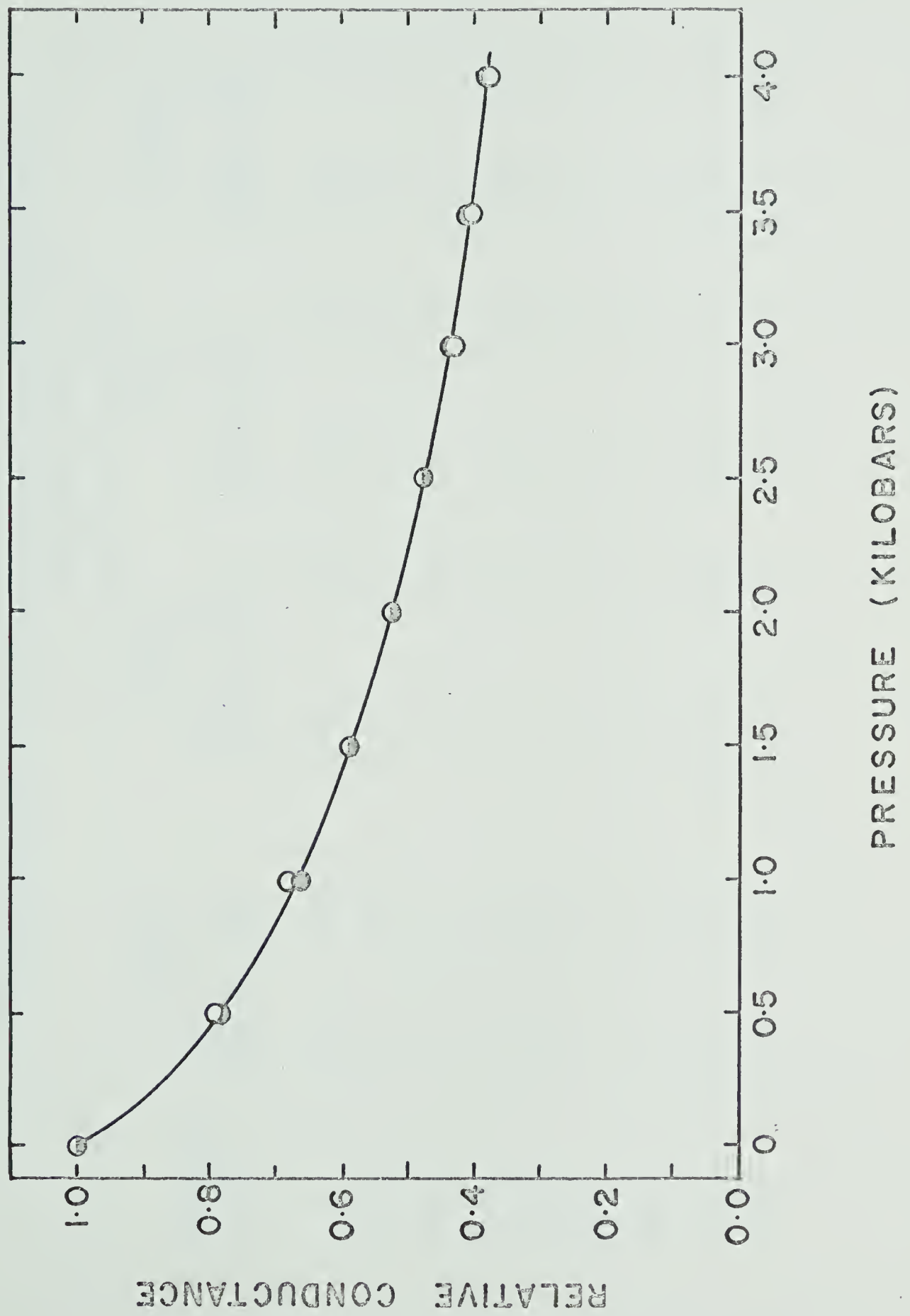


TABLE III-D-IX

Conductance and Relative Conductance Cyclopentane 30 °C

I = Conductance .mhos x 10¹¹

II = Relative Conductance

Pressure Bars	Cell B		Cell C		Cell B		Cell C	
	4.6 x 10 ¹⁴ eV/ ml sec		4.6 x 10 ¹⁴ eV/ml sec		1.6 x 10 ¹⁴ eV/ml sec		1.6 x 10 ¹⁴ eV/ml sec	
	I	II	I	II	I	II	I	II
1	3.40	1.00	2.96	1.00	1.66	1.00	1.46	1.00
500	2.81	0.82	2.40	0.81	1.37	0.82	1.23	0.84
1000	2.46	0.72	2.08	0.70	1.22	0.73	1.05	0.72
1500	2.16	0.64	1.82	0.61	1.08	0.65	0.92	0.63
2000	1.92	0.56	1.62	0.55	0.96	0.58	0.81	0.55
2500	1.71	0.50	1.45	0.49	0.86	0.52	0.71	0.50
3000	1.54	0.45	1.31	0.44	0.78	0.47	0.65	0.45
3500	1.41	0.41	1.19	0.40	0.70	0.42	0.59	0.40
4000	1.29	0.38	1.10	0.37	0.63	0.38	0.54	0.37

function of pressure in Figure III-D-14. Once again the pressure dependence of the relative conductance is independent of the dose rate and the cell employed for the determination.

(6) Methylcyclohexane

Methylcyclohexane, the second of the cyclic hydrocarbons studied, was investigated at 30°C. Apart from the magnitude of the induced conductance being the smallest observed for any hydrocarbon studied under the same experimental conditions, methylcyclohexane behaved in an analogous manner to the other hydrocarbons.

Figure III-D-15 illustrates the pressure dependence of the conductance as obtained with cells B and D. Results are shown for each cell at two dose rates, 4.9 and 1.6×10^{14} eV/ml sec. The conductances interpolated from these experiments are shown in Table III-D-X at 500 bar increments of pressure. The pressure dependence of the relative conductance is shown in Figure III-D-16. The actual experimental values are shown.

The reproducibility from experiment to experiment for the observed relative conductance amounts to about 5%. The relative conductance of 0.23 at 4000 bars corresponds to a 4.4 fold change in conductance.

FIGURE III-D-14

Relative Conductance versus Pressure Cyclo-
pentane 30°C

O Cell B Dose rate 1.6×10^{14} eV/ml sec

● Cell C Dose rate 4.6×10^{14} eV/ml sec

Pressure Vessel A

Interpolated values

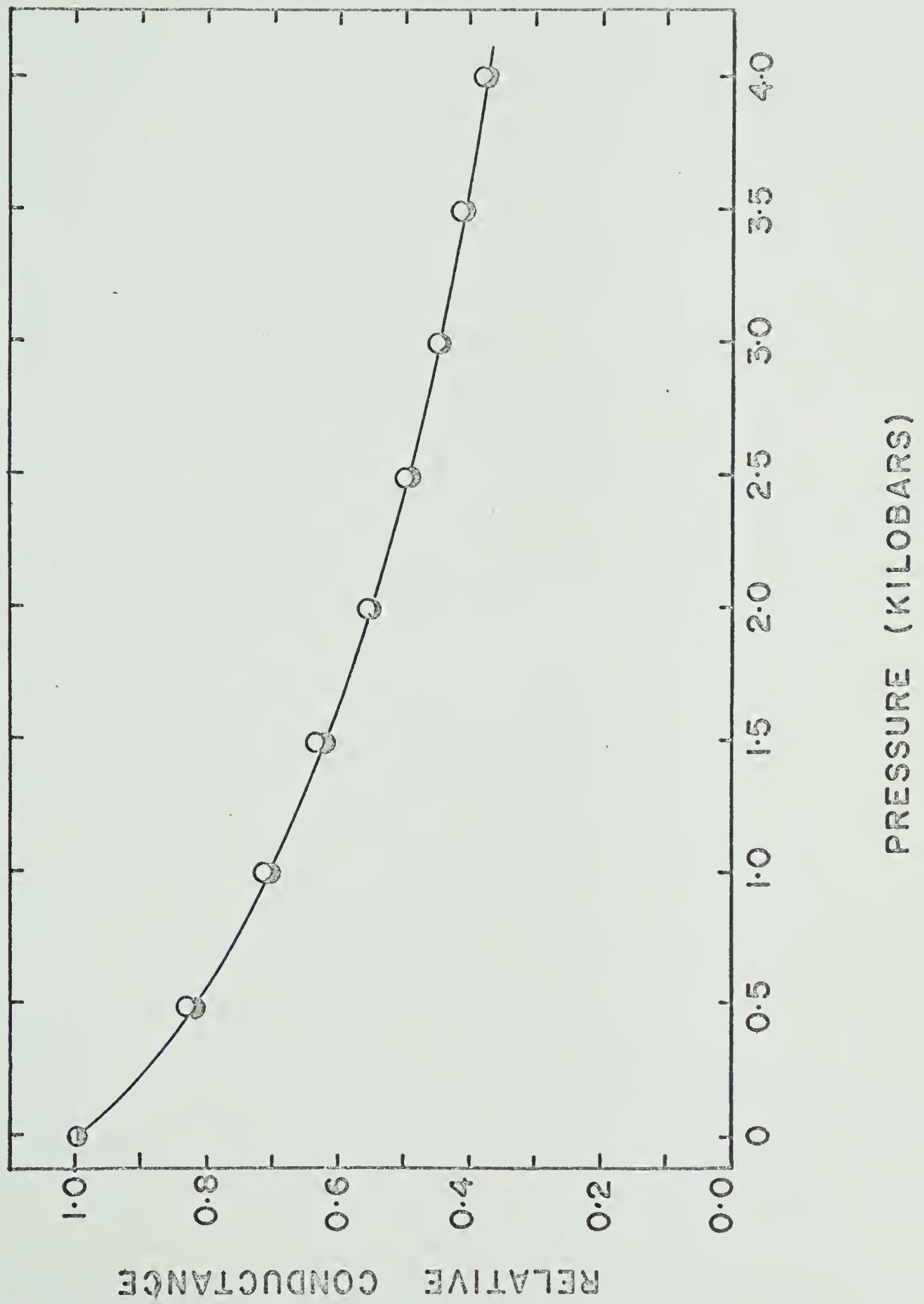


FIGURE III-D-15

Conductance versus Pressure Methylcyclo-
hexane 30°C

O Cell B Dose rate 4.90×10^{14} eV/ml sec

O Cell B Dose rate 1.60×10^{14} eV/ml sec

□ Cell D Dose rate 4.90×10^{14} eV/ml sec

■ Cell D Dose rate 1.60×10^{14} eV/ml sec

Experimental values

Pressure Vessel A

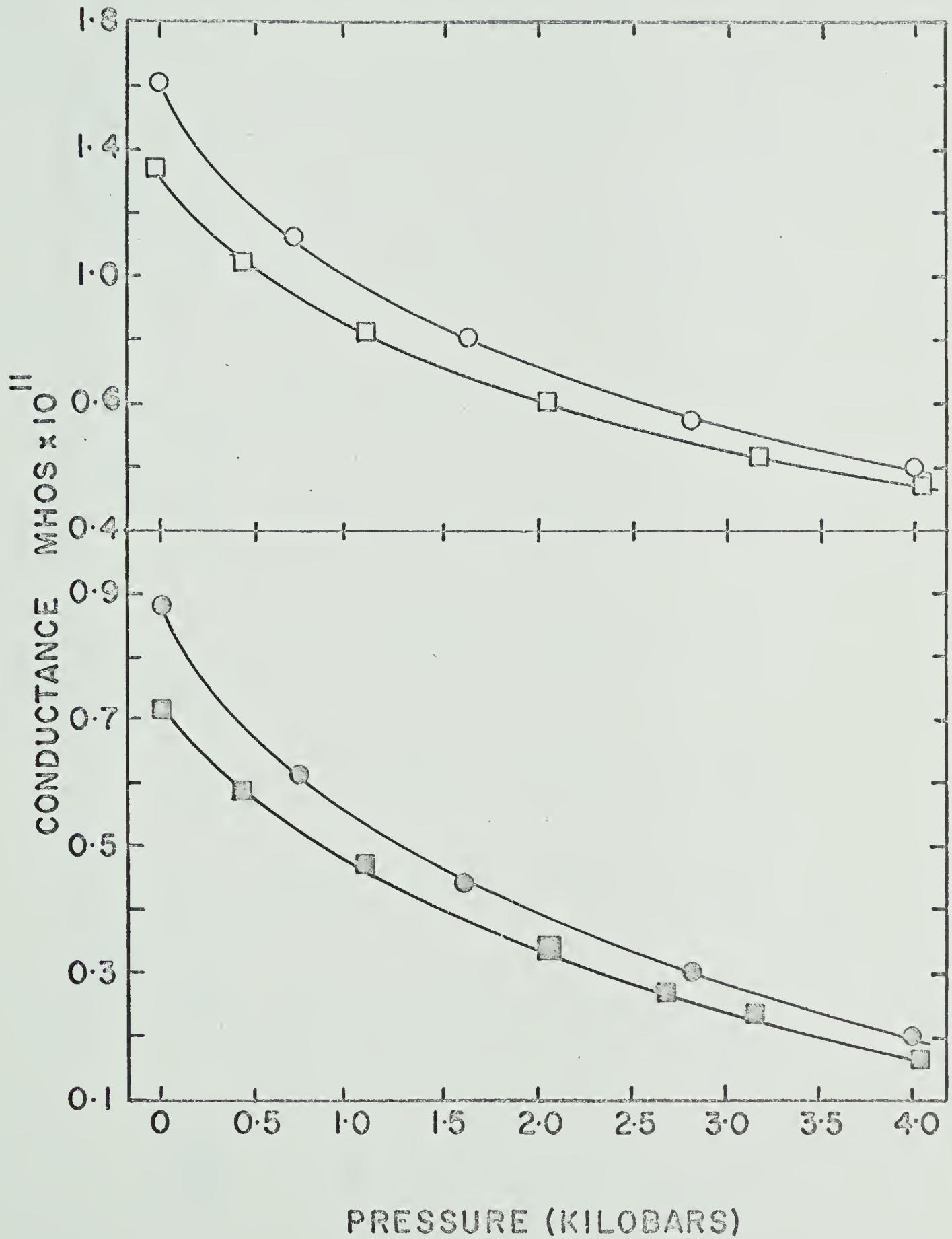


TABLE III-D-X

Conductance and Relative Conductance Methylcyclohexane 30°C

Pressure Bars	Cell B		Cell D		Cell B		Cell D	
	4.9 x 10 ¹⁴ eV/ml sec	I	II	4.9 x 10 ¹⁴ eV/ml sec	I	II	1.6 x 10 ¹⁴ eV/ml sec	I
1	1.62	1.00	1.00	1.35	1.00	1.00	0.88	1.00
500	1.22	0.75	0.76	1.03	0.76	0.77	0.68	0.79
1000	1.00	0.62	0.63	0.85	0.63	0.64	0.56	0.64
1500	0.84	0.52	0.53	0.72	0.53	0.52	0.46	0.56
2000	0.72	0.44	0.46	0.62	0.46	0.44	0.39	0.47
2500	0.61	0.38	0.39	0.52	0.39	0.37	0.33	0.40
3000	0.52	0.32	0.33	0.45	0.33	0.32	0.28	0.35
3500	0.47	0.29	0.29	0.39	0.29	0.28	0.24	0.28
4000	0.38	0.23	0.25	0.34	0.25	0.23	0.20	0.22

FIGURE III-D-16

Relative Conductance versus Pressure Methyl-
cyclohexane 30°C

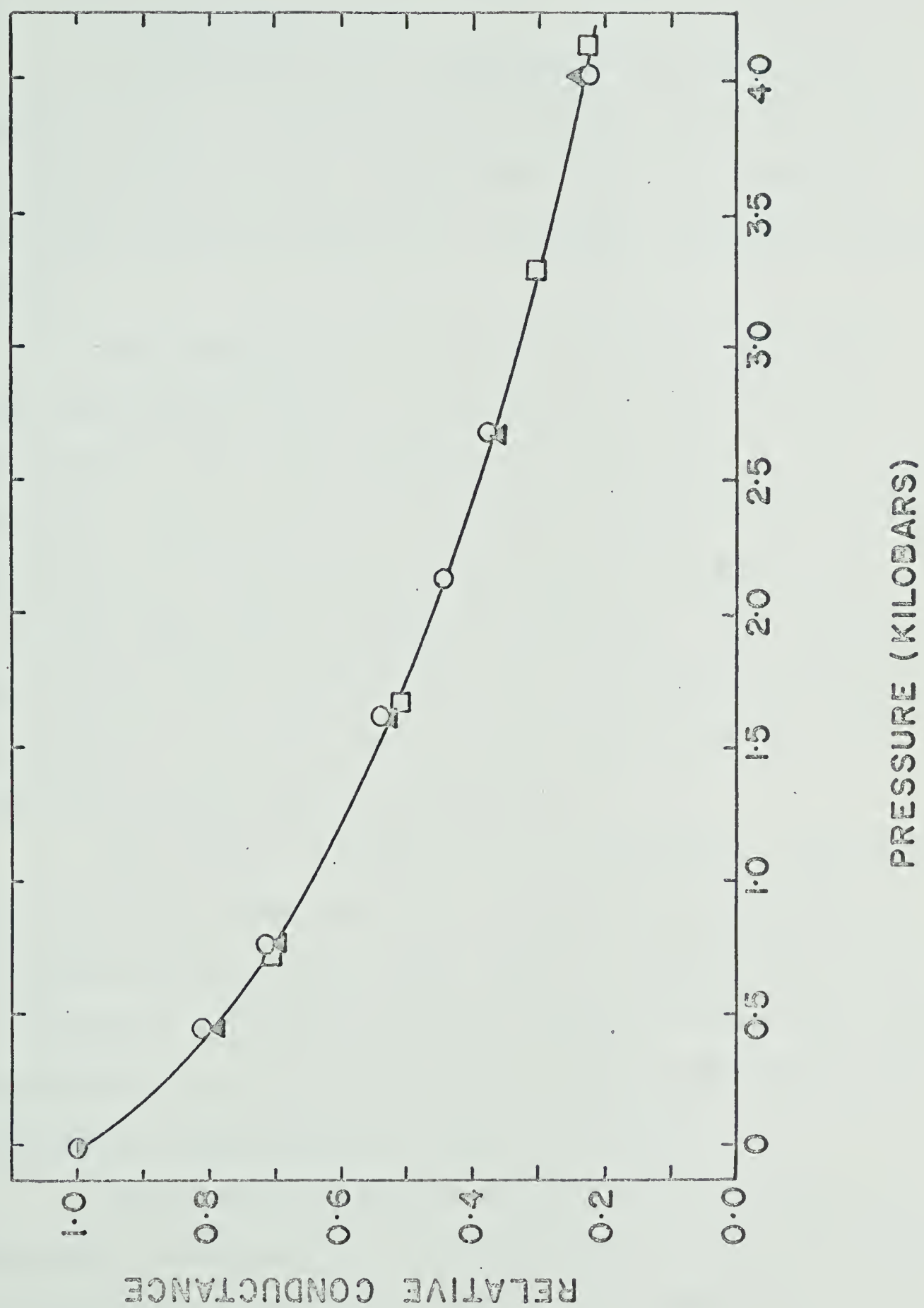
O . Cell D 1.6×10^{14} eV/ml sec

▲ Cell D 4.9×10^{14} eV/ml sec

□ Cell B 4.9×10^{14} eV/ml sec

Pressure Vessel A

Experimental values



(7) 2,2-Dimethylbutane

2,2-Dimethylbutane (neohexane) was found to be unique amongst the hydrocarbons studied in that the radiation induced current in this hydrocarbon was dependent upon the irradiation time (i.e. dependent upon the absorbed dose).

The dependence of the cell current at 100 volts upon the absorbed dose is illustrated in Figure III-D-17. The results shown were obtained at a dose rate of 4.2×10^{14} eV/ml sec using cell F. The initial current at 100 volts was 3.58×10^{-9} amps which rose rapidly to a maximum of 4.3×10^{-9} amps after 3 minutes irradiation. The current then slowly fell over the next 60 to 70 minutes irradiation and finally rose slowly to a steady value of 5.30×10^{-9} amps after 1000 minutes irradiation.

The effect of continuously irradiating a sample that had previously been used for a conductance experiment up to 4000 bars pressure is also shown in Figure III-D-17. A considerable quantity of gas was produced during the irradiation because at the end of the experiment the bellows was extended by approximately double its length.

Some results obtained for the effect of pressure upon the conductance of 2,2-dimethylbutane are illustrated in Figure III-D-18. The values of the conductance at one atmosphere pressure correspond to 3 minutes irradiation.

FIGURE III-D-17.

Cell Current versus Absorbed Dose

2,2-dimethylbutane 30°C

Atmospheric Pressure.

O Cell F Dose rate 4.2×10^{14} eV/ml sec

□ Cell F Dose rate 4.2×10^{14} eV/ml sec
after 55 minutes irradiation at same
dose rate and pressures up to 4000
bars.

Pressure Vessel A

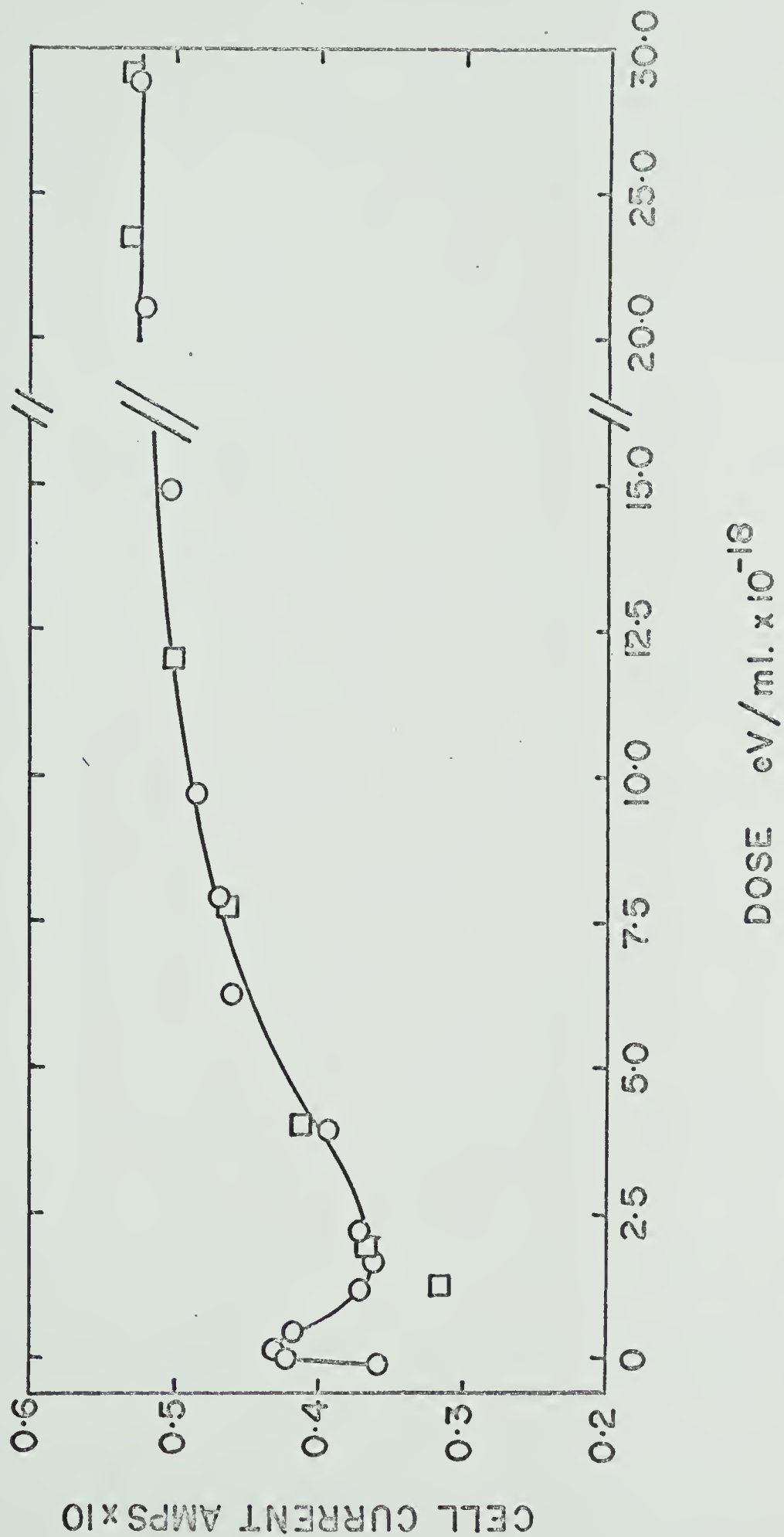


FIGURE III-D-18

Conductance versus Pressure 2,2-dimethyl-
butane 30°C

All Cell F

O Dose rate 4.2×10^{14} eV/ml sec

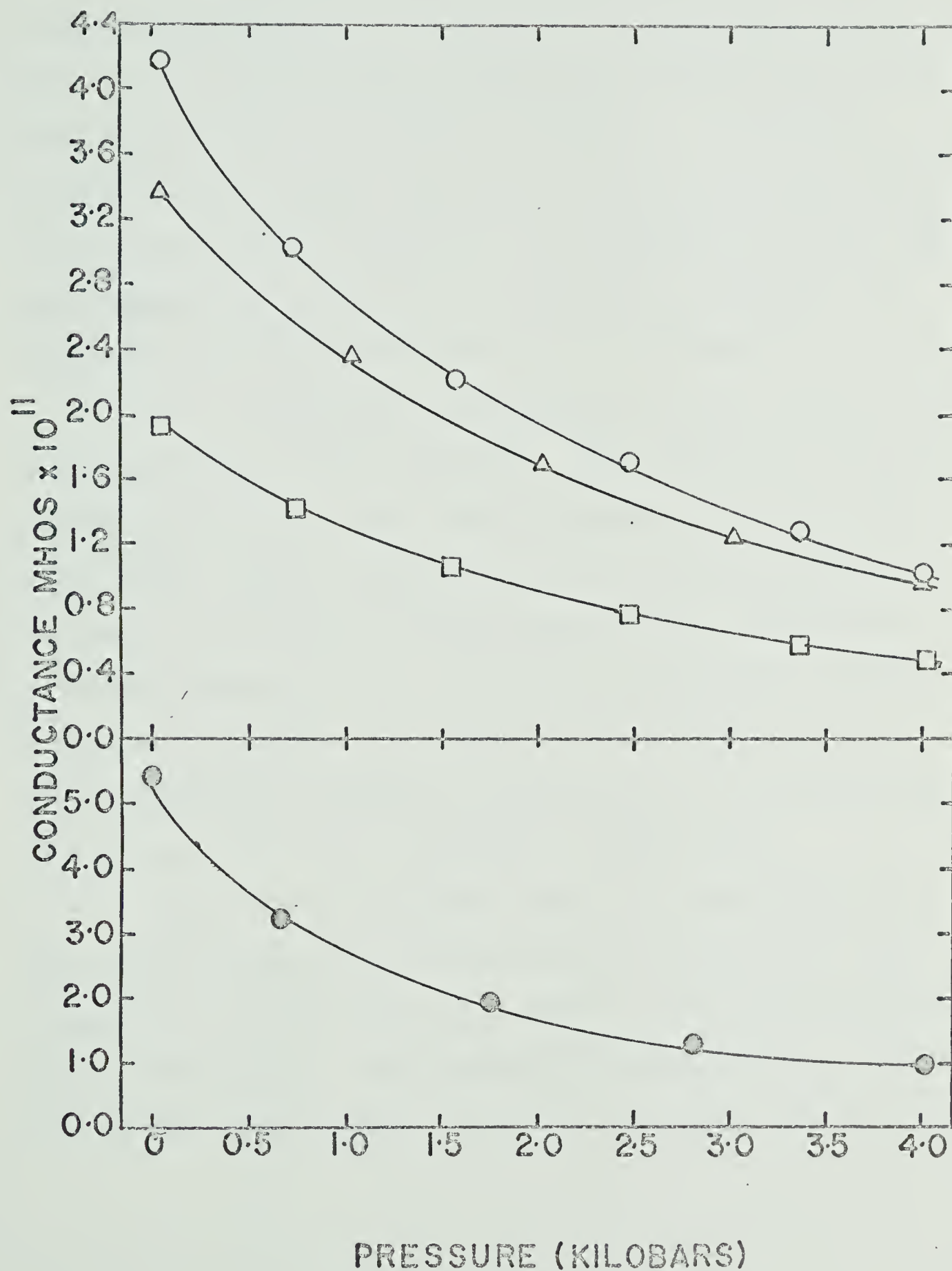
□ Dose rate 1.4×10^{14} eV/ml sec

Δ Dose rate 4.2×10^{14} eV/ml sec

Pressure reducing cycle [Experiment B - Table III-D-XI]

O Dose rate 4.2×10^{14} eV/ml sec
after irradiation to steady cell
current at 100 volts (total dose
prior to experiment 37.5×10^{18}
eV/ml).

Pressure Vessel A



The conductance on the pressure decreasing cycle fell below that determined on the pressure increasing cycle. The latter variation was not due to a change in the dose rate as previously discussed on page 179. Also shown in Figure III-D-18 are the results obtained for the effect of pressure upon a sample of 2,2-dimethylbutane that had been previously irradiated at atmospheric pressure for 1500 minutes (total dose about 3.7×10^{18} eV/ml).

The interpolated conductances for each experiment are recorded in Table III-D-XI. The calculated relative conductances, based upon the atmospheric pressure value after three minutes irradiation are in surprisingly good agreement considering the variation of the conductance with the absorbed dose. The pressure dependence of the relative conductance is illustrated in Figure III-D-19. The conductance changes by a factor of 4.2 on increasing the pressure from one atmosphere to 4000 bars.

The effect of pressure upon the conductance of the sample that had been previously irradiated for 1500 minutes was greater than on a sample that had received no prior irradiation. The conductance decreased by a factor of 5.2 over the pressure range one atmosphere to 4000 bars.

TABLE III-D-XI

Conductance and Relative Conductance 2,2-Dimethylbutane 30°C

I = Conductance mhos $\times 10^{11}$
 II = Relative Conductance.

Pressure Bars	Cell F ^b		Cell F		Cell F		Cell F ^a	
	4.2 $\times 10^{14}$ eV/ml sec		4.2 $\times 10^{14}$ eV/ml sec		4.2 $\times 10^{14}$ eV/ml sec		4.2 $\times 10^{14}$ eV/ml sec	
	I	II	I	II	I	II	I	II
1	3.99	1.00	3.37	1.00	4.18	1.00	1.95	1.00
500	3.38	0.77	2.77	0.82	3.25	0.78	1.55	0.79
1000	2.52	0.63	2.35	0.70	2.66	0.64	1.25	0.64
1500	2.14	0.54	2.00	0.59	2.26	0.54	1.06	0.54
2000	1.80	0.45	1.67	0.50	1.92	0.46	0.90	0.46
2500	1.52	0.38	1.42	0.42	1.63	0.40	0.77	0.39
3000	1.31	0.33	1.23	0.36	1.40	0.33	0.65	0.33
3500	1.12	0.28	1.05	0.31	1.20	0.29	0.55	0.28
4000	0.95	0.24	0.94	0.28	0.98	0.23	0.47	0.24

^aValue after irradiation to steady value of the cell current (see text)^bPressure releasing cycle.

FIGURE III-D-19

Relative Conductance versus Pressure

2,2-dimethylbutane 30°C

O

Cell F 4.2×10^{14} eV/ml sec

O

Experimental points. Two consecutive experiments

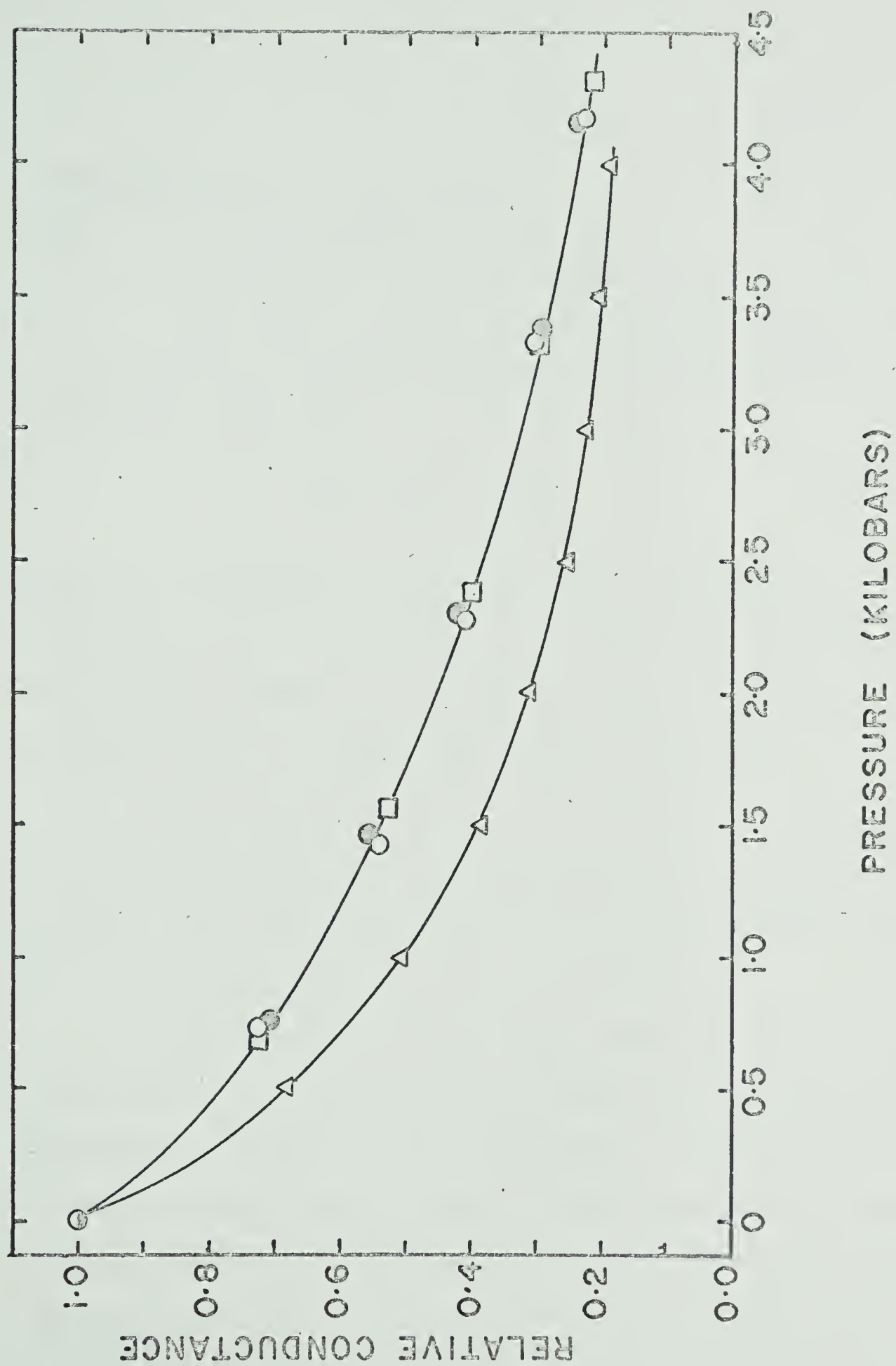
□

Cell F 1.4×10^{14} eV/ml sec

Δ

Cell F 4.2×10^{14} eV/ml sec after a total dose of 37.5×10^{18} eV/ml sec.

Pressure Vessel A



Section IV

D I S C U S S I O N

Radiation Induced Conductance

(A) G_{fi} at Atmospheric Pressure

The value of G_{fi} at one atmosphere pressure may be calculated from the relation previously given in Section I (page 13).

$$G_{fi} = 100 \frac{k\kappa^2}{Iu^2} \quad (I-v)$$

When k is expressed in $\text{cm}^3/\text{ion sec}$, κ in mho/cm , I in eV/ml sec and u in $\text{cm}^2/\text{V sec.}$, in order to obtain G_{fi} in units of ions/100 eV, the relation must be multiplied by $1/e^2$, where e is the ion charge in coulombs.

The ratio k/u may be separated out from relation I-v and calculated from Debyes Theoretical relation (I-vi). For the hydrocarbons used in the present studies k/u lies in the range 0.9 to $1 \times 10^{-6} \text{ V/cm}$.

In order to calculate G_{fi} , the sum of the individual positive and negative ion mobilities must be known. Literature values for the mobilities or radiolytic ions in hydrocarbons vary by about a factor of two (see Table I-C-1), the experimental values for the mobility depending upon the purity of the hydrocarbon and upon the experimental technique employed for their determination.

To remove uncertainty in G_{fi} values calculated from relation I-v, the mobilities of the ions should be determined simultaneously with the steady state conductance. In the present work ion mobilities were not determined. Experimentally, such determinations are very difficult when the cell is contained inside a high pressure vessel because it is impossible to transmit a narrow beam of pulsed radiation through the vessel without scattering.

In general, the mobility of a negative ion in an hydrocarbon is related to the viscosity of the hydrocarbon by,

$$u_- = a_- \eta^{-b_-} \quad (IV-i)$$

where a_- and b_- are constants. A similar expression exists for the positive ions. Reported values of b_- lie between 0.83 (69) and 1.00 (74) whereas for positive ions, b_+ varies from 0.96 (69) to 1.5 (74). Recent results from this laboratory (61, 154) gives b_+ 0.94 and b_- 0.99. The results of the latter study were used to calculate G_{fi} in the present work.

Figure IV-A-I show the log-log plot of mobility versus viscosity for positive and negative radiolytic ions in several hydrocarbons (154). The mobilities of the respective ions in the hydrocarbons used in the present

work were obtained by interpolation from the full lines of this graph, using the known hydrocarbon viscosity.

Table IV-A-I contains the interpolated mobilities and the calculated values of G_{fi} at one atmosphere pressure. The G_{fi} values are the average of numerous determinations, some of which were not included in the last section. Values obtained using pressure vessel B are not included because of the large uncertainty in the dose rate in this vessel. Also included in Table IV-A-I are values of G_{fi} calculated using other literature values for u where available.

The values of G_{fi} at atmospheric pressure are of the correct order of magnitude but are roughly 40% lower than the average of the literature values for the same hydrocarbon (see Table I-C-1). It should be noted that the literature values vary by as much as a factor of three.

Owing to the uncertainty in the actual ion mobilities in the present system extensive speculation about the cause of the low values is not worthwhile. It is possible that the dose rates reported in the last section are too high, however, an error of about 40% is unlikely.

The mobilities of the positive ions used in the calculations may also be too high. The dashed line in

FIGURE IV-A-I

Ion Mobility versus Viscosity Log Log Plot

- n-pentane
- ∇ 2,2-dimethylpropane
- Δ n-hexane
- 2,2-dimethylbutane
- cyclohexane

open points negative ion

20°C

closed points positive ion

slope dashed line -1.5.

TABLE IV-A-I
G_{fi} (atmospheric pressure) and Ion Mobilities

Compound	Temp.	$u_+ \times 10^3$ cm ² /V sec	$u_- \times 10^3$ cm ² /V sec	G _{fi} +0.01	G _{fi} ^a
n-pentane	30	0.84	1.63	0.07	0.07 (62)
n-hexane	3	0.51	0.91	0.06	0.08 (67)
	30	0.65	1.23	0.07	0.05-0.09 (56,62,67)
	56	0.80	1.52	0.07	0.08 (67)
n-octane	3	0.29	0.53	0.07	0.08 (67)
	30	0.40	0.73	0.09	0.10 (67)
	56	0.50	0.94	0.11	0.13 (67)
methylcyclohexane	30	0.30	0.56	0.04	-----
cyclopentane	30	0.48	0.90	0.07	-----
2,2-dimethylbutane	30	0.57	0.90	0.30	-----
	30	0.57	0.90	0.60 ^b	

^aG_{fi} calculated using mobilities in references cited.

^bSample that had been irradiated for 1500 minutes at 4.2 x 10¹⁴ eV/ml sec.

Figure IV-A-1 has a slope of -1.5 in accordance with the reported mobility - viscosity dependence of Adamczewski et al. (65,66,75). The location of the line is arbitrarily placed assuming the mobility of an ion in a solvent of viscosity 0.3 cp is $0.6 \text{ cm}^2/\text{eV sec}$.

The mobility of the positive ion assuming such behaviour in methylcyclohexane is reduced by about 35% and the corresponding G_{fi} increased by about 12%. The calculated G_{fi} for methylcyclohexane is still low but no other values are available for comparison.

The high G_{fi} value for 2,2-dimethylbutane is in agreement with those reported by other workers (61,68,154). The increase in the steady state conductance with increasing dose was also observed in glass cells which were more amenable to rigorous cleaning. The decline in the conductance after a dose of about $7 \times 10^{16} \text{ eV/ml}$ and eventual rise (Figure III-D-17) were not observed in glass systems.

The initial rise in conductance may be the result of the removal of electron scavengers present in the original sample and the further decline then arising from the production of electron scavengers from the direct radiolysis of the sample. There is no apparent reason why the steady state conductance should then increase.

(B) Effect of Pressure on G_{fi}

From relation I-v (page 13) the ratio of G_{fi} at any pressure to that at one atmosphere pressure and at the same temperature is given by

$$\left(\frac{G_{fi}^P}{G_{fi}^1} \right) = \frac{\frac{k_p}{u_p}}{\frac{k_1}{u_1}} \frac{I_1 u_1 \left(\frac{\kappa_p}{\kappa_1} \right)^2}{I_p u_p} \quad (IV-ii)$$

When the dose rate is expressed in eV/ml sec the ratio I_1/I_p may be replaced by the ratio ρ_1/ρ_p where ρ is the density of the sample at the respective pressure. Further from Debyes relation,

$$\frac{\frac{k_p}{u_p}}{\frac{k_1}{u_1}} = \frac{\epsilon_1}{\epsilon_p} \quad (IV-iii)$$

and relation IV-ii may be written

$$\frac{G_{fi}^P}{G_{fi}^1} = \frac{\epsilon_1}{\epsilon_p} \frac{\rho_1}{\rho_p} \frac{u_1}{u_p} \left(\frac{\kappa_p}{\kappa_1} \right)^2 \quad (IV-iv)$$

The only unknown ratio in IV-iv is u_1/u_p , the pressure dependence of the ion mobilities. As was mentioned in the last section, the ion mobilities were not measured in the present work and difficulties arise as to the correct mobility values to use, when considering the

data.

Two limiting cases may be considered, one in which the Stoke-Walden relationship is assumed to be applicable (i.e. b_+ and b_- in relation IV-i are assumed to be unity) and the second, in which G_{fi} is assumed to be independent of pressure.

(a) Assume that Stokes-Walden-Rule Applies

If b_+ and b_- are both unity, the ratio u_l/u_p in IV-iv may be replaced by η_p/η_l therefore

$$\frac{G_{fi}^P}{G_{fi}^l} = \frac{\epsilon_l}{\epsilon_p} \frac{\rho_l}{\rho_p} \frac{\eta_p}{\eta_l} \left(\frac{\kappa_p}{\kappa_l} \right)^2 \quad (\text{IV-v})$$

The pressure dependence of the ratio $(G_{fi}^P)/(G_{fi}^l)$ at 30°C is illustrated in Figure IV-B-1 for pentane, hexane and octane and in Figure IV-B-2 for methylcyclohexane, cyclopentane and 2,2-dimethylbutane. Figure IV-B-1 also includes the results obtained for n-hexane at 3 and 56°C. The pressure dependence of the dielectric constant at these temperatures was calculated from the present results at 30°C together with Mopsiks (126) data at -25, 0 and 25°C. The pressure dependence of ϵ for n-octane at temperatures other than 30°C is not available.

The scatter in the data arises from the dependence of $(G_{fi}^P)/(G_{fi}^l)$ upon the square of the conductivity.

FIGURE IV-B-1

$(G_{fi}^P)/(G_{fi}^L)$ versus Pressure

O n-pentane 30°C

□ n-hexane 30°C full line

dashed lines I 3°C

II 56°C

Δ n-octane 30°C

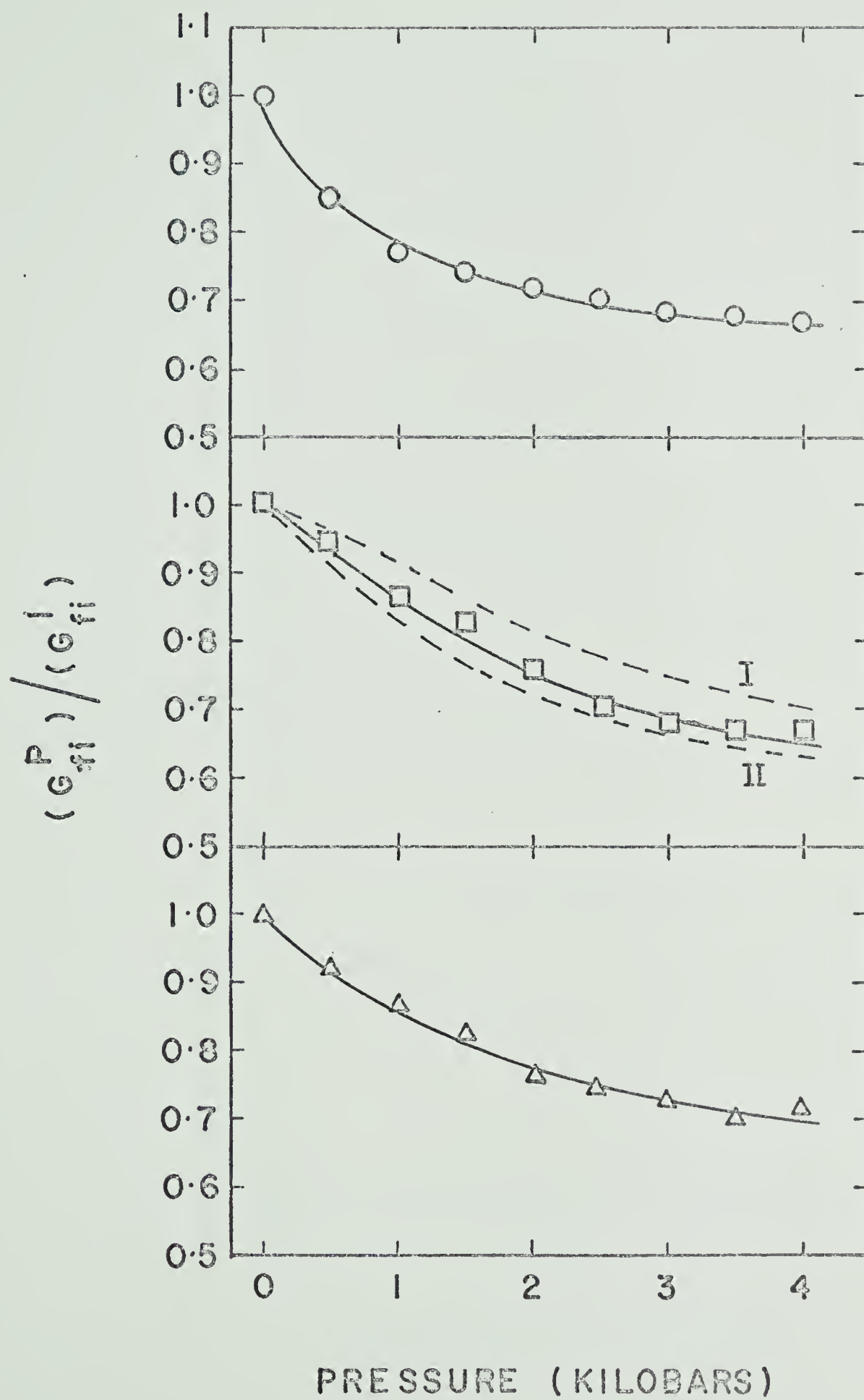


FIGURE IV-B-2

$(G_{fi}^P)/(G_{fi}^L)$ versus Pressure

O Methylcyclohexane

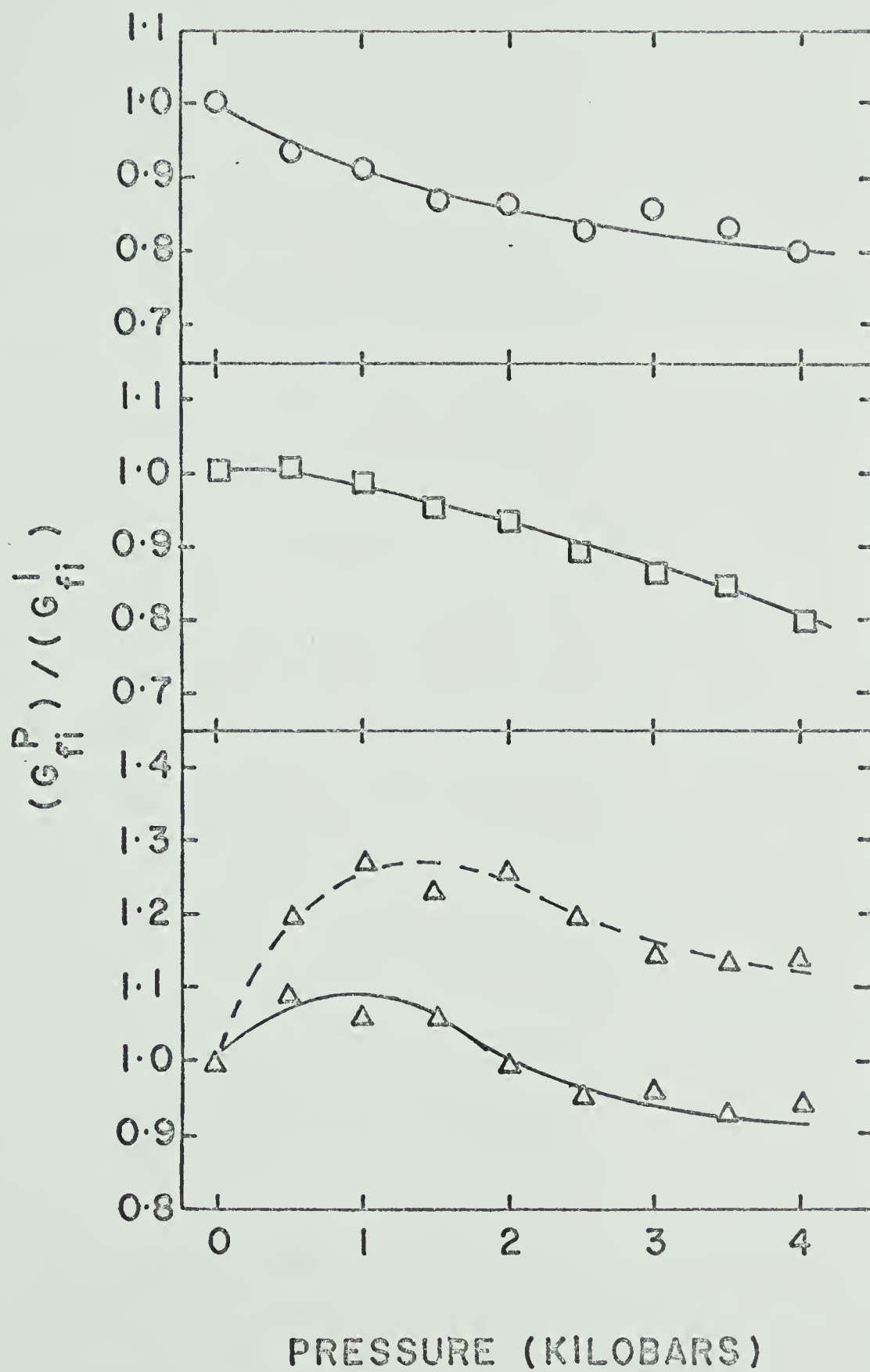
□ Cyclopentane

Δ 2,2-Dimethylbutane

full line pressure increasing
cycle.

dashed line pressure decreasing
cycle

All 30°C.



In general if the Stoke-Walden relationship is applicable G_{fi} is decreased on increasing the pressure from one atmosphere to 4000 bars by about 33% for n-pentane and hexane, and by 30% for n-octane. For n-hexane the change in G_{fi} with pressure is temperature dependent but because of the experimental error little significance can be attached to the observed variation.

The decrease in G_{fi} for the cyclic hydrocarbons over the same pressure range at 30°C is less than for the straight chain hydrocarbon and amounts to about 20%. The variation of G_{fi} with pressure for 2,2-dimethylbutane is unusual in that it first increases and then decreases, the values at one atmosphere and approximately 2000 bars being equal. This behaviour is probably unreal and is associated with the dose dependence of the induced conductance. If the conductance as determined on the pressure reducing cycle is used to calculate (G_{fi}^P/G_{fi}^1) , a curve of similar shape is obtained but G_{fi} increases further with pressure.

(b) Assume that G_{fi} is independent of pressure.

If G_{fi} is considered to be independent of pressure then it must be assumed that Walden rule does not apply,

hence

$$(u_+ + u_-) \propto \eta^{-b} \quad (\text{IV-vi})$$

and

$$\left(\frac{\eta_p}{\eta_1} \right)^b = \frac{\epsilon_p}{\epsilon_1} \frac{\rho_p}{\rho_1} \left(\frac{\kappa_1}{\kappa_p} \right)^2 \quad (\text{IV-vii})$$

The power b to which η_p/η_1 must be raised in order to make it equal to the right hand side of the equation IV-vii can be calculated. The dependence of the calculated b value on the applied pressure is illustrated in Figure IV-B-3.

The value of b for hexane and octane is about 1.20 at one atmosphere pressure and is, within experimental error, independent of pressure. The value for *n*-pentane is about 1.4 at atmospheric pressure and decreases with increasing pressure. Methylcyclohexane shows a similar decrease in b with increasing pressure the extrapolated value at 1 atmosphere being about 1.15. Cyclopentane on the other hand exhibits a value less than unity at atmospheric pressure which increases with increasing pressure.

For hexane and octane, the results suggest that

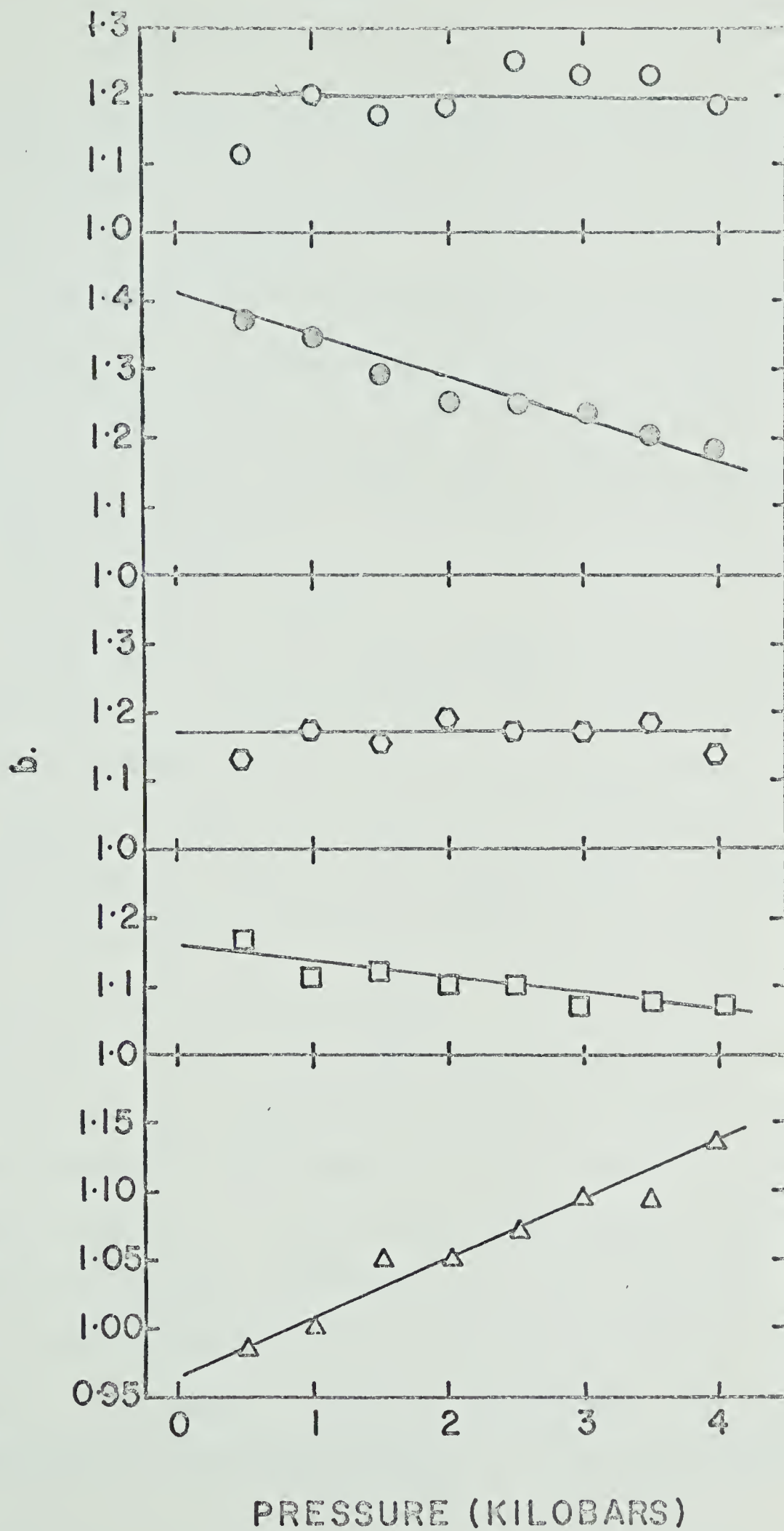
$$u \propto \eta^{-1.20}$$

FIGURE IV-B-3

Power b in Relation IV-vii

- O n-hexane
- n-pentane
- n-octane
- methylcyclohexane
- Δ cyclopentane

All 30°C



which is in close agreement with the value predicted on the basis of some ion mobility measurements ($b_- \sim 1$ and $b_+ \sim 1.5$) (65,66,75).

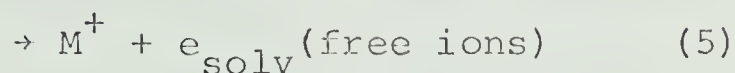
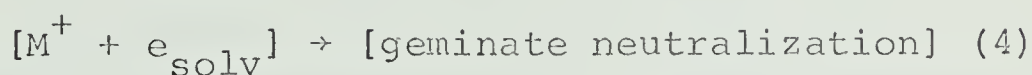
The cause of the different values for the other hydrocarbons is not immediately apparent. Quantitatively, the more spherical ions may be expected to follow more closely to Stokes Law. However, pentane and methylcyclohexane do not fit any more closely than do the other hydrocarbons.

The variation of b with pressure, if real, is interesting. In applying Stokes Law it is generally assumed that the volume of the ion is independent of the applied pressure (at least up to 4000 bars the maximum pressure used in the present work). Quantitatively it is difficult to say anything about the ions because their nature is unknown. Examination of Figure IV-A-1 shows that the experimental results (154) obtained for the mobilities of the positive ions exhibit greater scatter about their line than those of the negative species. This is surprising because the positive ion is always considered to be the positive ion of the hydrocarbon under irradiation whilst the nature of the negative species depends upon the impurities present in the hydrocarbon. It is also possible

that several negative and positive species exist.

Radiolytic ions may be solvated in low dielectric constant liquids. The amount of electrostriction around a cavity of roughly molecular size which contains a charge is greater in low dielectric liquids than in high dielectric constant liquids (155), and electrostriction may be important in the localization process of thermalized electrons. From the point of view of the bulk compressibility of the hydrocarbon under irradiation compared to that in the absence of radiation electrostriction may be neglected because the concentration of the ions is small ($\sim 10^{-9}$ M).

The variation of G_{fi} with pressure may be predicted on the basis of the model developed by Freeman (25,49). Consider the two reactions (see Section I)



The "critical escape distance" (page 13) which determines whether reaction 4 or 5 occurs, decreases with increasing pressure because of the increased dielectric constant. In the present hydrocarbons ϵ increased by between about 11% (methylcyclohexane) and 16% (n-pentane) when the pressure was increased to 4000 bars. On the other hand

the initial separation distance of the parent ion and its corresponding electron (or negative ion) also decreases with increasing pressure because the range of an electron is assumed to be inversely proportional to the density of the liquid. The latter may not be true for low energy electrons close to thermal energy. The density increases for the present hydrocarbons studied on increasing the pressure to 4000 bars by between 12% (methylcyclohexane) and 29% (n-pentane).

The values of y , the ion separation distance, was taken from the calculation of Freeman (49) for n-hexane at 20°C and corrected for the density at 30°C, using the known temperature dependence of the density. The values were then further altered for use at 4000 bars and 30°C using the determined pressure dependence of density. It was assumed that $N(y)$, the number of electrons with the separation distance y , was independent of pressure and that only y was changed. The results obtained for $\phi(y)$, which is the probability of escape (given by $e^{-r/y}$), and G_{fi} at one atmosphere and 4000 bars are shown in Table IV-B-I. The G_{fi} values were calculated using the expression given previously (I-xii) assuming that $G(\text{total ionization})$ was four. The calculated decrease in G_{fi} is 6% when the pressure is increased

TABLE IV-B-1

G_{fi} 30°C n-hexane 1 atmosphere and 4000 bars

1 atmosphere				4000 bars		
<u>N(y)</u>	<u>(y)</u>	<u>$\phi(y)$</u>	<u>N(y) $\phi(y)$</u>	<u>(y)</u>	<u>$\phi(y)$</u>	<u>N(y) $\phi(y)$</u>
2150	20	---	0	16	----	0
1100	22	---	0	18	----	0
600	27	---	0	22	----	0
476	37	---	0	30	----	0
270	63	0.009	3	51	0.006	2
116	102	0.056	6	82	0.044	5
64	148	0.137	9	119	0.114	7
41	199	0.228	9	160	0.198	8
28	257	0.319	9	206	0.287	8
21	319	0.398	8	256	0.364	8
16	388	0.469	8	312	0.438	7
13	462	0.530	7	371	0.550	7
15	564	0.594	9	453	0.566	8
14	716	0.663	9	575	0.638	9
10	912	0.725	7	733	0.703	7
8	1126	0.770	6	904	0.753	6
6	1359	0.806	5	1092	0.791	5
8	1734	0.844	7	1393	0.831	7
10	2342	0.882	9	1881	0.872	9
34	3143	0.911	31	2524	0.903	31
<hr/>				<hr/>		
5000			142			134

$$r_{1 \text{ atm}} = 294 \text{ \AA}$$

$$r_{4000} \text{ bars} = 258 \text{ \AA}$$

$$G_{fi} = \frac{N(y)\phi(y)}{N(y)} \times G(\text{total ionisation})$$

$$(G_{fi})_{1 \text{ atm}} = 0.114$$

$$(G_{fi})_{4000 \text{ bars}} = 0.107$$

from one atmosphere to 4000 bars. Similar variations are found for the other hydrocarbons studied.

The above model therefore predicts that G_{fi} is practically independent of pressure. At this stage it is impossible to distinguish which of the two above limiting cases is the more correct.

(C) Radiation Induced Conductance

The radiation induced conductance of all the hydrocarbons studied decreased with increasing pressure. The conductance was found to be independent of the applied field strength up to 2500 V/cm, the maximum field employed. This behaviour is in agreement with other studies (24,80) at similar dose rates (10^{14} eV/ml sec).

On the assumption that ionic migration may be treated as a rate process, and that G_{fi} is independent of pressure, the volume of activation, defined by relation I-xvi, (page 25) may be calculated. ΔV^\ddagger is a composite value for the positive and negative species and corresponds to the volume increase required for the ions to migrate from one equilibrium position to another such position.

Some plots of $\log \kappa$ versus pressure are shown in Figure IV-C-1. In order to calculate ΔV^\ddagger from such plots the slope of the curve is required. At one atmosphere

FIGURE IV-C-1

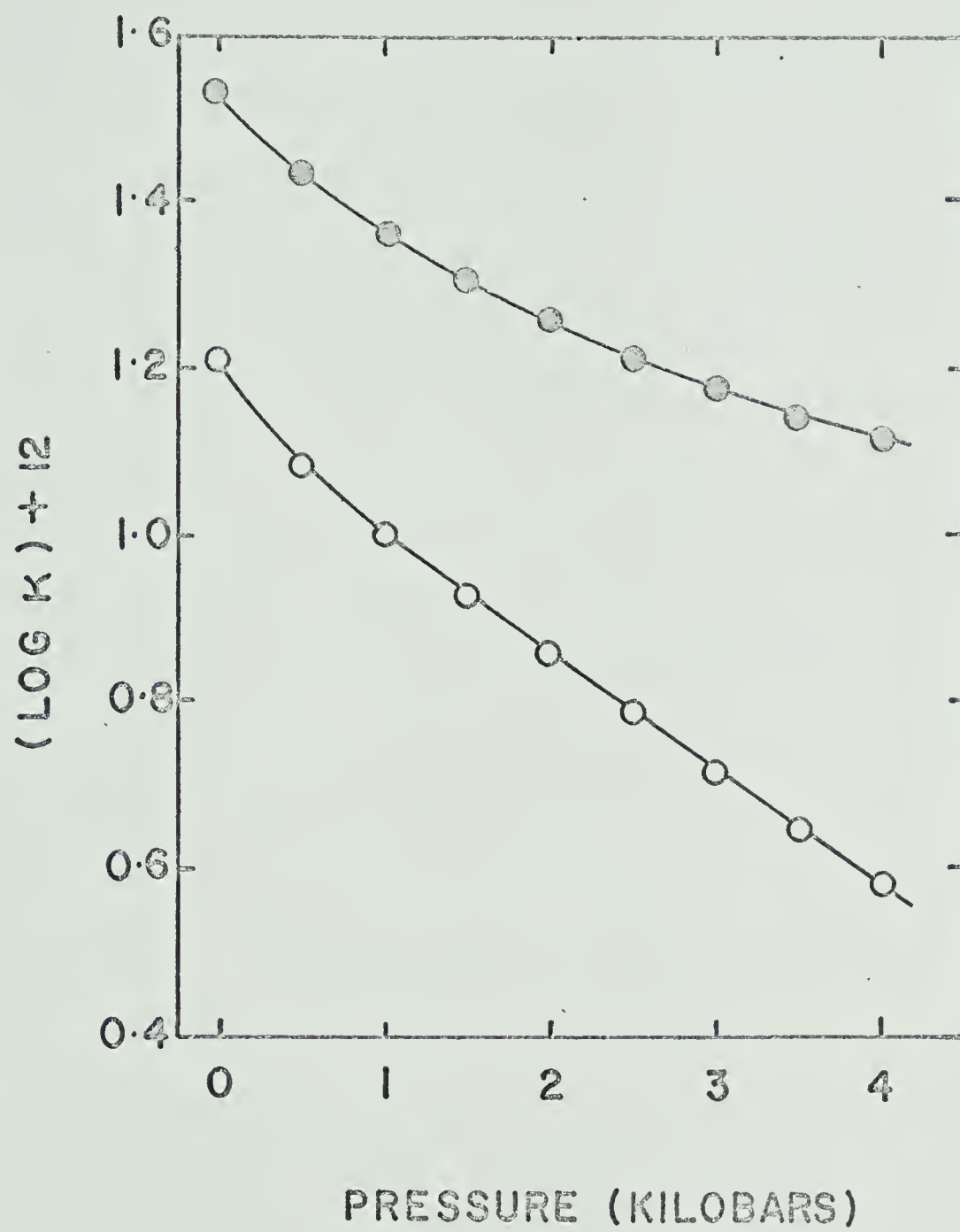
log κ versus Pressure 30°C

● n-pentane Cell C

Dose rate 4.0×10^{15} eV/ml sec

○ methylcyclohexane Cell B

Dose rate 4.9×10^{14} eV/ml sec.



pressure the slope is difficult to obtain accurately because of the rapid change of κ with pressure over the first few hundred bars increase in pressure. The alternative technique of plotting $\Delta V_{\text{mean}}^{\ddagger}$ versus the mean pressure and extrapolating to one atmosphere does not help in the present circumstances. The values of ΔV^{\ddagger} obtained at one atmosphere pressure also exhibit variation from experiment to experiment because of the inaccuracies in the conductance measurements.

Values of ΔV^{\ddagger} calculated by the slope method are shown in Table IV-C-I. The values quoted at one atmosphere pressure are the average values of several determinations and are probably accurate to within $\pm 3 \text{ cm}^3/\text{mole}$. Values at higher pressures exhibited less variation from determination to determination and are probably accurate to within $\pm 1 \text{ cm}^3/\text{mole}$.

At atmospheric pressure ΔV^{\ddagger} is approximately 9 to 14% of the molar volume of the hydrocarbon. The volume of activation decreases with increasing pressure and at 4000 bars is between 4 and 8% of the molar volume of the hydrocarbon at the same pressure. ΔV^{\ddagger} for methylcyclohexane and 2,2-dimethylbutane reached a limiting value around 2000 bars. The latter hydrocarbons also exhibited the greatest viscosity changes with pressure

TABLE IV-C-1

Volums of Activation for Induced Conductance

Compound	Temp.	1 atm ($\pm \sim 3$ cm ³ /mole)	1000	2000 $\pm \sim 1$ cm ³ /mole	3000	4000	$\frac{\Delta V^\dagger \times 100}{\text{molar volume}}$	% 1 atm
n-pentane	30	13	7.0	5.0	4.0	3.5	12%	
n-hexane	3	11	7.0	6.0	5.0	4.5	--	
	30	12	8.0	6.0	5.0	4.0	9 %	
	56	13	8.0	6.5	5.0	4.2	--	
n-octane	3	13	8.0	7.8	---	---	---	
	30	12	8.2	6.8	6.0	6.0	11%	
	56	14	9.0	7.0	6.5	6.5	---	
methylcyclohexane	30	18	9.0	8.0	8.0	8.0	14%	
cyclopentane	30	10	6.8	6.0	4.8	4.0	14%	
2,2-dimethylbutane	30	14	9.2	8.1	8.1	8.1	10%	
	30	20 [†]	14	10	5.5	3.3	14%	

[†] Sample after irradiation at 4.2×10^{14} eV/ml sec for 1500 minutes.

and it appears that molecular structure may play some role in the ionic migration process.

The values of ΔV^\ddagger are similar to those reported in other studies. ΔV^\ddagger for several salts in methanol (103), nitrobenzene (103) and N,N-dimethylformamide (104) are positive and increase with solvent volume (i.e. decrease with increasing pressure) and ion size. For example, (103) ΔV^\ddagger for sodium nitrate in methanol at atmospheric pressure is about 12% of the molar volume of the methanol whereas for tetrabutylammoniumpicrate in the same solvent it is about 24%. It was also suggested that as the density increases ΔV^\ddagger approaches a limiting low value. ΔV^\ddagger was also reported to decrease with increasing temperature but little significance can be attached to the observed temperature variation of ΔV^\ddagger for hexane and octane in the present studies, because of the experimental uncertainty in the values of ΔV^\ddagger .

In summary, the volumes of activation are consistent with the radiolytic ions being of molecular size. ΔV^\ddagger exhibits a pressure dependence similar to that found in higher dielectric constant media.

S U M M A R Y

At the commencement of this work, it had been suggested (155) that cavities in low dielectric constant liquids may play a role in the trapping and solvating of thermalized electrons. Cavity theories of electron solvation had been previously developed for the solvation of electrons in water and ammonia (157,158,159). Increasing the pressure upon a liquid results in the reduction of the interstitial cavities and it seemed possible that the initial separation distance of the electron and parent positive ion may have been altered. The present results indicate that no major change in the separation distance, apart from that which arises from changes in density and dielectric constant, occurs up to pressures of 4000 bars.

No adequate description of the effect of molecular structure upon electron range has yet been achieved, and it is unfortunate that in 2,2-dimethylbutane, in which the electron may have a range greater than in the straight chain hydrocarbons (61, 154), the conductance is dependent upon the absorbed dose.

In conclusion it may be stated that regardless of whether the radiolytic ions obey Stokes Law or not, no

major changes in G_{fi} occur on increasing the pressure to 4000 bars. In order to develop this project further, work should be undertaken at higher pressures and techniques developed to enable the radiolytic ion mobilities to be determined simultaneously with the steady state induced conductance.

R E F E R E N C E S

1. W. C. Roentgen, Ann. der Phys. 64, 1 (1898).
2. O. Glasser and M. Boveri, in "Wilhelm Conrad Roentgen and the Early History of Roentgen Rays". C. C. Thomas Springfield, Illinois (1934).
3. L. Benoist and D. Hurmulescu, Comp. Rend. 122, 235 (1896).
4. J. J. Thomson, Proc. Roy. Soc. 59, 274 (1896).
5. J. S. Townsend, "Electricity in Gases", Clarendon Press, Oxford (1915).
6. P. Curie, Comp. Rend. 134, 420 (1902).
7. H. Becquerel, Comp. Rend. 136, 1173 (1903).
8. D. H. Wilkinson, "Ionization Chambers and Counters," Cambridge University Press, Cambridge, (1950).
9. J. W. Boag, "Ionization Chambers" in "Radiation Dosimetry" edited G. J. Hine and G. L. Brownell, Academic Press Inc., New York 1956.
10. J. J. Thomson and G. P. Thomson, "Conduction of Electricity through Gases". Cambridge University Press, Cambridge, 1928.
11. J. W. Roag and T. Wilson, Brit. J. Appl. Phys. 3, 222 (1952).
12. G. R. Freeman, Radiation Reviews, 1, 1 (1968).
13. G. Jaffe, Ann. Physik, 42, 303 (1913).
14. G. Jaffe, Ann. Physik, 1(5), 977 (1929).

15. G. Jaffe, Physik Z. 30, 849 (1929).
16. F. L. Mohler and L. S. Taylor, Bur. Stand. J. Res., 13, 659 (1934).
17. L. S. Taylor, Bur. Stand. J. Res., 17, 557 (1936).
18. C. S. Pao, Phys. Rev., 64, 60 (1943).
19. H. A. Kramers, Physica 18, 665 (1952).
20. A. N. Gerritsen, Physica 14, 381 (1949).
21. A. N. Gerritsen, Physica 14, 407 (1949).
22. C. T. R. Wilson, Proc. Roy. Soc., A87, 277 (1912).
23. L. Onsager, Phys. Rev., 54, 554 (1938).
24. G. R. Freeman, J. Chem. Phys., 39, 1580 (1962).
25. G. R. Freeman and J. M. Fayadh, J. Chem. Phys., 43, 86 (1965).
26. T. J. Lewis, Progress in Dielectrics, 1, 97 (1959).
27. D. W. Swan, Brit. J. Appl. Phys., 13, 208 (1962).
28. I. Adamczewski, Brit. J. Appl. Phys., 16, 759 (1965).
29. A. Rogazinski, J. de Phys. et Radium, 7, 329 (1936).
30. A. Rogazinski, Phys. Rev., 60, 648 (1941).
31. F. W. Spiers, Chapter (1) in Ref. 9.
32. A. J. Swallow, "Radiation Chemistry of Organic Compounds". Pergamon Press, Oxford (1960).
33. A. W. Topchiev, "Radiolysis of Hydrocarbons", Elsevier Publishing Company (English Edition) New York 1964.
34. H. Essex, J. Phys. Chem., 58, 42 (1954).

35. G. Goldstein and S. A. Reynolds, Nuclear Data, 1A, 435 (1965).
36. H. E. Johns and J. S. Laughlin, Chapter 2 in Ref. 9.
37. S. Fine and C. F. Hendie, Nucleonics, 13(3), 36 (1955).
38. A. H. Compton and S. K. Allison, "X-rays in Theory and Experiment" 2nd Edition Van Nostrand, New York (1935).
39. H. A. Bethe, Handbuch der Physik 24, 273 (1933).
40. D. V. Cormack and H. E. Johns, Radiation Research 1, 133 (1954).
41. L. G. Walker, Ph.D. Thesis, University of Alberta (1967).
42. M. Burton, Record of Chemical Progress, 19, 13 (1958).
43. B. F. J. Schonland, Proc. Roy. Soc., A108, 187 (1925).
44. J. R. Young, J. Appl. Phys., 27, 1 (1956).
45. M. Davis, Phys. Rev. 94, 243 (1954).
46. A. Hummel, A. O. Allen and F. H. Watson, J. Chem. Phys., 44, 3431 (1966).
47. A. H. Samuel and J. L. Magee, J. Chem. Phys., 21, 1080 (1953).
48. R. L. Platzman in "Basic Mechanisms in Radiobiology" National Academy of Sciences, Washington (1953).
49. G. R. Freeman, J. Chem. Phys., 46, 2822 (1967).

50. D. E. Lea in "Actions of Radiation in Living Cells", Cambridge University Press, Cambridge (1955).
51. M. Lefort, Ann. Rev. Phys. Chem., 9, 123 (1958).
52. H. E. Johns, Chapter 12 in Ref. 9.
53. A. Mozumder and J. L. Magee, Radiation Research 28, 203 (1966).
54. G. R. Freeman, J. Chem. Phys., 37, 988 (1963).
55. A. O. Allen and A. Hummel, Disc. Faraday Soc., 36, 95 (1963).
56. A. Hummel and A. O. Allen, J. Chem. Phys., 44, 3426 (1966).
57. P. Debye, Trans. Electrochem. Soc., 82, 265 (1942).
58. M. v. Smoluchowski, Z. Physik. Chem. 92, 129 (1917).
59. P. Chang and C. R. Wilke, J. Phys. Chem., 59, 592 (1955).
60. V. L. Talrose, Chapter 2 in "Actions Chimiques et Biologique des Radiations", Ed. M. Haissinsky, Mainson, Paris (1967).
61. P. H. Tewari and G. R. Freeman J. Chem. Phys. (in press)
62. W. Schmidt, Z. Naturforsch., 23B, 126 (1967).
63. A. Jahns and W. Jacobi, Z. Naturforsch., 21A, 1400 (1966).
64. F. Williams, J. Am. Chem. Soc., 86, 3954 (1964).
65. I. Adamczewski, Nature 137, 994 (1936).
66. O. Gzowski, Nature, 194, 173 (1962).

67. O. Gzowski, Z. Phys. Chem., 221, 288 (1962).
68. W. F. Schmidt and A. O. Allen, J. Chem. Phys.,
(in press).
69. I. Adamczewski and B. Jachym, Acta. Phys. Pol., 30,
767 (1967).
70. G. R. Freeman in "Radiation Research", G. Silini
Ed. Interscience Publishers, New York, 1967 p.113.
71. H. Schnyders, L. Meyer and S. A. Rice, Phys. Rev.
Letters, 15, 187 (1965).
- 72.. L. Meyer, H. T. Davis, S. A. Rice and R. J. Donn-
elly, Phys. Rev., 126, 1927 (1962).
73. W. E. Wentworth, R. S. Becker and R. Tung, J.
Phys. Chem., 71, 1652 (1967).
74. I. Adamczewski, Brit. J. Appl. Phys., 16, 759 (1965).
75. I. Adamczewski, Atomproxis. 9, 327 (1961).
76. B. Jachym, Acta. Phys. polar 29, 23 (1964).
77. J. C. Russell and G. R. Freeman, J. Chem. Phys., 48,
90 (1968).
- 77a. K. Schmidt and W. Buck, Science, 151, 70 (1966).
78. R. Gibaud, J. Chim. Phys., 64, 521 (1967).
79. A. Mozumder and J. L. Magee, J. Chem. Phys., 47, 939
(1967).
80. G. R. Freeman, Disc. Faraday Soc., 36, 250 (1963).
81. A. Hummel and A. O. Allen, J. Chem. Phys., 46, 1602
(1967).

82. D. Blanc and J. Mathieu, J. Phys. Radium 21, 675 (1960).
83. D. Blanc, J. Mathieu and J. Boyer, Nuovo Cim. 19, 929 (1961).
84. D. W. Goodwin and K. A. McFadyen, Proc. Roy. Soc., 66B, 85 (1953).
85. H. House, Proc. Phys. Soc., 70B, 913 (1957).
86. N. B. Green, J. Appl. Phys., 26, 1257 (1955).
87. J. O. Hirschfelder, C. F. Curtis and R. B. Bird, "Molecular Theory of Gases and Liquids", John Wiley and Sons Ltd., (1954).
88. H. Eyring, J. Chem. Phys., 4, 283 (1936).
89. H. O. Hirschfelder, D.P. Stevenson and H. Eyring, J. Chem. Phys., 5, 896 (1937).
90. S. Glasstone, K. J. Laidler and H. Eyring, "Theory of Rate Processes" McGraw-Hill (1941).
91. H. Eyring and T. Ree, Proc. Nat. Acad. Sci., 47, 526 (1961).
92. H. Eyring and R.P. Marchi, J. Chem. Ed. 40, 562 (1963).
93. P. W. Bridgman, "The Physics of High Pressures" G. Bell and Sons Ltd., London (1931).
94. M. G. Evans and M. Polanyi, Trans. Faraday Soc., 31, 875 (1935).
95. S. D. Hamann "Physico-chemical Effects of Pressure" Butterworth Scientific Publications, London 1957.

96. S. D. Hamann, Chapter 8 in "High Pressure Physics and Chemistry", Volume 2, Ed. R. S. Bradley, Academic Press, London (1963).
97. K. E. Weale in "Chemical Reactions at High Pressures" E. and F. N. Spon Ltd., London (1967).
98. E. McLaughlin, Trans. Faraday Soc., 35, 28 (1959).
99. H. M. Cohen and D. Turnbull, J. Chem. Phys., 21, 1364 (1959).
100. W. A. Steele and W. Webb, Chapter 4(ii) in Ref. 96.
101. A. J. Batschinski, Z. Physik Chem., 84, 643 (1913).
102. S. B. Brummer and G. J. Hills, Trans. Faraday Soc., 57, 1816 (1961).
103. S. B. Brummer and G. J. Hills, Trans. Faraday Soc., 57, 1823 (1961).
104. S. B. Brummer, J. Chem. Phys., 42, 1636 (1965).
105. F. Barrieria and G. J. Hills, Trans. Faraday Soc., 64, 1359 (1968).
106. R. J. Greet, and J. H. McGill, J. Phys. Chem., 71, 1746 (1967).
107. R. A. Horne and D. S. Johnson, J. Phys. Chem., 70, 2182 (1966).
108. R. M. Fuoss and F. Accascina, in "Electrolytic Conductance", Interscience, New York, (1966).
109. J. F. Skinner and R. M. Fuoss, J. Phys. Chem., 69, 1437 (1965).

110. C. M. Apt, F. F. Margosian, I. Simon, J. H. Vreeland and R. M. Fuoss, J. Phys. Chem., 66, 210 (1962).
111. J. F. Skinner and R. M. Fuoss, J. Phys. Chem., 70, 1426 (1966).
112. D. D. Tanner, private communication.
113. A. O. Allen, "The Radiation Chemistry of Water and Aqueous Solutions", p.22, D. Van Nostrand Company Inc., New York, (1961).
114. N. B. S. Handbook #54, "Protection against Radiation from ^{226}Ra , ^{60}Co and ^{137}Cs ".
115. F. Waibel, Ann. d. Physik., 72, 161 (1923).
116. C. Franche, Ann. d. Physik., 77, 159 (1925).
117. W. E. Danforth, Phys. Rev., 38, 1224 (1931).
118. J. C. Jamieson, J. Chem. Phys., 21, 1385 (1953).
119. International Critical Tables, Vol. III. National Research Council, McGraw Hill, New York 1933.
120. Y. Rocard in "Principles of Electricity and Magnetism" Pitmans and Sons Ltd., London, (1959).
121. P. W. Bridgman, Proc. Am. Acad., 66, 185 (1931).
122. J. W. M. Boelhouwer, Physica 26, 1021 (1960).
123. H. E. Eduljee, D. M. Newitt and K. E. Weale, J. Chem. Soc., 3086, (1951).
124. N. L. Brown, Annual Report of the Conference on Electrical Insulation, National Academy of Sciences, National Research Council Publication 1238 (1964).

125. R. M. Hubbard and G. G. Brown Ind. Eng. Chem.
(Anal. Ed.) 15, 212 (1943).
126. F. I. Mopsik, Bur. Stand. J. Res., 71A, 287 (1967).
127. Z . T. Chang, Chinese J. Phys., 1, 1 (1924).
128. P. W. Bridgman, Phys. Rev., 3, 153 (1914).
129. L. Onsager, J. Am. Chem. Soc., 58, 1486 (1936).
130. P. Debye, in "Polar Molecules" Dover, New York (1947).
131. Von S. Kyropoulos, Z. fur Physik, 40, 507 (1926).
132. J. G. Kirkwood, J. Chem. Phys., 4, 592 (1936).
133. A. Michels, P. Sanders, and A. Schipper, Physica
2, 753 (1935).
134. A. Michels, A. Jaspers and P. Sanders, Physica 1,
627 (1954).
135. A. Michels, C. A. Ten Seldam and S. D. J. Overdijk,
Physica 17, 781 (1951).
136. H. G. David, S. D. Hamann and J. F. Pease, J. Chem.
Phys., 19, 1491 (1951).
137. F. G. Keyes and J. L. Oncley, Chem. Rev., 19, 195
(1936).
138. C. A. Ten Seldam and S. R. de Groot, Physica 18,
905 (1952).
139. P. W. Bridgman, Proc. Am. Acad. Arts and Science,
77, 140 (1948).
140. D. L. Dugle and G. R. Freeman, J. Phys. Chem., 70, 1256
(1966).

- 141. A. E. Flowers, Proc. Amer. Soc., Testing Materials 14, 565 (1914).
- 142. M. D. Hersey and H. S. Shore, Mech. Eng. 50, 221 (1928).
- 143. M. D. Hersey, J. Wash. Acad. Sci., 6, 525 (1916).
- 144. R. B. Block, J. App. Phys., 13, 56 (1942).
- 145. Handbook of Chemistry and Physics 41st Edition
Chemical Rubber Publishing Co., Ohio (1960).
- 146. C. B. Dow, J. Appl. Phys., 8, 367 (1937).
- 147. E. M. Greist, W. Webb and R. W. Schiessler, J.
Chem. Phys., 29, 711 (1958).
- 148 H. Lamb in Hydrodynamics Article 371 Cambridge
University Press 6th Edition (1932).
- 149. Article 330 in Ref. 148.
- 150. P. W. Bridgman Proc. Amer. Acad. 61, 57 (1926).
- 151. P. W. Bridgman, National Acad. Science 11, 603
(1925).
- 152. J. R. Partington "An Advanced Treatise on Physical
Chemistry" Volume II Chapter VII and references
therein. Longmans, Green & Co. Ltd., London (1951).
- 153. A. J. Matheson, J. Chem. Phys., 44, 695 (1966).
- 154. P. H. Tewari and G. R. Freeman, paper submitted for
publication July 1968.
- 155. G. R. Freeman, unpublished work presented at the
Gordon Research Conference on Radiation Chemistry,
New Hampton, N.H. August 1966.

- 156. G. R. Freeman, J. Chem. Phys., 40, 907 (1964)
- 157. J. Jortner, S. A. Rice and E. G. Wilson in
"Metal Ammonia Solutions", Ed. L. Lepoutre and
M. J. Sienko, W. A. Benjamin Inc., New York 1964.
- 158. J. Jortner, S. A. Rice in "Solvated Electron"
Advances in Chemistry Series 50, (1965).
- 159. J. Jortner, Radiation Research Supplement #4
(1964).

B29902